An Investigation of Radiometer and Antenna Properties for Microwave Thermography

Malika Mimi

Department of Physics and Astronomy

University of Glasgow

Glasgow

Thesis

Presented for degree of Doctor of Philosophy

to the University of Glasgow,

October 1990

ProQuest LLC.
789 East Eisenhower Parkway
P.O. Box 1346
Ann Arbor, MI 48106 – 1346

In the name of God, Most Gracious, Most Merciful.

Time shows that nothing lasts but Faith, Goodness, Truth, and Virtue.

Victory and Help, conditions for and against: true fealty, patience, and self-restraint: strength and gentleness

To the memory of my brother Yasine

and

To my parents

whose love, support, and encouragement

over the years have to a large extent

made the writing of this thesis possible.

Declaration

This thesis has been composed by the undersigned. It has not been accepted in any previous application for a degree. The work of which it is record has been done by myself, unless indicated otherwise in the text. I further state that no part of this has already been or is being concurrently submitted for any such degree or qualification at any other university.

Malika Mimi

Acknowledgements

This work was carried out whilst I was a student in the Department of Physics and Astronomy, University of Glasgow and in receipt of a research studentship award from Algerian government the Ministry of High Education.

I would like to thank Professor I.S. Hughes the ex-head of the department of Physics and Astronomy especially for the financial support to attend conferences and Professor P.R. Ferrier the present head of the department of Physics and Astronomy for the financial support to attend conference. I am very grateful to my supervisor Dr. D.V. Land for this constant enthusiasm for this work, for his many helpful and constructive suggestions and for sending me to the 17th European Microwave Conference in Rome, Italy in September 1987 and to the Advances in Medical Microwave Imaging meeting in Lille University , France in November 1989. I also thank Dr. A.Watt, Dr. V. Brown, Dr. R. Jennings, A. Campbell and A.Seath whom I benefited from their help.

Special thanks must be given to R. Setoodeh for his friendship and help.

Table of contents

Chapter II

The microwave radiometer

Chapter III

Microstrip circuits for radiometer input switching circuits

Chapter IV

Microwave thermography antennas

Chapter V

Microwave correlation radiometry: Theory

Chapter VI

Microwave correlation radiometry: Practical Implementation

Chapter VII

Electromagnetic fields measurements and the nonresonant perturbation technique

Chapter VIII

Nonresonant perturbation technique: Practical Implementation

Summary

Microwave thermography obtains information about the subcutaneous body temperature by a spectral measurement of the intensity of the natural thermally generated radiation emitted by the body tissues. At lower microwave frequencies the thermal radiation can penetrate through biological tissue for significant distances. The microwave thermal radiation from inside the body can be detected and measured non-invasively at the skin surface by the microwave thermography technique, which uses a radiometer to measure the radiation which is received from an antenna on the skin. In the microwave region the radiative power received from a volume of material has a dependence on viewed tissue temperature $T(\underline{r})$ of the form,

$$P = kB \int_{vol} c(\underline{r})\, T(\underline{r})\, dv$$

where k is the Boltzmann's constant, B the measurement bandwidth, $c(\underline{r})$ is the relative contribution from a volume element dv (the antenna weighting function). The weighting function, $c(\underline{r})$, depends on the structure and the dielectric properties of the tissue being viewed, the measurement frequency and the characteristics of the antenna. In any practical radiometer system the body microwave thermal signal has to be measured along with a similar noise signal generated in the radiometer circuits.

The work described in this thesis is intended to lead to improvement in the performance of microwave thermography equipment through investigations of antenna weighting functions and radiometer circuit noise sources. All work has been carried out at 3.2 GHz, the central operating frequency of the existing Glasgow developed microwave thermography system.

The effects of input circuit losses on the operation of the form of Dicke radiometer used for the Glasgow equipment have been investigated using a computational model and compared with measurements made on test circuits. Very good agreement has been obtained for modelled and measured behaviour. The losses contributed by the microstrip circuit structure, that must be used in the radiometer at 3.2 GHz, have been investigated in detail.

Microwave correlation radiometry, by "*add and square*" method, has been applied to the received signals from a crossed-pair antenna arrangement, the antennas being arranged to view a common region at a certain depth. The antenna response has been investigated using a noise source and by the nonresonant perturbation technique. The received pattern formed by the product of the individual antenna patterns gives a maximum depth in phantom dielectric material. The depth can be adjusted by changing the spacing of the antennas and the phase in an antenna path. However, the pattern is modulated by a set of positive and negative interference fringes so that the complete receive pattern has a complicated form. On uniform temperature distributions the total radiometric signal is zero with the positive and negative contributions cancelling each other out. The fringe modulation can be removed by placing the antennas close enough together, The pattern is then simple and gives a modest maximum response at a known depth in a known material. The radiometer system remains sensitive to the temperature gradients only and the wide range of dielectric properties and tissue structures in the region being investigated usually makes the system response difficult to interpret.

For crossed-pair antennas in phase the effective penetration depth in high- and medium-water content tissues is about 2.5 cm at a frequency of 3.2 GHz. The field pattern observed was of the form expected from the measurements of the individual antenna behaviour with the appropriate interference pattern superimposed.

The *nonresonant perturbation* technique has been developed and applied to assist the development of the medical application of both microwave thermographic temperature measurement and microwave hyperthermia induction. These techniques require the electromagnetic field patterns of the special antennas used to be known. These antennas are often formed by short lengths of rectangular or cylindrical waveguide loaded with a low-loss dielectric material to achieve good coupling to body tissues. The high microwave attenuation in biological materials requires the field configurations to be measured close to the antenna aperture in the near-field wave. The *nonresonant perturbation* is a simple technique which can be used to measure electromagnetic fields in lossy material close to the antenna. It has been applied here to measure accurately the antenna weighting function and the effective penetration depth in tissue simulating dielectric phantom materials.

The antenna patterns have been measured at 3.25 GHz in different dielectric phantom materials representing from low- to high-water content tissues, using dielectric spheres and sheets. The relative response $Ln(E^2)$ has been found to fall approximately linearly with distance from the antenna aperture along its central axis. The distance over which $Ln(E^2)$ is reduced by a factor of $e^{-2\alpha z}$, the effective penetration depth, has been measured and compared to the calculated *TEM* wave penetration distance in the phantom material. For a TE_{11}-mode circular antenna in high- and medium-water content material the effective penetration depth is farmed to be close to the plane-wave penetration depth, the ratio of them being approximately 90%. In fat simulating phantom material the effective penetration depth is rather smaller than the plane-wave penetration depth, the ratio being approximately 70%.The results show that the TE_{11}-mode circular antenna gives a better microwave thermographic performance than the more commonly used TE_{01}-mode rectangular antennas.

Chapter I

Microwave thermography

I.1- Introduction:

Microwave thermography or thermometry is a particular use of radiometry in the measurement of the thermal noise emitted by the body tissues. This technique has been widely used and extensively investigated in medical applications for the detection, the diagnosis and the monitoring of diseases which produce changes in the body' s normal temperature distributions.

Variations in the temperature in the subcutaneous tissue and over the body surface reflect variations in the physiological properties of blood flow and metabolic heat production. Changes in metabolism produce thermal changes in the body which can be investigated by the microwave thermography technique. The improved sensitivity of this technique makes it preferable when compared with infra-red technique.

At infra-red wavelengths tissue penetration distances are extremely small, of the order of 0.1 mm, and observable thermal radiation can come from only the skin surface. The infra-red skin temperature pattern which is observed is the result of a complex combination of thermal conduction of heat from internal body sources through the subcutaneous tissues, the state of perfusion of the cutaneous tissues, and a delicate thermal balance at the skin surface dependent on radiative, convective and evaporative heat losses (Draper and Boag, 1971; Lipkin and Hardy, 1954). The need for very stable heat loss from the skin during infra-red measurements thus normally requires stabilisation of the temperature of the surface. Microwave thermography attempts to observe directly the thermal radiation due to internal body sources, by minimizing the contribution from the skin tissue.

Research studies in medical applications have been carried out in order to investigate microwave temperature measurements in the human body. Several kinds of diseases have been studied, including detection of cancers of the breast, thyroid, brain and bone (Mamouni et al., 1981; Shaeffer et al.,1981; Carr et al., 1983; Barrett et al., 1980; Gautherie et al., 1979a; 1979b; Leroy, 1982; Land, 1987a; Brown, 1989) osteo-articular and inflammatory diseases (Fraser et al., 1987; Brown, 1989) as well as of the temperature during a heating process, for example, in hyperthermia for the treatment of cancer (Plancot et al., 1987). The significant advantage of microwave thermography for monitoring these diseases is its ability to take advantage of the relative transparency of body tissues at microwave frequencies. This transparency of tissues to microwave thermal radiation allows information to be obtained about internal body temperature patterns from measurements made at the skin surface. The average temperature within a volume, extending to depths 1 - 5 cm depends on frequency and tissue type (Fig. I.1). This figure illustrates the variations of tissue properties with frequency (data collected from Cook, 1951a; 1951b, 1952; Herrick, 1950; England, 1950) in terms of the e^{-1} (or 37 %) penetration depth for the power of the incident plane-wave radiation. At 3 GHz the plane-wave penetration depth is about 5 cm in tissue with a low water content, such as fat, and is about 0.8 cm in high water content tissue such as muscle and skin. It can be seen that the penetration depth in both low- and high- water content decreases significantly with increasing frequency. At frequencies above 10 GHz the penetration depths are only a few millimetres. At the higher microwave frequencies microwave thermography will then give results very similar to those obtained with infra-red thermography.

This microwave measurement of internal temperature is related predominantly to physiological conditions in the deeper tissues rather than the effects of heat transfer to the environment. Experience has shown that diseases or physiological states in which a thermal phenomenon occurs at a depth of up to several centimeters can be examined and have frequently been detected by

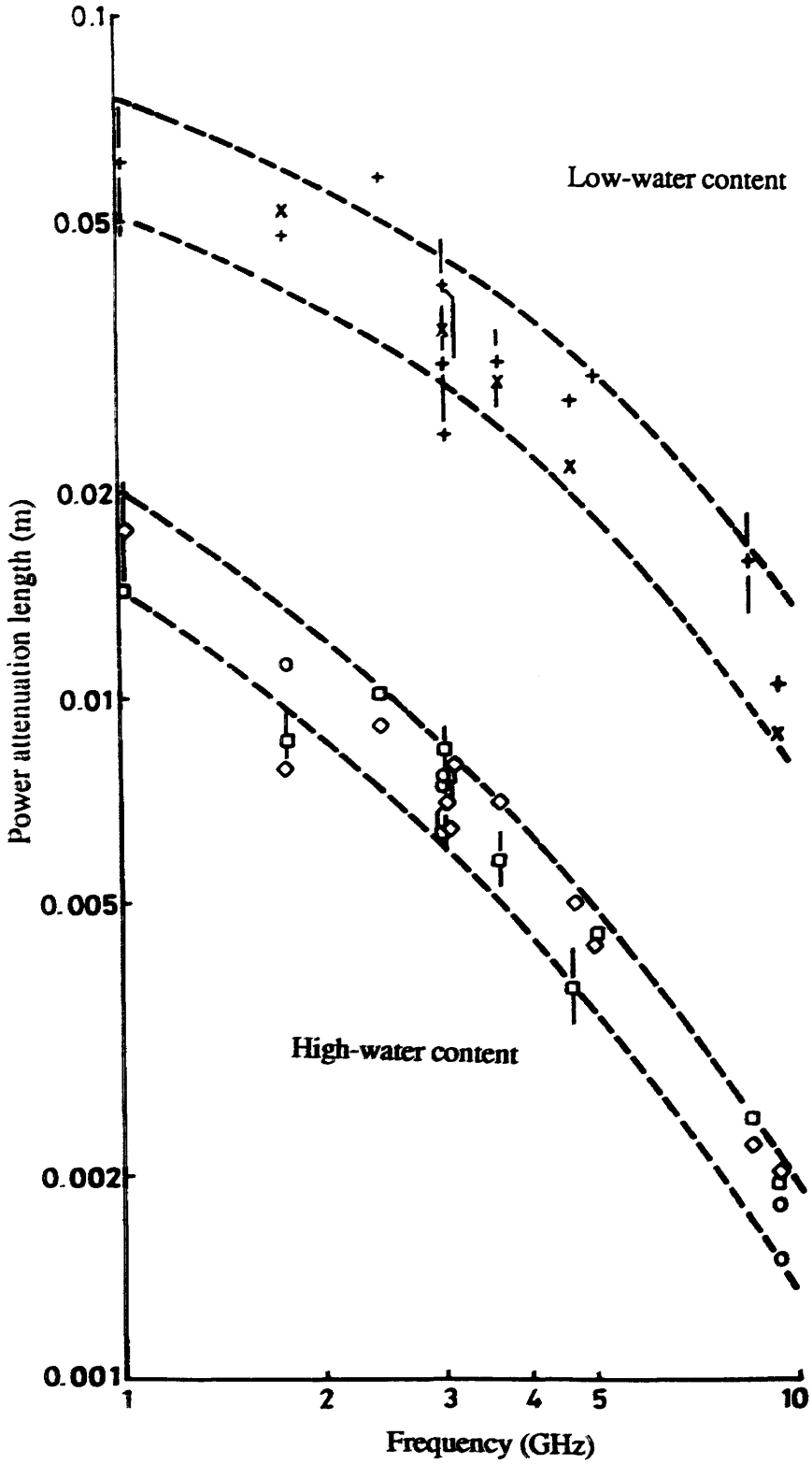

Fig. L1- Microwave penetration depth in human tissue

□ Muscle
○ Blood
◇ Skin
\+ Fat
× Bone

microwave thermography. Therefore, microwave thermography has been chosen to detect the thermal radiation from body tissues by a radiometer system which consists of two essential elements; a microwave radiometer which measures the power of the thermal signal; and an antenna which receives the power from the tissue, providing a transition between the radiation emitted by the tissue and the system. This system will be described in the following chapters.

I. 2- The object of the study.

The object of this work is to improve existing microwave radiometry techniques for medical applications. This may be achieved by reducing the effects of losses in the special input circuits required for the microwave radiometer and also the spatial response patterns of various radiometer antenna arrangements.

For the investigation of antenna spatial response patterns a new technique, *nonresonant perturbation*, has been used. The *nonresonant perturbation* technique was applied to measure accurately the penetration distances of the electromagnetic fields which are proportional to the temperature within the tissue. The measurements of antenna electromagnetic field configurations for various materials simulating body tissues have been analysed experimentally as well as numerically.

The use of microwave correlation radiometry was first suggested for medical application by Mamouni et al., (1981). Two identical antennas are used to look at a region at some depth in the body and the signal from this volume is cross-correlated. Mamouni et al., (1983); Leroy, (1982); Bellari et al., (1984a; 1984b); Hill et al, (1985); and Newton (1986) have published work on the practical implementation of the idea. In the present study the correlation microwave antennas are combined with the *nonresonant perturbation* technique to develop a technique for the measurement of the electromagnetic fields in biomedical applications.

In section I.3, below, microwave thermography is briefly described. The basic principles of clinical thermography and thermometry are discussed in section

I.4. Hyperthermia and the techniques for hyperthermia induction are described briefly in section I.5, with a discussion of the use of microwave radiometry for the non-invasive monitoring of hyperthermia temperature. Section I.6 reviews recent and current work in the field of microwave thermometry.

Chapter II discusses in detail the microwave radiometry technique and describes the microwave radiometer used in this study. The design and testing of the microstrip circuits for the microwave radiometer input switching device are described in Chapter III. Chapter IV describes the performance of the microwave thermography antennas related to tissue properties and modelling of the microwave temperature. Chapters V and VI respectively discuss the theory and the practical work of *microwave correlation radiometry*. The *nonresonant perturbation* technique is presented in Chapter VII. Chapter VIII describes the application of the *nonresonant perturbation* technique to a single TE_{11}-mode cylindrical waveguide antenna and to the correlation microwave thermography. The author's conclusions are presented in Chapter IX.

I. 3- Principles of microwave thermography.

The apparent microwave thermal radiation temperatures measured at the surface of the human body can be derived from consideration of the thermal radiation emission of an ideal black-body source and the propagation of electromagnetic radiation through dielectric materials. The radiation at any wavelength from a black-body depends only on its temperature and is independent of the nature of the material of this body. Planck's Law describes the intensity of the radiation from the black-body at a temperature T in the wavelength region λ and $\lambda + d\lambda$. This is given by:

$$B_\lambda \, d\lambda = \frac{2hc^2}{\lambda^5 \left(e^{\frac{ch}{\lambda KT}} - 1 \right)} \, d\lambda \qquad (I.1)$$

where $B_\lambda \, d\lambda$ is the emitted power passing through a unit surface area, into a unit

solid angle about a particular direction, in a unit wavelength interval about $d\lambda$, h, c, and K are respectively Planck's constant (Js), the velocity of the radiation (ms^{-1}), and Boltzmann's constant (JK^{-1}), T is the temperature of the source material (K).

Figure I.2 shows the intensity spectrum of black-body emission at a temperature of T= 300 K, approximately that of the human body. At wavelengths between 0.2 and 20 μm both white and black skin behave as a black-body (Mitchell et al., 1967). Maximum intensity occurs at a wavelength λ = 10 μm. Infra-red thermography operates near the radiation maximum in the wavelength range 3-15 μm (Jones, 1987). Although the wavelength dependence of the thermal radiation results in the intensity in the microwave or centimetric wavelength part of the spectrum being reduced by a factor of 10^8 compared with the infra-red maximum nevertheless microwave radiometers, of a form originally developed for radio astronomy, can readily detect radiation at this intensity.

Radiation is usually defined in terms of intensity, either spectral intensity which refers to radiation emitted in a small frequency interval about a central frequency or total intensity which refers to the combined radiation over all frequencies. In microwave thermography it is the spectral intensity in a small band of microwave frequencies which is the relevant quantity.

Intensity, I_ν, is related to the amount of radiative power, dP, in a specific frequency band, $d\nu$, which is transported across an element of area, $d\sigma$, and in directions confined to an element of solid angle $d\omega$,

$$dP = I_\nu \cos\theta \, d\omega \, d\sigma \, d\nu \qquad \text{(I.2)}$$

where θ is the angle between the direction considered and the outward normal to the surface $d\sigma$.

From Eq. I.1 the intensity of radiation emitted by a black body, B_ν, is often referred to as the "Planck function" and is given by:

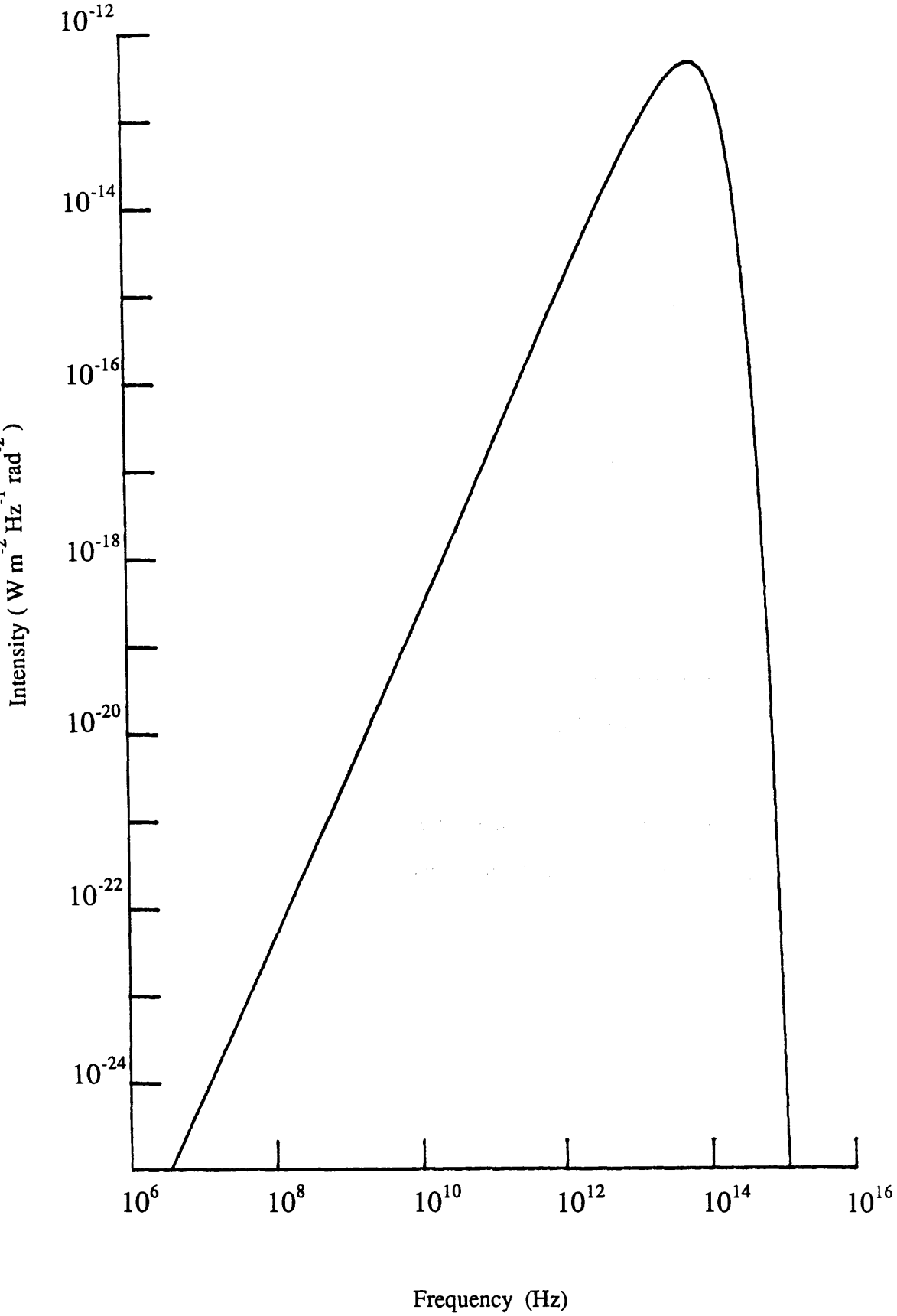

Fig. I.2- Intensity spectrum of a black body at a temprature of 300 K

$$B_\nu(T) = \frac{2h\nu^3}{c^2\left[e^{\frac{h\nu}{KT}} - 1\right]} \qquad (I.3)$$

At microwave frequencies below 10 GHz for source temperatures about 300 K, where $\frac{h\nu}{kT} << 1$, Planck's Law is given by the Rayleigh-Jeans's Law approximation:

$$B_\nu(T) = \frac{2KT\nu^2}{c^2} \qquad (I.4)$$

The intensity, $B_\nu(T)$, given in Eq. I.3 and I.4, is in terms of a frequency bandwidth $d\nu$, whereas Eq. I.1 the intensity was given in terms of a wavelength interval, $d\lambda$.

For non black-bodies the intensity is dependent on both the temperature and the nature of the material and will be less than that emitted by a black-body at the same temperature.

For a small element dm of an isotropic non black-body in an isotropic field of radiation the power emitted in a bandwidth $d\nu$, in directions confined to an element of solid angle $d\omega$, can be expressed as:

$$j_\nu \, dm \, d\omega \, d\nu \qquad (I.5)$$

where j_ν is the emission coefficient for frequency ν.

A pencil of radiation passing through a thickness dz of this material will be reduced from its original intensity In to $I_\nu + dI_\nu$ where

$$dI_\nu = -k_\nu \rho I_\nu dz \qquad (I.6)$$

where k_ν is the mass absorption coefficient and ρ is the density of the material.

An important relation between these two quantities of emission and absorption is given by Kirchhoff's Law (Chandrasekhar, 1939) which states that the ratio of the emission to absorption coefficients of any body in thermodynamical equilibrium is equal to the intensity of the radiation emitted by a black-body at the same temperature T:

$$B_\nu(T) = \frac{j_\nu}{k_\nu} \tag{I.7}$$

A small cylinder of material at a temperature above absolute zero, with cross-sectional area $d\sigma$ and length dz, which has radiation of intensity I_ν incident in the z direction on one face and intensity $I_\nu + dI_\nu$ emerging from the second face in the same normal direction will both absorb part of the incident radiation and emit radiation. The power per unit bandwidth through the cross-section of the cylinder in a direction confined to a solid angle $d\omega$ about the z direction is given by $I_\nu d\sigma\, d\omega$ of which an amount $k_\nu \rho I_\nu dz\, d\omega d\sigma$ is absorbed by the cylinder. The power per unit bandwidth emitted by the cylinder is equal to $j_\nu \rho dz\, d\omega d\sigma$ and in a steady condition,

$$dI\, d\sigma\, d\omega = \rho\, j_\nu\, d\sigma\, d\omega dz - \rho k_\nu I_\nu\, d\sigma d\omega dz \tag{I.8}$$

or

$$\frac{dI_\nu}{dz} = j_\nu \rho - k_\nu \rho I_\nu \tag{I.9}$$

This equation is known as the equation of transfer (Chandrasekhar, 1939). An approximation of the intensity of the radiation , $B_\nu(T)$which was given in equation I.4, for the bandwidth $\Delta\nu$ gives the corresponding power, $KT\Delta\nu$, which is the Nyquist Law.

The radiometric signal power received by a suitably impedance matched antenna in contact with the body is the power:

$$P = KT\Delta v. \qquad (I.10)$$

Thus at microwave frequencies the emitted power is proportional to the temperature of the emitting material.

The radiation transfer techniques (Brown, 1989) rely to a great degree on the differing absorption properties exhibited by high- and low- water content tissues (fat, skin, and muscle), Fig. I. 1. The interference effects between the tissue layers permits consideration of the radiative transfer in terms of power, and therefore at microwave frequencies in terms of temperature. Chandrasekhar, (1950) examined and discussed a case of a tumour in breast fat using the plane parallel solution to the equation of radiative transfer to calculate the excess temperature (ΔT_b) of incident radiation at the skin/antenna interface. This temperature, depends on the characteristics of the properties of the tissue and the measurement conditions, which is given by relationship I.11.

$$\Delta T_b = \Delta T \left(1 - \frac{1}{e^{k_t \Delta z_t}} \right) \left(\frac{t_{fs}}{e^{(k_f \Delta z_f + k_s \Delta z_s)}} \right) \qquad (I.11)$$

where ΔT is the mean excess temperature of the tumour ambient; k_t , k_f , and k_s are the power absorption coefficients (inverse of the penetration depth) of the tumour, fat, and skin respectively; Δz_t, Δz_f and Δz_s are the sizes of the tumour, overlying fat layer, and skin layer; t_{fs} is the power transmission coefficient from fat to skin. At 3 GHz the temperature, ΔT_s; was evaluated by Myers and Barrett, (1977) using the tissue properties data collected from England, (1950); Johnson and Guy, (1972).

$$\Delta T_b = 0.28\ \Delta T \qquad (I.12)$$

I. 4- Thermography and Thermometry.

Temperature is an important parameter in the physiology of the human body. In this study investigations of the effects of subcutaneous temperature changes are carried out. It has been used in clinical measurements ever since Hippocrates used his hand to assess a patient's temperature in about 400 BC. Sanctorius of Padua, (1612 AD) first used the thermometer to measure body temperature following the development of the air-thermometer invented by Galileo in 1595 AD. By the 1870's temperature measurement was generally adopted as a medical procedure (Solsona, 1978).

Measuring the general temperature of the body remains to this day an important technique for monitoring disease. Normal body "core" temperature is approximately 37 ^{o}C but might vary about this throughout the day by as much as 1 ^{o}C. It is dangerous to life when the core temperature rises above 41 ^{o}C or falls below 35 ^{o}C.

Particular diseases may cause specific patterns of temperature change during the period of illness. Study can assist diagnosis of the disease. Therefore, measuring general body temperature provides useful information. Several diseases and disorders cause recognizable changes in temperature. Tumours cause temperature increases in the region of 1 or 2 ^{o}C, due to the increased vascular activity and metabolism associated with the tumour. Inflammatory diseases such as arthritis are known to cause localized temperature increases. Blood flow plays a major role in the heat regulating mechanism of the body, so disorders and diseases of the vascular system often effect local or regional temperature changes. There are two methods of measuring the internal temperature (invasive and non-invasive). These techniques are employed to give information about the thermal condition of the deeper tissue and so provide information about their vascular and metabolic states. The above techniques are at present mainly used in research. Skin temperatures can be measured successfully by infra-red or liquid crystal thermography. All methods have some disadvantages in terms of performance, cost

and complexity for routine use but microwave thermography techniques are simple to use with sufficient sensitivity to detect thermal anomalies and suitable for operation in clinical environments at very reasonable cost. It is now necessary to evaluate different applications for improving these techniques.

I. 4. 1- Internal temperature measuring techniques.

a- Invasive techniques:

The measurement of the internal temperature may be achieved by inserting narrow probes containing thermistor or thermocouple sensors into the tissue. Non-metallic temperature probes have been developed for use in electromagnetic fields as applied in hyperthermia treatment of cancers (Vaguine et al., 1984; Wickersheim et al., 1985). Haimovici, (1982) has used thermocouples inserted into shoulder, hip, knee and ankle joints to investigate normal joint temperatures and the temperatures in patients suffering from various osteo-articular disease. It is only possible to investigate the temperature in a limited volume of tissue with such techniques. However, invasive techniques are undesirable due to the danger of physical damage, infection of the tissue, and discomfort to the patient.

b- Non-invasive techniques:

There are various methods of non-invasive thermometry which can be used to determine the internal temperatures other than microwave thermography. Non-invasive methods are particularly required for monitoring hyperthermia treatment of cancers. This treatment involves heating tumour tissue to a temperature of 42 - 45 ^{o}C. These techniques rely on the temperature dependent properties of the tissue being known.

The feasibility of temperature control by microwave radiometry has also been studied extensively. It has been shown also that non-invasive microwave radiometry is a preferable substitute for the undoubtedly traumatic invasive

techniques. Most of these non-invasive methods are still at the stage of research and development.

(i)- **Microwave Radiometry**:

Microwave radiometry* is an alternative technique to measure the subcutaneous temperature up to several centimetres. Microwave radiometry is based on using small matched antenna brought into contact with the skin and designed for local measurements (Land, 1987a; Brown, 1989; Mamouni et al., 1983; Bardati et al., 1985; Myers et al., 1980).

(ii)- **Microwave Tomography**:

The technique of active imaging involving illumination of the body tissues with microwave radiation is termed microwave tomography. Appropriate tomographical techniques might be used to reconstruct an image of the observed part of the body which depends on the permittivity and conductivity of the tissue (Bolomey et al., 1982; Peronnet et al., 1983). This technique is at an early stage of development.

(iii)- **Ultrasonic Tomography**:

The technique of ultrasonic tomography relies on the temperature dependence of the speed of sound in tissue, but cannot be used in regions containing bone or gas. Ultrasonic techniques have been developed for the examination of the breast (Johnson et al., 1977).

(iv)- **NMR Imaging**:

The tissue temperature depends on the nuclear magnetic relaxation mechanism for moments in a static magnetic field, involving thermal interactions with the surrounding environment. Parker, (1984) discusses the potential

*- *Discussed in Chapter II in more detail*

application of NMR imaging as a non-invasive technique utilizing localized temperature monitoring to achieve high spatial localization with a resulting resolution of 2 ^{o}C.

(v)- **X-Ray Computed Tomography**:

The images generated by computed tomography are based on differences in the linear attenuation of X-rays which is related to the density and the atomic number of tissues. The change in tissue density, and hence absorption of X-rays with temperature can provide a technique with an estimated resolution of 1 ^{o}C (Fallone et al., 1982). The ultrasonic and X-Ray techniques are costly and there is an element of risk for the patient.

I. 4. 2- Skin temperature measuring techniques:

Skin temperature is often required to assess the change induced by an internal or external stimulus within a given area. Temperature measurement within the tissue is vital. Temperatures between 37 ^{o}C and 40 ^{o}C will actually stimulate tumour growth. Above 45 ^{o}C all cells are killed so there is danger of doing serious damage to normal tissue in the vicinity of the tumour.

a- Thermistor and thermocouple probes:

There is a variety of thermistor and thermocouple probes available for point measurement of skin temperature (Cetas, 1985; Ring, 1986). They must, however, be placed in contact with the skin and so may affect the delicate balance of heat transfer at the skin surface, altering the quantity which is to be determined. They do not provide an overall picture of the temperature distribution on the skin surface unless a large and time consuming number of measurements is made.

b- Liquid crystal plate thermography:

This technique uses liquid crystal compounds which exhibit iridescent colours which change with crystal temperature in the cholesteric phase and thus shows the skin temperature pattern as coloured images. A thin blackened plastic sheet containing liquid crystals dispersed in a translucent polymer is placed firmly and uniformly against the surface to be examined and the resulting image is usually photographed to obtain a permanent record of the thermal image. This technique requires thermal contact with the skin, so the examination of body regions of complex morphology is very difficult. For this reason, clinical applications are at present mainly confirmed to breast examination. The absolute temperature range of response is typically about 3 °C (Jones, 1987).

c- Infra-red thermography:

Infra-red thermography is achieved by a scanner fitted with an infra-red detector. Remote sensing of the thermal radiation emitted from the skin surface is thus effected in the infra-red spectrum at wavelengths near to the maximum of emission about 10 μm. Real time display of the temperature distribution over the body area of interest can be displayed on an oscilloscope screen or in either colour or both black and white on a television image tube . Scanning speeds range from one to fifty frames per second depending on the imaging system being used. A thermal resolution of 0.2 °C is provided by most systems designed for routine clinical use, although more complex systems with resolutions of 0.1 °C are available (Jones, 1987; Gautherie and Ring, 1980). The optimum depth of tissue detectable by infra-red radiation is in the range of 0.1 to 0.5 mm.

Lawson, (1957) first showed that in most patients with breast carcinoma the skin over the tumour was warmer than that in the surrounding areas. In subsequent studies Lloyd Williams et al., (1961) describe the application of infra-red thermometry to the diagnosis of swellings in the breast, and Gershon-Cohen and Haberman in 1964 confirmed these observations.

The advantage of measuring skin temperature by infra-red thermography rather than, applying thermometric devices, such as thermocouples, to the surface is that infra-red measurement is almost instantaneous, and that contact with the skin is unnecessary.

I. 5- Hyperthermia.

Hyperthermia is the treatment of disease, particularly certain cancers, by the process of heating regions of the body containing the carcinoma tissue.

Generally, malignant cells are intrinsically more heat sensitive than normal cells in the temperature range 42 - 43.5 ^{o}C. This difference allows for a measure of specificity in the treatment of cancer, malignant cells being killed whilst normal cells survive. There are two types of hyperthermia therapy, whole body or regional, and local. For the whole body or a region of the body, such as a limb, hyperthermia is limited to temperature in the 41.8 to 42.0 ^{o}C range. This can be achieved using hot bath or radiofrequency heating. Local hyperthermia or the delivery of heat to a specific portion of the body is more suitable for clinical situations involving tumours that are not widespread or where only a portion of the body needs to be treated. If particularly heat sensitive organs, such as liver or brain, are outside the heated field, higher temperature can be used for local hyperthermia than can be used for whole body therapy. The use of higher temperatures should allow local hyperthermia to be more successful in tumour treatment than whole body hyperthermia. Several techniques have been used to produce local heating in the human body.

a- Radio-frequency heating:

Two basic forms for the coupling of radiofrequency power to body tissues are used - capacitive coupled and inductively coupled.

In capacitive radiofrequency, the tissue is placed between two applicators or

electrodes. Heating depends on tissue resistance and current flow. Radiofrequency energy couples more readily to fatty tissue than to muscle (Selawry et al., 1958). It appears at present that radiofrequency heating techniques, using implanted electrodes for the production of local hyperthermia, are ideally suited to the treatment of small, well defined tissue volumes (Sutton, 1971).

Inductive radiofrequency heating depends mainly on tissue dielectric properties with the dissipated power density σE^2. Both kinds of local hyperthermia and regional hyperthermia use frequencies in the range of 20 to 30 MHz.

b- Ultrasound:

The significant advantage of ultrasound heating is that it may be focussed to concentrate the energy for dissipation into very small volumes of tissue. It appears to be well suited for producing and sustaining controlled levels of uniform hyperthermia in deep tissue up to 5 cm beneath the skin surface sites (Goldman et al., 1965). Cabanac et al., (1971) and Gerner et al., (1975) presented studies investigating the improvement of the applicators used for such cases. It has been concluded that direct contact applicators are required.

c- Microwave heating:

Numerous investigators have used microwaves to generate local heat. Heating depends on electrode power output, applicator radiation pattern, and tissue absorption of microwave energy. Microwave heating complements radiofrequency heating to a certain extent in that muscle tissues are more closely coupled than fatty tissue (Cloudsley -Thompson, 1963). Microwave heating appears to be a technique ideally suited to the heating of larger regional tissue volumes and may be appropriate to whole body hyperthermia.

The ability to induce hyperthermia can be very variable and unpredictable because of temperature distribution and tissue inhomogeneity, and because of the

natural effect of blood flow in regulating tissue temperature.

Generally, non-invasive thermometry in clinical hyperthermia has attracted a great deal of attention. Various ultrasound techniques have been investigated (Nasoni et al., 1982; Robert et al., 1982; Christensen, 1983) but progress has been limited by major problems which lead to non-unique temperature reconstruction. Fallone et al., (1982) used X-ray tomography in phantom studies and have shown that adequate spatial and temperature resolutions can be achieved.

The potential of microwave radiometers for non-invasive temperature sensing in tissues located within 3 cm from the skin is more promising. Several improvements to these devices have been reported (Mamouni et al., 1977; Carr et al., 1982; Lüdeke and Köhler, 1983) and the development of multi-receiver systems (Semet et al., 1984), correlation techniques (Mamouni et al., 1983; Haslam et al., 1984; Newton, 1986) and multifrequency radiometers together with multispectral analysis (Miyakawa, 1981; Schaller, 1984a; Plancot et al., 1984; Newton, 1986; Bardati et al., 1987) should lead to systems in which spatial resolution, temperature resolution and response time satisfy the requirements for hyperthermia monitoring.

Plancot et al., (1987) presented numerical analyses of hyperthermia and radiometry temperature measurements for *TEM* propagation. Microwave systems combining microwave radiometers operating at 1-2 GHz or 2-4 GHz frequency range have been developed, tested and used in hyperthermia therapy.

The hyperthermic treatment of cancers has been further investigated and improved by Christensen and Dumey, (1981). They have examined the basic mechanisms of several heating modalities including electromagnetic methods at both high and low frequencies with a variety of applicators.

Microwave hyperthermia induction requires the electromagnetic field configurations of the applicators used to be known. The *nonresonant perturbation* technique has been used to improve the measurement of the electromagnetic field (discussed in Chapter VII).

I. 6- Literature review of microwave thermography.

Microwave thermography for medical use was first proposed by Enander and Larson in 1974. Since then several groups have investigated this technique and research has been carried out to develop convenient radiometric equipment. Lüdeke et al., (1979) developed an improved radiometer at 3.1 GHz, to simultaneously and independently measure temperature and emissivity to minimize temperature measurement error. The radiometer was designed for a temperature range of 28 - 42 ^{o}C and an emissivity change up to 20 % .

Edrich and Hardee, (1974; 1976) have presented radiometer measurements of 45 GHz which showed that the human body emits thermal radiation at millimeter wavelengths which can be used to produce thermography imaging. They also studied complex permittivity and the penetration depth of muscle and fat tissues between 40 and 90 GHz. Edrich and Smith, (1978) describe a non-invasive technique to measure the temperature of human joints using a 68 GHz radiometer system. These millimetre wavelength measurements used a mechanically scanned parabolic reflector antenna in air approximately 1 m from the body. Gautherie et al., (1979a) studied several patients with breast carcinoma using two millimeter wave scanners at 30 and 68 GHz respectively. A highly sensitive Dicke radiometer has been used for the analyses. Robert et al., (1980) compared microwave thermography imaging at centimeter and millimeter wavelengths with infra-red thermography analyses. The results indicate that the microwave thermography method can non-invasively detect and thermally image deep tissue.

Myers and Barrett, (1980) presented results of a clinical study of breast cancer detection at 1.3 and 3.3 GHz. They also described the performance of a 6 GHz radiometer. All three radiometers are of similar design. They comprise a conventional Dicke-switched, or comparison superheterodyne radiometer, with 100 MHz intermediate frequency bandwidth, centered at 60 MHz. The input to the first stage tunnel-diode amplifier is switched at 8 Hz between the antenna, and a

matched load maintained at 22.0 ± 0.1 ^{o}C by a thermoelectric refrigerator. The resulting square-wave signal is detected at the intermediate frequency by a square-law crystal detector whose output is synchronously demodulated. Barrett and Myers, (1986) presented the basic principles of radiation transfer in the microwave range to detect breast cancer at 6 GHz.

Mamouni et al., (1977) worked with different frequencies between, 8 - 12 GHz range. Since then they have been employed in improving the technique of microwave thermography for medical applications especially in the vicinity of 3 GHz, where results obtained give more encouraging results.

Carr et al., (1982) describe improvements in microwave system design, including: emissitivity, spatial resolution, microwave transmission characteristics, and microwave interference which tends to increase in importance with increasing frequency. The frequency selected for the microwave radiometer was 4.7 GHz which relates to the Dicke radiometer configuration. It has been shown that tumours detected by combined local heating and thermography. This method may also be applied as a simultaneous hyperthermia treatment and a monitoring of tissue temperature.

Iskander and Durney, (1983) proposed two microwave methods for measuring changes in lung water content, one method changes the phase of an active microwave signal transmitted through the thorax, and the other is based on measuring with a radiometer changes in the natural microwave radiation emitted by the body. They have constructed a 1 GHz Dicke-radiometer and made measurements on phantom materials to test its performance. It is possible to use very low frequencies in this case because the average lung water content is the object of interest and spatial resolution is not a consideration. The temperature of the lung remains constant due to the high rate of blood perfusion and changes in the observed microwave radiation are taken to be due to a change in the emission of radiation from the lung proportional to the water content.

Lüdeke and Köhler, (1983) described two types of radiometers. One utilises

a microwave front-end for the 1.7 to 2.5 GHz band and the other has a microwave front-end for the 10.7 to 12.7 GHz band. These microwave thermographic systems have been developed to improve the emissivity readings independent of temperature measurement. This has provided a temperature resolution of ± 0.1 K and an emissivity resolution with an accuracy of about ± 1%.

Recently, Abdul-Razzak et al., (1987) designed a microwave thermography system operating in the 9 - 10 GHz frequency band. Probes and scanning antennas have been designed to improve the resolution and to reduce the effects of noise. Measurements made on 25 patients with occlusive vascular disease and on 30 normal controls indicate a detection rate comparable with the present invasive and more costly technique. The possibility of increasing penetration depth in tissue is difficult, in view of the reflection of the radiation from deep regions in the body at the skin-air boundary.

Multi-frequency radiometry techniques have been used to measure temperature distribution in tissue (Newton, 1986) at two frequency bands. The optimum frequencies are 1 GHz and a higher frequency between 3 and 8 GHz. Bardati et al., (1986; 1987) "Universita' Tor Vergata, Rome" have investigated the problem of inversion of multi-frequency microwave radiometric data to provide a reconstruction of the temperature distribution in the tissue. The initial experimental tests of a prototype four channel radiometer, with central operating frequencies in the range 1.5 to 5.5 GHz, have been carried out and analysed (Bardati et al., 1987).

Correlation microwave radiometry has also been suggested for the improvement of single frequency, single antenna microwave thermography (Mamouni et al., 1983). This technique uses two identical radiometer channels and antennas. The antennas are arranged to view a common volume of tissue inside the body. The signal in each channel comprises of a component from the common region and a component from the rest of the antenna' s field of view, the common component may be separated out. The radiometer signal originating at depth inside the tissue may therefore be determined by adjusting the relative orientation of the

two antennas. The depth observed inside the tissue may be altered. Research into this technique is being continued in order to further improve the performance of microwave thermography.

The microwave thermography group at Glasgow University headed by Dr D.V. Land, (1983a; 1983b; 1984; 1986; 1987a; 1987b; 1988) is still in the early stages of the development of this technique. It has been demonstrated that it is possible to build a microwave thermography system with sufficient sensitivity to detect thermal gradients and also suitable for operation in clinical environments at a very reasonable cost (Land, 1987a). Researches in microwave thermography are being carried out to improve the investigation in medical applications. The computer modelling techniques for microwave thermography, developed by Land (1988), will be discussed in more detail in the following chapters. This work has been further investigated by Brown, (1989) for the detection of breast disease and knee joint damage.

Further studies on the microwave dielectric and thermal properties of tissue, and on the antenna patterns will improve the sensitivity of the microwave system techniques and applications. Microwave thermography correlation techniques are being investigated using a 90 ^{o} crossed-pair antenna arrangement which could be of practical interest. A novel technique for microwave hyperthermia induction, *nonresonant perturbation*, is proposed by Dr D.V. Land to investigate the electromagnetic field configurations.This technique has been used in conjunction with the correlation microwave thermography antennas to improve the detection of the penetration distance of the electromagnetic fields.

Chapter II

The microwave radiometer

II.1- Introduction and literature review:

II.1.1- Microwave radiometry:

The microwave radiometer technique relevant to this work has been developed since the late nineteen forties. The classic comparator microwave radiometer was first described by Dicke in 1946. The operation of this type of radiometer will be considered in detail in section II.2.

In 1954 Selove, presented in his paper an analysis of the sensitivity of radiometers at radio frequencies used to investigate radiation from astronomical sources. Two types of radiometer were considered. The first was a modulation type comparison radiometer, where square-wave modulation was used to improve the final detected signal. The comparator microwave radiometer designed with two channels used two separate frequency bands. The basis for improvement is that comparison is made by switching the signal on and off, then the signal is present only half the time. The second is a *d.c.* comparison radiometer in which the comparison voltage is unmodulated. Goldstein, (1955) also presented a comparison of two independent radiometer receivers which showed a greater sensitivity when the output was correlated. This was further investigated by Strom, (1957) who analysed the sensitivity of the Dicke radiometer using the comments of Goldstein, Tucker and Graham. These analyses achieved a more general treatment of the radiometer and found that the sensitivity was independent of detector characteristics. This relationship showed that the expression for the sensitivity agreed with that of Goldstein and Dicke. Strum, (1958) considered high-sensitivity microwave radiometry for a system where the temperature was significant by less

than 1 K. Fluctuations in gain and temperature of antenna, the waveguide system, the comparison source, the noise balancer, the receiver and other amplifying components were considered for the microwave radiometer system, and the influence of these factors on the threshold equation. Knight, (1962) considered a radiometer with asymmetrical square-wave modulation and correlation. The calculation is of the Goldstein type and was done by representing Gaussian noise entering the radiometer as a Fourier series of sinusoidal waves. Kelly et al., (1958) analysed a general comparison radiometer for arbitrary modulation and correlation and presented proof that a square-law detector is superior to any other detector law for Gaussian noise. Wait, (1967) considered the sensitivity of the Dicke radiometer, using a switching radiometer to compare microwave noise sources with a sum-and difference-correlation radiometer and discussed the literature of the Dicke switching radiometer. He proved that the most sensitive radiometer is a square-wave modulated radiometer with a wide band square-wave correlator.

Fig.II. 1 show the basic Dicke switching radiometer where T_1 , T_2 are noise source effective temperatures, ($T_1 = T_2$), connected to the transmission coefficients a_1 (t) , a_2 (t) respectively; the noise signal sources are 180° out of phase. The internal noise of the amplifier referred to the input of the amplifier has effective temperature T_n. The reference signal c (t) is referred to as the correlation and usually is sinusoidal or square wave; n , s , A , D , F1 , M , and F2 are the outputs of the amplifier noise , switch signal, amplifier, detector, band pass filter, multiplier and low pass filter respectively.

Medical applications have been improved by using microwave radiometry instead of infrared radiation because the detection depths are greatly significant. As explained in Chapter I microwave radiometry is being assessed for medical applications because the radiation penetration distances through body tissues are large enough to allow internal rather than surface temperature patterns to be examined. The following authors have published work on the design of microwave radiometers suitable for tissue temperature measurement. Lüdeke et al., (1979)

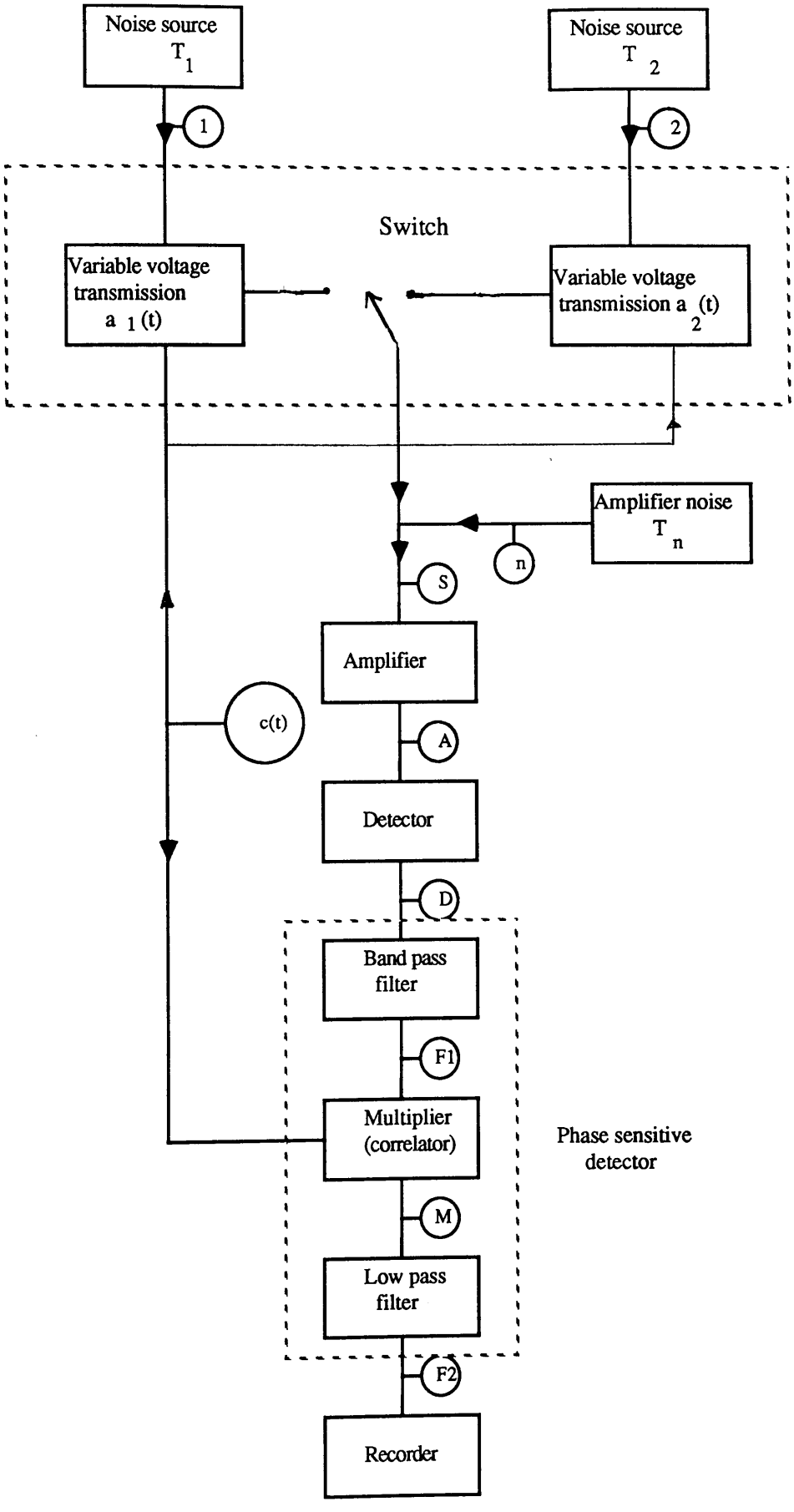

Fig. II.1 Dicke radiometer

developed an improved radiometer, which simultaneously measures temperature and emissivity, independent of a possible mismatch. Land, (1983b) designed and constructed a 3 GHz radiometer receiver*.

Myers et al., (1980) presented results of a clinical study of breast cancer detection at 1.3 GHz (wavelength 23 cm) and 3.3 GHz (wavelength 9 cm), and described the performance of their 6 GHz (5 cm) radiometer. This method has been used by Carr et al., (1981) to investigate the detection of cancer utilizing a combination of a passive microwave radiometer and an active transmitter with frequencies of 4.7 GHz for the radiometer and 1.6 GHz for the transmitter. In addition, Shaeffer et al., (1981) used also this non-invasive method to detect cancer, especially of the breast; measurements were made on several healthy male and female breasts. Since 1981 more interest has been shown in microwave radiometry for medical rather than in industrial applications. Carr et al., (1983) discussed the cases of a number of females at one frequency for an apparent temperature of about 0.4 ^{o}C. In 1983 Mamouni et al., improved this technique to include multiprobe scanning and the study of the possibilities of correlation microwave thermography. Enel et al., (1984) discussed the detection of the subcutaneous thermal gradients which exist in living tissues and the determination of their thermal and geometrical characteristics. They also investigated a radiometer system incorporating six probes scanned electrically with a bandwidth range between 2.5 and 3.5 GHz and a sensitivity of 0.1 ^{o}C. It has been shown that is possible to improve the spatial resolution of microwave radiometry and the need for multiprobes or multifrequency. Bardati et al., (1985) measured the subcutaneous temperature distribution for different frequencies in the range 1.5 - 6.5 GHz using a combination of both singular functions and Kalman filtering. The reconstructions obtained by singular functions alone, suffered from strong instability due to the relatively high noise level in measurements, whereas the combination with the Kalman filter led to more significant results. Microwave radiometric techniques

* - *more detail in section II.5*

have been used to investigate the behaviour of living tissues, for instance the geometrical characteristics (depth and size) and the temperature of local, thermal volume in homogenous tissue and lossy material. The first of these experiments were done by Bocquet et al., (1986) using water as lossy material at two frequencies, 1.5 and 3 GHz, to obtain information on the temperature gradients at depth. Microwave radiometry is able to provide significant information on metabolism and thermal conditions of subcutaneous tumor tissue. Brown, (1989) studied the development of the computer modelling techniques for microwave thermography. It has been found primarily that the microwave thermographic measurements on both the breast and knee joint reflect the level of perfusion in the breast tissue and the synovium respectively. Mamouni et al., (1989) developed a compution method of three dimensional structure for the weighting function, (Eq.II.1), the applicator associated with microwave radiometry in order to evaluate the influence of the structure of the material on the radiometric signals and to improve the imaging technique. N'Guyen et al., (1980a) have presented a method to combine microwave heating and microwave radiometry, which has given good results and shows that the method is sound.

The weighting function is defined by:

$$C_i(f) = K\,\sigma_i(f)\,|\,E_i^2(f)\,|\,\Delta V_i \qquad \text{(II.1)}$$

where σ_i is the conductivity, E_i is the electric field and K is constant of normalisation for the subvolume ΔV_i coupled to the applicator.

The total power of the microwave radiometer is given by a simple form:

$$P = G\,T_{sys} \qquad \text{(II.2)}$$

where T_{sys} is the system temperature, which accounts for the antenna noise signal, the input line losses, and the internally generated noise; G is the system gain constant.

II.1.2- Multi-frequency radiometry:

This technique has been proposed for medical application in order to obtain better resolution by the introduction of several radiometers. Newton, (1986) used a multi-frequency radiometer with several radiometers operating at different frequency bands to show that the penetration of microwave radiation in biological tissue depends on the frequency. These three two-frequency bands at 1 and 8 GHz, 1 and 5 GHz, and 1 and 3 GHz have been used to measure the temperature. The resulting data showed that the sensitivity of a multi-frequency radiometer was inferior to the sensitivity of single frequency radiometers, on the other hand the output of each radiometric channel depends on frequency, hence multi-frequency radiometric observations contain substantially more information than single-frequency measurements.

The total signal at the output of the radiometric channel with centre-band frequency f is given by:

$$S(f) = \int_z W(f, z)\, T(z)\, dz \qquad \text{(II.3)}$$

where $W(f, z)$ is the weighting function at the depth z and frequency f, $T(z)$ is the temperature profile at z. It has been established experimentally that the greater the number of radiometers used at any one time the more difficult it is to achieve an accurate result in both the weighting function and the reading. Although several difficulties still remain in retrieving temperature patterns in the human body from multispectral radiometric data Bardati et al., (1987a) has been able to produce experimental results that confirm that useful accuracy is indeed feasible up to moderate depths in the tissues. Experimental phantom material, simulating a highly absorbing homogeneous infinite muscle, was intentionally chosen for analysis by Bardati et al., (1987b). The multi-frequency microwave radiometer has been further investigated by Bardati et al., (1989) in order to determine the temperature variation

with depth in the human body . They considered a cross-section of the human neck of clinical interest for monitoring temperature during hyperthermia treatment. Six frequencies, between 1 and 4 GHz, and three positions of the antenna close to the axis of symmetry of the neck were considered. This technique can study the effects of the number of measurement positions on temperature reconstruction and improve the quality of the microwave radiometry system used for medical applications.

II.2-Description of the radiometer:

The microwave radiometer is a receiver specially developed to detect the random noise signals generated within animal tissues in the microwave region, particularly selecting signals of thermal radiation to facilitate sensitive temperature measurement within the Raleigh-Jeans region of the thermal radiation spectrum, In this region the frequency f (approximately 300 K) and the source temperature T, are such that $\frac{hf}{kT} << 1$ and the radiometric power varies linearly with the temperature making the region ideal for medical microwave radiometry. The measurement of a small amount of microwave noise with a simple receiver is impractical because the noise cannot be distinguished from the desired signal. The main problem of the total power radiometer (Eq.II.2), which makes it impractical for this application, is the degradation of the sensitivity by fluctuations in the gain of the system*. The output reading is proportional to the total input noise temperature and to the gain of the system.

$$\Delta = G\,(T_A + T_r) \qquad \text{(II.4)}$$

where G is the receiver gain, T_A is the source noise temperature and T_r is the receiver noise temperature. The changes in Δ are found by taking the total differential of Eq. II.4.

*- *RF Radiometer Handbook for details.* (See references)

$$\delta \Delta = \delta [G (T_A + T_r)] = G \delta (T_A + T_r) + (T_A + T_r) \delta G \qquad \text{(II.5)}$$

which is equivalent to an input temperature change of,

$$\frac{\delta \Delta}{G} = \delta (T_A + T_r) + (T_A + T_r) \frac{\delta G}{G}$$

$$\frac{\delta \Delta}{G} = \delta (T_A + T_r) = \delta T_{sys} = \Delta T_{sys} \qquad \text{(II.6)}$$

δT_{sys}, is the variation of T_A and T_r, which ΔT_{sys}

In an ideal system $\frac{\delta G}{G}$ would be zero and only changes in system temperature δT_{sys}, would contribute to $\delta \Delta$ In this system the noise limits the detectable system temperature δT_{sys} given by ΔT_{sys}. The effect of the gain variation can be removed by using a Dicke radiometer in which the frequency is high enough to maintain a stable gain over the switching period.The radiometer itself generates noises from its input port which is reflected back to the radiometer by devices connected to the input port.

II.3-The Dicke Switching Radiometer:

In 1946, Dicke suggested modulating a noise signal as a means of detecting the signal of interest from noise originating in the amplifying system and also to reduce the effects of gain fluctuations in the radiometer output due to receiver gain instabilities. He proposed a scheme in 1946 (Fig. II. 1), to reduce the effects of gain fluctuations in radiometers.

$$\Delta = G (T_a + T_r) - G (T_{ref} + T_r) = G (T_A - T_{ref}) \qquad \text{(II.7)}$$

$$\delta \Delta = \delta G (T_A - T_{ref}) \ , \ \frac{\delta \Delta}{G} = \delta \left(T_A - T_{ref} \right) < \delta (T_A - T_r)^*$$

*- *Proved by experiment (discussed in section II.11).*

where the system output is Δ; the antenna temperature, T_a; the reference temperature, T_{ref}; the receiver temperature, T_r; and the system gain factor, G.

Other types of radiometers have subsequently been described by the same authors but Dicke-type radiometers have remained very popular and have been widely used by radio-astronomers and now are used in medical applications.

The problems of radiometer designs are greatly reduced by the Dicke input switching radiometer because of this ability to separate and filter out noise. The output of this is increased by a factor of two compared to the ideal total power radiometer. This type of radiometer also has the advantage of eliminating a gain variation noise, and to detect and measure the thermal radiation at its input. The simplest type of radiometer is the "straight" receiver, in which rectification takes place directly at radio-frequency. The more usual radiometer is the superheterodyne type.

II. 4 - Superheterodyne Radiometer:

The superheterodyne radiometer has been used to improve the measurement techniques for temperature and attenuation of radio-astronomy devices since 1959 and carried out by Meredith et al., (1963). Superheterodyne receiver techniques have been successfully extended to a frequency of 140 GHz. The superheterodyne receiver is capable, even at short (millimeter) wavelengths, of detecting powers several orders of magnitude lower than the minimum power which can be detected with an infra-red type receiver. Its great advantage is that it operates at room temperature. The sensitivity is, however, limited by the lack of a precise impedance match of the modulator and the signal source (Meredith et al., 1964). The minimum temperature change, ΔT, which can be detected in the radiometer is conventionally assumed to be that giving a *d.c.* output equal to *rms* output noise voltage (Kraus, 1966) which is given by:

$$\Delta T = \frac{K\, T_{sys}}{\sqrt{\Delta\nu_{HF}\, \tau_{LF}}} \qquad (II.8)$$

where K is the sensitivity constant, T_{sys} is the system noise temperature at the applicator terminals, $T_{sys} = T_a + T_r$, where T_a and T_r are the antenna and the receiver temperatures respectively (K), $\Delta\nu_{HF}$ is the pre-detection bandwidth (Hz) and τ_{LF} is the post-detection equivalent integration time (s).

The constant K depends on the type of receiver and its mode of operation, but is of the order of unity. The system noise temperature at the applicator terminals depends on the applicator noise temperature, the receiver noise temperature, the physical temperature of the transmission line between the applicator and receiver and the efficiency of the transmission line.

II. 5- Description of a 3 GHz radiometer:

A 3 GHz radiometer* has been designed and constructed by Land, (1983b), University of Glasgow.It consists of a Dicke-switched radiometer and a single side-band superheterodyne with a 14 dB gain, a 2.5 dB noise figure *RF* pre-amplifier of bandwidth 2.5 to 3.5 GHz; the signal is converted by a mixer and local oscillator at 3 GHz.The *IF* amplifier has a bandwidth of 0 to 500 MHz, noise figure of 2.5 dB and a gain of 46 dB. A square law detector is used followed by low-noise *AF* amplifier with low frequency, (Fig. II. 2); prototype of this radiometer is shown in Fig. II. 3. The amplified and detected input signal, $G\,(T_A - T_{ref})$, at the 1 kHz switching frequency is further amplified, and synchronously detected and than passed through a low-pass filter. The gain variation depends on the temperature of the microwave pre-amplifier. The microwave difference signal and the reference source temperature signal are added and scaled to provide calibrated antenna temperature in degrees Celsius.

*- *Land D.V., (1987), " A Clinical Microwave Thermography System", IEE Proceeding, Vol. 134A, pp.193-200.*

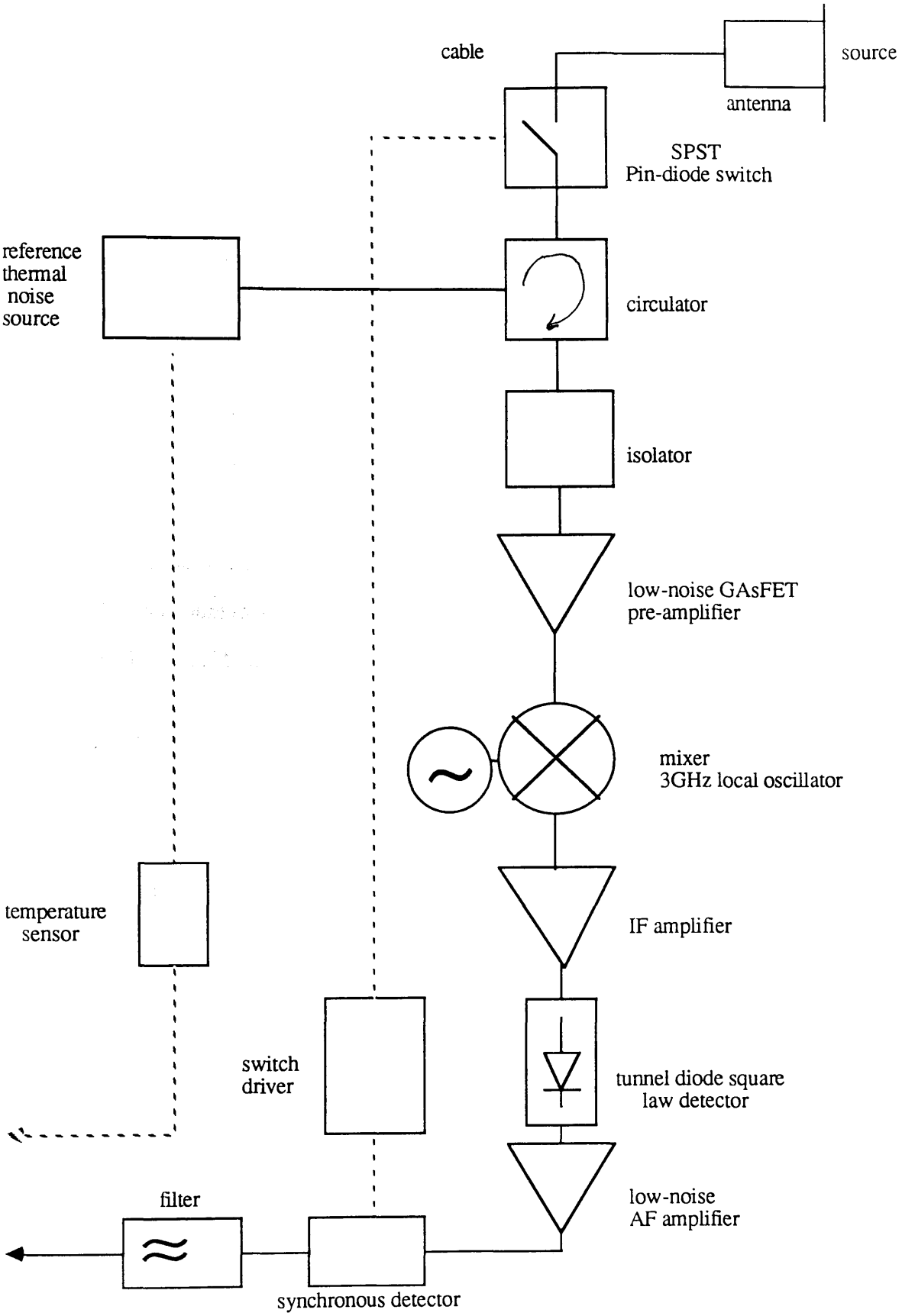

Fig. II. 2 3GHz microwave radiometer

Land, (1983a) utilized the Dicke input circuit to aid in determining the performance of his antenna designed to detect and measure the mismatch in interface between the antenna and the body for medical applications. The antenna is placed in contact with the skin and connected to a radiometer receiver which will convert the input to an output on a thermal signal. The accuracy of the measurement depends how close the source temperature is to the reference temperature. The reference noise source is a standard microwave 50 Ω coaxial load, heated to approximately 40 °C. Other, self-balancing, radiometers have been proposed (Lüdeke et al., 1978; 1979; 1983) which maintain the reference temperature equal to that of the source to correct the effect of reflection at the boundary. This is a more complex method than the one described above, with reduced receiver sensitivity and a longer response time for a given temperature resolution.

The optimum temperature resolution achievable with a radiometer receiver is given by Gabor, (1951).

$$\Delta T = Q \frac{T_r + T_s}{\sqrt{Bt}} \qquad \text{(II.9)}$$

where Q is the radiometer receiver constant in the range of 4.6 to 6.6, T_r is the effective noise temperature of the measuring system at the input, T_s is the source temperature, B is the receiver pre-detected noise signal bandwidth, and t is the receiver post-detected signal filter response time.

II. 6- Radiometer sensitivity:

Radiometer sensitivity is the smallest change in system noise input that can be detected and processed by the system to give a measurable output. Any fluctuation in the output is directly proportional to the noise power detected at the input (Eq. II.9). The sensitivity of the radiometer may be improved by increasing the pre-detection bandwidth but this is limited practically by the frequency over

which the antenna may be matched to the body tissues. Increasing the post-detection integration time will also improve the sensitivity but this is limited by the required response time of the system. The effect of reducing the noise temperature, T_r, while improving the sensitivity, becomes of progressively less value because the antenna noise temperature, T_a, due to the source, is always present. ΔT is a basic limitation to radiometer performance.

The Dicke radiometer is a square-wave modulation and its output fluctuations increase by a factor of two compared to the ideal total power radiometer. The performance of the 3 GHz radiometer used for this work is given by:

$$\Delta T = (T_S + T_R)\, K \sqrt{\frac{B_2}{B_1}} \qquad \text{(II.10)}$$

where ΔT is the temperature equivalent of the root-mean-square *(rms)* noise fluctuation of the output signal; T_S is the source noise temperature which is close to 310 K; T_R is the effective noise temperature at the input of the receiver; K is the radiometer constant (K = 2 here) ; and B_1 and B_2 are the receiver pre-detection and post-detection noise power bandwidths respectively B_1 is set by IF bandwidth, and $B_2 = \frac{0.35}{\tau_{LF}}$, where τ_{LF}, is the equivalent integration time; τ_{LF} was usually set at 2 seconds, critically damped. The *rms a.c.* noise temperature in the radiometer output is 0.04 K. It has been assumed that the peak-to-peak magnitude of the noise is eight times greater than the *rms* value (Meredith, 1964), since 95% of the signal will be within 3.92 times the rms value for Gaussian distribution. This 95% is 0.16 K and is a convenient measure of the temperature resolution of the system. The observed variation of the peak-to-peak magnitude was between 0.16 K - 0.18 K.

The temperature resolution is also affected by the stability of the system, and fluctuations in the gain caused mainly by the relatively slow ambient temperature changes. Low noise *GASFET* pre-amplifiers, are a significant

problem. They have about 1% change in gain for a temperature change of 1 K. However, the difference between the antenna temperature and the source temperature will always be less than 5 K, a change of 1 K will cause a maximum change in output of 0.05 K (Brown, 1989); a variation of more than 1 K in the operating temperature is not considered likely in the time to scan one patient, which is usually less than 10 - 20 minutes. The variation in gain does not therefore in practice reduce the temperature resolution, but affects the absolute temperature calibration of the system. The temperature resolution of the radiometer can be improved by reducing the receiver noise. Such an improvement has been demonstrated by Newton (1986), improving resolution from 0.16K to 0.025K . As sensitivity is increased the variations in gain will become relatively more important. The practical results of the sensitivity of the 3 GHz radiometer are discussed in section II. 11.

II. 7- Antennas:

The antenna used in Glasgow microwave thermography system was that designed by Land, (1983a). It is a cylindrical waveguide antenna, 2.5 cm internal diameter and 5.2 cm in length with a tapered fin-line type waveguide to coaxial line transition (Fig.II. 4). The antenna waveguide is loaded with a low-loss dielectric (Emerson and Cummings Eccoflo HiK dielectric powder, $\varepsilon_r^* = 12 - i\ 0.0084$). The waveguide modes which may propagate in the operating bandwidth of 3.0 - 3.5 GHz are TE_{11} - and TM_{01} -modes. The guide wavelength is characterized by the dielectric filling, which allows the dimensions of the guide to be smaller than those required for a hollow guide, and reduces the wavelength by a factor of $\sqrt{\varepsilon_r'}$ in unbounded volume of dielectric. For the cylindrical waveguide antenna used in Glasgow microwave thermography system the cut-off frequency for the TE_{11} -mode is 2.03 GHz and for the TM_{01} -mode is 2.65 GHz. The waveguide to coaxial line transition is so arranged to couple to only the TE_{11} -mode.

ε_T^* *is the complex relative permittivity (dielectric constant and loss factor)*

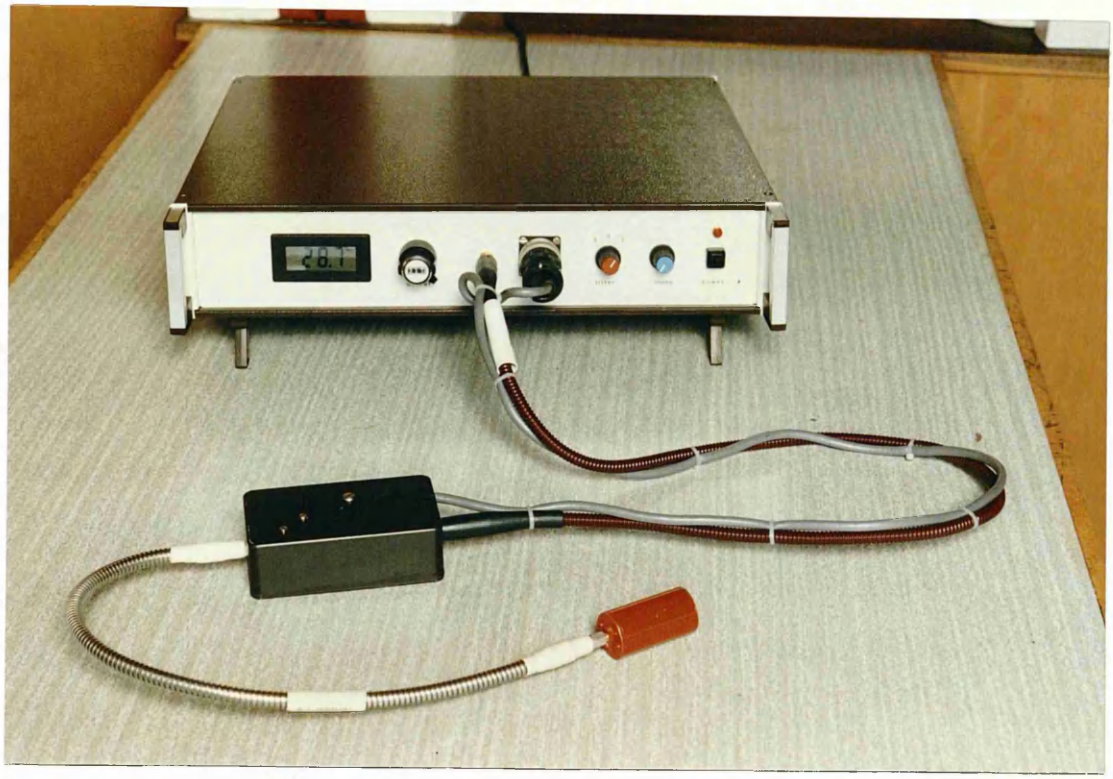

Fi.g II.3 Prototype of a 3 GHz radiometer

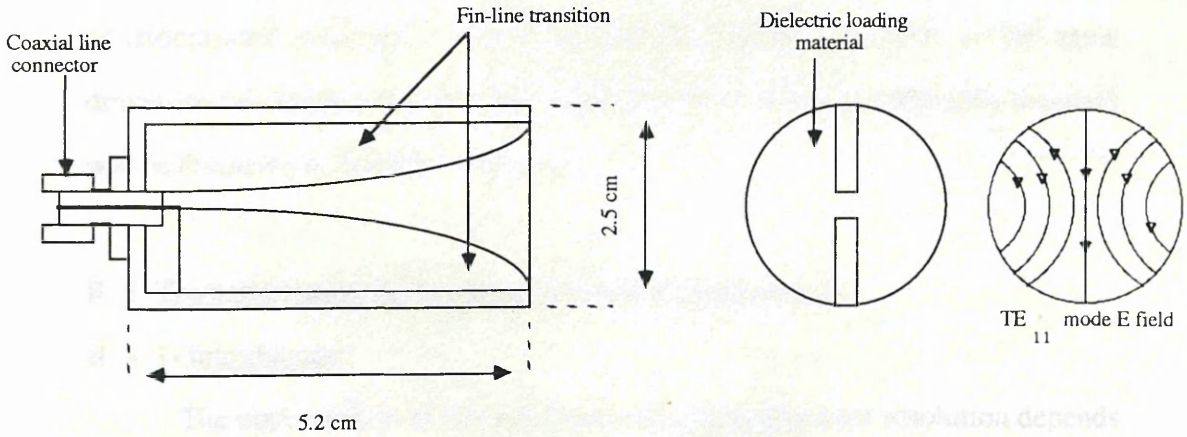

Fig. II. 4 Cylindrical waveguide antenna used in Glasgow microwave thermography

The rectangular waveguide antenna operating in TE_{10}-mode is used widely in clinical microwave thermography . Guy, (1971b) used rectangular waveguide antenna operating in the TE_{10}-mode for several dimensions, and showed the effect of the aperture width on the heating patterns in the muscle layer of a planar tissue model consisting of a layer of fat 2 cm thick above a semi-infinite layer of muscle. Heating microwave antennas are appropriate to receiving microwave antennas through the reciprocity principles (discussed in more detail in Chapter IV). Cheung et al., (1981) designed a TE_{10}-mode rectangular waveguide antenna, which was used to study the experimental and the theoretical results of the attenuation in liquid phantom for three different applicators. The Microwave Thermography Group at l'Université de Lille, France also used TE_{10}-mode rectangular waveguide antennas along with probes in their studies (Robillard et al., 1980, 1982, N'Guyen et al., 1980a, and Audet et al., 1980). Moreover, Erik, (1987) used TE_{10} - and TE_{20} - mode waveguide antennas to analyse the penetration depth of two different liquid phantoms for different aperture widths and frequencies. By the reciprocity theorem this antenna will receive a maximum signal from the muscle or the liquid phantom and then have the best response within the depth. From the diffraction considerations rectangular and cylindrical waveguide antennas of the same dimensions should have very similar behaviour. Microwave thermography antennas will be discussed in detail in Chapter IV.

II. 8- The performance of the radiometer system input circuits:

II. 8. 1- Introduction:

The improvement of the radiometer system temperature resolution depends on the reduction of the input noise by reducing antenna and circuit losses (particularly Dicke switching elements) and on improving amplifier performance.

II. 8. 2- Noise Signals:

In general, the random disturbance caused by the noise, disturbs the desired signal and reduces the certainty of an observation or measurement. Microwave thermal noise arises from vibrations of conduction electrons and holes due to their finite temperature (North, 1942; Miller et al., 1967).

II. 8. 3- Available noise power, N:

The available noise power, is the maximum rate at which energy can be absorbed from the body. This power is KTB where K is the Boltzmann's constant, T is the absolute temperature, and B is the bandwidth of the transmission path. The thermal noise power available, KTB , although dependent on bandwidth, is independent of frequency in the Raleigh-Jeans region (see section I.3), and of the value of the source impedance.

II. 8. 4- Noise temperature,T:

The noise temperature of a generator at a specified frequency is defined as the temperature of a passive system having the same available noise power per unit bandwidth. The thermal equilibrium situation is actually the only condition by which the output from a standard is truly known. In order to determine the noise temperature of a generator with non-zero reflection coefficient, a "lossless" tuner can be used to bring the reflection coefficient to zero, which would allow the temperature to be measured by standard techniques.

$$T = \frac{N}{KB} \qquad \text{(II.10)}$$

II. 8. 5- Effective noise temperature, T_e:

The effective noise temperature is the temperature which yields the power emerging from the output of the noise source when it is connected to a non-

reflecting, non-emitting load. The relationship between the noise temperature T and effective noise temperature T_e is: $T_e = T(1 - |\rho|^2)$

where ρ is the reflection coefficient of the noise source.

II. 8. 6- Noise figure (noise factor), F:

The noise figure is defined as the ratio of the available signal to noise ratio *(SNR)* at the input to the available *SNR* at the output. This is generally a function of frequency but is usually independent of bandwidth, and it is a very important criterion in communication systems.

$$F = \frac{S_i N_o}{S_o N_i} \qquad F = \frac{T_e + T_o}{T_o} \tag{II.12}$$

where S_i, S_o and N_i, N_o are noise signals and the available noise power of the input and output respectively. It is very important that the noise figure F is independent of the antenna characteristics, since it is assumed that the source temperature is fixed at 300 K. The difference between the noise figure of two receivers, therefore, is not a direct measure in the change in performance of the operating "real-life" system. The best measure is the change of the operating noise temperature, but even this assumes that no change in antenna gain has taken place that will change S_i.

II. 9- Thermal radiation measurement:

The intensity of thermal radiation emitted by a black surface (a perfect emitter and absorber) radiating into a medium, is given by Planck's Law which is already described in Chapter I.

Fabre and Leroy, (1981) presented a method of analysing the thermal noise emission of lossy material, where they considered a coaxial cell filled with a lossy material connected to a matched receiver at thermodynamic equilibrium at the

temperature T_o. The power emitted is $(1 - |\rho|^2)\, KT_o\, \Delta F$, and the variation of ΔT the temperature of the cell involves the variation ΔT_m of the noise temperature received,

$$\Delta T_m = (1 - |\rho|^2)\, \Delta T \qquad \text{(II.13)}$$

A basic Dicke switching circuit radiometer was developed by Land, (1983b) at a frequency of 3 GHz to investigate the radiation from the human body. This technique was chosen to minimise the effect of antenna mismatch. The practical limitations, for temperature measurement arise mainly from losses between antenna and receiver, and from non-ideal switch parameters, including non-symmetrical switch operation which acts alternatively as a transmission or reflection element. This method has recently been further developed for clinical applications and is the essential part of the equipment used in clinical microwave thermography. Land, (1987a) has discussed the behaviour of the internal body temperature patterns at clinically useful depths within the body (Fig. II. 5), where the numerical temperature patterns closely agree with patterns calculated using simple thermal microwave modelling. In practice, the reflection coefficient of the termination is very small, but the equivalent temperature of the noise source must be corrected for transmission losses. A particular radiometer can be described in terms of its resolution, stability, and the dependence of its output on the noise generator's reflection coefficient. Resolution and stability depend primarily on the first-stage amplifier noise figure, gain and on the type of radiometer. In the Dicke-type radiometer the receiver or reference temperature is fixed and lies near, but is not equal to, the source temperature T_s. This receiver is represented by a normal load resistance at the temperature T_{rec}. The theoretical investigation shows that this system can have a significant measurement error depending on the reflection coefficient of the antenna due to:

-Multiple reflections between antenna and switch;

-Interference on the receiver-side, noise reflection from the switch in the "on" state with reflection from the antenna;

-Non-symmetrical thermal emission from the *PIN-switch* depending on the antenna matching. Theoretical study has shown that the radiometer signal is linear with the temperature, and with the reflection coefficient. This is proved by measurement.

II. 10- Analysis of the Dicke radiometer input circuit:

The input circuit of the Dicke type radiometer used for this work has been investigated to assess its effect on the performance of the radiometer system. The results of this analysis have been compared with measurement made on the radiometer. Numerical analyses of the case shown below have been studied at the different temperature signals for the two switch positions.

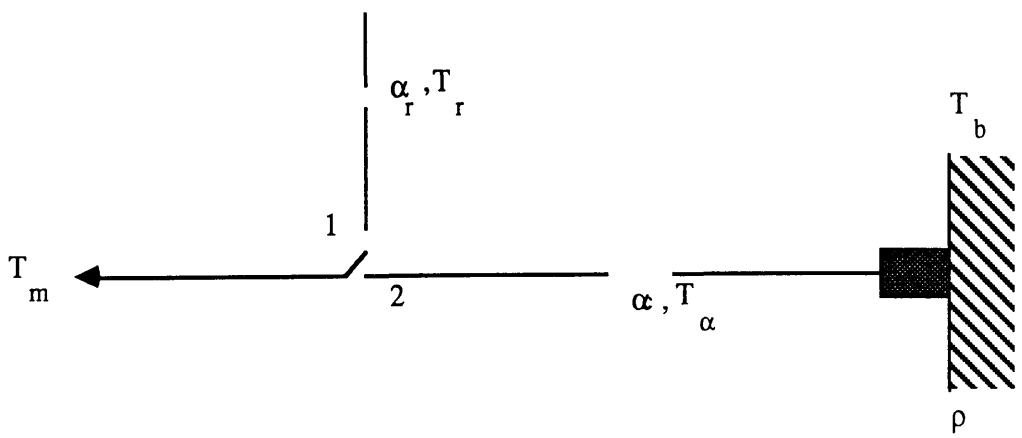

where α_r, α, T_r, T_α are the power attenuation constants and temperatures through the attenuating region (coaxial cables and switch),ρ is the reflection coefficient at antenna/body interface, T_b is the body temperature and T_m is the received input temperature.

The incident and the reflected temperature is obtained using this process.

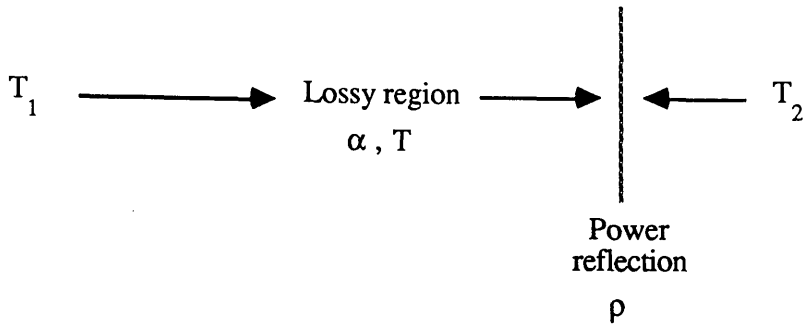

The diagram shows how to obtain the total effective temperature through a lossy region.

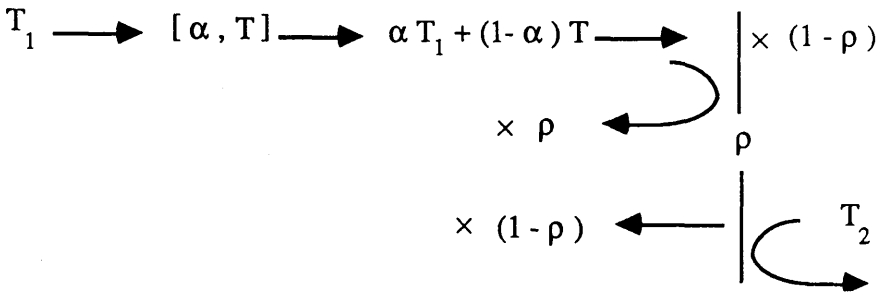

so the total effective temperature in this case is:

$$\rho [\alpha T_1 + (1 - \alpha) T] + (1 - \rho) T_2$$

If the reflection at the boundary is 100% ($\rho = 1$) the above expression becomes:

$$\alpha T_1 + (1 - \alpha) T$$

which is similar to the original instance where the switch is in position 1.

The second case was considered with the switch in position 1, we assume

that reflection at the interface switch/reference load is 100%. The diagram in this case is:

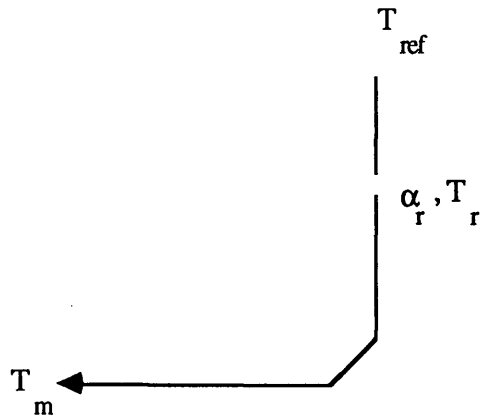

The temperature T_m is seen at the interface as:

$$T_m = \alpha_r T_{ref} + (1 - \alpha_r) T_r \qquad \text{(II.14)}$$

where T_{ref} is the effective reference load temperature.

With the switch is in position 2. The mismatch between the signal source and the switch will cause a reflection of radiation which will affect the measured signal.

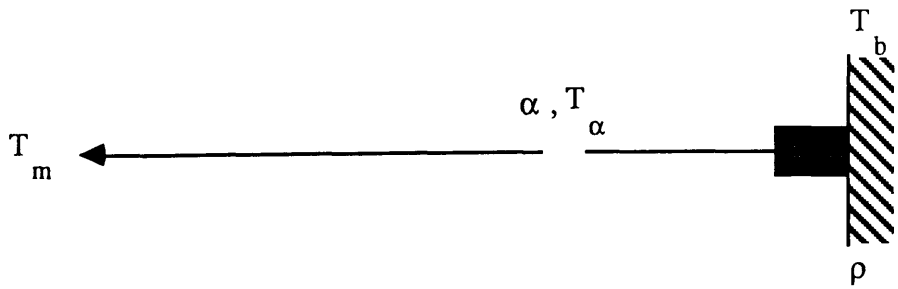

At the interface T_m is seen as:

$$\alpha T_m + (1 - \alpha) T_\alpha$$

This is reflected as:

$$\rho[\alpha T_m + (1 - \alpha) T_\alpha]$$

The effective noise temperature of the signal going to the attenuation is then:

$$\rho [\alpha T_m + (1 - \alpha) T_\alpha] + (1 - \rho) T_b \qquad \text{(II.15)}$$

The apparent temperature beyond the attenuating region is T_a, where T_a is equal to:

$$T_a = \alpha [\rho \alpha T_m + \rho (1 - \alpha) T_\alpha + (1 - \rho) T_b] + (1 - \alpha) T_\alpha \qquad \text{(II.16)}$$

The difference between the signals associated with each of these states is measured by a Dicke radiometer. Considering $T_r = T_\alpha$ and $\alpha_r = \alpha$, the expression becomes:

$$\rho \alpha^2 T_{ref} + \rho (1 - \alpha^2) T_\alpha + (1 - \rho) T \qquad \text{(II.17)}$$

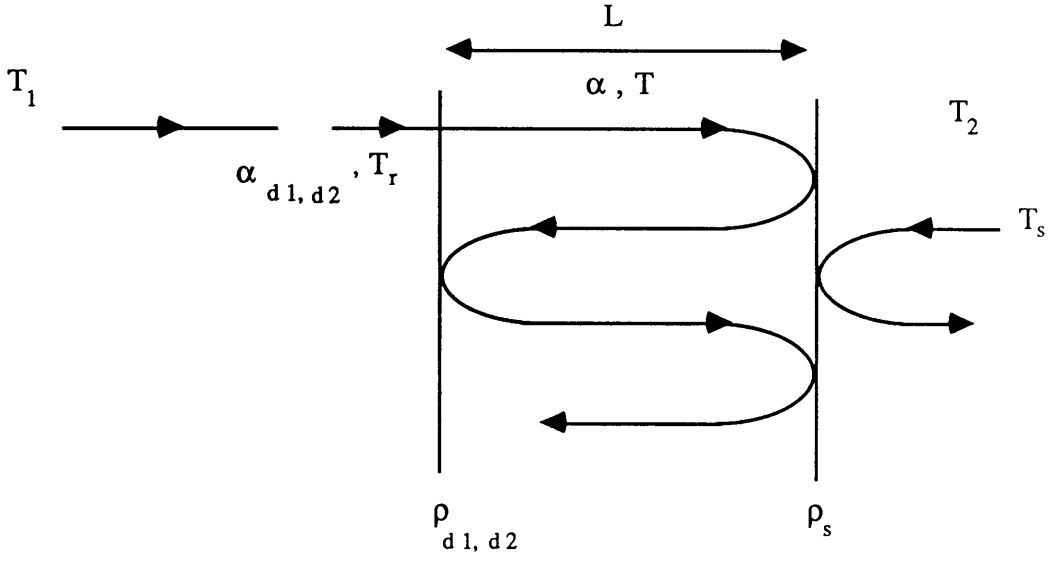

Where ρ_d and ρ_s are the reflection coefficients of the the first and the second boundaries, the power attenuation at the switch is α_d, and α is the attenuation constant between the boundaries. The two effective temperatures (T_1 ,T_2) of the incident and reflected waves to the switch are defined by these expressions.The temperature T_1, resulting from the loss of signal at the switch and the reference

load at temperatures T_r and T_{ref}. The total temperature T_1 can be written as:

$$T_1 = \alpha_d T_{ref} + (1- \alpha_d) T_r \qquad \text{if} \qquad T_r = T \tag{II.18}$$

Consider two different cases for the temperature T_2. First, a matched load between the signal source and the switch gives a specific range of temperature which can be written as:

$$T_2 = \alpha_s T_s + (1- \alpha_s) T \tag{II.19}$$

Second, because there is a mismatch between the signal source and the switch the temperature $T_2 = T_s$. The two reflection coefficients of the boundaries, ρ_s and ρ_d are defined by:

$$\rho_s \exp(- 2\gamma_s L) = \frac{Z_o - Z_2}{Z_o + Z_2} \qquad \text{and} \qquad \rho_d = \frac{Z_1 - Z_{out}}{Z_1 + Z_{out}} \tag{II.20}$$

The mismatch between the signal source and the switch will cause reflections of radiation which will change the measured signal. The mismatch at the interfaces between the source and switch and between the switch and reference load will cause reflections of radiation which will also change the measured signal. These reflection coefficients can be combined to give an effective reflection coefficient when there is no loss and there is loss between the reflection coefficients ρ_s and ρ_d.

$$\rho_{eff\ 1\ or\ 2} = \frac{\rho_{d1\ or\ d2} + \rho_s \exp(- 2 \gamma_s L)}{\rho_{d1\ or\ d2} \exp(- 2 \gamma_s L) + 1} \tag{II.21}$$

with $\gamma_s = \alpha_s + j\beta \quad ; \beta = \frac{2\pi}{\lambda}$

When one considers the effective reflection coefficient ρ_{eff}, depends on the values of ρ_d, ρ_s and the propagation constant, which is defined above. The measured signal now becomes:

$$\alpha_d [\rho_{eff} (\alpha_d T_1 + (1 - \alpha_d) T) + (1 - \rho_{eff}) T_s] + (1 - \alpha_d) T \qquad (II.22)$$

For the two states the signal now becomes:

$$\alpha_d (\rho_{eff2} - \rho_{eff1}) [\alpha_d (T_1 - T) - (T_2 - T)] \qquad (II.23)$$

Computational modelling shows the variation of the effective reflection coefficient with respect to source temperature and the reference temperature. Fig. II. 6a shows the relationship between the signals of the two boundaries with the effective reflection coefficients.

The measured signal is directly proportional to the source and the reference temperatures T_1 and T_2 as well as the effective reflection coefficient.

Fig. II. 6b shows the numerical analyses of the effective reflection coefficient with the measured signal for different values of the power attenuation (α_d) (Eq. II.23) at the switch for the range of 0.89 to 0.99 at a frequency of 3.2 GHz and at 300 K source temperature and 313 K reference load temperature.

II. 11- Measurement of microwave radiometer behaviour:

A microwave thermal noise source consists of a matched resistive termination maintained at fixed temperature and a transmission line to transmit the thermal noise generated from the termination. The source temperature can be established by a conventional thermometer (Fig. II. 5), and the loss distribution of the transmission circuit can be calculated under the operating conditions using a sliding short-circuit method (described in section III).

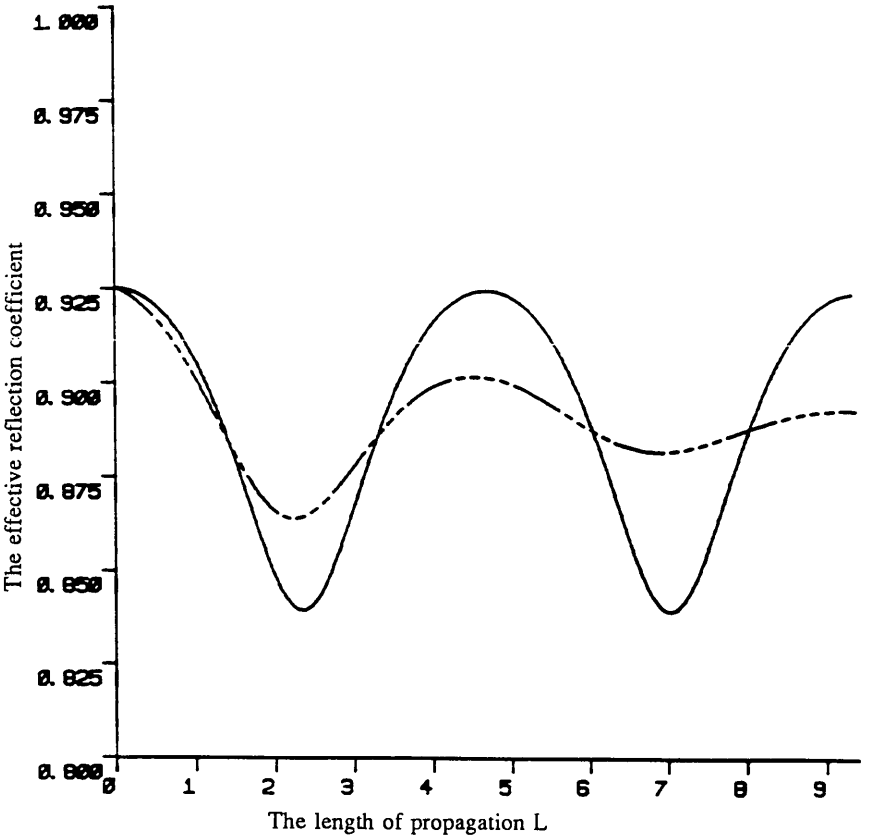

a- The variation of the signal between two media

The propagated signal
The attenuated signal

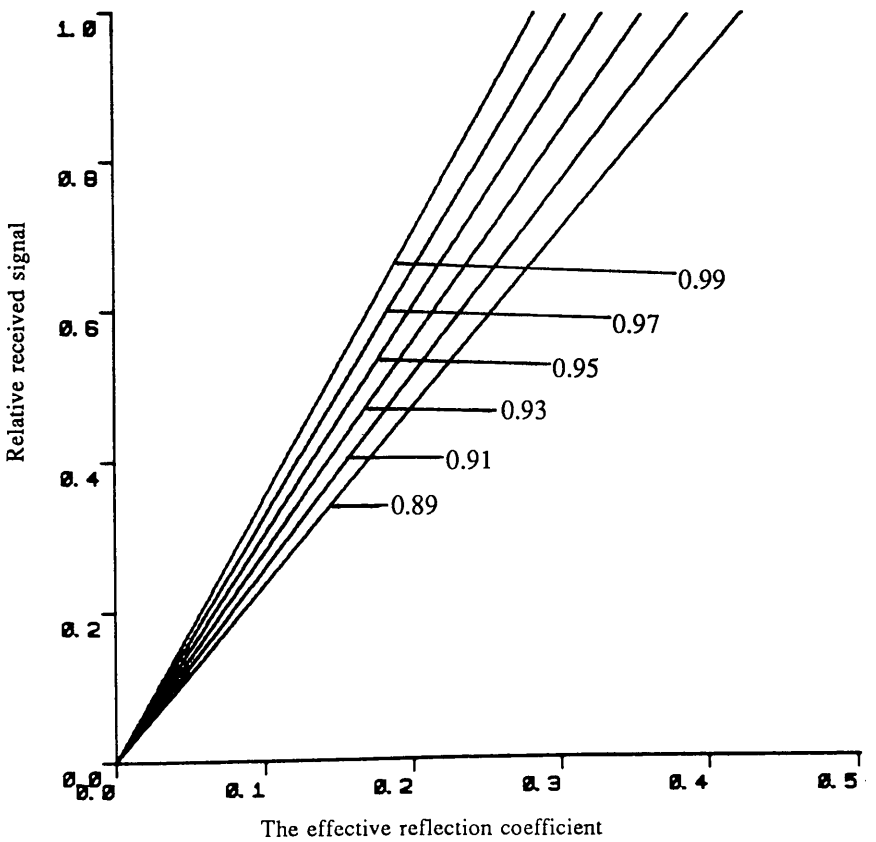

b- The variation of the effective reflection coefficient signal between two media for different attenuation constants α_d

Fig. II.6- The computational modelling of the reflection coefficient with the attenuation constant.

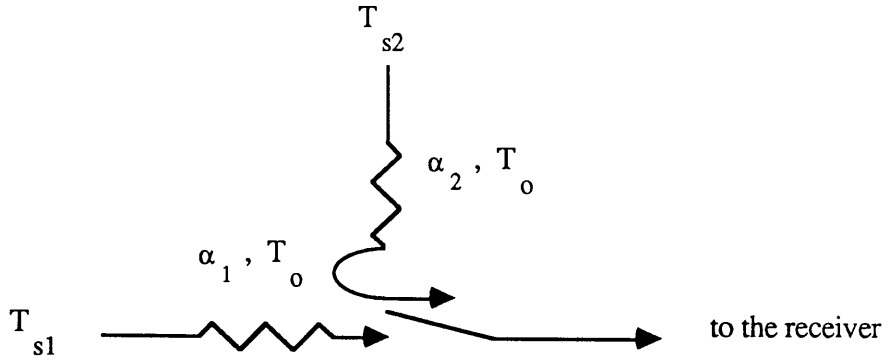

where α_1, α_2 and T_{s_1}, T_{s_2}, T_o are the power attenuation of cables and temperatures of load 1, load 2 and cables respectively.

The difference signal measured by the receiver at the switching frequency for the above arrangement is given by:

$$\Delta = G\,\alpha_1\,T_{s1} + G\,(\alpha_1 - \alpha_2)\,T_o - G\,\alpha_2\,T_{s2} \qquad \text{(II.24)}$$

$$= G\,\alpha_1\,(T_{s1} + T_o) - G\,\alpha_2\,(T_{s2} + T_o) \quad \text{if } \alpha_1 = \alpha_2 = \alpha$$

$$= G\,\alpha\,(T_{s1} - T_{s2}) \qquad \text{(II.25)}$$

where G is the system gain.

The equation II.25 illustrates that the lossy components in the two paths are (α_1, α_2) at the ambient temperature T_o. This is a reasonable approximation of the practical case.

$$\Delta = G\,(\alpha_1 - \alpha_2)\,T_S - G\,(\alpha_1 - \alpha_2)\,T_o \quad \text{if } T_{s1} = T_{s2} = T_s \qquad \text{(II.26)}$$

The same technique has been used to investigate cable losses using a matched source. We replaced the antenna/body interface by matched load 1, and the reference load by matched load 2 (Fig. II. 7). The temperature at load 1 varies between 0 and 50 °C at intervals of 5 °C and the reference temperature varies between 0 and 50 °C at intervals of 10 °C at a frequency of 3.2 GHz. The signal

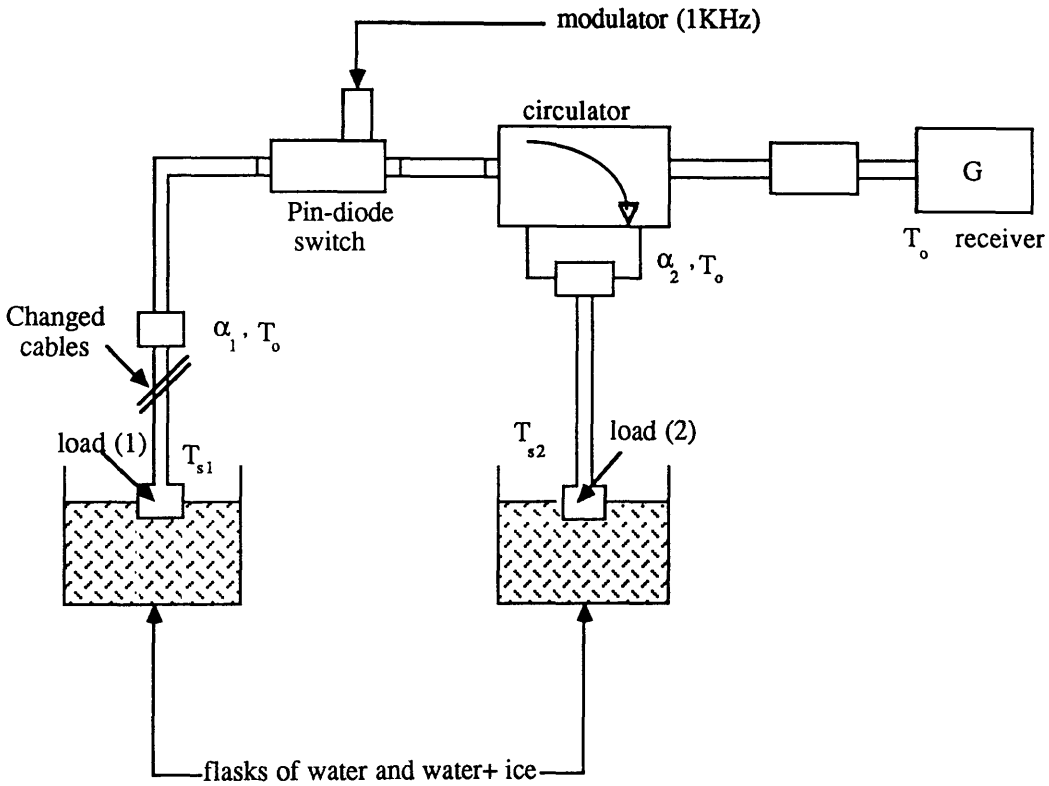

Fig. II.7 Radiometer input circuit arrangement for testing input circuit behaviour

received (Δ) from the radiometer is directly proportional to the difference between the temperatures. Measurements are taken at room temperature (20 °C) for a range of lengths of various types of microwave cables between the switch and load 1 *(9, 17, and 33 cm, RG 223/U 8, RG 223/U 56, RG 223/U 110, RG 223/U 145, and RG 223/U 175 cm).* This serves to provide a range of input circuit losses (α), Tab. II.1. The results in Fig. II. 8, Fig. II. 9 and Fig. II. 10 show that the output temperature of the radiometer agrees closely with the theoretical analyses (Eq. II.25). The experiment demonstrated that the attenuation constant of the reference load increases in proportion to the microwave cable lengths for *RG 223/U* and decreases in proportion to an increase in copper cable length.

Figures II. 11 and II. 12 show, in three dimensional form, numerical and experimental analyses for various lengths of different types of microwave cables between the switch and load 1 *(9, 17, and 33 cm, RG 223/U 56, RG 223/U 110, and RG 223/U 145)* to provide a range of input circuit losses (α). It was found that the temperature distribution of the microwave radiometer reading (Δ) was proportional to the source temperatures (T_{s_1} , T_{s_2}) Eq.II.24. It has been proved that a 3 GHz radiometer system with a spatial resolution of about 1 °C is suitable for clinical applications.

Table II.1- The attenuation constants of different microwave cables.

Attenuation of cables	Attenuation of the reference load	Receiver gain G = 1 + G'	G '	Microwave cables (cm)
0.867	0.766	1.441	0.441	RG 223/U 8
0.868	0.932	1.214	0.214	RG 223/U 56
0.847	0.935	1.180	0.180	RG 223/U 110
0.838	0.908	1.182	0.182	RG 223/U 145
0.872	0.832	1.216	0.216	Copper 9*
0.872	0.785	1.453	0.453	Copper 17
0.874	0.767	1.563	0.563	Copper 33

* - *matched load 2 fixed cable length (9 cm).*

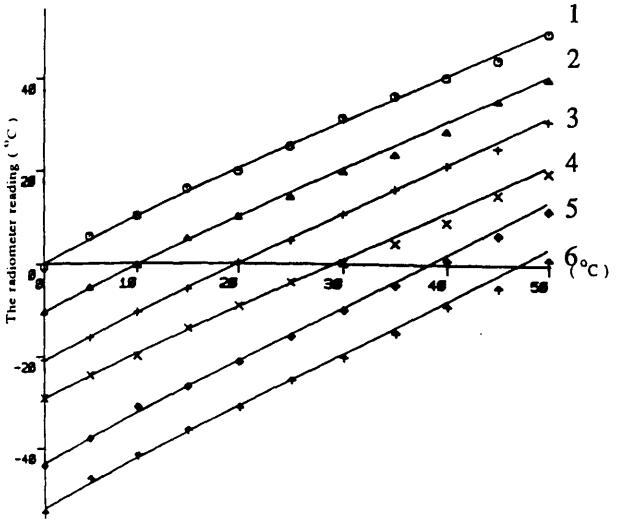

a- The variation of the radiometer received signal with the source temperature T_{s_1} using the matched load of 9 cm cable length.

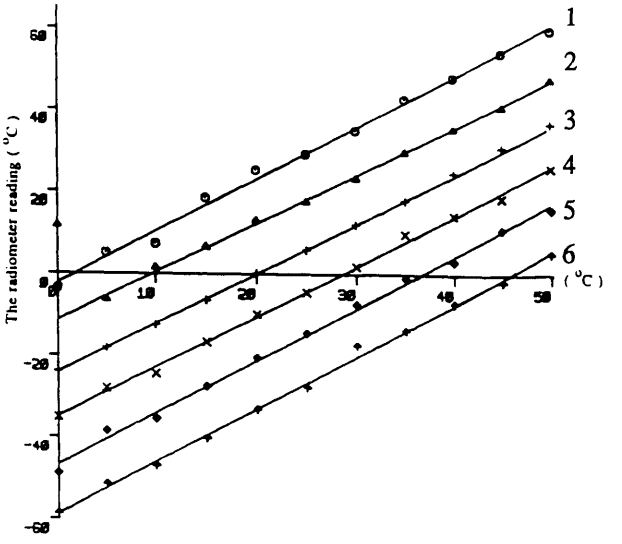

c- The variation of the radiometer received signal with the source temperature T_{s_1} for a 8 cm cable length.

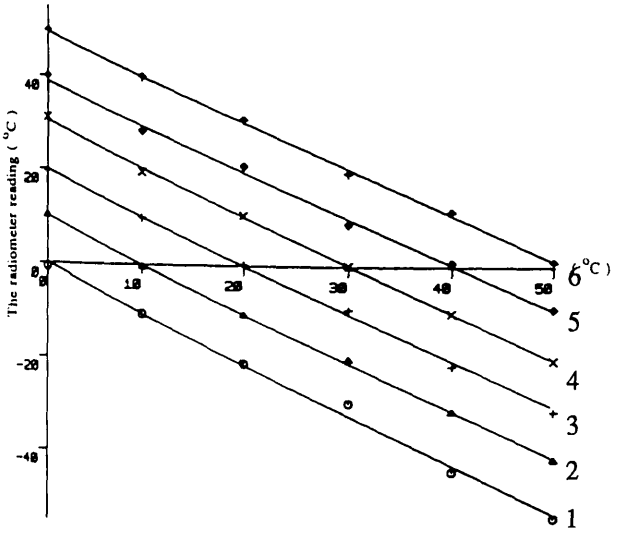

b- The variation of the radiometer received signal with the source temperature T_{s_2} using the matched load of 9 cm cable length.

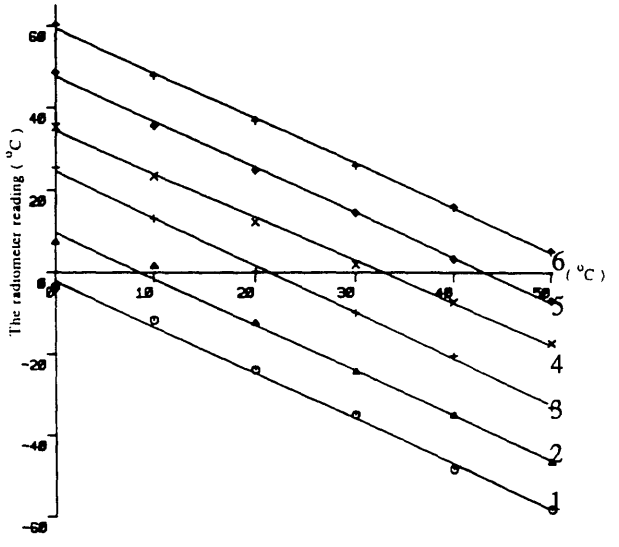

d- The variation of the radiometer received signal with the source temperature T_{s_2} for a 8 cm cable length.

Fig. II.8- The variation of the apparent source temperature when 8 & 9 cm length RG 223/U cables were used in the antenna and reference arms of the radiometer input circuit.

= 0 °C, 2 = 10 °C, 3 = 20 °C, 4 = 30 °C, 5 = 40 °C, and 6 = 50 °C

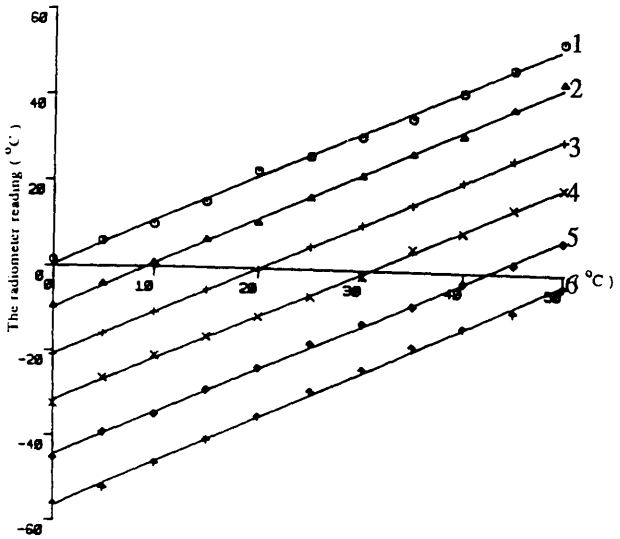

a- The variation of the radiometer received signal with the source temperature T_{s_1} for a 56 cm cable length.

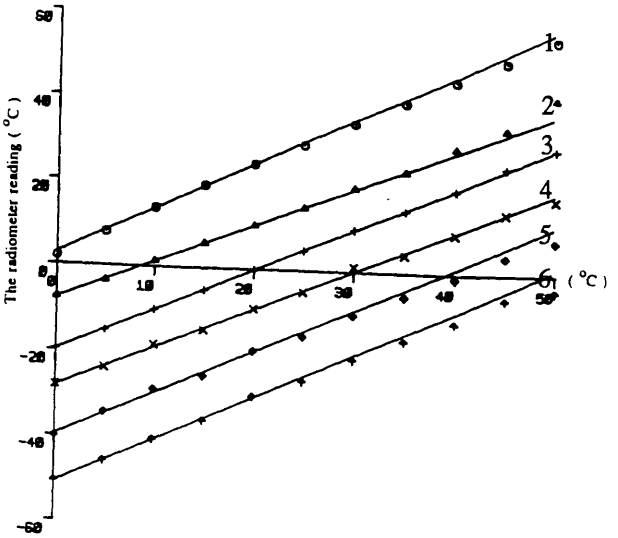

c- The variation of the radiometer received signal with the source temperature T_{s_1} for a 110 cm cable length.

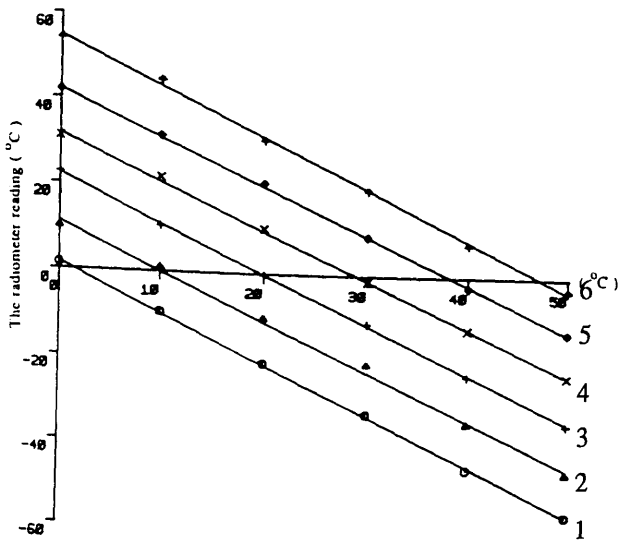

b- The variation of the radiometer received signal with the source temperature T_{s_2} for a 56 cm cable length.

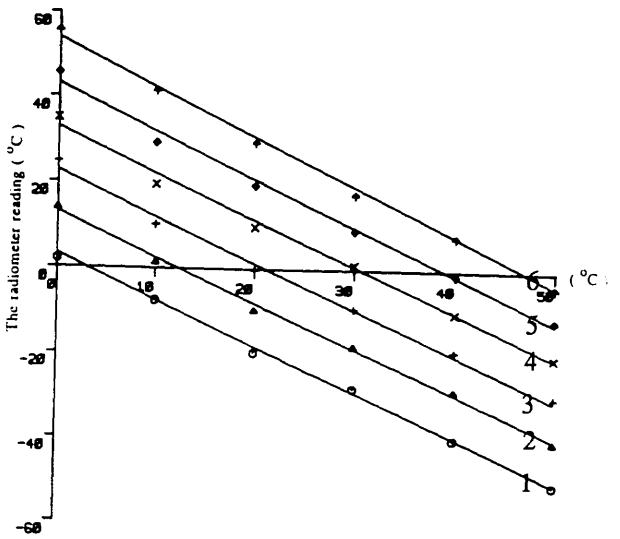

d- The variation of the radiometer received signal with the source temperature T_{s_2} for a 110 cm cable length.

Fig. II.9- The variation of the apparent source temperature when 56 & 110 cm length RG 223/U cables were used in the antenna and reference arms of the radiometer input circuit.

: 0 °C, 2 = 10 °C, 3 = 20 °C, 4 = 30 °C, 5 = 40 °C, and 6 = 50 °C

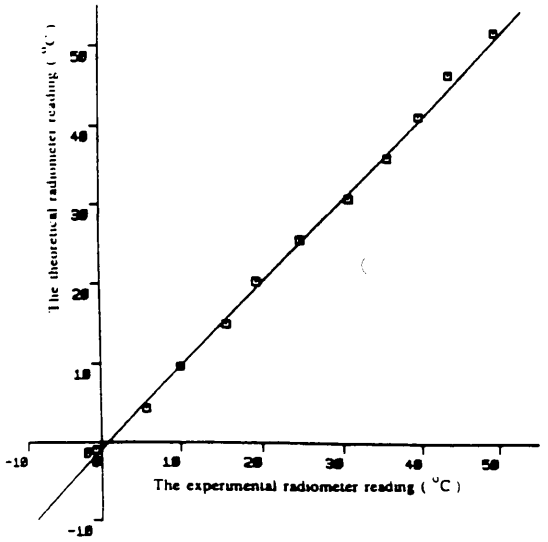

a- The comparison of the experimental and the theoretical analyses of the microwave radiometer received signal for a matched load of 9 cm cable length.

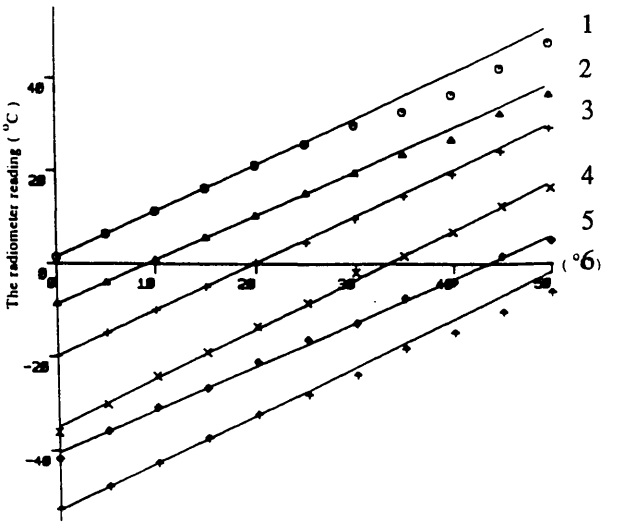

c- The variation of the radiometer received signal with the source temperature T_{s_1} for a 145 cm cable length.

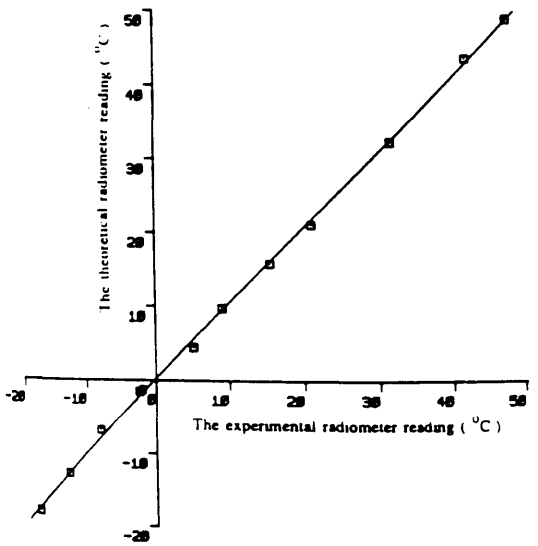

b- The comparison of the experimental and the theoretical analyses of the microwave radiometer received signal for a 56 cm cable length.

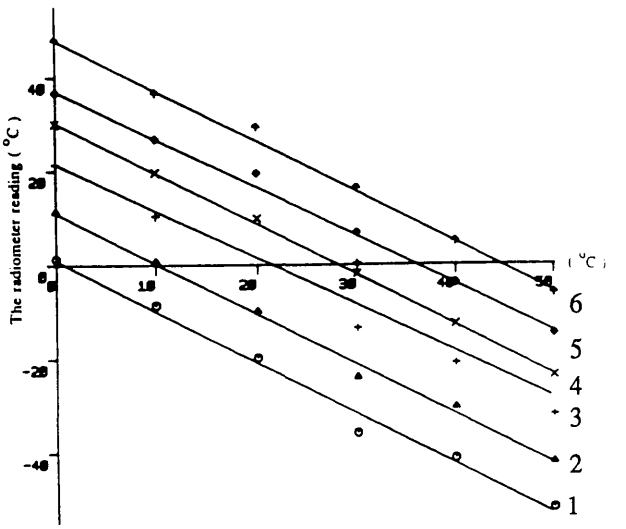

d- The variation of the radiometer received signal with the source temperature T_{s_2} for a 145 cm cable length.

Fig. II.10- The numerical and the experimental analyses of the radiometer received signal with the source and reference temperatures.

= 0 °C, 2 = 10 °C, 3 = 20 °C, 4 = 30 °C, 5 = 40 °C, and 6 = 50 °C

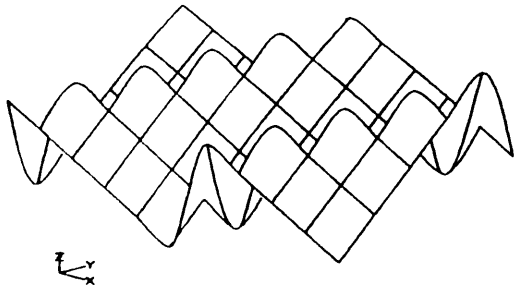

a z: -52 to 51

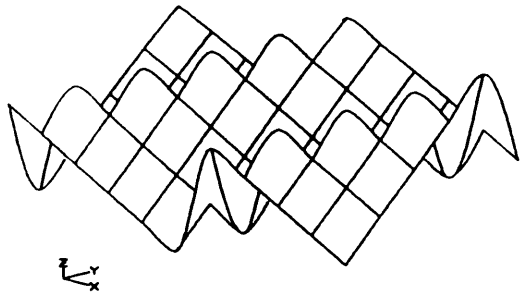

a z: -53 to 52

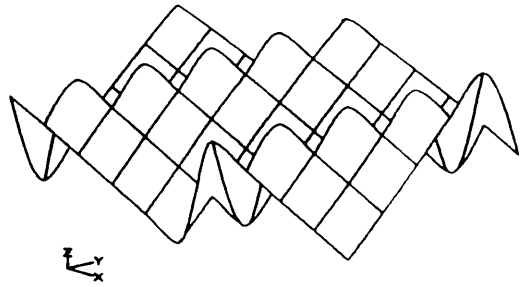

a z: -55 to 54

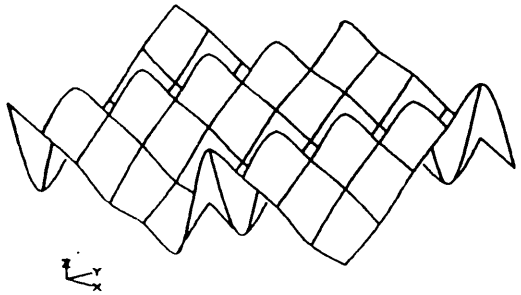

b z: -53 to 48

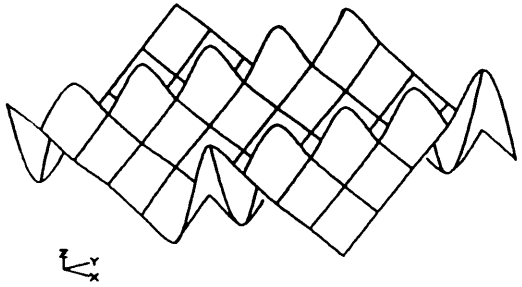

b z: -51 to 55

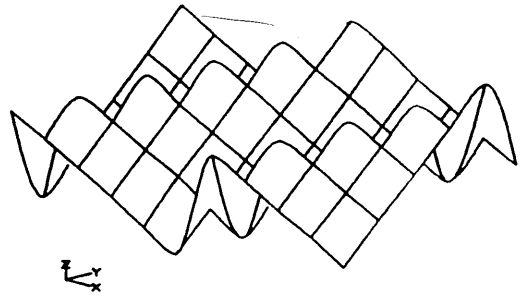

b z: -56 to 54

The received signal of a matched load for 145 cm length RG 223/U cable: a- represent the theoretical analysis, b- represent the experimental analysis.

The received signal of a matched load for 110 cm length RG 223/U cable: a- represent the theoretical analysis, b- represent the experimental analysis.

The received signal of a matched load for 56 cm length RG 223/U cable: a- represent the theoretical analysis, b- represent the experimental analysis.

Fig. II.11- The variation of the apparent source temperatures (T_{s1}, T_{s2}) with the microwave radiometer received signal (Δ) when 145, 110 and 56 cm length RG 223/U cables were used in the antenna and reference arms of the radiometer input circuit.

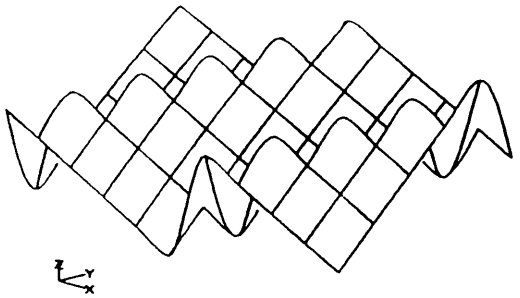

a z: -52 to 52

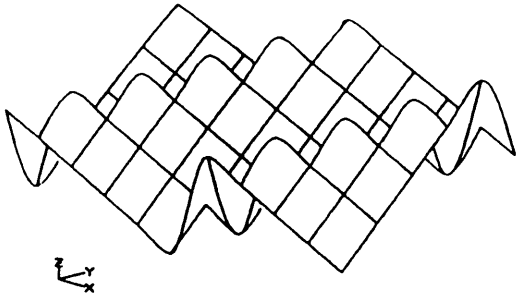

a z: -60 to 61

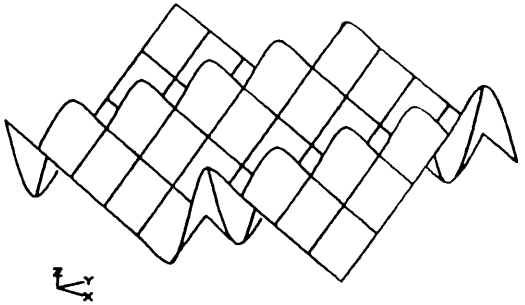

a z: -63 to 65

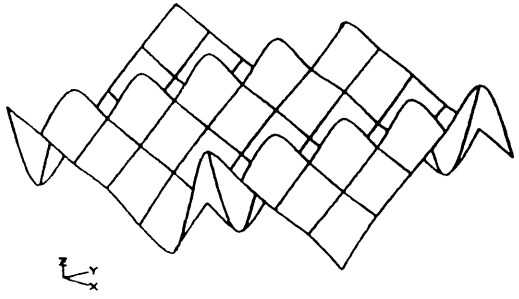

b z: -54 to 50

The received signal of a matched load for 9 cm length copper cable: a- represent the theoretical analysis, b- represent the experimental analysis.

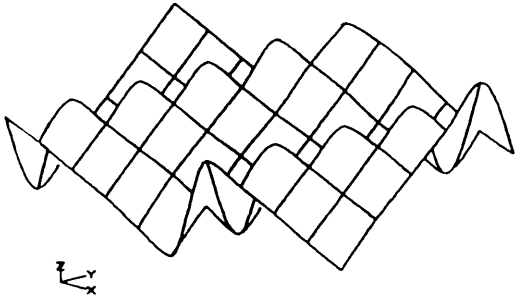

b z: -61 to 59

The received signal of a matched load for 17 cm length copper cable: a- represent the theoretical analysis, b- represent the experimental analysis.

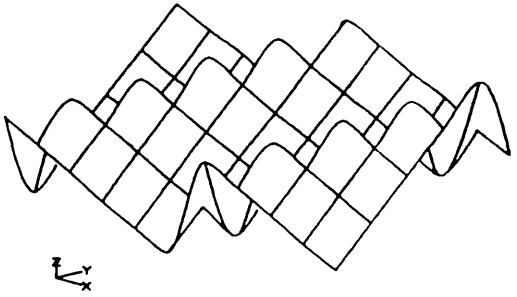

b z: -61 to 64

The received signal of a matched load for 33 cm length copper cable: a- represent the theoretical analysis, b- represent the experimental analysis.

Fig. II.12- The variation of the apparent source temperatures (T_{s1}, T_{s2}) with the microwave radiometer received signal (Δ) when 9, 17 and 33 cm length copper cables were used in the antenna and reference arms of the radiometer input circuit.

When the two temperatures (T_{s_1} , T_{s_2}) are approximately equal and close to the freezing point of the water, the error is about 0.2 °C. For higher temperatures, or when the source and the reference temperatures differ, the error can be about 3 °C. The radiometer reference temperature should be set close to the source temperature to have relevant results. This was successfully applied in a 3 GHz microwave radiometry system used for clinical applications (Glasgow hospitals). The modelling for the radiometer temperature measurements (above diagram) shows the behaviour of the received signal with respect to the temperature; the linearity of the temperatures with respect to the received signal; and the attenuation power measured from the expression (Eq. II.25). This analysis shows that when the difference between the antenna temperature and the source temperature is 2 °C, a change of 1 °C will cause a maximum change in the output of 0.1 °C. A variation of 1 °C is not significant and does not affect the measurements of the ambient temperature. The temperature value 0.1 °C is a very small variation in the output of the radiometer using cables for testing, as the losses inside these cables are considered and included in the output. These results are used to compare the losses of the cables with the antenna internal losses and have shown that there is very good agreement between the theoretically modelled and measured radiometer input circuit performance.

It is concluded that the model of the radiometer input circuits analysed in section II.10 properly represents the behaviour of the actual radiometer circuits used in the Glasgow microwave thermography equipment. Since the circuit used is a form of the general comparator on Dicke radiometer circuit, this model, with an appropriate choice of the effective receiver input temperature, can be applied to all comparator type radiometer input circuits.

and the source temperatures, Eq. II.26, and this has been proven by the experiment.

The theory of the apparent temperature beyond the attenuating region and the difference signal (Δ) at the receiver in microwave radiometer input switching circuit were derived for the practical cases. This theory, which is based on the above equations, predicts attenuation considerably lower than other theories now being used in industry; and the temperature resolution is about 1 ^{o}C as has been experimentally demonstrated.

Chapter III

Microstrip circuits for radiometer input switching circuits

III. 1- Introduction:

The purpose of this chapter is to discuss the great importance of low-loss microstrip circuits for radiometer input circuits. The performance of the radiometer system input circuits has been discussed in section II.8, which required low-loss input circuits between, for example, the antenna and the circuit switching element, between the switching element and circulator/reference load/amplifier, and for combining the signals from two or more antennas (crossed antennas).

Microstrip lines are a convenient form of transmission line for the construction of radiometer input circuits. The microstrip is a parallel pair of conductors deposited on either side of a thin dielectric substrate which provides the necessary mechanical stability. A parallel two conductor line of this type may need development because:

(i) A radio-frequency shield may be required to eliminate radiation losses and cross-coupling problems to other circuits. The shield dimensions or the sheet conductivity of the shielding material have to be carefully chosen in order to suppress transverse electric excitation, magnetic modes and box resonances.

(ii) The proximity of the air-dielectric interface to strip conductor can lead to excitation of plane-trapped surface waves. This problem can be solved by:-

a) using a substrate with two dielectric constants or

b) selecting a product of a sufficiently small operating frequency band for the microstrip or

c) removing the air-dielectric interface into the far field region.

(iii) If the substrate is a semi-conductor, surface passivation may be necessary to protect against atmospheric contamination; this can be achieved by applying a thin dielectric film to the substrate.

The dielectric losses are readily calculated by either empirical formulas (Schneider, 1969; Welch and Pratt, 1966) or plane-wave approximation (Caulton et al., 1966). When using the plane-wave approximation method for low-loss substrates, conductor loss is dominant (Krowne, 1988). But in the case of monolithic microwave integrated circuits, where substrates such as silicon, germanium or teflon are used, dielectric loss becomes the dominant one, and therefore has to be treated more rigorously.

III. 2- The microstrip design requirements:

For design purposes, it is necessary to know the characteristic impedance, phase velocity and the attenuation constant of the dominant microstrip mode and how they are affected by geometrical factors. Also, the electronic properties of the substrate and the conductors and the effects of the operating frequency on them. Of particular importance for this application is the attenuation constant of the dominant mode. The dielectric properties have not received much attention in the papers on microstrip lines although Welch and Pratt, (1966) investigated the dielectric attenuation for mixed dielectric systems, and so were made the subject of further experimentation.

One major advantage of all microstrip configurations with an air gap is that the effective dielectric constant is small. This means that the effective dielectric loss tangent is substantially reduced, and all circuit dimensions can therefore be increased, which in turn, leads to less stringent mechanical tolerances. The open-strip transmission line was initially abandoned by microwave designers in favour of the balanced strip transmission line because of the radiative nature of the open-strip line. The use of thin high dielectric material greatly reduces radiation from the open-strip and has recently been actively used for integrated microwave printed circuits.

The line radiation is reduced by the concentration of the field in the dielectric region. The width of a microstrip line on a dielectric substrate can be adjusted to control its impedance. When the impedance is controlled by dimensions in a single plane, the circuit manufacture can be conveniently carried out by photolithography techniques and photoetching of thin film.There are several transmission structures that satisfy the requirement of being planar. The most common of these are:

- microstrip.
- slotline.
- coplanar waveguide.
- coplanar strips.

Generally microstrip lines are manufactured from standard teflon, impregnated fibreglass or polystyrene printed circuit boards 0.79 to 1.59 mm thick with copper lines of 1.59 to 3.18 mm wide. For integrated circuits alumina, sapphire, beryllium, or high resistivity semi-conductors 2.54 to 7.62 mm thick are used as substrates for the line. The conductors can be, copper, aluminum, gold or silver and are of the order of 2.032 to 7.62 mm wide.

III. 3- The different type of microstrips:

Two known types of microstrip were investigated in this work. Both had a similar geometry in that they consisted of narrow strip conductors of width W and thickness t, separated by a dielectric substrate of width much greater that W and thickness H (Figs. III. a, III. b). The first type the dielectric was a supportive layer of teflon, in the second the dielectric was an air gap.

The characteristic impedances of the two microstrips of the respective dielectric substrates had different values. The relative permittivity ε_r of the dielectric substrate materials had to be taken into consideration together with the geometric cross-section $\frac{w}{H}$ for each microstrip transmission line.

In general according to Kraus, (1984), the characteristic impedance of strip

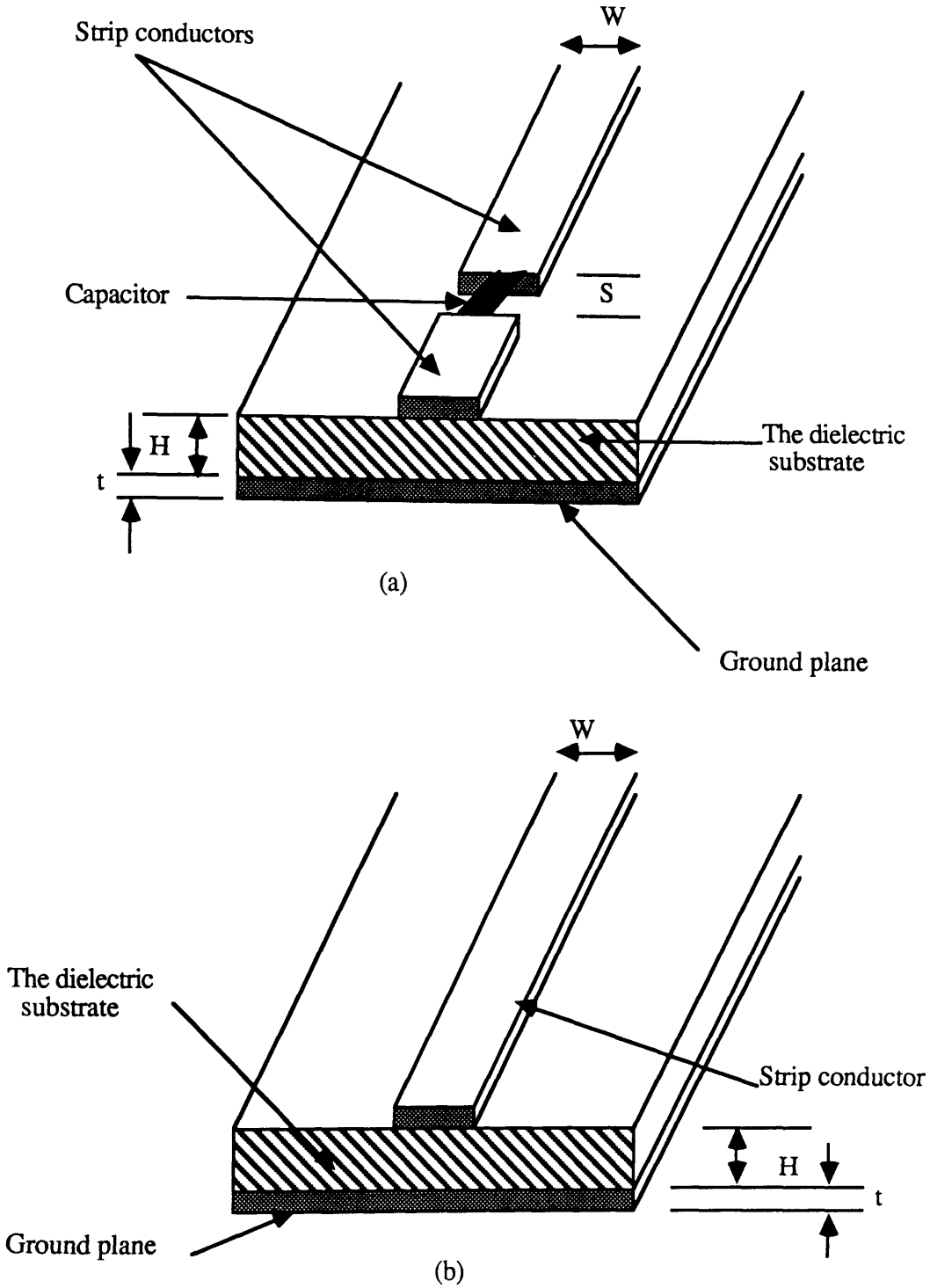

S is the distance between two copper strips.
H is the dielectric thickness.
W is the strip width
t is the thickness of the foil.

Fig. III.a- Microstrip configuration. a- microstrip line with a capacitor 1000pF, b- a straight microstrip line.

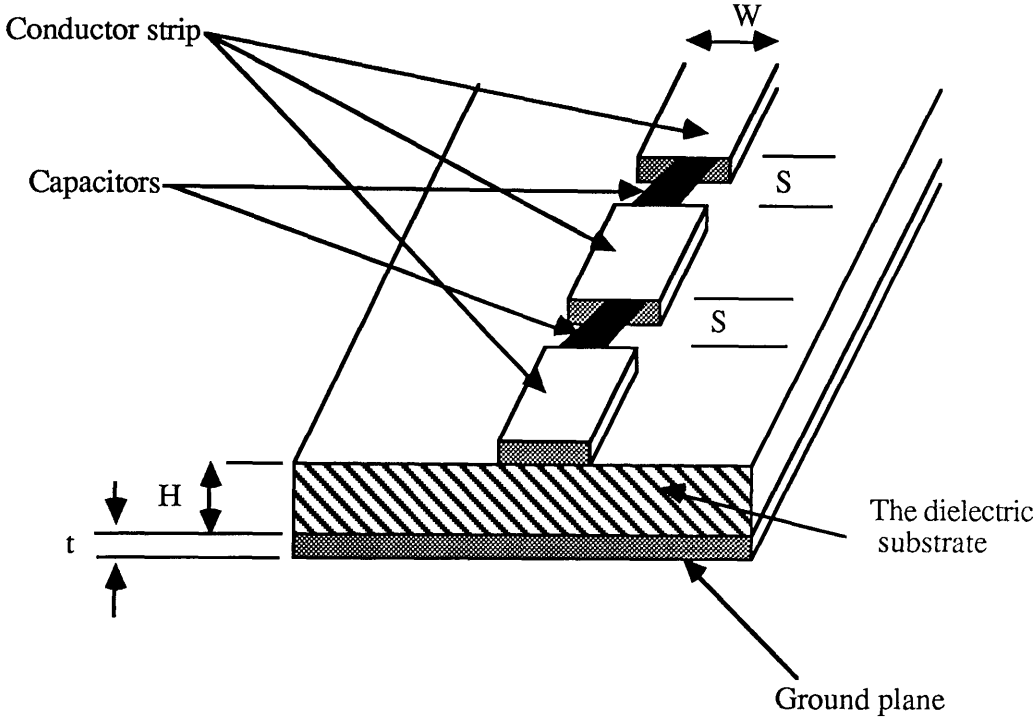

W is the width of the strip.
H is the dielectric thickness.
S are the gaps between the strips
t is the thickness of the foil.

Fig. III.b- Microstrip configuration with two capacitors each is 1000pF.

lines with W greater than the dielectric thickness H is given by the equation:

$$Z_o = \frac{377}{\sqrt{\varepsilon_r}\left[\frac{W}{H} + 2\right]} \qquad \text{(III.1)}$$

where 377 is the intrinsic impedance of vacuum or the characteristic impedance of free-space, ε_r is the relative permittivity of the substrate, W is the conductor width and H is the dielectric thickness.

In practice the microwave energy propagates both in the dielectric substrate and in the air region adjacent to the conductor resulting in the effective relative permittivity constant $\varepsilon_{r_{eff}}$ which should be considered as a function of microstrip geometry $\frac{W}{H}$. The effective relative permittivity is much lower than the relative permittivity ε_r, which is defined by:

$$\varepsilon_{r_{eff}} = \frac{\varepsilon_r + 1}{2} + \frac{\varepsilon_r - 1}{2} F\left(\frac{W}{H}\right) \qquad \text{(III.2)}$$

where

$$F\left(\frac{W}{H}\right) = \begin{cases} \left\{1 + 10\frac{W}{H}\right\}^{-\frac{1}{2}} & \frac{W}{H} \geq 1 \\ \left\{1 + 10\frac{W}{H}\right\}^{-\frac{1}{2}} + g\left(\frac{W}{H}\right) & \frac{W}{H} \leq 1 \end{cases} \qquad \text{(III.3)}$$

and in the present work this must be taken into consideration as a function of the microstrip geometry when deriving conclusions using the relative effective permittivity constant defined by the relationship:

$$\varepsilon_{r_{eff}} = \frac{\varepsilon_r + 1}{2} + \frac{\varepsilon_r - 1}{2}\left[1 + 10\frac{H}{W}\right]^{-\frac{1}{2}} \qquad \text{(III.4)}$$

Schneider, (1968) presented analyses using equation III.4 which yields final results with an accuracy of ± 2% for $\varepsilon_{r_{eff}}$ and an accuracy of ± 1% for $\sqrt{\varepsilon_{r_{eff}}}$.

III. 4- Microstrip measurement:

III. 4. 1- Description of the board preparation:

For the manufacture of the microstrip lines used in this research project two types of base material were selected 1) - double sided copper-clad *Glass fibre* reinforced epoxy board, 2) - double sided copper-clad non-woven glass microfibre *PTFE* laminate *(RT/duroid ®†)*.

The dimensions of the boards are 69.9 mm in length, 28.6 mm in width and 1.6 mm thick. The microstrip boards were produced by the usual photo-resist etching process.

III. 4. 2- Techniques for standing-wave detector measurements:

The measurement of standing-wave ratios requires typical apparatus which is based on the signal source, standing-wave measuring section and the termination. This is terminated by a suitable termination, a short-circuited line of known length, and a movable short circuit. This technique, suggested by Ginzton, (1957) provides a nearly perfect approximately 100% reflection to the main transmission line, and is useful for checking the accuracy of the equipment. To adjust and check the equipment prior to use the oscillator should be adjusted for the desired power output and allowed to stabilize. The modulation of the signal generator permits simplification of detecting equipment and increases the sensitivity (Fig.III. c). Simple sinusoidal modulation is impractical since the frequency of most microwave oscillators depends on the applied potentials. Therefore, to obtain amplitude modulation with little incidental frequency modulation, it is generally necessary to employ square-waves. The use of square-wave modulation does not require the detecting system to reproduce all the frequency components of the detected signal.

† *Rt/duroid ® microwave laminate is a registered trademark of Rogers Corporation*

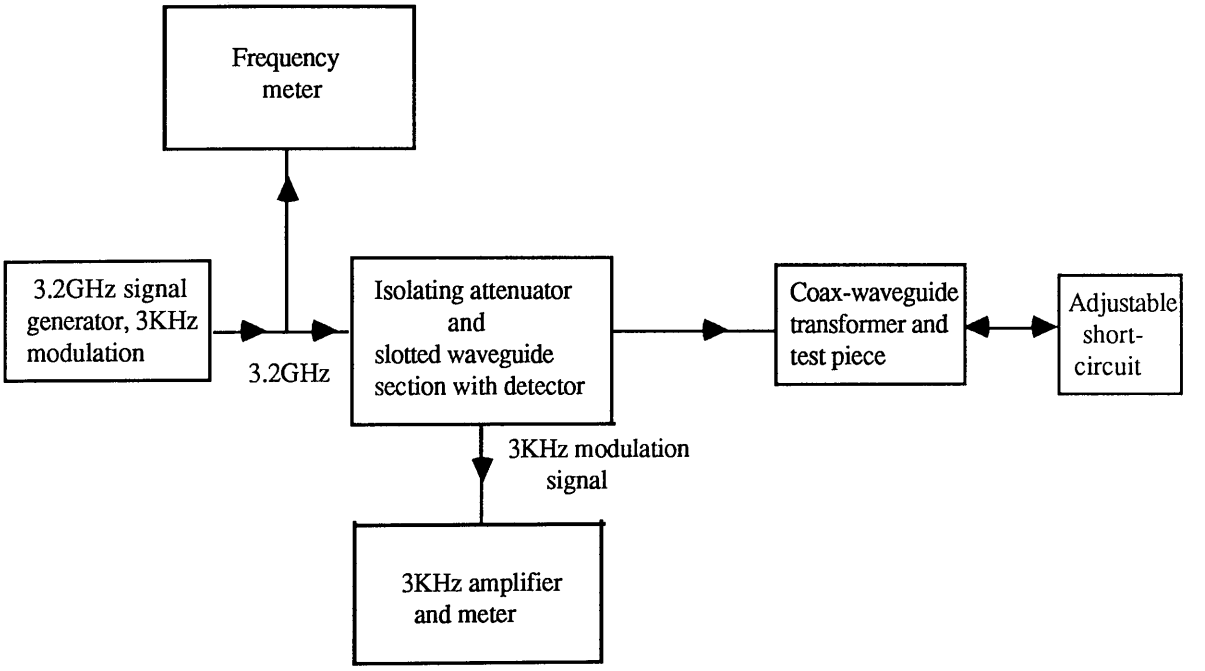

Fig. III.c-The equipment set-up

The usual practice is to reduce the bandwidth of the detecting amplifier to respond only to the fundamental component of the detected frequency. The standing-wave detector should be terminated with a matched impedance. Near the ends of the slot the response can become significantly different from the ideal and these regions should be noted and avoided where possible during any experimental measurements using a standing-wave detector. Low standing-wave ratios are critical and particular care in most of the adjustments is not essential as high sensitivity is not required. On the other hand, high sensitivity is required for the large variation in voltages associated with high standing-wave ratios and an accurate knowledge of the detector response law, is needed.

III. 4. 3- The method of measurements:

If a high value of voltage standing-wave ratio *(VSWR)* is to be measured, the accuracy of the calibration of the detector indicator and the associated attenuators becomes extremely important. Ginzton, (1957) considered a method known as the double minimum which can be used to measure the high *VSWR* by merely observing the shape of the standing-wave pattern near the voltage minimum. The advantage of this method is the reduction of errors due to probe loading because it is always located in the region of the low impedance.To apply this method, accurate measurements of small displacements of the probe carriage are recorded as it is moved in the vinicity of the voltage minimum. This can best be done by attaching a small micrometer dial indicator to the probe carriage. The procedure is as follows: first, find the value of the voltage minimum, then the adjacent two positions are found at which the output is twice the minimum value. If the detector response is square-law, the standing-wave ratio is given by,

$$r = \frac{V_{max}}{V_{min}} = \frac{\lambda_t}{2\pi x_o} \qquad \text{(III.5)}$$

where x_o is the probe displacement, and λ_t is the transmission line wavelength.

The measurement of small values of attenuation can be measured by either a substitution method or direct measurement of the power ratio with or without component. The attenuation of any lossy terminal network may be determined from the following quantities: 1) the effect of the insertion of such a network on the voltage distribution and the phase shift in a short-circuited section of lossless line following the unknown component, 2) the magnitude of the voltage standing-wave ratio of unknown component terminated by a short-circuit (Ebert, 1945).If the unknown unit is terminated by a short-circuit and the ratio of the incident to reflected power is known, P_1 and P_2, the attenuation of the unknown unit can be computed. The power P_2, having been totally reflected from the short-circuit, is again attenuated while passing through the unknown unit. This power is called P_3. The attenuation of the unit can be written as (Weber, 1947).

$$\alpha = 10\,\mathrm{Ln}\left[\frac{P_1}{P_2}\right] = 10\,\mathrm{Ln}\left[\frac{P_2}{P_3}\right] = 5\,\mathrm{Ln}\left[\frac{P_1}{P_3}\right] \qquad \text{(III.6)}$$

The quantity $\frac{P_1}{P_3}$ is, however, the ratio of incident to reflected power and is independent of generator impedance. If r is the *VSWR*, then

$$\frac{P_3}{P_1} = \frac{r-1}{r+1} \qquad \text{(III.7)}$$

then the final expression for the attenuation constant becomes:

$$\alpha = 10\,\mathrm{Ln}\left[\frac{r+1}{r-1}\right] \qquad \text{(III.8)}$$

III. 5- Results of measurements on test microstrip lines:

The results are presented of accurate experimental measurements on microstrip lines to find the line attenuation at the radiometer frequency of 3.2 GHz, using the "double minimum" method, and for line characteristic impedances of 40 - 60 Ω.

III. 5. 1- Results of initial measurements on test microstrip assemblies:

The measurement of standing-wave ratios with the double minimum method gives an accurate value of about 0.5% when the *VSWR* is above approximately 10. The position of the minimum can be located more accurately by averaging two positions of equal indicator readings set on either side of the minimum. Adjusting the input attenuators to set a minimum detector signal level means that the indicated residual measurement noise is below the mid-point of the *VSWR* meter scale. The probe is moved to the left and to the right side of the minimum position to find the wanted two minimum points which establish the width of the minimum. All measurements are taken at 3.2 GHz using a suitable amplitude modulated signal source.

III. 5. 2- Checking the accuracy of this method using lengths of coaxial cable of known attenuation as standards:

The method described was used above to measure the attenuation constant of two cable types *GE 83010* and *RG 223/U* at 3.2 GHz. The measured values are compared with the manufacturer's published values. The results of these measurements showed good agreement with the expected attenuation values of the respective cables (Tab. III.1).

The losses of *PTFE* and glass fibre substrate microstrip were measured by noting the difference in attenuation between 40 - 60 Ω of 69.9 mm in length interconnected to the measurement system. The boards were connected and measurements of the standing-wave ratios recorded after locating the minimum along the travelling-wave. Two different kinds of microstrips were tested: the first ones were straight (without a gap) and the second had a gap which formed a series capacitor, of capacitance 1000 pF.

Table III.1- Insertion loss of RG 223/U and GE 83010.

cable type	VSWR	loss (dB)
RG 223/U	42.35 ± 0.5	0.24
GE 83010	48.84 ± 0.5	0.21

A summary of typical results obtained using the standing-wave detector measurement technique is given in Tab. III.2, III.3, III.4 and III.5. It shows that the standing-wave ratio is high and decreases when the attenuation constant and the characteristic impedance increases, Tab. III.2 and III.3 illustrate how the measured data of the attenuation constant varies with the strip width of the *PTFE* and *glass fibre* microstrips for the characteristic impedance range 40 - 60 Ω. Tab. III.4 and III.5 present the similar measured data but the microstrip configurations are different. The conducting strips are coupled with small capacitors.

Table III.2- variation of the *PTFE* microstrip attenuation with strip width.

Impedance (Ω)	√VSWR	Loss (dB/m)
40	6.030 ± 0.05	0.554
45	5.881 ± 0.05	0.579
50	5.674 ± 0.05	0.622
55	5.490 ± 0.05	0.664
60	5.290 ± 0.05	0.715

Table III.3- variation of the *glass fibre* microstrip attenuation with strip width.

Impedance (Ω)	√VSWR	Loss (dB/m)
40	4.400 ± 0.05	1.964
45	3.198 ± 0.05	2.042
50	3.172 ± 0.05	2.540
55	3.184 ± 0.05	2.496
60	2.972 ± 0.05	2.616

Table III.4- The attenuation constants of *glass fibre* microstrip using a capacitor

Impedance (Ω)	√VSWR*	√VSWR**	Loss* (dB/m)	Loss**(dB/m)
40	3.401	2.761	1.957 ± 0.1	2.947 ± 0.1
45	3.292	2.593	2.776 ± 0.1	3.217 ± 0.1
50	3.483	3.087	2.186 ± 0.1	3.012 ± 0.1
55	3.332	3.487	2.876 ± 0.1	2.168 ± 0.1
60	3.180	2.774	2.971 ± 0.1	2.752 ± 0.1

Table III.5- The attenuation constants of *PTFE* microstrip using a capacitor

Impedance (Ω)	√VSWR*	√VSWR**	Loss* (dB/m)	Loss**(dB/m)
40	4.451	4.473	1.477 ± 0.1	1.669 ± 0.1
45	4.858	5.687	1.227 ± 0.1	0.622 ± 0.1
50	4.902	5.205	1.032 ± 0.1	0.980 ± 0.1
55	4.628	4.593	0.955 ± 0.1	1.040 ± 0.1
60	4.750	4.454	0.929 ± 0.1	1.083 ± 0.1

Figures III.1 and III.2 show the variation of the attenuation with the strip width of two different materials *RT/duroid* ® and *Glass fibre*, where the loss decreases gradually when the ratio of the width of the strip with the dielectric substrate thickness increases. The *RT/duroid* ® attenuation range was 0.5 - 0.8 dB/m and the Glass fibre attenuation range varies between 1.9 - 2.7 dB/m. Since the loss of *RT/duroid* ® is small compared with the Glass fibre material, the microwave component designers use *RT/duroid* ® as microstrip transmission lines for microwave circuits.

Figures III.3 and III.4 show the measurements made with the same microstrip *RT/duroid* ® with a capacitor gap at both ends. The capacitor is fixed near one end of the strip (1.7 mm from the end of the strip) and when the capacitor

* *The capacitor is near the connector (connected to the standing-wave measuring system)*

** *The capacitor is connected to the termination of the transmission line (near the end).*

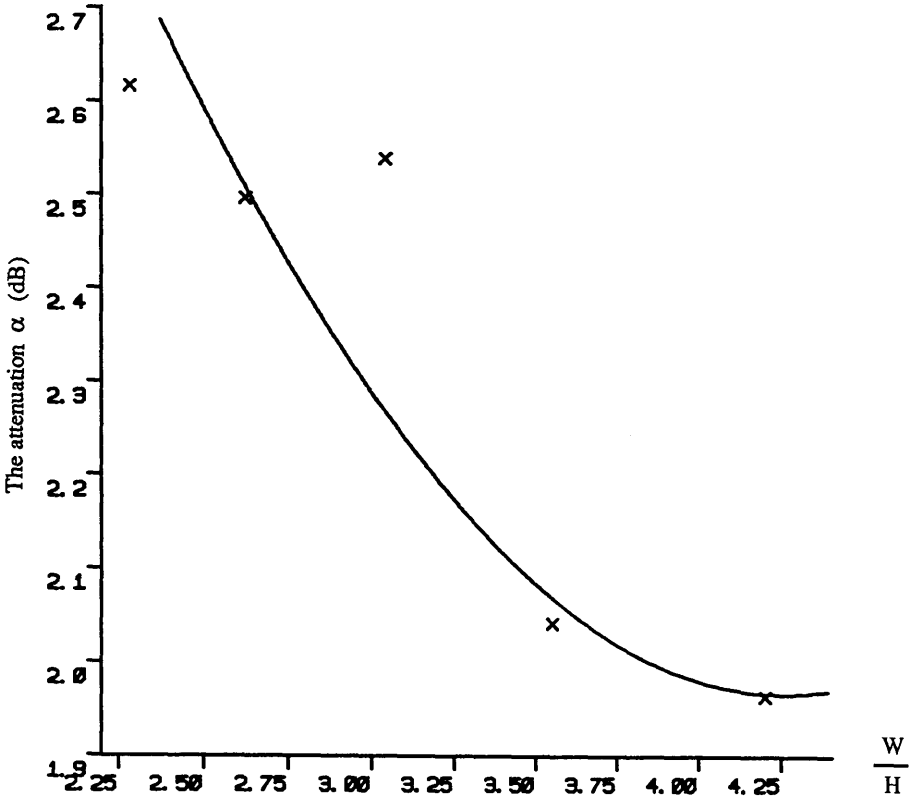

Fig. III.1- The variation of the attenuation with the strip width, (H = 1.59 mm, $\varepsilon_r = 2.2$), microstrip constructed by Glass fibre without a capacitor

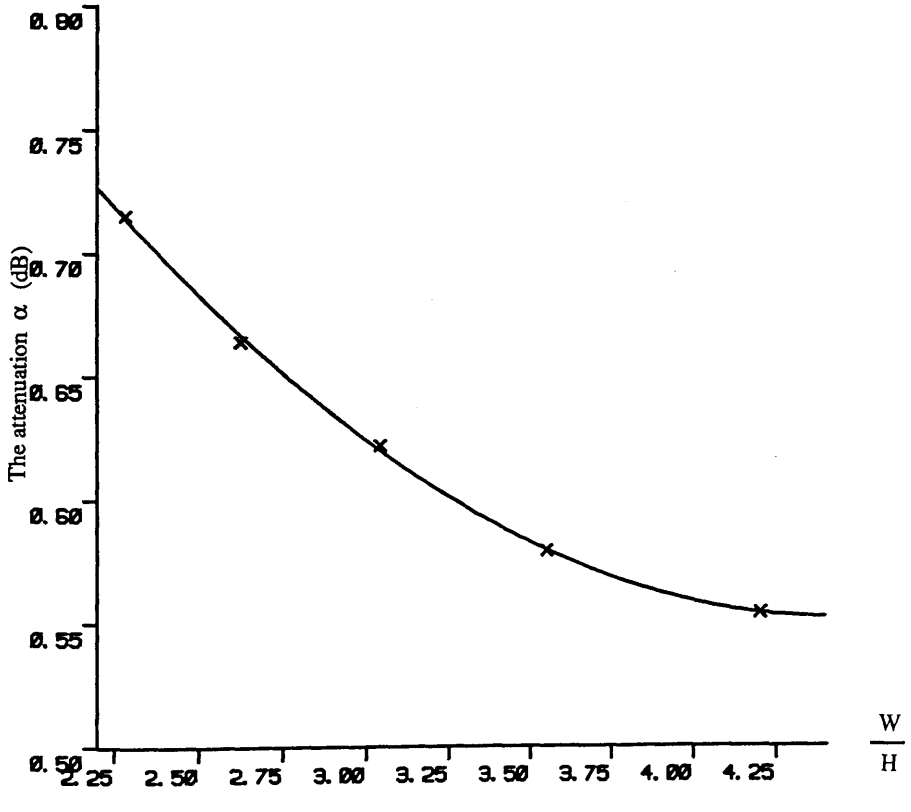

Fig. III.2- The variation of the attenuation with the strip width, (H = 1.59 mm, $\varepsilon_r = 2.2$), microstrip constructed by RT/duroid® without a capacitor.

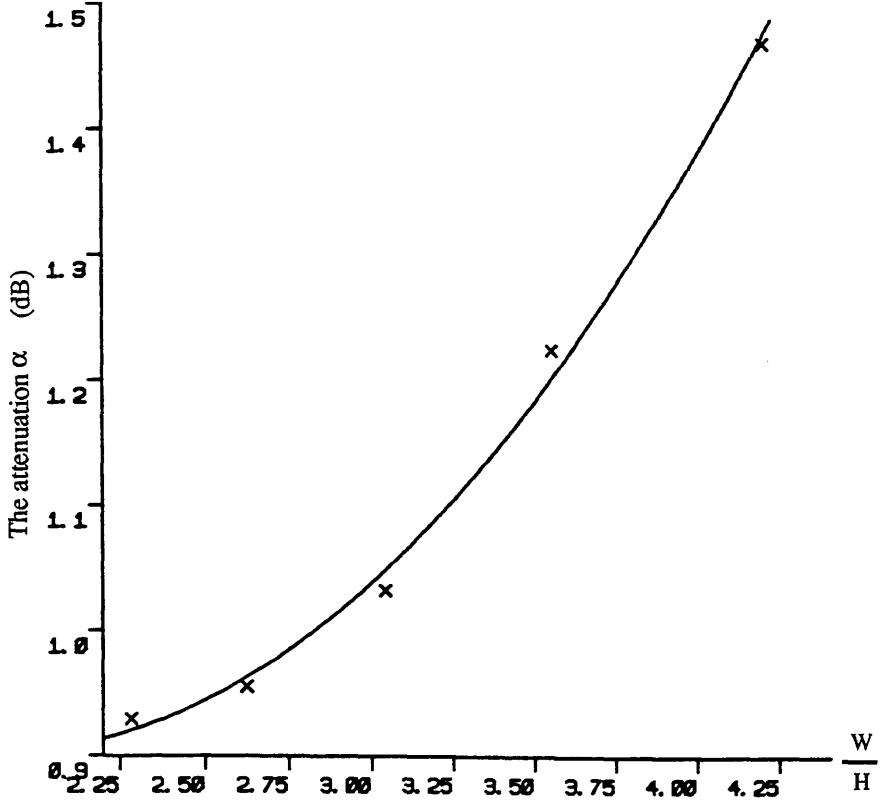

Fig. III.3- The variation of the attenuation with the strip width, (H = 1.59 mm, ε_r = 2.2), microstrip constructed by RT/duroid® with a capacitor close to the connector measurement system.

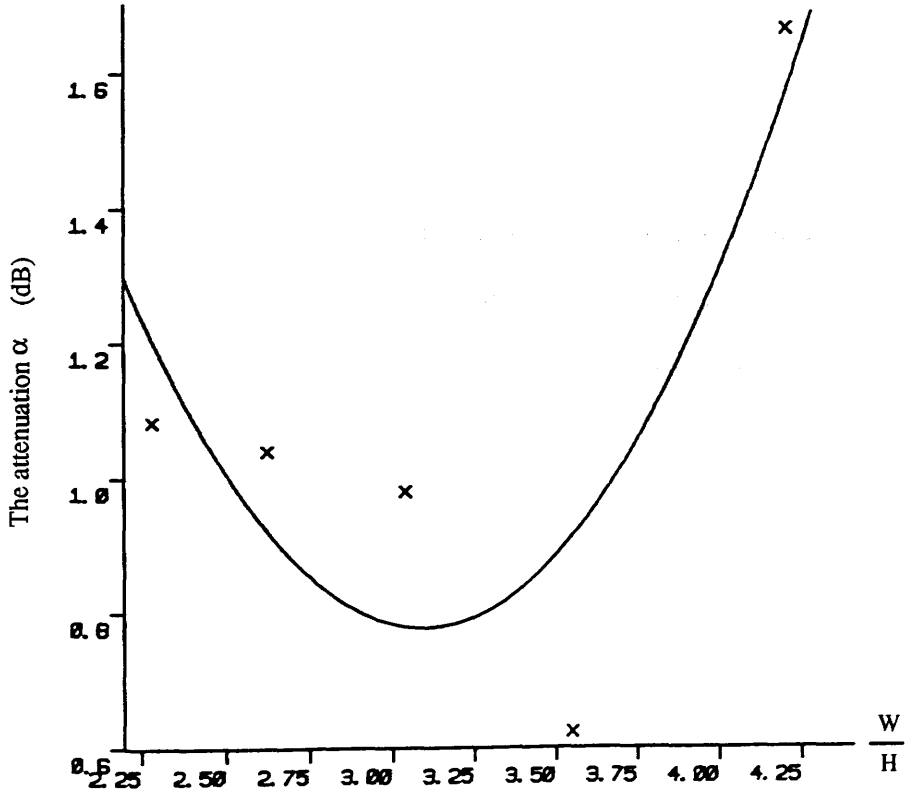

Fig. III.4- The variation of the attenuation with the strip width (H = 1.59 mm, ε_r = 2.2), microstrip constructed by RT/duroid® with a capacitor close to the transmission line (termination).

is near the connector measurement system the loss increases as the characteristic impedance increases and the range of the attenuation is 0.9 - 1.5 dB/m. In the opposite case the loss decreases rapidly. It is not convenient to have a capacitor in the circuit with *RT/duroid* ® material.

Figures III.5 and III.6 represent the results for the *Glass fibre* microstrip with a capacitor for both ends. The losses decrease when the capacitor is near the connector measurement system but the range is higher (2.0 - 3.0 dB/m) than for the straight strip, and when the strip is reversed it increases for the same characteristic impedance range and its value is between 2 - 3.2 dB/m.

Figures III.7 and III.8 show the measurement results with one capacitor fixed at each end of the strip. The results are not significant for either materials and show that the straight line microstrip using *RT/duroid* ® material gives efficient attenuation values. The losses are small, suggesting that using this material as a *PIN-diode* switch or other component will minimize the degradation of the sensitivity of the radiometer.

Figure. III.9 represents the variation of the square root of the effective relative permittivity with the strip width. The effective relative permittivity is proportional to the characteristic impedance. These results prove the efficiency of using microstrip lines as transmission lines for the radiometer input circuits, so *PIN-diode* switches are convenient for a microwave radiometer design. The theoretical estimates which have been compared with the above at 1, 2, 4, and 6 GHz for different widths and thus different impedances show good agreement with the experimental results.

The results of the characteristic impedance measured at 3.2 GHz using the Kraus, (1984) method are compared with the manufacturer's data *(RT/duroid* ®*)* given at 2 GHz for the characteristic impedance range 20-110 Ω, (Fig. III.10). Good agreement is found, the characteristic impedance decreasing when the ratio of the strip width with the dielectric thickness increases.

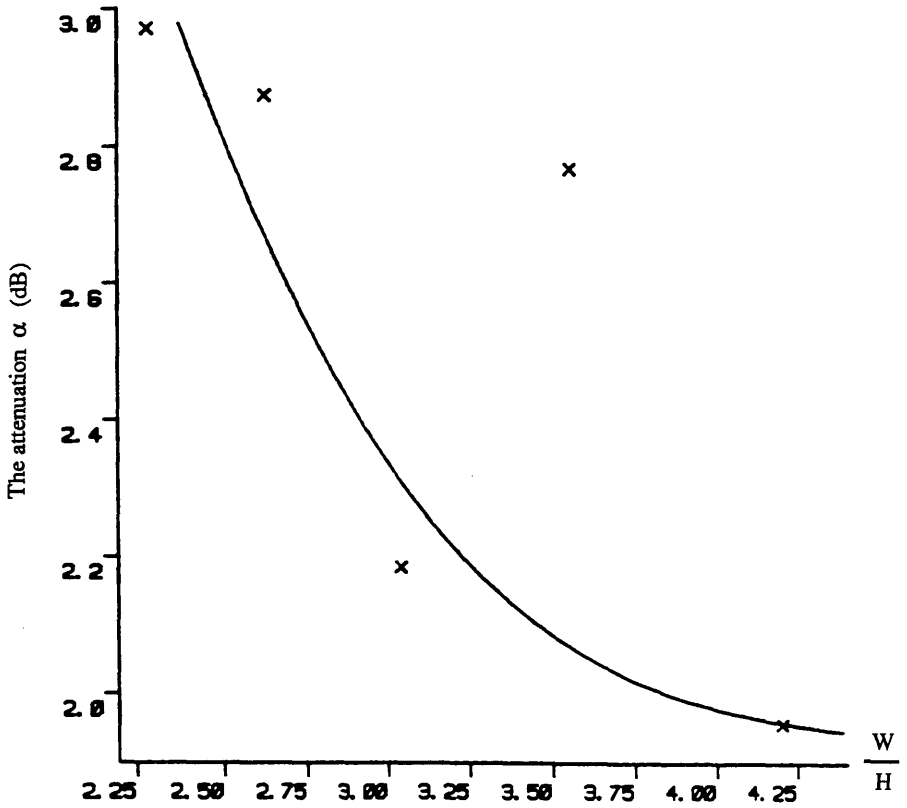

Fig. III.5- The variation of the attenuation with the strip width, (H = 1.59 mm, ε_r = 2.2), microstrip constructed by Glass fibre with a capacitor close to the connector measurement system.

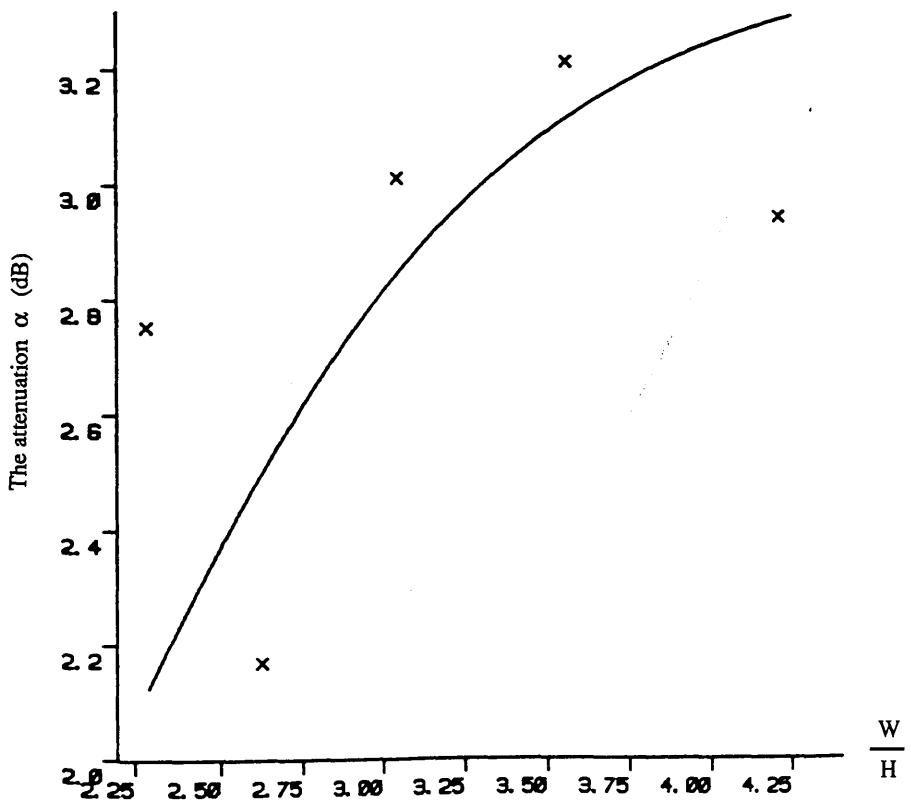

Fig. III.6- The variation of the attenuation with the strip width, (H = 1.59 mm, ε_r = 2.2), microstrip constructed by Glass fibre with a capacitor close to the transmission line (termination).

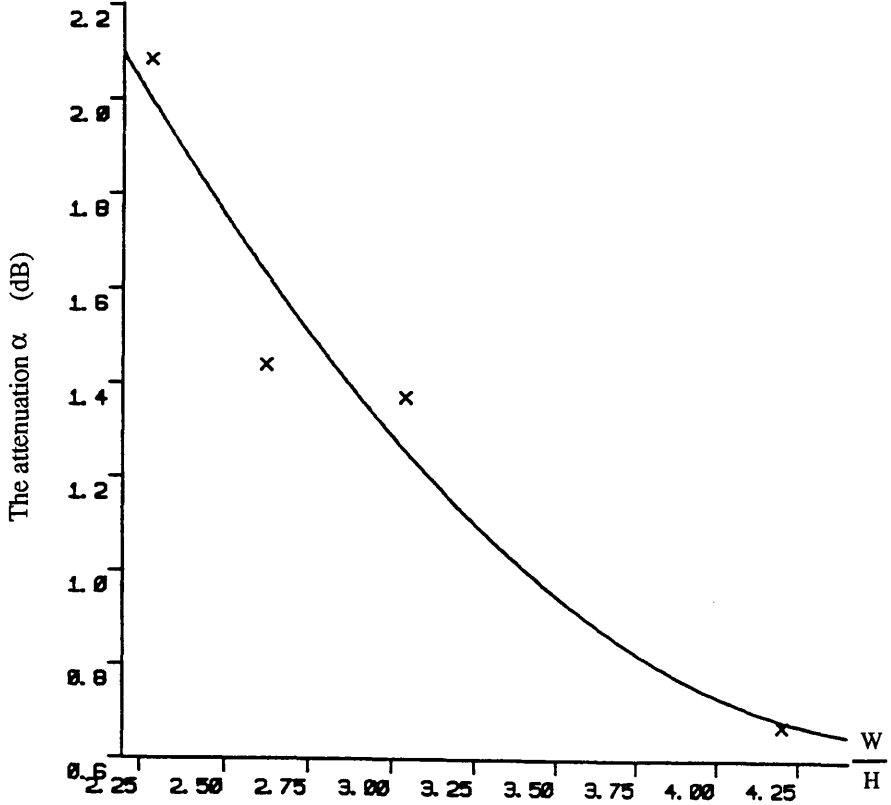

Fig. III.7- The variation of the attenuation with the strip width, (H = 1.59 mm, ε_r = 2.2), microstrip constructed by RT/duroid® with two capacitors the distance from each end to the capacitor is 1.70 cm.

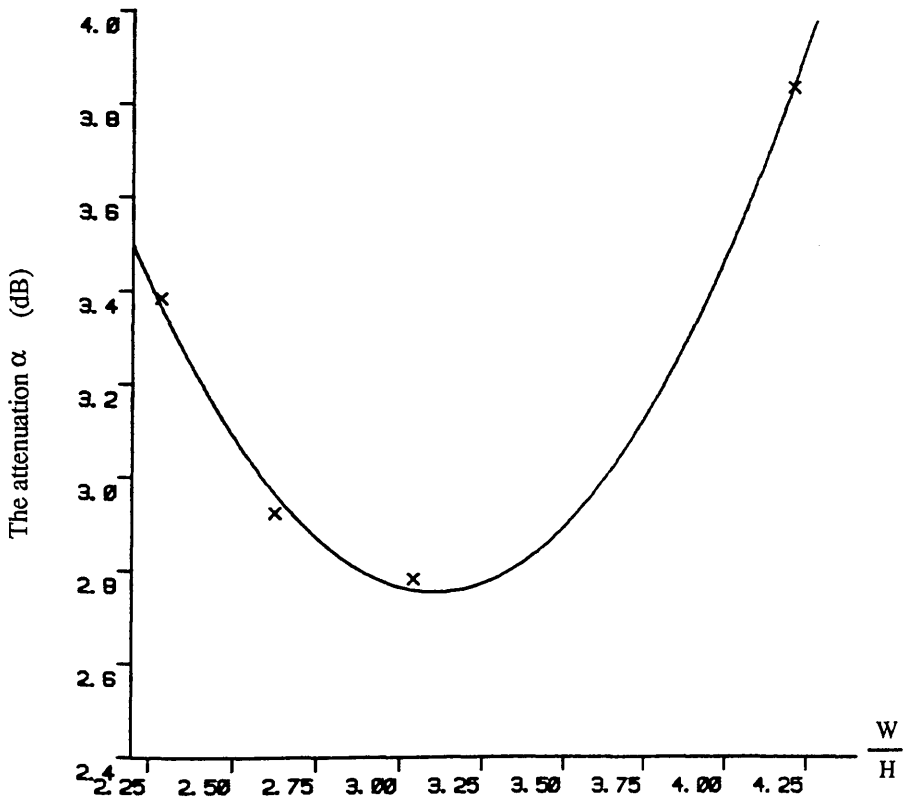

Fig. III.8- The variation of the attenuation with the strip width (H = 1.59 mm, ε_r = 2.2), microstrip constructed by Glass fibre with two capacitors the distance from each end to the capacitor is 1.7 cm.

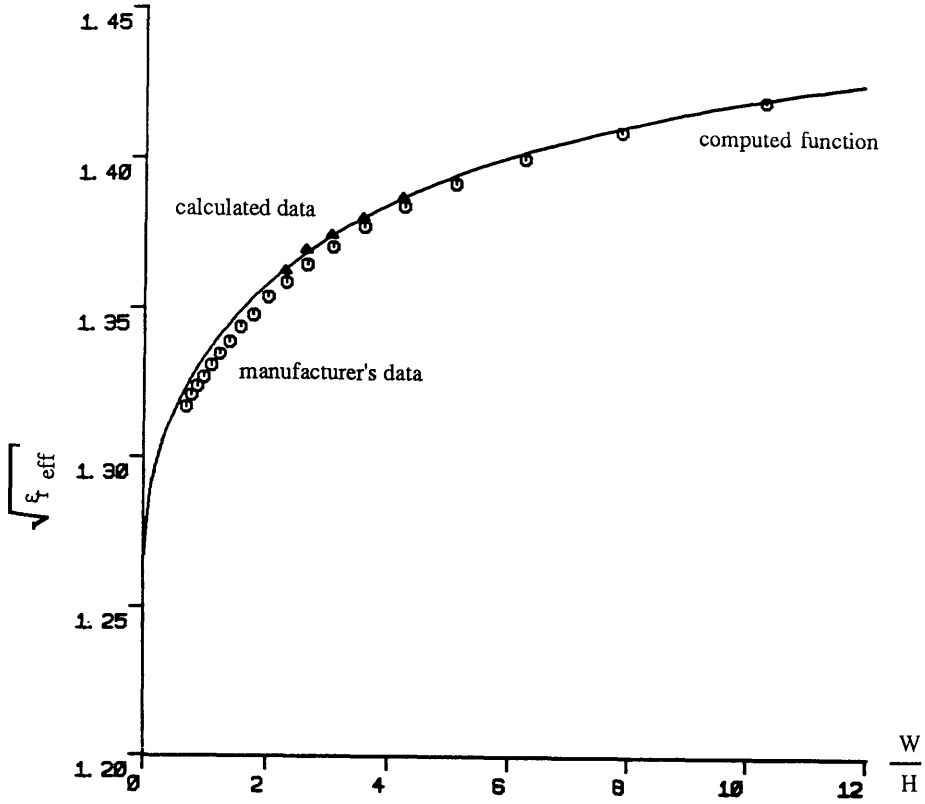

Fig. III.9- The variation of the square root of the effective relative permittivity with the strip width, (H = 1.59 mm, $\varepsilon_r = 2.2$), microstrip constructed by RT/duroid®

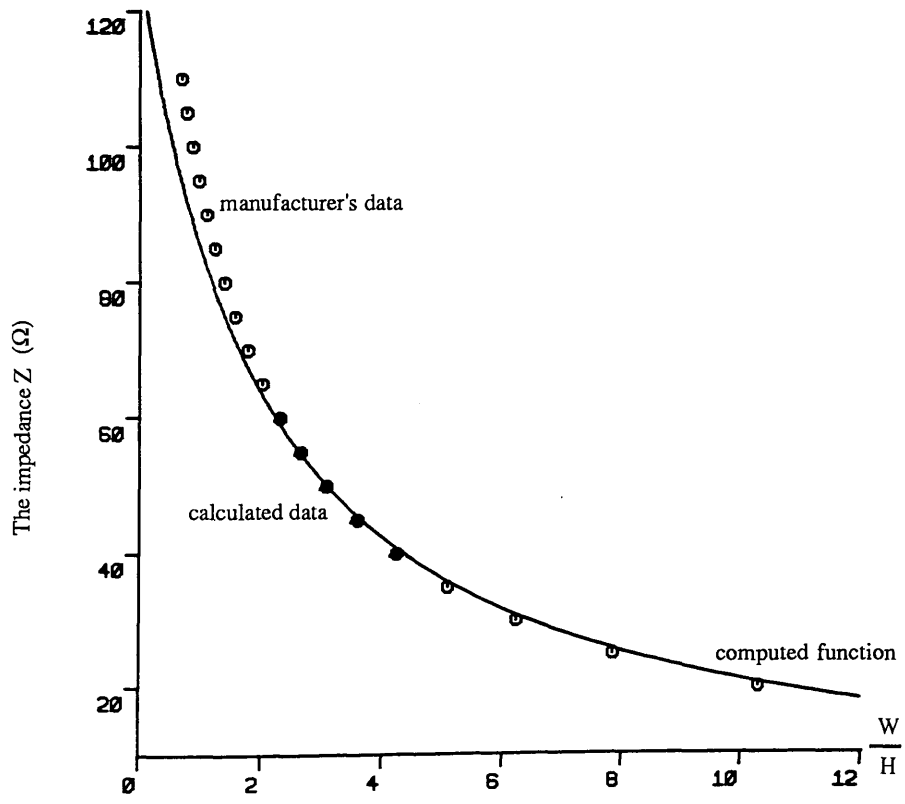

Fig. III.10- The variation of the impedance with the strip width (H = 1.59 mm, $\varepsilon_r = 2.2$), microstrip constructed by RT/duroid®

III. 6- Literature review:

In recent years, a number of authors have considered the properties of dielectrics in transmission lines. Attention have been devoted improving the significant losses of sensitivity due to the characteristic impedance and thickness of the strip and the dielectric substrate.

Welch and Pratt, (1966) discussed losses in microstrip transmission systems for integrated microwave circuits. Microstrip attenuation due to lossy dielectric substrate, α_d, which was calculated by Assadourian and Rimai, (1952) (Eq.III.9). These equations have been improved and verified by Welch and Pratt "the effective filling factor", q, was used giving encouraging results.

$$\alpha_d = \left[\frac{\mu}{\varepsilon}\right]^{\frac{1}{2}} \frac{\sigma_d}{2} \qquad \text{(III.9)}$$

where σ_d is the conductivity, μ is the permeability and ε is the permittivity of the dielectric substrate; α_d is independent of the geometry of the microstrip.

The effective dielectric constant (ε_{eff}) has a value intermediate between the dielectric constant of the substrate (ε) and the dielectric constant of the surrounding medium. For this calculation an "effective filling factor",q, (Wheeler, 1965) has been introduced.

$$q = \frac{\varepsilon_{eff} - \varepsilon_o}{\varepsilon - \varepsilon_o} \qquad \text{(III.10)}$$

$$\varepsilon_{eff} = q\varepsilon + (1 - q)\varepsilon_o \qquad \text{(III.11)}$$

The final expression of the attenuation is given by:

$$\alpha'_d = q\left(\frac{\varepsilon}{q\varepsilon + (1-q)\varepsilon_o}\right)^{\frac{1}{2}} \alpha_d \qquad \text{(III.12)}$$

Simpson and Tseng, (1976) presented a different technique of calculating the dielectric loss in microstrip lines. This technique is based on an extension of the moment method which has been used widely to calculate other microstrip characteristics such as impedances. The numerical analyses of the attenuation constant (Eq. III.8) were compared with theoretical data using different methods of calculation (Schneider, 1969) and were also compared with experimental data from Hyltin, (1965). Simpson and Tseng presented a theory for analysing the behaviour of the microstrip lines. Experimental measurements of the attenuation constant have been done to verify the theory. These measurements agreed well using the equation below.

$$\alpha = \frac{\frac{\sigma}{2}\int E^2 \, ds}{2P} \qquad \text{(III.13)}$$

where $P = \frac{1}{2}\frac{V^2}{Z_o}$ is the total power.

Kumar et al., (1976) presented a method for the calculation of the characteristic impedance of microstrip by evaluating the associated capacitance. They compared the numerical results to the experimental results given by Kaupp, (1967). Kumar et al., developed basic equations for the characteristic impedance which is just the characteristic impedance of a wire-over-ground transmission line, Eq. III.9 and for the effective relative permittivity constant determined through the signal propagation delay of the lines, Eq. III. 10.

$$Z_o = \frac{60}{\sqrt{\varepsilon_r}} \operatorname{Ln} \frac{4h}{d}; \qquad h >> d \qquad \text{(III.14)}$$

where h is the dielectric substrate thickness and d is the strip thickness.

$$T_d = \sqrt{\mu\varepsilon} \qquad \text{(III.15)}$$

$$T_d = 1.016\sqrt{\varepsilon_r} \qquad \text{(III.16)}$$

$$\varepsilon_{r_{eff}} = 0.475\,\varepsilon_r + 0.67 \qquad \text{(III.17)}$$

where $\varepsilon_{r_{eff}}$ and ε_r are the effective relative permittivity and the relative permittivity respectively.

Figure III.11 shows the variation of the characteristic impedance with the strip width and the dielectric thickness (data collected from Kumar et al., 1976 and Kaupp, 1967) at 25 MHz. The relative permittivity of the dielectric substrate is about 4.7, the foil (strip) thickness is about 0.7112 mm and the dielectric substrate thickness is in the range of 2.032 to 17.016 mm. It can be seen that the characteristic impedance decreases gradually as the ratio of the strip width with the dielectric substrate thickness, $\frac{w}{H}$ increases. For large values range of the strip width the characteristic impedance is very low.

Pucel et al., (1968) proposed approximate expressions for the conductor losses extending to a wide range of geometrical parameters and applicable only to the microstrip on the dielectric substrate. They considered dielectric losses in the substrate, ohmic skin losses in the strip conductor and the ground plane. The analyses of the dielectric losses were based on Welch and Pratt expressions used with their formulae for skin loss attenuation. It showed that the experimental data is in agreement with the results from the technique used for measuring low attenuation losses. Wheeler, (1965) discussed the improvement in the numerical calculation (Wheeler, 1964) of the relation between the transmission line properties, such as wave resistance and the shape ratio (strip width over separation). This relation depends on the dielectric constant of the sheet material. Two shape ratios characterised by strips "wide" or "narrow" width relative to their separation have been considered. It has been found possible to compute the effective dielectric constant to a fair accuracy by choosing the shape ratio and the dielectric constant of the material.

Horton et al., (1971) discussed the variation of microstrip losses with thickness of strip. The losses were calculated for a variety of frequencies and

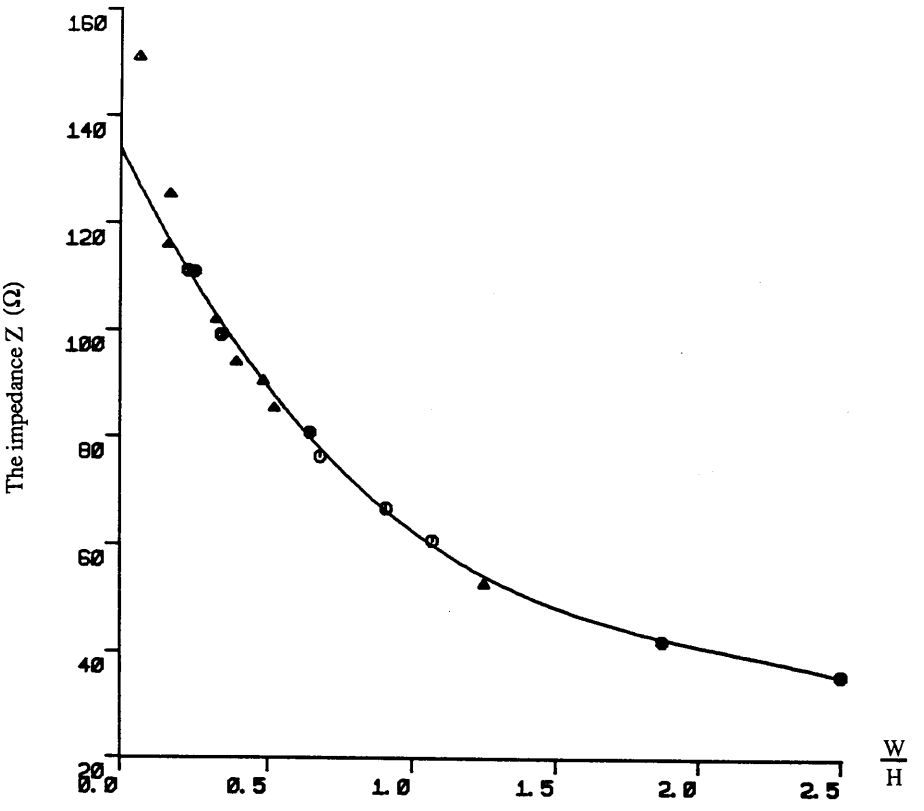

Fig. III.11- The variation of the impedance with the strip width and the dielectric thickness (2.032 mm < H < 17.016 mm, $\varepsilon_r = 4.7$)

Kaupp, 1967

o Kumar et al., 1976

• Kaupp and Kumar et al.

$\frac{w}{H}$ = 0.5, 1.0 and 2.0; the relative permittivity of the dielectric substrate ε_r was taken as 11 They concluded that the selection of thickness can improve the quality factor of the lines by as much as 10%. Gunston and Weale, (1969) discussed the variation of the characteristic impedance of single and coupled microstrip with strip thickness, operating at 1 GHz. They considered the foil (strip) and the dielectric substrate thickness t and H respectively in combination, the range of $\frac{t}{H}$ is 0.01 to 0.05 for the relative permittivity of the substrate *9.6* and 0.05 to 0.20 for the substrate permittivity *4.3*. The variation of the characteristic impedance with the foil thickness t is so small as to be negligible. It has been concluded that the finite thickness of the strip must be taken into account when evaluating circuit performance. John and Arlett, (1974) discussed the behaviour of the characteristic impedance and the effective relative permittivity using the above equations where the permittivity is independent of the strip width and the dielectric substrate thickness.

Caulton et al., (1966) presented a study of the properties of microstrip lines. The theoretical design data based on the work of Wheeler, (1965), were consistent with measurements of characteristic impedance, wavelength, and attenuation constant. Bahl and Garg, (1977) presented an accurate closed form expression for the variation of characteristic impedance and effective relative permittivity constant of microstrip with finite strip thickness. It has been found that the results for the characteristic impedance, Z_o, and the square root of the effective relative permittivity,$\sqrt{\varepsilon_{r_{eff}}}$, were correct to within 2% for $0 \leq \frac{t}{H} \leq 0.2,\ 0.1 \leq \frac{w}{H} \leq 20,$ and $\varepsilon_r \leq 16$. Their method is widely applied in the design of thick microstrips used in computers and thick film microwave integrated circuits.

The performance of microstrip and coupled microstrip transmission lines has been improved by a rigorous analysis of the phase constant, the characteristic impedance and the attenuation constant due to the dielectric losses of the lossy substrate (Assadourian and Rimai, 1952; Yamashika and Mittra, 1968; Bryant and

Weiss, 1968; Schneider, 1969; Williams and Schwarz, 1983; Mirshekar-Syahkal, 1983). It was also observed that the range of applicability of the above theory was based on the geometrical parameters. Finite thickness of the dielectric substrate is required in the microstrip transmission lines for microwave integrated circuits. The effect of loss and frequency dispersion on the performance of microstrip and coupled microstrip lines has been further studied by Rao, (1974) based on earlier studies by Johns and Bolljahn.

Gupta et al., (1979) described the numerical analyses of the behaviour of the microstrip lines at different frequencies with respect to attenuation constants, characteristic impedance, the effective relative permittivity and the standing-wave ratio. They compared the properties of microstrip transmission lines with published analysis.They considered in their analysis the effective filling factor, earlier considered by Welch and Pratt, (1966) to define the effective dielectric constant, ε_{eff} (Eq. III.11). The attenuation constant, Eq. III.13, has been used as well in their analysis.

Smith and Chang, (1980) extended the basic technique to the finite width dielectric microstrip transmission line through numerical analysis and experimental investigation. Further investigation for finite width has been modified to include modelling with ground plane as well as dielectric substrate (Smith and Chang, 1985). The computed characteristic impedance as a function of the $\frac{w}{H}$ ratio has been analysed for several values of strip width. Their numerical analysis showed that the finite width dielectric and ground plane can be used to predict the effect of ground plane truncation on the transmission characteristics of microstrip circuits. Chang and Klein, (1987) reported a technique for microstrip transmission line loss reduction using dielectric layers. Experimental results have shown that the loss can be substantially reduced by a proper shield. The variational method was used to calculate the effect of shielding on the effective dielectric constant and characteristic impedance. The theoretical calculation agreed very well with the experimental results. Cano et al., (1988) discussed the computation of the frequency dependence

of microstrip and unilateral thin lines on a biaxial substrate. They suggested that the theory might be useful in the design of microwave integrated circuits.

Leung and Balanis, (1988) considered the distortion of short pulses propagating along microstrip transmission lines. The dielectric substrates considered were isotropic materials with relatively high loss characteristics. Results showed that attenuation and dispersion distortions change with the strip width, substrate height, and substrate dielectric constant.

Standley and Cheung, (1988) studied the performance of some microstrip structures using superconducting materials. They found that at high temperature superconducting materials can be used to fabricate microwave circuits with very low insertion loss and high quality factor at frequencies of several giga hertz or higher.

The method used at the present work (Eq. III.1, Eq. III.4) shows good agreement with the manufacturer's data and are compared with the measurements of the characteristic impedance by Kumar et al., (1976) and Kaupp, (1967).

Chapter IV

Microwave thermography antennas

IV. 1- Introduction and literature review:

Microwave thermography antennas based on cylindrical and rectangular waveguides with various cross sections or on microstrip or similar techniques have been developed for use in direct contact with the skin at frequencies above about 200 MHz. The contact is not perfect as there is often a small air gap between the skin and the applicator. This must be kept small because the impedance mismatch to air could reduce the signal by an order of magnitude. Since the dimensions of these applicators can be made comparable with the wavelength, energy is largely transmitted into the tissue in a wave propagating from the aperture of the applicator.

For simplicity, applicators have often been designed as rectangular cross section waveguides and operated at a frequency 10% to 30% greater than the lowest frequency at which propagation can occur in the applicator or antenna. For a given operating frequency, the linear dimensions of an applicator may be reduced from those of an air-filled device if it is loaded with a suitable dielectric material. These simple applicators have approximately 60% of the aperture yet provide sufficient effective microwave energy. Applicators using different excitation and geometry which may achieve more uniform heating have been developed (Stuchly and Stuchly, 1978; Kantor and Witters, 1983; Vaguine et al., 1982; Lin et al., 1982). In particular, waveguide applicators with a ridged cross section offer a number of advantages (Paglione and Sterzer, 1981). Recently, Hand and Hind, (1986a) reviewed the design and performances of several types of waveguide applicators. Guy et al., (1978) presented a TE_{10}-*mode* waveguide applicator which consisted of a 12 $\times$ 6 cm waveguide with a 64 cm tapered section that increased its cross-

section to a 12 × 16 cm, loaded with aluminum-oxide sand (dielectric constant approximately 4). These applicators have been used for electromagnetic heating at low frequencies where greater depth of penetration is obtained and at high frequencies where microwave energy can be focused on selected areas of the body. A 13 cm square waveguide applicator with stripline feed was designed by Guy, (1978) to produce an even temperature distribution with the highest temperatures in the muscle. A light weight dielectric matching material was used which was porous and allowed for air flow (2.5 cm thick Echo foam, HiK Flex dielectric, 4.0).

Microwave applicators based on microstrip or related techniques can offer a number of advantages including small size, light weight, the ability to conform to the tissue surface and flexibility of radiation pattern. Mendecki et al., (1979) described a 2.45 GHz printed circuit antenna loaded with dielectric powder which could conform closely to tissue contours. A microstrip ring applicator was reported by Bahl et al., (1980b) and Bahl, (1982) described a microstrip loop antenna. The operating frequency, bandwidth and heating characteristics of microstrip applicators can depend critically on the load presented to them (Bahl and Stuchly, 1980a; Sandhu and Kolozsvary, 1983) although predictable performance can be achieved if a suitably thick bolus is used. Johnson et al., (1984) developed a series of low profile applicators which are relatively insensitive to tissue load. They consist of resonant patches sandwiched between dielectric slabs and operated at frequencies between 200 MHz and 915 MHz. By incorporating ferrite material into this type of applicator, an operating frequency as low as 27 MHz can be achieved and for microwave frequencies this material can be used (Johnson et al., 1985). Sandhu et al., (1977) designed two types of applicators operating at frequencies of 915 and 2450 MHz. The applicator is essentially square cross section waveguide closed at one end and open at the application end. The waveguide is excited in the TE_{10}-*mode*, using a coaxial line probe antenna. The 915 MHz applicator waveguide is loaded with low-loss dielectric material (Hik-Eccoflo and Hik-Stycast from Emerson and Cummings, including MA 02021) with a dielectric constant $\varepsilon = 6.0$.

It is found that it is capable of producing fairly uniform (± 0.5 °C) heating up to a depth of 3 cm. Tanabe et al., (1983) described a microstrip spiral antenna which offers good coupling, broad bandwidth and a circularly symmetrical treatment field. Henderson et al., (1988) presented a microstrip circular antenna which offers limited scanning beam. These authors have developed a 915 MHz array of such applicators designed to heat large areas of the chest wall. An array of rectangular patch radiators designed for the same purpose was reported by Sandhu and Kalozsvary, (1984). The dependence of heating characteristics on the size and operating frequency of applicators has been discussed by several authors (Guy, 1971b; Tuner and Kumar, 1982; Hand and Johnson, 1986b); in general, applicators small in relation to the wavelength exhibit relatively poor penetration.

IV.2 Microwave antenna response function:

Consider an antenna in contact with a lossy material of the same impedance and connected to a terminating resistor by a lossless transmission line which is also impedance matched to the antenna. If the system is in thermodynamic equilibrium at uniform temperature T, then the terminating load, being a resistor at temperature T, radiates an average power of KT watts per unit bandwidth through the transmission line and into the lossy material. The condition of thermodynamic equilibrium requires that the antenna must also receive KT watts per unit bandwidth from the lossy material. If the antenna, transmission line and load are at a temperature different from the lossy medium the antenna must still receive the same power per unit bandwidth. the power per unit bandwidth, P, received by the antenna may also be expressed as:

$$P = \frac{1}{2} \int_V I_\nu (\underline{r})\, P_n (\underline{r})\, dV \qquad \text{(IV.1)}$$

where $I_\nu (\underline{r})$ is the intensity of the radiation emitted by the volume element dV at

position $\underline{r}$, with origin at the position of the antenna. $P_n(\underline{r})$ is the normalized power response pattern of the antenna given by:

$$P_n(\underline{r}) = \frac{P(\underline{r})}{\max(P(\underline{r}))} \qquad \text{(IV.2)}$$

and is referred to as the antenna pattern. The factor $\frac{1}{2}$ in Eq. IV.1 arises because the radiation is of an incoherent, unpolarized nature and, because any antenna is responsive to only one polarisation component, only half of the incident power is received.

By the reciprocity theorem (Slater, 1942) the transmitting and receiving power patterns of an antenna are identical. This means that the power dissipated in a volume element when the antenna is radiating into lossy medium is proportional to the power received from that volume element when the antenna is receiving. The power, P, dissipated in a subvolume dV is given by:

$$P = \frac{1}{2}\sigma |E_o|^2 dV \qquad \text{(IV.3)}$$

where σ is the conductivity ($\Omega^{-1}m^{-1}$), and $\underline{E} = \underline{E}_o e^{i\omega t}$ is the electric field.

The receiving power response pattern must be proportional to this and so

$$P_n(\underline{r}) = A|\underline{E}(\underline{r})|^2 \qquad \text{(IV.4)}$$

where A is a constant of proportionality.

From Eq. IV.4 the intensity of radiation emitted in the region of the Rayleigh-Jeans Law by a small thickness, dz, of homogeneous material is given by:

$$I_\nu(\underline{r}) = \frac{2\nu^2 k T(\underline{r})}{c^2} 2\alpha\, dz \qquad \text{(IV.5)}$$

Using Eq. IV.2 and IV.3 in Eq. IV.1 we have:

$$P = \frac{\nu^2 k}{c^2} A \int_V 2\alpha T(\underline{r}) |E(\underline{r})|^2 dV \qquad \text{(IV.6)}$$

For a uniform temperature T it has already been stated from thermodynamical considerations that the power received per unit bandwidth is proportional to KT and so we must have:

$$\frac{\nu^2 A\, 2\alpha}{c^2} \int_V |E(\underline{r})|^2 dV = 1 \quad \text{or} \quad \frac{2\alpha}{\lambda^2} \int_V P_n(\underline{r})\, dV = 1 \qquad \text{(IV.7)}$$

In general, for a lossy material, it is a difficult problem to determine theoretically the distribution $E(\underline{r})$. The antenna pattern, however, may be described approximately by an exponential variation in the direction of the central axis of the antenna in a single region of tissue, while the lateral response is considered to be uniform over an area of effective aperture size, A_e, and zero outside this area.

$$\begin{cases} P_n(\underline{r}) = e^{\frac{z}{\delta'}} & \text{if } (x,y) \in A_e \\ = 0 & \text{if } (x,y) \notin A_e \end{cases} \qquad \text{(IV.8)}$$

where δ' is the effective power penetration depth which is related to the effective field attenuation constant, α, by the equation:

$$\delta' = \frac{1}{2\alpha} \qquad \text{(IV.9)}$$

This is the normalized power pattern having a maximum value of 1 at z = 0 and for this form of the power pattern Eq.IV.7 requires that,

$$A_e = \frac{\delta}{\delta'}\lambda^2 \qquad \text{(IV.10)}$$

where δ is the plane-wave penetration depth.

The effective power penetration depth must always be less than the plane-wave power penetration depth (discussed in more detail in Chapter VII and VIII).

IV.3- Microwave radiometer antenna pattern:

The microwave radiometer antenna pattern gives the contribution of a small volume element of the tissue to the total signal. It is a difficult problem to calculate theoretically the antenna pattern, which depends on several parameters such as the operating frequency, dimensions and geometry of the guide, dielectric loading of the guide and dielectric properties of observed tissue as well as on the geometry of the tissue.

The antenna pattern may be determined either theoretically by numerical methods, in which case the tissue geometry is usually assumed to be in planar layers, or experimentally using dielectric phantom materials simulating the dielectric properties of the tissue (more detail in Chapter VIII).

Table IV.1 illustrates a number of direct contact antennas used in clinical microwave thermography. The most commonly used contact antenna for clinical application is a dielectric filled rectangular waveguide antenna operating in TE_{10}-mode. It is most important that the dimension of the antenna be less than the wavelength corresponding to the cut-off frequency.

Table IV.1- Direct contact antennas used in clinical microwave thermography.

Frequency (GHz)	Antanna	dimensions (cm)	ε'_r	reference
3.3	Rect. waveg.	2.3 × 1.0	11	Barrett, 1977
1.3	Rect. waveg.	2.3 × 1.0	30	Myres et al., 1979
6.0	Rect. waveg.	2.3 × 1.0	2	Myres et al., 1979
4.7	Rect. waveg.	1.83 × 0.92	9.8	Carr et al., 1982
3.0	Rect. waveg.†	2.2 × 1.1	25	Enel et al., 1984
1.5	Rect. waveg.†	3.3 × 1.65	25	Boquet, 1989
1	Rect. waveg.	10 × 4.3	9	Mamouni, 1989
1	Rect. waveg.	6 × 2.9	25	Mamouni, 1989
3	Rect. waveg.	3 × 1.5	9	Mamouni, 1989
3	Rect. waveg.	2 × 9.5	25	Mamouni, 1989
3	Rect. waveg.	5 × 2.4	4	Mamouni, 1989
9	Rect. waveg.	1.1 × 0.6	4	Mamouni, 1989
0.915	Rect. waveg.	12 × 6	4	Guy, 1978
1.1, 2.6, 4.0, 5.5	T.R. waveg.*	~ 4.8 × 2.2 ~ 2.3 × 1.0	6	Bardati et al., 1987
0.915	Sq. waveg.	13 × 13	4	Guy, 1978
2.6 - 3.95	Sq. waveg.	7.6 × 7.6	10	Stuchly, 1978
2.45 ± 0.05	Cir. waveg.	15.2 (ø)	?	Kantor et al., 1978
2.45	Cir. waveg.	8.0 (ø)	10	Stuchly et al., 1980
9.6 - 10	Cir. waveg.	2.7 (ø)	10	Stuchly et al., 1980
3.2	Cir. waveg.	2.5 (ø)	12	Land, 1987

†- *6 antennas arranged in a 2 ×3 grid to form a multi-probe.*

* - *multi-frequency radiometry system.*

T.R. - *Truncated rectangular, Rect. waveg. - rectangular waveguide, Sq. waveg. - square waveguide, Cir. waveg. - circular (cylindrical waveguide*

An increase in the dielectric constant of the waveguide filling requires a reduction in the dimensions of the guide in order to restrict propagation to the TE_{10}-mode. This means that the guide dimensions are determined within certain limits by the type of dielectric loading if multi-mode propagation is to be avoided. The dielectric loading of the guide and the waveguide dimensions also determine the transverse- wave impedance of the guide. The impedance mismatch at the antenna/tissue interface causes a reflection of the radiation signal from the tissue and it is desirable that this reflection should be minimized.

IV.4- Dielectric properties of tissues:

To design and assess the performance of electromagnetic devices for clinical applications one must first consider the magnetic and electric properties of tissues. A brief summary of the biological tissues which are non-magnetic and have a permeability equal to that of free space ($4\pi 10^{-7}$ Hm^{-1}) has been reported in this chapter. The interaction with electric fields is determined by the permittivity which may be expressed in complex form as:

$$\varepsilon^* = \varepsilon_o (\varepsilon' - i \varepsilon'') \qquad \text{(IV.11)}$$

where ε', the dielectric constant, is a measure of the energy which may be stored in the tissue, and ε'', the loss factor, is a measure of the energy dissipated by the medium.ε_o, the permittivity of free space, is 8.854×10^{-12} Fm^{-1}. The loss factor ε'' is often expressed in terms of the electrical conductivity σ and the frequency of the electromagnetic field f. Thus:

$$\varepsilon'' = \frac{\sigma}{2\pi f \varepsilon_o} \qquad \text{(IV.12)}$$

The high frequency electric field interacts with the tissue by producing a

drift of free electrons and ions, polarisation of atoms and molecules and rotation of dipole molecules. The electric field in the tissue, $\underline{E}$, gives rise to a conduction current $\underline{J}_c$.

$$\underline{J}_c = \sigma \underline{E} \tag{IV.13}$$

the interaction related to the bound charges gives rise to a frequency dependent displacement current, $\underline{J}_d$,

$$\underline{J}_d = \frac{\partial (\varepsilon' \underline{E})}{\partial t} \tag{IV.14}$$

the relationship between the conduction loss and the dielectric loss is:

$$\frac{\underline{J}_c}{\underline{J}_d} = \frac{\sigma}{2\pi f \varepsilon_o \varepsilon'} = \frac{\varepsilon''}{\varepsilon'} \tag{IV.15}$$

this is known as the loss tangent *(tanδ)*.

The local absorbed power density at a point *(x,y,z)* in tissue is defined by:

$$P = \frac{\sigma E_{xyz}^2}{2} \tag{IV.16}$$

where E_{xyz} is the magnitude of the electric field at that point. In hyperthermia the specific absorption rate *(SAR)* is often used, where

$$SAR = \frac{\sigma}{\rho} \frac{E_{xyz}^2}{2} \tag{IV.17}$$

where ρ is the tissue density (Kgm^{-3}).

Penetration of electromagnetic fields into tissues is often described in terms of the plane wave penetration depth δ. This is the distance through a uniform medium after which the magnitude of the E-field of a plane electromagnetic wave is reduced by a factor e^{-1}, and is given by:

$$\delta = \frac{2c}{\omega\left(\sqrt{\varepsilon'^2 + \varepsilon''^2} - \varepsilon'\right)^{\frac{1}{2}}} \qquad \text{(IV.18)}$$

The absorbed power density is reduced to approximately 13.5% within this distance.

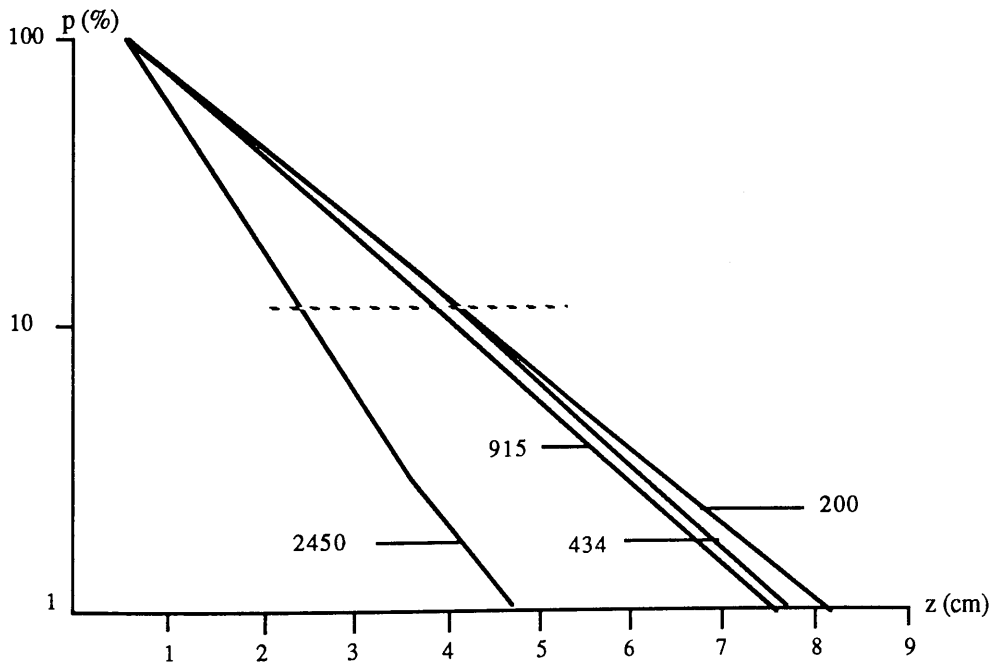

Fig. IV.3- Frequency dependence of penetration into uniform muscle from applicator with 10 cm × 10 cm aperture. p is the absorbed power density normalized to the peak value at depth z = 0.5 cm.

The above figure shows the frequency dependence of penetration into a semi infinite homogenous medium (muscle) from a TE_{10}-mode applicator with a 10×10 cm aperture. The values of E_y^2 (proportional to specific absorption rate), normalized at 5 mm from the plane of the aperture, are plotted against distance from the aperture along the central axis perpendicular to the plane of the aperture. The distances over which E_y^2 is reduced by a factor of e^{-2} "the effective penetration depths" are less than the plane wave penetration depths at each of the frequencies considered.

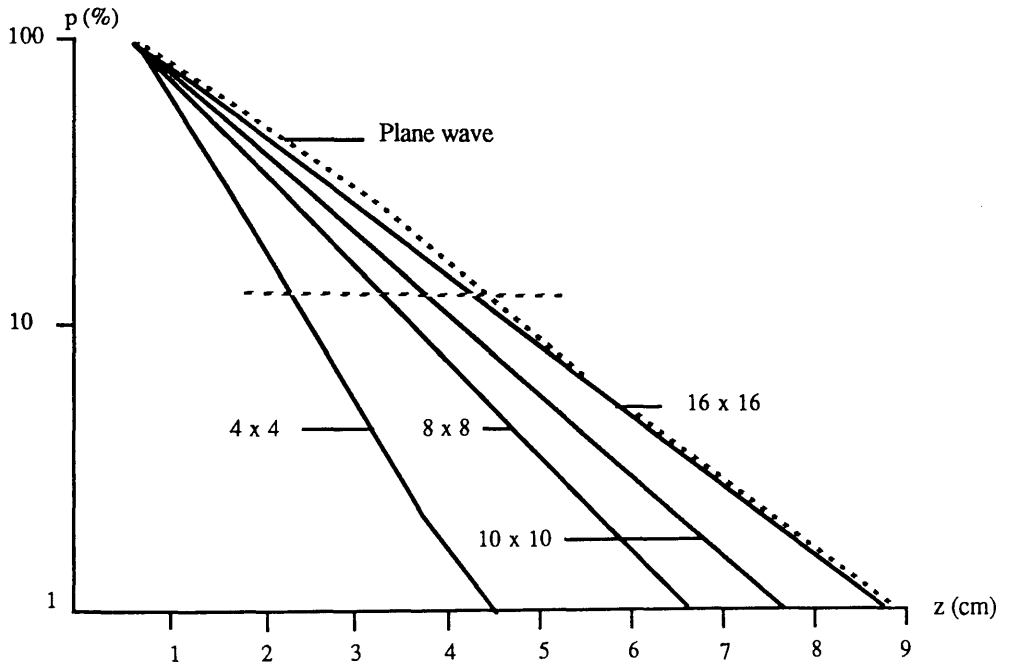

Fig. IV.4- Penetration into uniform muscle from 434 MHz applicators fro various aperture sizes. p is the absorbed power density normalized to the peak value at depth z = 0.5 cm.

The above figure shows the results of similar calculations for TE_{10}-mode applicators with various size apertures operating at 434 MHz. The effective penetration depth decreases as the size of the applicators is reduced and, for apertures small compared with the wavelength in the medium, becomes quite sensitive to aperture size.

A common feature of direct contact applicators is that energy is transmitted

from the waveguiding structure to the tissue in the form of propagating wave. The wave propagation within hollow cylindrical waveguides can take place only if certain relationships between the dimensions of the waveguide and the operating frequency are satisfied. Before discussing the characteristics of particular applicators, the existence of different types of guided electromagnetic wave should be noted.

IV.5- TEM-mode waveguide:

Transverse electromagnetic waves *(TEM)* are those in which there is no component of electric or magnetic field in the direction of propagation, the electric and magnetic fields lie totally in the transverse plane. Although such waves may propagate along a system of two or more conductors (along a coaxial line), they cannot exist within uniform hollow cylindrical guides. Waves which can propagate within such guides have either an electric or magnetic field component in the direction of propagation. Those with magnetic field component in this direction and with electric fields restricted to the transverse plane are known as Transverse Electric waves *(TE)* whilst those with an electric field component in the direction of propagation and only a transverse magnetic field are referred to as Transverse Magnetic waves *(TM)*. Boundary conditions make it desirable that electric fields should be predominantly parallel to skin surface and tissue interface and so applicators are usually designed to support propagation of *TE* waves.

IV.5.1- Rectangular TE-mode waveguide antennas:

Many direct contact applicators are based on waveguides with rectangular cross section. To obtain components of the electric field for *TE* waves in the co-ordinate system shown in the Fig. IV. 1, Maxwell's equations must be solved subject to boundary conditions at the walls of the applicator which are assumed to be perfectly conducting. The electric field components (Johnk, 1975) are:

$$E_x = \left[\frac{j\omega\mu}{h^2} \frac{n\pi}{b} A \right] \cos\left(\frac{m\pi x}{a}\right) \sin\left(\frac{n\pi y}{b}\right) \underline{i} \qquad \text{(IV.19)}$$

$$E_y = \left[\frac{-j\omega\mu}{h^2} \frac{n\pi}{a} A \right] \sin\left(\frac{m\pi}{a} x\right) \cos\left(\frac{n\pi}{b} y\right) \underline{j} \qquad \text{(IV.20)}$$

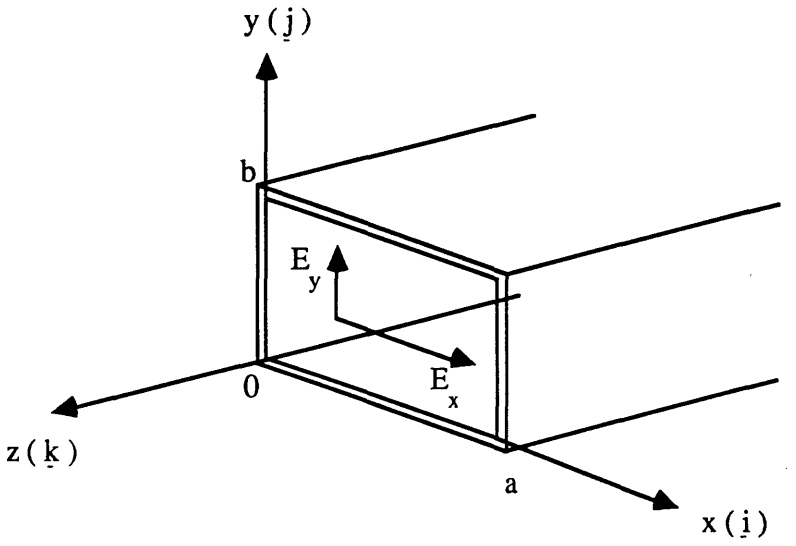

Fig. IV. 1- Coordinate system for applicator with rectangular cross section.

with the propagation constant $\gamma_{mn} = \sqrt{\left(\frac{m\pi}{a}\right)^2 + \left(\frac{n\pi}{b}\right)^2 - \omega^2\mu\varepsilon}$

$h^2 = \gamma_{mn}^2 + \omega^2\mu\varepsilon = \left(\frac{m\pi}{a}\right)^2 + \left(\frac{n\pi}{b}\right)^2$ and A is a constant; m and n are either integers or zero (but not both equal to zero). It has been assumed that the applicator contains dielectric material having permittivity ε and permeability μ and that the fields within it vary with z and t as $exp\ (j\omega t + \gamma_{mn} z)$. This transverse wave has m half sine variations in the x direction and n such variations in the y direction and propagation can occur only when the frequency is greater than the cut-off frequency $f_{c_{mn}}$ where:

$$f_{c_{mn}} = \left[\frac{1}{2\pi \sqrt{\mu\varepsilon}} \right] \sqrt{ \left(\frac{m\pi}{a} \right)^2 + \left(\frac{n\pi}{b} \right)^2 } \qquad \text{(IV.21)}$$

since for lower frequencies γ_{mn} becomes a real attenuation factor.

For rectangular applicators *(a > b)* the mode having the lowest cut-off frequency "the dominant mode" is TE_{10} for which:

$$f_{c_{TE_{10}}} = \left[\frac{1}{2a \sqrt{\mu\varepsilon}} \right] \qquad \text{(IV.22)}$$

It follows from the equation (IV.4) that wave propagation can take place in a rectangular applicator only when its largest dimension is greater than half the wavelength in an unbounded region of the medium used to load the applicator. Operation in the TE_{10}-mode can be ensured by choosing the dimensions of the applicator and operating frequency f such that f is typically 10% - 30% greater than $f_{c_{TE_{10}}}$. Linear dimensions may be reduced from those of an air filled device by loading the applicator with material of suitable dielectric constant. The performance of the applicator or antenna is also determined by the reflections which may occur at the applicator/tissue interface.

Table IV.2 illustrates some dielectric materials used for the microwave thermography antennas in order to achieve the reduction in dimensions required in medical applications . However, it should be remembered that as the aperture of an applicator is made smaller, the effective penetration depth is reduced significantly below that for plane waves at the same frequency (discussed in detail in Chapter VII).

A disadvantage of TE_{10}-mode applicators is that only approximately 60% of the aperture provides effective heating. Microwave applicators should provide: 1) the uniform heating of a specified volume; usually of muscle, with minimal heating of fat and skin; 2) uniform heating over a selected area in the plane parallel to the

applicator's aperture; 3) minimum leakage . Other applicators have been developed in attempts to achieve the above requirements. Multimode aperture type applicators have been designed and tested by Stuchly and Stuchly, (1978). TE_{10}- and TE_{30}-mode square waveguide applicators operated at *S* band, having the aperture dimensions 7.6 cm × 7.6 cm, and filled with low loss dielectric material of dielectric constant 10. Other designs incorporating inhomogeneously loaded waveguides, ridged waveguides and circular waveguides have been considered. (see later).

Table IV.2- Properties of some commercially available dielectric materials.

Material	Form	Dielectric constant	tanδ	Density (g cm-3)	Manufacturer
DA-9 Alumina	*	9.5 ± 3%	1×10^{-4}	3.9	TT
D-15 Mg-Ti	*	15 ± 3%	2×10^{-4}	3.5	TT
D-30Ni-Al-Ti	*	31 ± 5%	2×10^{-4}	4	TT
D-100 Titania	*	96 ± 5%	1×10^{-3}	4	TT
Magnesium Calcium Titanates	*	14 to 140 ± 5%	2×10^{-3}	3.5 to 3.8	TT
Silastic 9161 RTV	+	4.0	7×10^{-3}	1.6	DC
Sylgard 186	+	3.0	1×10^{-3}	1.1	DC
Eccoflo HiK	•	2 - 5 - 12.0	$4\text{-}7 \times 10^{-3}$	1.6-2.7	EC
Stycast HiK 500F	†	3 - 12 ± 3%	2×10^{-3}	2.2	EC
Stycast 35	**	1.9 - 5	$5\text{-}9 \times 10^{-4}$	0.7-2.3	EC
Stycast HiK Castable	**	6 - 19	1×10^{-3}	2-3	EC
Eccofoam HiK	◊	1.1 ± 10% to 6 ± 7%	1×10^{-3} to 3×10^{-2}	0.8	EC

TT = Trans-Tech; DC = Dow Corning; EC = Emerson & Cuming.

** - solid-bars; † - solid sheets, rods or bars; + - castable silicone elastomer; ** - casting resin; ◊ - open cell foam sheet; • - powder.*

IV.5.2- Circular TE-mode waveguide antennas:

For applicators of circular cross section with radius a (Fig.IV.2) the electric field components for TE waves expressed in cylindrical co-ordinates (Ramo et al., 1965) were:

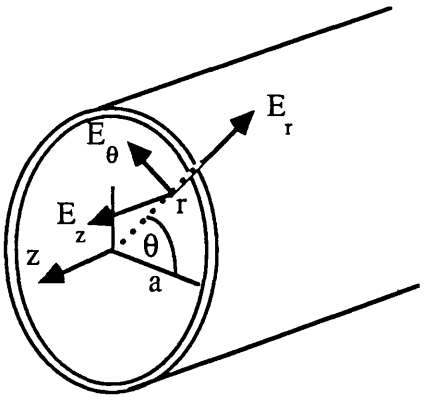

Fig.IV.2- Coordinate system for applicator with circular cross section

$$E_r = \left[\frac{j\omega\mu}{h^2} \frac{n}{r} A \right] J_n (hr) \sin (n\phi)\, \underline{r} \qquad \text{(IV.23)}$$

$$E_\phi = \left[\frac{j\omega\mu}{h} A \right] J_n' (hr) \cos (n\phi)\, \underline{\phi} \qquad \text{(IV.24)}$$

where $h^2 = \gamma_{mn}^2 + \omega^2\mu\varepsilon$; γ_{mn} is the propagation constant; $J_n(hr)$ is a Bessel function of order n and $J_n'(hr)$ is its derivative with respect to (hr).

For this TE wave, the integers 1 and n describe the number of radial and circumferential variations across the aperture.

The cut-off frequency $f_{cTE_{n,1}}$ is given by:

$$f_{c_{TE_{n,1}}} = \frac{\rho_{n,1}}{2\pi a \sqrt{\mu\varepsilon}} \qquad \text{(IV.25)}$$

where $\rho_{n,1}$ is the nth root of $J_n'(ha) = 0$.

The dominant mode is TE_{11} for which $\rho_{11} = 1.84$ and so, the cut-off frequency is

given by:

$$f_{c_{TE_{11}}} = \frac{1.84}{2\pi a\sqrt{\mu\varepsilon}} = \frac{0.293}{a\sqrt{\mu\varepsilon}} \qquad \text{(IV.26)}$$

Thus wave propagation can take place in a circular cylindrical applicator only when the radius is greater than about 0.3 × free space wavelength. The cut-off frequency for the next higher mode (TM_{01}) is $1.305\, fc_{TE_{11}}$.

Several circular direct contact applicators have been published. Kantor and Witters, (1983) describe two circular polarised applicators for use at 915 MHz which give symmetrical heating patterns and are designed to produce low levels of stray radiation. The circular applicator can be readily modified to minimise leakage fields (Stuchly and Stuchly., 1980; Neelakantaswamy and Rajaratnam, 1982). A TE_{11}-mode applicator with a variable aperture for operation at 430 MHz is described by Vaguine et al., (1982) whilst Lin et al., (1982) have developed an applicator consisting of three concentric circular cylinders. The TE_{11}-mode is supported between the inner and middle cylinders. However, the TE_{21}-mode (or a TE_{11}-mode at a different frequency) can propagate between the middle and outer cylinders. The inner cylinder can be used to introduce a cooling agent to the skin or ionising radiation if simultaneous hyperthermia and radiotherapy are prescribed.

IV.6- Dielectric properties of tissue at 3 GHz:

Several authors have considered the dielectric behaviour of tissue and attempted to relate the water content to the dielectric properties (Schwan and Foster, 1977; Schepps and Foster, 1980; Foster et al., 1980). Dielectric properties vary greatly with the tissue type and with the frequency. Tissues may be divided into two main categories, high water content tissue, such as muscle and skin and low water content tissue, such as fat and bone. The values of measured dielectric properties of tissue have been tabulated by Stuchly and Stuchly, (1980); by Foster and Schwan, (1986); and, more recently, by Campbell*. The difference in complex

* - *PhD thesis in preparation.*

permittivities between the same tissues from various non-aquatic mammals is small in the frequency range 0.1 to 10 GHz (Stuchly and Stuchly, 1984) compared to fat tissue. The difference between measurements using excised (in vitro) or living (in vivo) tissues (Foster and Schwan, 1986) is also small. Any consistent difference due to either of these factors is indistinguishable among the variations due to tissue heterogeneity.

The values of measured dielectric properties of human tissue at 3 GHz and 37 °C, in vitro, as compiled from the literature, are given in Table IV.3, together with calculated plane wave power penetration depths.

The study of Guy, (1971a) and the theoretical studies of Tuner and Kumar, (1982); Nilson, (1984); and Plancot, (1983) show that aperture dimensions should be greater than half a wavelength (in the medium) to avoid excessive power absorption in the superficial tissues and generally no greater than two wavelengths to avoid higher order heating patterns. Although simple plane layered models are useful for predicting the performance of applicators when the radius of curvature of the tissue is considerably greater than the wavelength, they are unable to account for the effects of geometry which may become significant when the radius of curvature is comparable with or less than the wavelength. Ho et al., (1971) analysed the power absorption due to TE_{10}-mode aperture sources (433 to 2450 MHz) in contact with triple layered cylinders which simulated human limbs. The heating produced in the fat region relative to that in muscle was minimized when the height of the aperture was equal to one wavelength in the fat. Authors mentioned in Chapter II used different types of waveguide for different frequency ranges and aperture sizes. The frequency range from,10 MHz to 10 GHz, was covered in this study.

Table IV.3- Dielectric properties of human tissues and organs at a frequency of 3 GHz and 37 °C.

Tissue Type	ε'	ε''	σ (sm^{-1})	2α (m^{-1})	δ (mm)	Reference
Whole Blood						
	56	16.18	2.7	136.02	16.90	Jenkins et al., 1989
	53	14.98	2.5	129.46	17.77	England, 1950
	60	19.77	3.3	160.61	14.32	Stuchly and Stuchly, 1980
	58	17.38	2.9	143.56	16.02	Stuchly and Stuchly, 1980
	56	16.18	2.7	136.02	16.90	Stuchly and Stuchly, 1980
	55-56	15-18.6	2.5-3.1	127-156.2	15-18	Herrick et al., 1950
	56	15.9	2.65	133.5	17.2	Cook, 1952
Bone						
	8.4	1.32	0.22	28.62	80.04	Cook, 1951
	7.5	1.0	0.17	23.40	98.30	Herrick et al., 1950
Bone Marrow	4.2-5.8	0.72-1.4	0.12-0.23	22.07-36	64-104	Herrick et al., 1950
Brain	32	17.38	2.9	193.27	11.90	Lin, 1975
Breast Carcinoma	62	14.98	2.5	119.70	19.22	England et al., 1949
	57	17.98	3.0	149.80	15.35	
Fat						
Breast	3.9	0.90	0.15	28.64	80.32	Cook, 1981
Abdonimal wall	4.9	1.44	0.24	40.87	56.27	Cook, 1951
near faecal fistula	7.0	1.74	0.29	41.32	55.66	Cook, 1951

Tissue Type	ε'	ε''	σ (sm^{-1})	2α (m^{-1})	δ (mm)	Reference
Fat						
sole of foot	11.6	2.25	0.38	42.10	54.68	Cook, 1951
Breast	5.2	1.56	0.26	42.98	53.51	England, 1950
	7.2	1.74	0.29	40.74	56.45	England et al., 1949
	3.9-7.2	0.66-1.38	0.11-0.23	21-32.32	71-110	Herrick et al., 1950
Liver	42-43	12-12.2	2-2.04	116.34-117.28	19-20	Herrick et al., 1950
Muscle						
Soleus	51	17.98	3.0	158.37	14.52	Cook, 1951
Pectoralis major	50	17.38	2.9	154.62	14.88	Cook, 1951
" "	52	19.17	3.2	167.3	13.75	Cook, 1951
	45-48	13-14	2.2-2.3	124-125	18-19	Herrick et al., 1950
Ocular lens cortical		41	12.58	2.1	123.64	18.60
	Dawkins et al., 1981					
Skin						
Near faecal fistula	51	14.98	2.5	131.98	17.43	Cook, 1951
Breast	40	12.58	2.1	125.18	18.37	Cook, 1951
Instep sole	42	13.18	2.2	127.98	17.97	Cook, 1951
	41	16.78	2.8	164.86	13.95	England, 1950
	50	14.98	2.5	133.29	17.26	England et al., 1949
	52	16.78	2.8	146.39	15.71	England et al., 1949
	40-45	11.98-16.18	2-2.7	119.22-151.74	19.29-15.16	Stuchly and Stuchly, 1980

Chapter V

Microwave correlation radiometry Theory

V. 1- Introduction and the literature review:

Microwave correlation radiometry is a possible alternative technique to multi-frequency radiometry, discussed in Chapter II, for obtaining a measurement of the subcutaneous temperature gradient in living tissue. In its simplest form this technique consists of combining the outputs of two antennas feeding a microwave correlation radiometer. Microwave correlation is based on the coherent detection of noise, here presented as the correlated signal from the two antennas.

The use of microwave correlation radiometry may improve the sensitivity for disease detection by localization of the thermal gradient in the tissues (Leroy, 1982).

The coherence theory and its application to correlation radiometry has been discussed extensively in the literature and has been used in radio-astronomy since the 1950's and more recently in medical radiometry applications. Page, et al., (1953) presented a method for the measurement of auto- or cross-correlation functions. These functions performed by a correlator are delay, multiplication, and integration. Faris, (1967) discussed the sensitivity of a correlation radiometer for two cases. The first case related to the case of two different sources connected to opposite arms of a matched hybrid junction. The signals in each arm were applied to amplifiers, when the received signal at the output was the product of the two signals. The second case considered two identical amplifiers, with different effective temperatures. Faris analysed the effects of a differential time delay or a differential phase shift in the two radiometer channels. In both of these cases the

results are affected by a decrease in sensitivity. Ko, (1967) presented a theory for radio-astronomical measurements of partial coherence. It has been found that coherence functions were related to the spectrum, the brightness distribution, and the polarisation of the electromagnetic fields. Swensn and Mathur, (1968) derived the response of a two element radio interferometer to a coherent field, with no restriction on the bandwidth or antenna properties. These studies resulted in an improvement in spatial resolution in the far-field detection case appropriate to astronomy.

There has been considerable interest in the application of correlation radiometry to medical microwave thermography for diagnosis and therapy. Mamouni et al., (1981) described a method to achieve better control of the radiometrically varied tissue volume. This method was based mainly on the analyses of an interference pattern signal received from the applicator apertures of a volume V, it was the combination of two or more signal probes. These probes were placed in parallel (Fig. V. 1). Leroy, (1982) carried out the same technique using several probes to improve the volume of the scanned tissues. He found that the technique gave a high spatial resolution in the millimeter frequency ranges; but the penetration depth was comparatively poor (less than 1 mm). It is found that for high permittivity and very lossy materials, such as muscle, skin and brain, the penetration depth defined by an attenuation e^{-1} of the field on the axis of the probe is approximately that of the *TEM*. In other tissues, such as fat and bones, results are quite different and the signal measured is vastly different from the *TEM* case. Correlation thermography was further used by Mamouni et al., (1983) to improve techniques of microwave thermography for medical applications. They used two probes, "P_1" and "P_2", (TE_{10}-rectangular waveguide, 2.2 cm × 1.1 cm in dimensions with loading dielectric constant $\varepsilon' = 25$) connected to a correlator and in contact with lossy material to achieve better localization of the thermal gradients in the varied volume. This system helped to improve the correlator and simplify its operation. The outputs of the two probes were connected via a 180 ° hybrid to a

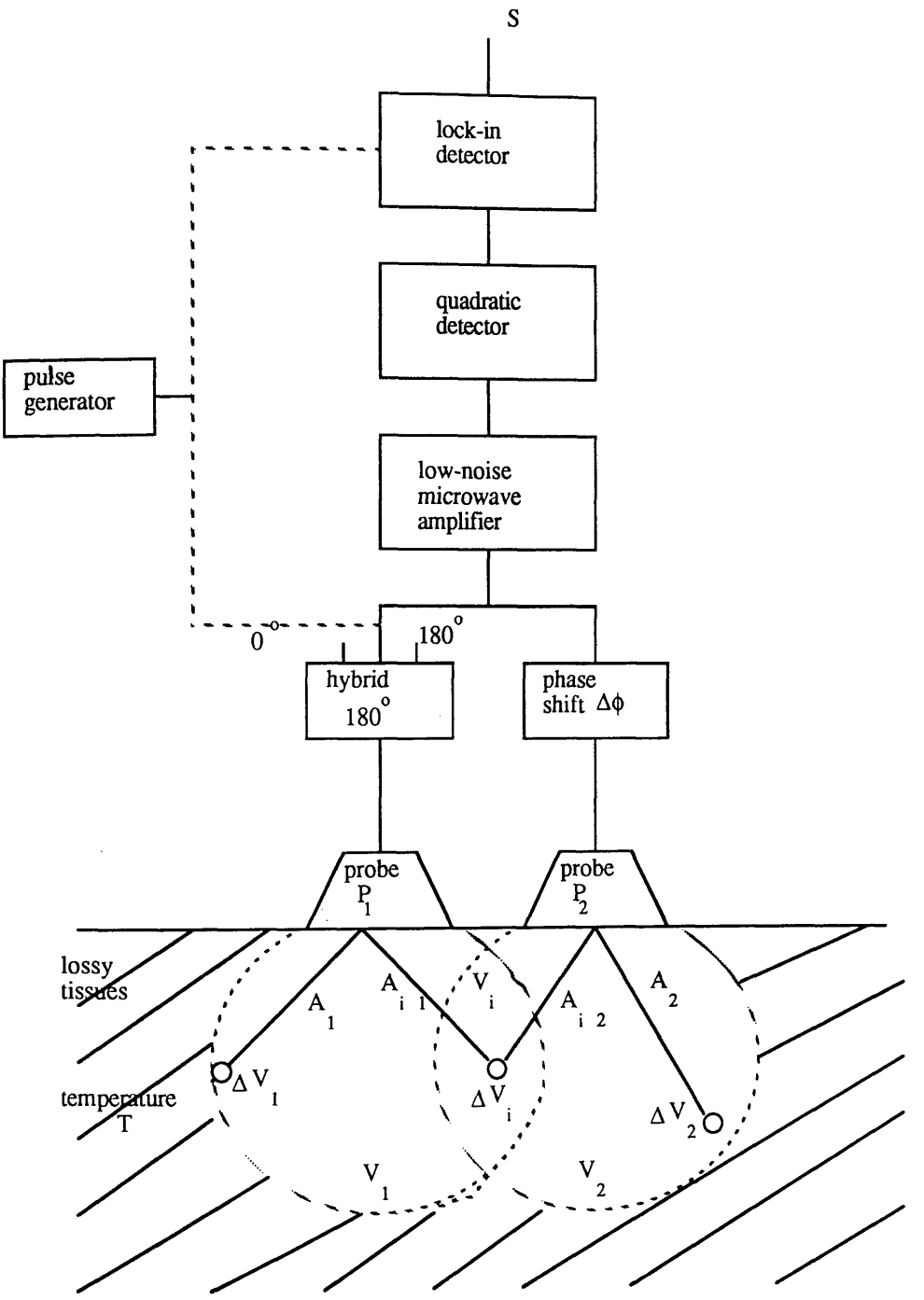

Fig. V.1 System of correlation radiometer
[from Mamouni et al., 1981]

noise source. The receiver consisted of a *S-band* low noise preamplifier followed by a heterodyne receiver and a numeric filter monitored by microprocessor. The resulting gain was about 70 dB with a noise factor about 7 dB. The bandwidth was 2.2 to 3.8 GHz (Fig. V.2). Mamouni et al., compared these results with classical single antenna thermography using the same probes and receiver and showed that the correlation volume processes have more selective output signals but the resultant signal amplitudes in microwave correlation radiometry are smaller than in the classical method.

Bellari et al., (1984b) studied the thermal structure associated with lossy materials using the correlation method. This consists of a coherent detection of the thermal noise, from two probes with 30° between their axes, which are connected to a microwave correlator. The output signal depends on the thermal emission of the volume scanned by both probes and on the delay times associated with the propagation of the noise signals in the lossy material and in the two branches of the correlator. The system used was a similar to Figure V. 1 except that it has been modified by the introduction of *S band* low noise amplifiers in the two branches of the correlator. The bandwidth was 2.6 to 3.4 GHz together with a noise factor of 4 dB led to a sensitivity better than 0.1 °C for a time constant of one second. The localisation of the thermal gradient was very noticeable as a function of the position of probes and was able to define its signal with an accuracy of nearly 1 mm corresponding to the closest possible spacing of the antenna mid-lines. Hill et al., (1985) discussed the cross-correlation of thermal radiation from two sources received by two antennas, at fixed distances from the sources and from another microwave correlation radiometer, in order to combine the spatial and thermal resolution in a dense transmission medium for two thermal sources in air. The radiation from different points on a surface of constant delay for a dielectric constant 49 which is typical of dense tissue was theoretically studied. Numerical calculations were carried out using two thermal sources to determine the surface of

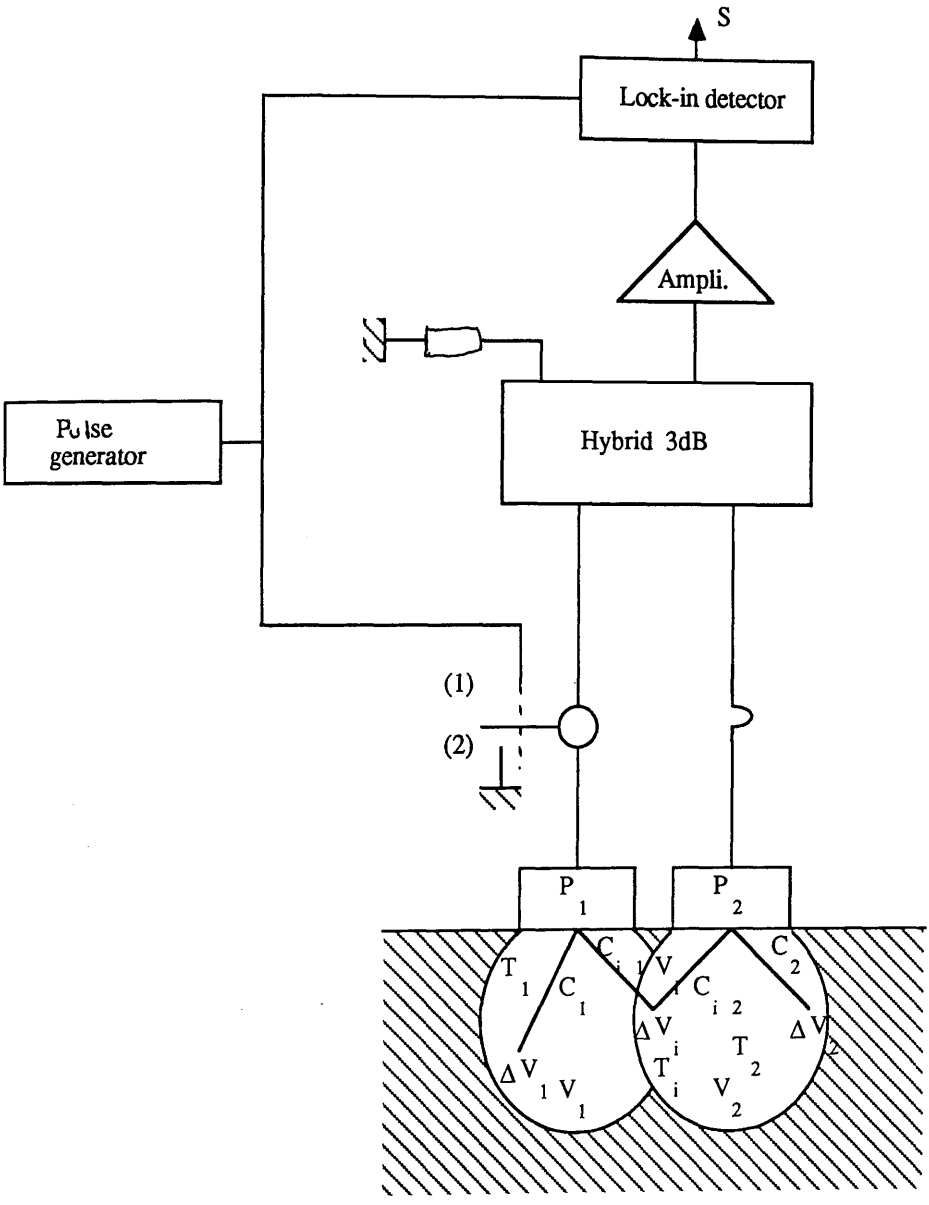

Fig. V.2 Synoptic of a system of correlation microwave thermography.
[from Mamouni et al., 1983]

constant delay in air (where the dielectric constant is 1). This technique showed that as the receiver bandwidth increased the apparent coherence time of the radiation decreased, permitting a compact volume of the tissue to be examined.

The correlation technique was thoroughly investigated by Newton, (1986) using two TE_{11}-cylindrical waveguide antennas and two TE_{10}-rectangular waveguide antennas with two identical channels. The first was angled at 48° and the closest separation of the antennas was possible is 4.4 cm. The second was angled at 30° and the closest separation of the antennas was 1.75 cm. In this study Newton used two designs of correlation radiometer; an *add-and-square* correlator of a 180 ° hybrid combined with a single pole double throw *(SPDT) PIN*-diode switch to add the two signals and perform the phase switching (Fig.V.3); and a *multiplicative* correlator with two channels of correlation radiometers designed and constructed by Land, (1983a); (Fig. V. 4). This consists of two radiometer channels each comprising two isolators and pre-amplifier at the front-end followed by a mixer and *IF* amplification. Different muscle phantom materials have been used to define the optimum penetration depth of the electromagnetic field at different distances between the antennas. It has been found that by placing the antennas closer together, a simple received pattern with one central fringe in the interference pattern can be achieved. The orientation and size of antennas were adjusted to reach a maximum penetration distance.

V. 2- Modes of correlation radiometer operation:

V. 2. 1- Introduction:

The classical signal antenna microwave thermography *(MWT)* used for medical radiometry applications is capable of detecting the existence of thermal structures of relatively large size but not too deep. The microwave correlation radiometry *(MWCR)*, is the complimentary to *MWT*, and is preferred for studying either the limits of thermal zones, when the differences in temperature are great, or for localizing small thermal structures and improving the spacial

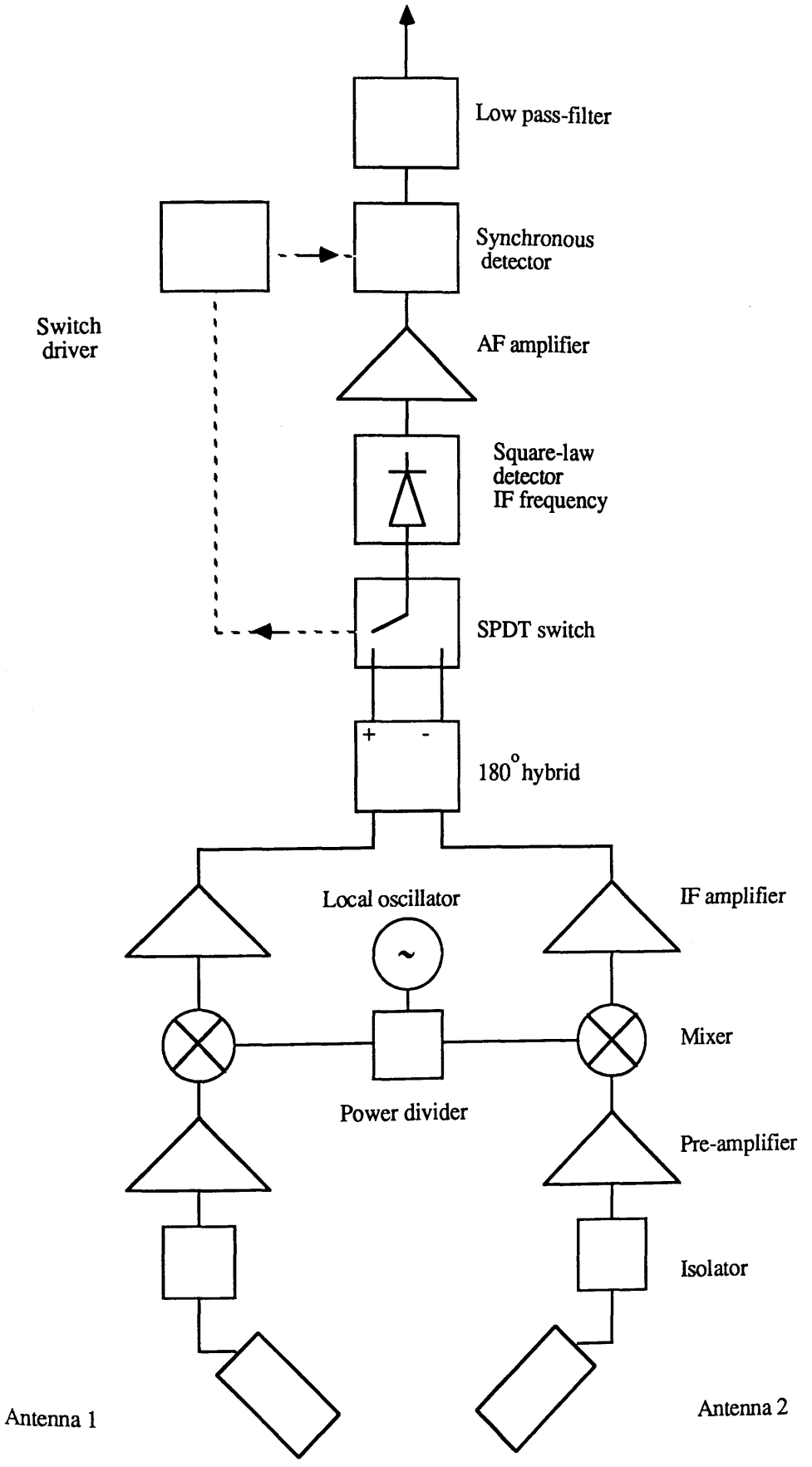

Fig. V.3 Schematic diagram of the add & square correlation radiometer

[from Newton, 1986]

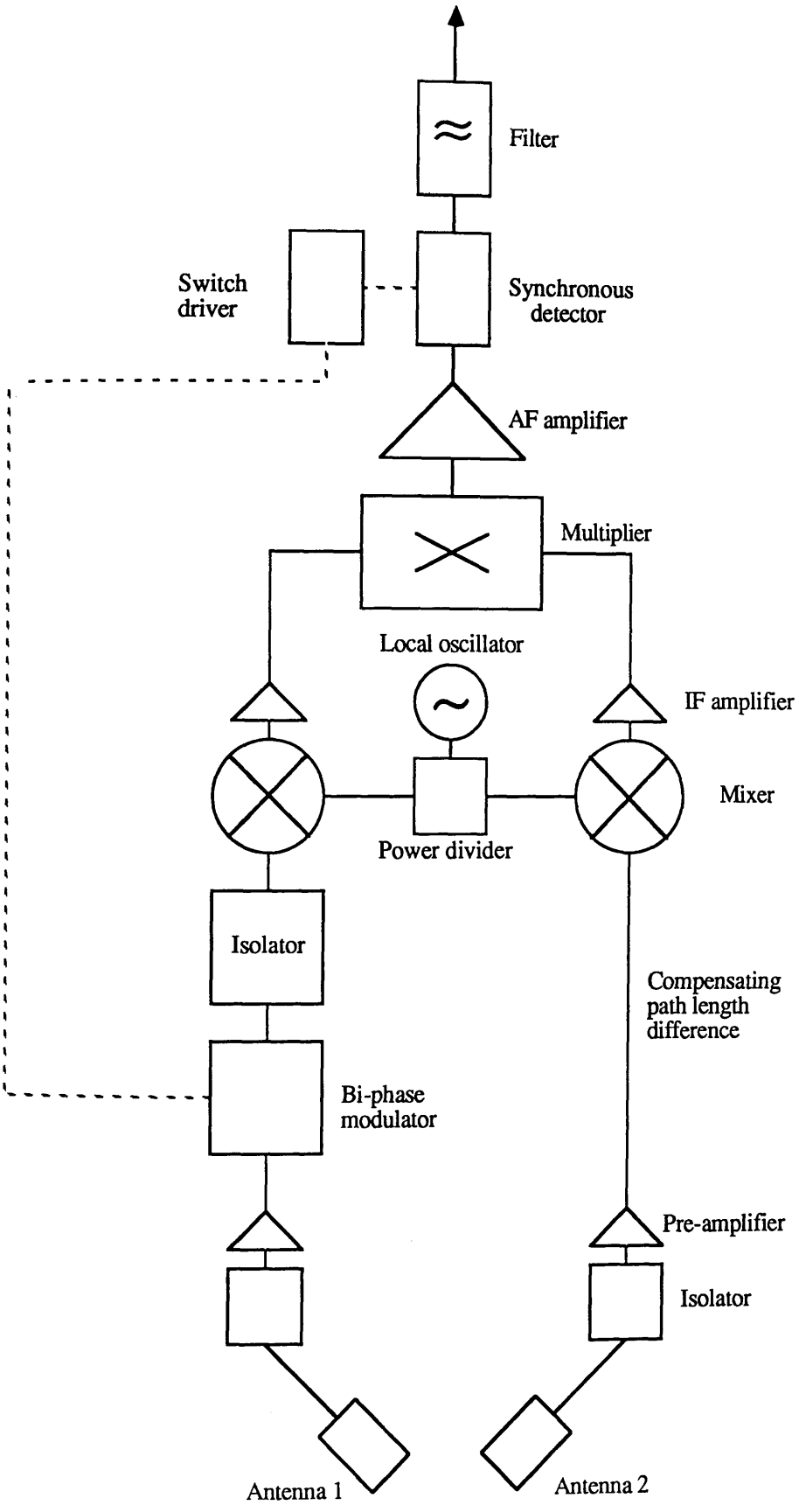

Fig. V.4 Schematic diagram of the multiplicative correlation radiometer

[from Newton, 1986]

resolution.

There are several types of correlation radiometer design with various degrees of sensitivity, and consideration has to be given to gain, stability and cost of the various types. Two main ways of calculating the cross-correlation signals received from two channels have been studied.

1) They can be multiplied together using a double balanced mixer as multiplier (Newton 1986). This is the *multiplicative* correlation radiometer.

2) They can be added together. The resulting signal is then squared by means of a square law detector. This is called an *add and square* correlation radiometer, (Newton, 1986).

V. 2. 2- The multiplicative correlation radiometer:

Figure V. 4 shows a schematic diagram of a *multiplicative* correlation radiometer, consisting of two radiometer channels. This radiometer was part of a radio-astronomy interferometer described in McClintock, (1981) and by Newton, (1986), who analysed the sensitivity of the technique for a range of frequency. With the *multiplicative* correlator, the received signal has correlated and uncorrelated components and the output is extracted from the correlated component only. The auto-correlation function of the thermal noise signal is given by:

$$c(t) = s(t)\ s(t-\tau) \qquad (V.1)$$

where τ is a time delay and is equivalent to a path length difference. This can be varied by inserting different lengths of coaxial cable into one of the channels. The total signal is proportional to the sync and the cosine functions for the bandwidth $d\omega$ and the path length difference τ.

V. 2. 3- The *"add-and-square"* correlation radiometry:

The *"add-and-square"* technique for the correlation of thermal radiation from two antennas was used in the experiments described in this work. This method which was described by Newton, (1986), uses two signals which are first added together and the result is then squared. A two-antenna microwave correlation radiometer integrates radiation over a distance that is of fixed time delay differential to the two antennas and also is within the volume of tissue common to both antennas. This distance is defined such that the difference in transit time of the radiation from any point P within that volume to each of the antennas is a constant τ (Fig. V. 5b), where $\tau = \frac{x_1 - x_2}{c}$. The analysis of this method will be described later in the chapter.

V. 3- Microwave correlation radiometry:

The arrangement investigated in this work uses two identical antennas, with a fixed distance between them, and with their axes at 90° (Fig. V.5a). By the reciprocity theorem the signal in each one is characterized by its radiation pattern. The signal radiated is a function of the geometry of the antennas (Fig. V. 5), the operating frequency, and the aperture field illumination. The component parts of the two antenna signals, resulting from the common region, are correlated (Fig. V.6, V.7, and V.8) and the components from the region not common to both antennas are uncorrelated. The output signal depends only on the common signal which is obtained by cross correlation of the two signals. The most important function in the coherence theory is the cross correlation of the signals received from two different directions. The coherence function is defined in the following section.

V. 3.1- The received pattern of the correlation radiometer:

The thermal noise signal received from a volume of tissue at any point P (Fig. V. 5) in the general field of view of the antennas is the signal received by the

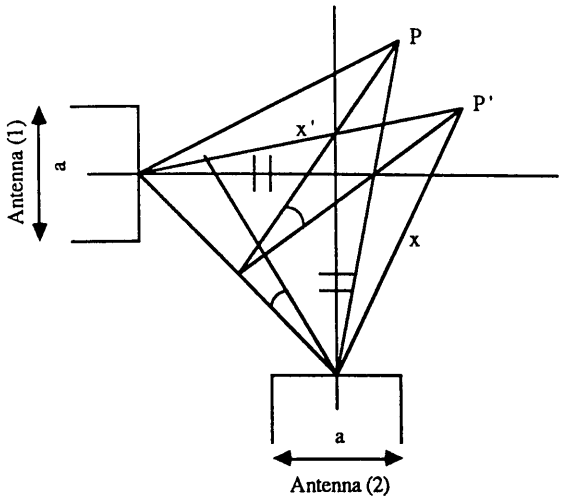

a- Arrangement of the two antenna positions 90 degrees phased.

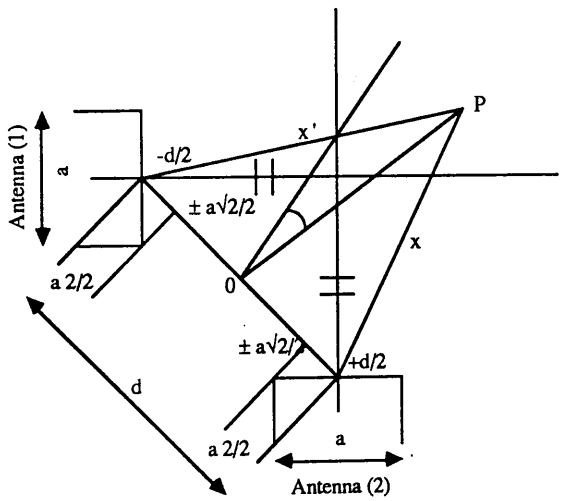

b- Diagram for an extended antennas.

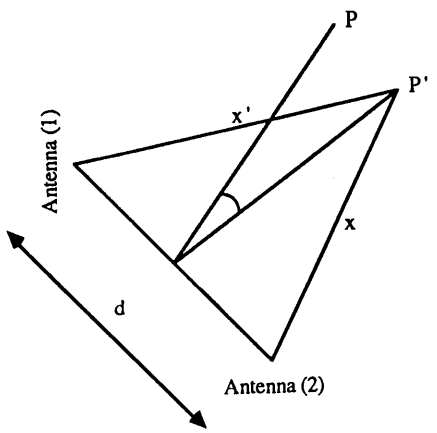

c- Diagram for a point antennas.

Fig. V.5- Correlation radiometer received signal arrangement.

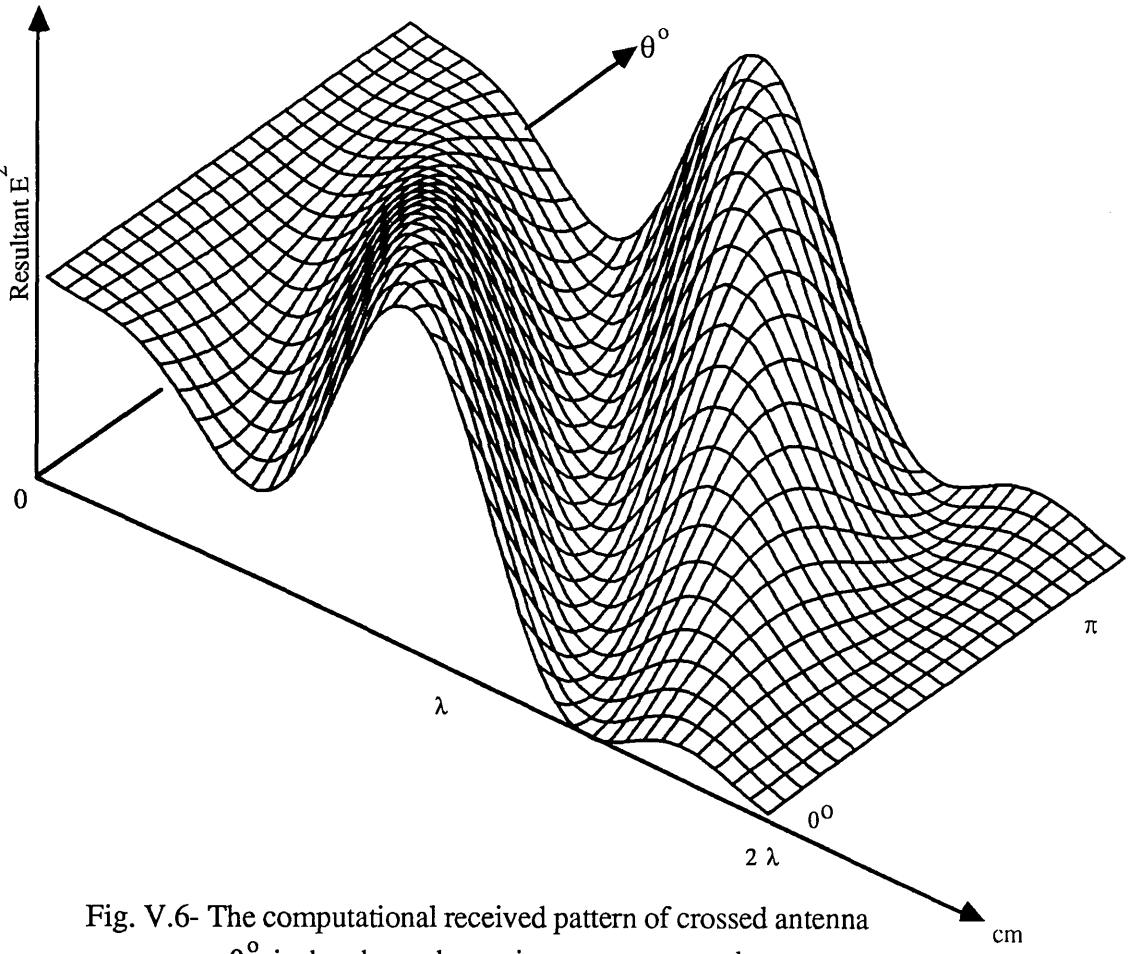

Fig. V.6- The computational received pattern of crossed antenna
θ° is the phase change in one antenna path.
2λ is the distance from one antenna.

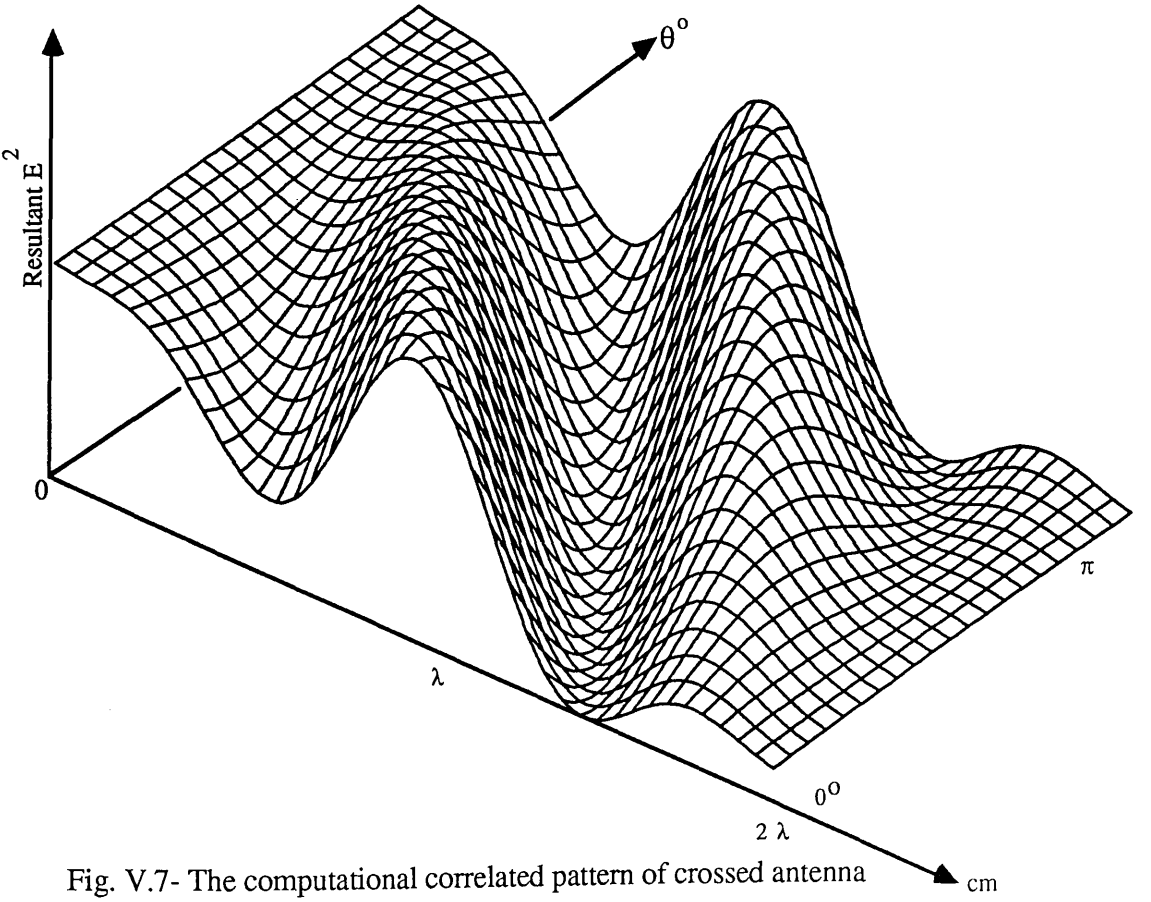

Fig. V.7- The computational correlated pattern of crossed antenna
θ° is the phase change in one antenna path.
2λ is the distance from one antenna.

radiometer from antenna *1* and antenna 2 at point *P* which are denoted by E_1 and E_2. The output signal is obtained by cross correlation of the two signals (Fig. V. 8). The most important function in coherence theory is the cross correlation of the signals received from two different directions at two different times. This is defined (Swenson and Mathur, 1968) as:

$$r(t) = \lim_{t \to \infty} \frac{1}{2T} \int_{0}^{T} E_1(x_1, t)\ E_2(x_2, t - \tau)\ dt \qquad (V.2)$$

or by,

$$r(t) = \langle E_1(x_1,t) \cdot E_2^*(x_2,t - \tau) \rangle \qquad (V.3)$$

where τ is the transit time delay of the radiation from any point *P* in the field of view to each of the antenna, $\tau = \frac{x_1 - x_2}{c}$.

The correlated signal received from the radiometer is given by:

$$R_p = \overline{\underline{E}_1 \times \underline{E}_2} \qquad (V.4)$$

where:

$$E_1 = E_o \exp(-\alpha x_1) \sin^2\left[\frac{\pi}{\lambda} x_2\right] \qquad (V.5)$$

$$E_2 = E_o \exp(-\alpha x_2) \sin^2\left[\frac{\pi}{\lambda} x_1\right] \qquad (V.6)$$

$$R_p = E_1 E_2 \cos\left[k(x_1 - x_2)\right] \qquad (V.7)$$

$$R_p = E_o^2 \exp\left[-\alpha(x_1 + x_2)\right] \sin^2\left(\frac{\pi}{\lambda} x_1\right) \sin^2\left(\frac{\pi}{\lambda} x_2\right) \cos\left[k(x_1 - x_2)\right] \qquad (V.8)$$

where E_1 and E_2 are the electric fields from the antenna *1* and *2* respectively and E_o is the field magnitude of the thermal noise emitted by the tissue at the point *P*.The output signal R_p of the correlation radiometer, due to the radiation emitted by tissue at the point *P*, is proportional to the signal power and hence the temperature, since *T* is proportional to E_o^2. The difference in path length to the two antennas is $cos\ [\ k\ (x_1 - x_2)\ ]$. This factor produces an interference pattern across the field of view from the point *P* to the two antennas of $n\lambda$, where, λ is the wavelength in tissue and n = 0, 1, 2, etc. The intensity will be zero wherever $k\ (\ x_1 - x_2\ ) = \frac{\pi}{2}, \frac{3\pi}{2}, \frac{5\pi}{2}$, and so on; the minima for the interference pattern is defined by $k\ (\ x_1 - x_2\ ) = \frac{\pi}{\lambda} d\ sin\ \theta$, and the maxima will then be determined by $d\ sin\theta = n\ \lambda$. The interference pattern depends on the product of the antenna received signals which are related to the relative orientation of the two antennas (Fig. V. 9).The path length difference $(\ x_1 - x_2\ )$ to point *P* is approximately $d\ sin\theta$, so the output received signal at point *P* is given by:

$$R_p \propto \text{real}\left[\exp\left(i\,k\,\frac{d}{2}\sin\theta\right)\exp\left(-i\,k\,\frac{d}{2}\sin\theta\right)\right] = \cos\left(k\,d\,\sin\theta\right) \qquad (V.9)$$

Thus the pattern is the product of the cosine fringes. This expression is true for just the point of intersection of the antenna axes.

For the aperture antennas with width *a* the output R_p is given by:

$$R_p \propto \text{real}\left[\int_{\frac{d}{2}-\frac{a\sqrt{2}}{2}}^{\frac{d}{2}+\frac{a\sqrt{2}}{2}} \exp\left(i\,k\,\sin\theta\,x\right)dx \int_{-\left(\frac{d}{2}-\frac{a\sqrt{2}}{2}\right)}^{+\left(\frac{d}{2}+\frac{a\sqrt{2}}{2}\right)} \exp\left(i\,k\,\sin\theta\,x\right)dx\right] \qquad (V.10)$$

$$= \text{real}\left[\frac{\exp\left(i\,k\,\sin\theta\right)}{\left(k\,\sin\theta\right)^2}\sin^2\left(k\,\frac{a\sqrt{2}}{2}\sin\theta\right)\right] \qquad (V.11)$$

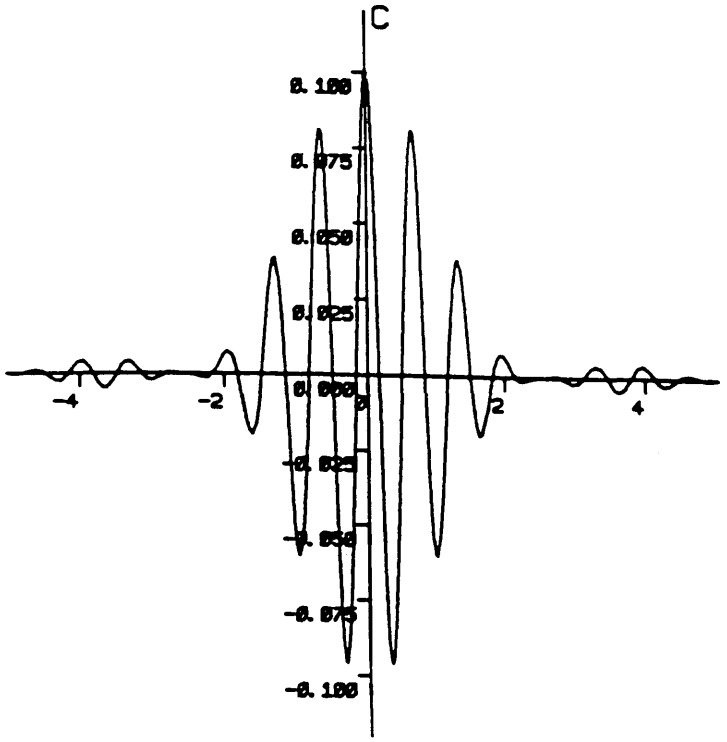

Fig. V.8- The cross-section pattern of the correlated signal.

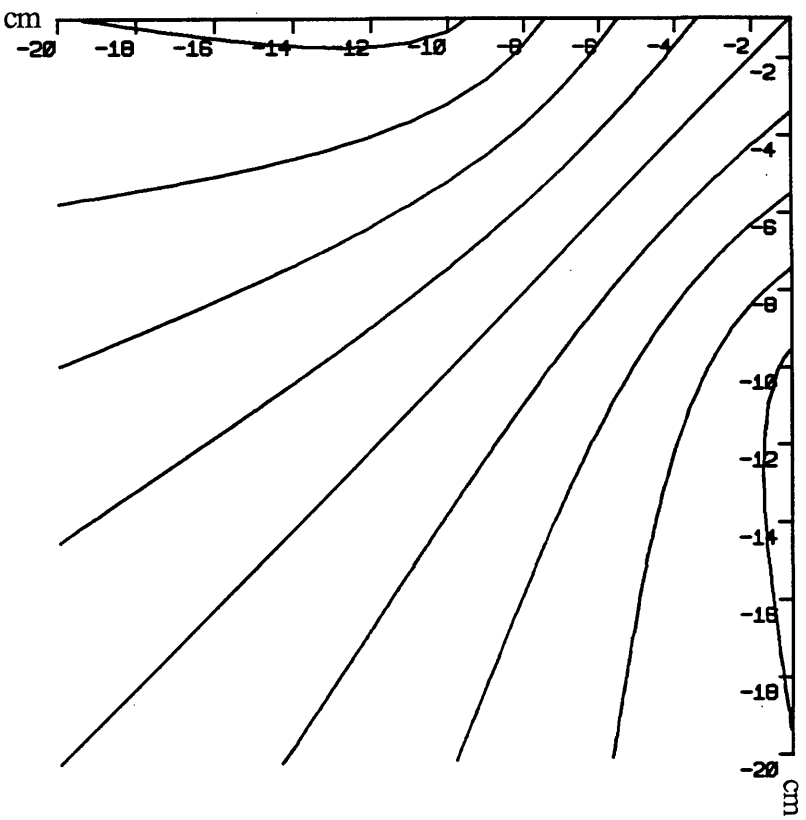

Fig. V.9- The interference pattern of the correlated signal.

The magnitude of the real part of this expression is given by:

$$R_e(R_p) = 2a^2 \cos(k d \sin\theta) \frac{\sin^2\left(k\frac{a\sqrt{2}}{2}\sin\theta\right)}{\left(k\frac{a\sqrt{2}}{2}\sin\theta\right)^2} \qquad (V.12)$$

Hence the pattern is the product of the cosine fringes by a sinc function modulation where the aperture width a is given by:

$$k\frac{a\sqrt{2}}{2}\sin\theta = y \qquad (V.13)$$

N.B. thus $\cos(k d \sin\theta)\frac{\sin^2 y}{y^2} = \cos(k d \sin\theta)\left[\frac{\sin y}{y}\right]^2$

If the width aperture a is just a point, y will tend to 0 and,

$$\lim_{y\to 0}\frac{\sin y}{y} = 1$$

so the output signal will be expressed by the following equation.

$$2a^2\cos[k d \sin\theta] \qquad (V.14)$$

Equation V.12 can be applied for any type of aperture, but the smaller the better because the magnitude of the output signal should preferably be large. The above analysis considered the pattern at only one frequency.

The radiometer detects a signal across a wide bandwidth of frequency, but only the signals at the same frequency from the same tissue element are coherent. Signals from the same tissue element, but at different frequencies, are incoherent so

it is valid to consider the correlation pattern at one frequency at a time. The total signal from position P is given by the integral over the bandwidth.

$$R_p = \int_{\omega} R_p(\omega)\, d\omega = \int_{\omega} \frac{1}{2} E_1(\omega)\, E_2(\omega) \cos[\, k\,(x_1 - x_2)\,]\, d\omega \qquad (V.15)$$

with $k = \frac{\omega}{c}$

If the frequency dependence of the electric fields $E_1(\omega)$ and $E_2(\omega)$ is neglected and the effect of the bandwidth on the path length is the only term considered, then the total signal from a particular point with path length difference $(x_1 - x_2)$ will be proportional to:

$$\int_{\omega_o - \frac{\Delta\omega}{2}}^{\omega_o + \frac{\Delta\omega}{2}} \cos(\omega\tau - \frac{\pi}{4})\, d\omega = \frac{1}{\tau} \sin(\omega\tau - \frac{\pi}{4}) \Bigg]_{w_o - \frac{\Delta\omega}{2}}^{\omega_o + \frac{\Delta\omega}{2}} \qquad (V.16)$$

$$= \Delta\omega \cos(\omega_o\tau - \frac{\pi}{4}) \frac{\sin(\frac{\Delta\omega}{2}\tau)}{(\frac{\Delta\omega}{2}\tau)} = \Delta\omega \cos(\omega_o\tau - \frac{\pi}{4})\, sinc(\frac{\Delta\omega}{2}\tau) \qquad (V.17)$$

where ω_o is the centre frequency, $\Delta\omega$ is the bandwidth and τ is the time delay.

The result of Eq. V.16 is the pattern for broad band signal and is the same as that for one single frequency, $cos\,[\,k\,(x_1 - x_2)\,]$, but has an additional $sinc$ function modulation, depending on bandwidth and path length difference. The $sinc$ function modulation reduces the magnitude of the signal with increasing path length difference, and with increasing distance from the central axis. Thus the effect of using a broadband signal is to reduce the outer fringes (Fig. V.10). In practice the effect is small (Newton, 1986).

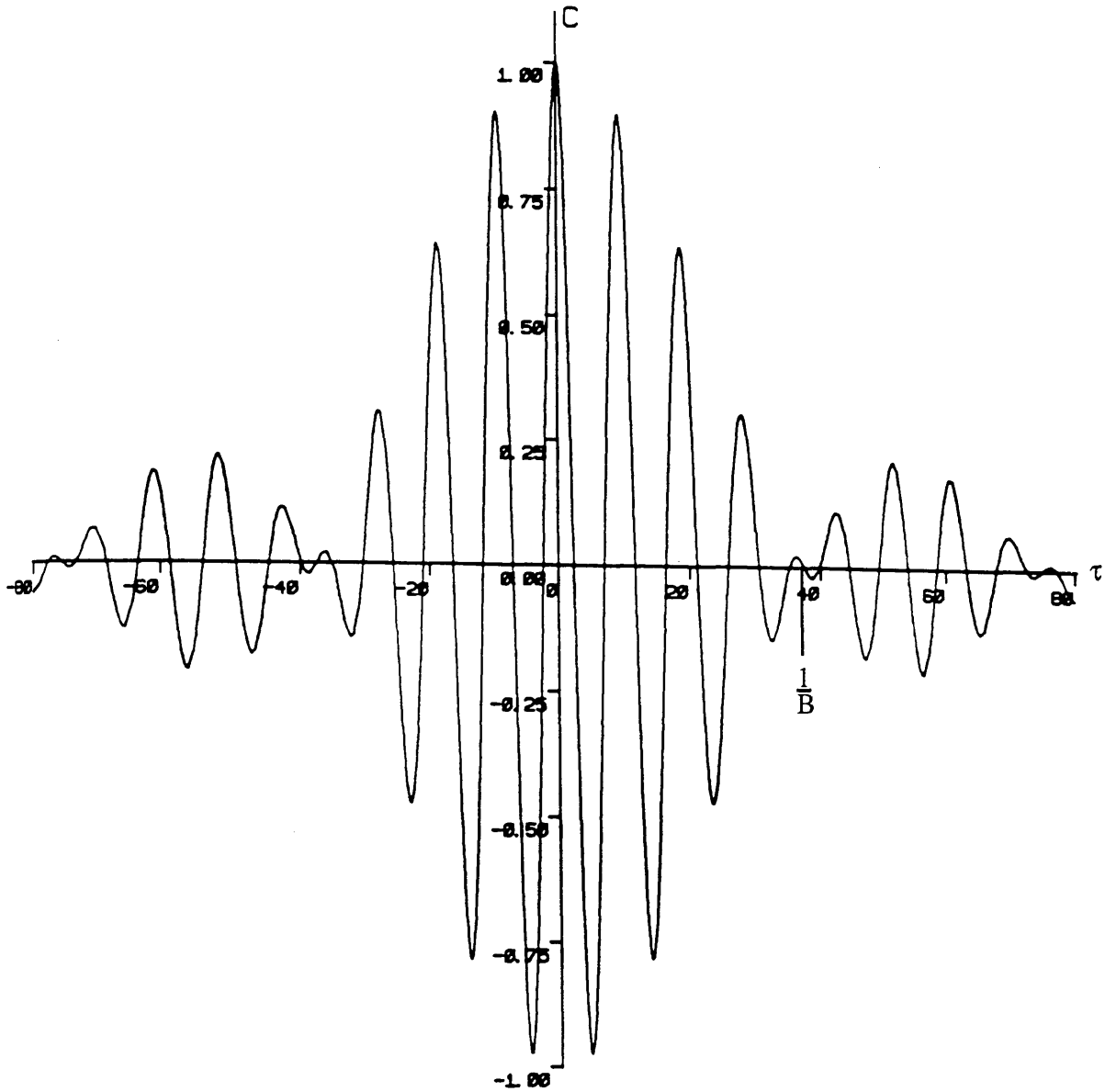

Fig. V.10- The auto-correlation function of the received signal for the frequency band 2.6 - 3.2 GHz, $C = \cos(2\pi f\tau)\ \mathrm{sinc}(B\pi\tau)$.

V.3.2- The received pattern of "an *add and square*" correlation radiometer:

The two signals are first added together and the result is then squared.

$$R_p = \overline{\left[E_1 + E_2\right]^2} \tag{V.18}$$

where:

$$E_1 = E_o\, e^{-\alpha x_1}\, \sin^2\left(\frac{\pi}{\lambda} x_2\right) \tag{V.19}$$

$$E_2 = E_o\, e^{-\alpha x_2}\, \sin^2\left(\frac{\pi}{\lambda} x_1\right) \tag{V.20}$$

where E_1 and E_2 are the electric fields from the antenna *1* and *2* respectively and E_o is the field magnitude of the thermal noise emitted by the tissue at the point *P*.

$$R_p = \overline{E_1^2 + E_2^2 + 2\, E_1\, E_2 \cos\theta} \tag{V.21}$$

The output is the sum of correlated and uncorrelated components, which is proportional to the total power received from the channels, with single channel radiometer outputs. The received signal depends only on the correlated component. This can be solved by introducing $R_p\,(\frac{\pi}{2})$, where the phase from one antenna to another is shifted by 90°. The output becomes:

$$R_p\,(\frac{\pi}{2}) = \overline{E_1^2 + E_2^2 + 2\, E_1\, E_2 \cos\,(\,\theta + \frac{\pi}{2}\,)} \tag{V.22}$$

The correlator will give a square wave output of a magnitude, which depends only on the correlated signal. Phase switching is an essential element of the design for

the *add and square* correlator (Fig. V. 3). This signal is then:

$$R_p - R_p(\frac{\pi}{2}) = 2\sqrt{2}\ E_1 E_2 \cos(\theta - \frac{\pi}{4}) \qquad (V.23)$$

$$= 2\sqrt{2} E_o^2 e^{-\alpha(x_1 + x_2)} \sin^2\left(\frac{\pi x_1}{\lambda}\right)\sin^2\left(\frac{\pi x_2}{\lambda}\right)\cos\left(k(x_1 - x_2) - \frac{\pi}{4}\right)$$

where $\theta = \omega\tau = 2\pi f(\frac{x_1 - x_2}{c}) = k(x_1 - x_2)$

$$= 2\sqrt{2} E_o^2 e^{-\alpha(x_1 + x_2)} \sin^2\left(\frac{\pi x_1}{\lambda}\right)\sin^2\left(\frac{\pi x_2}{\lambda}\right)\cos\left(\omega\tau - \frac{\pi}{4}\right) \qquad (V.24)$$

The correlator gives a square wave output of magnitude, $2\sqrt{2}\ E_1 E_2 \cos(\theta - \frac{\pi}{4})$, which now depends on only the correlated signal. Phase switching is thus an essential part of the design of an *add and square* correlator.

For the sensitivity of an *add and square* correlator it is necessary to take into consideration the auto-correlation function of the output. The signal in the square wave detector is $\frac{1}{\sqrt{2}}[E_1(t) + E_2(t)]$. The factor of $\frac{1}{\sqrt{2}}$ appears because, in practice, the addition of the two signals results in a halving of the power in each signal. Thus the output $R(t)$ from the square law detector will be given by:

$$R(t) = \frac{1}{2}\left(\overline{\left[E_1(t) + E_2(t)\right]\left[E_1(t) + E_2(t)\right]}\right) \qquad (V.25)$$

In Appendix A the auto-correlation function of the output is defined as:

$$C_R(t) = C^2_{E_1 + E_2}(0) + 2C^2_{E_1 + E_2}(\tau) \qquad (V.26)$$

$$C_{(E_1+E_2)}(\tau) = \frac{1}{2}\left(\overline{\left[E_1(t)+E_2(t)\right]\left[E_1(t-\tau)+E_2(t-\tau)\right]}\right) \qquad (V.27)$$

$$= \frac{1}{2}\left(\overline{E_1(t)\times E_1(t-\tau)} + \overline{E_2(t)\times E_2(t-\tau)} + \overline{E_1(t)\times E_2(t-\tau)} + \overline{E_2(t)\times E_1(t-\tau)}\right)$$

$$= \frac{1}{2}C_{E_1}(\tau) + \frac{1}{2}C_{E_2}(\tau) + C_{E_1 . E_2}(\tau) \qquad (V.28)$$

if $C_{E_1}(\tau) \approx C_{E_2}(\tau) \approx C_E(\tau)$ and $C_{E_1 . E_2}(\tau) = C_{E_c}(\tau)$

then

$$= C_E(\tau) + C_{E_c}(\tau) \qquad (V.29)$$

therefore the auto-correlation function becomes:

$$C_R(\tau) = \left[C_E(0) + C_{E_c}(0)\right]^2 + 2\left[C_E(\tau) + C_{E_c}(\tau)\right]^2 \qquad (V.30)$$

if $C_{E_c}(\tau) \ll C_E(\tau)$

$$C_R(\tau) = C_E^2(0) + 2C_E^2(\tau) \qquad (V.31)$$

The sensitivity of an *add and square* correlator radiometer has been compared to that for a single channel ideal total power radiometer. This shows similarities of sensitivity for both cases.

The modelling and the experimental analysis of the microwave correlation radiometer will be discussed in detail in Chapter VI.

Chapter VI

Microwave correlation radiometry Practical Implementation

VI. 1- Introduction:

In Chapter V the theory of the correlation microwave radiometry and the correlation function were discussed. The application of this theory to the microwave radiometry will be analysed numerically and experimentally verified.

Several authors have published work on correlation radiometry and discussed the effect of the spacing of antennas on the maximum depth attained. Mamouni et al., (1983) suggested a useful method to study thermal zones limits when the differences in the temperatures are great or for localising small thermal structures to improve the spatial resolution. The spatial resolution is improved because the width of each individual fringe in the pattern is much narrower than that for a single antenna. The interference pattern can be moved by changing the path length difference. Bellarbi et al., (1984b) and Hill et al., (1985) used the interference pattern to locate sharp thermal gradients and changed the path length difference to automatically scan the pattern without moving the antennas. Haslam, (1984) suggested doing correlation radiometry with only two antennas for different antenna apertures. These microwave correlation radiometer antennas have been applied in radio-astronomy to measure the received signal in aperture synthesis. Several problems have been found, for considering the microwave correlation radiometric techniques, which were spaced antennas, and hence an interference pattern, for detecting thermal gradients. A reduction in sensitivity is difficult because of the limited overlap of the individual antenna received patterns.

In the last few years several theoretical and practical studies have been made

in correlation microwave radiometry (see Newton, 1986, discussed in Chapter V). Mamouni et al., (1983) suggested a new a microwave correlation technique to investigate the thermal gradient in the subcutaneous tissues and to improve the performance of the applicator used in medical application. These studies were carried out by Mamouni, (1988) to improve the detection of the electromagnetic fields in lossy materials. The results of their work in nearly parallel antenna correlation radiometry were not encouraging to use their antenna arrangement. The Glasgow interest in the diagnoses of breast and limbs joint diseases using a 90° crossed-pair antenna arrangement could be of practical interest.

The *add and square* correlation radiometer, considered in this work, was constructed using a 180° hybrid combined with a single pole double throw *(SPDT) PIN* diode switch to add the two signals and perform the phase switching. This radiometer has been designed and constructed in the Glasgow University. Two TE_{11}-mode cylindrical waveguide antennas are used at fixed distances and 90° angled, (Fig. VI. 1), in order to improve the investigated volume under investigation in the treatment of cancer by hyperthermia therapy, and in the detection of disease in the female breast and in the major joints.

VI. 2- The *add and square* correlation radiometer:

VI. 2. 1- General design:

Figure V. 3 shows a schematic diagram of the *add and square* correlation radiometer. The two *IF* signals are added together by the 180° hybrid. The hybrid, combined with the *PIN* diode *SPDT* switch, produces the phase switching, which is necessary in an *add and square* design of correlator to separate the correlated component of the signal from the background. The output from one of the hybrids output ports is the sum of the two input signals (half the power of each channel). The square law detection gives:

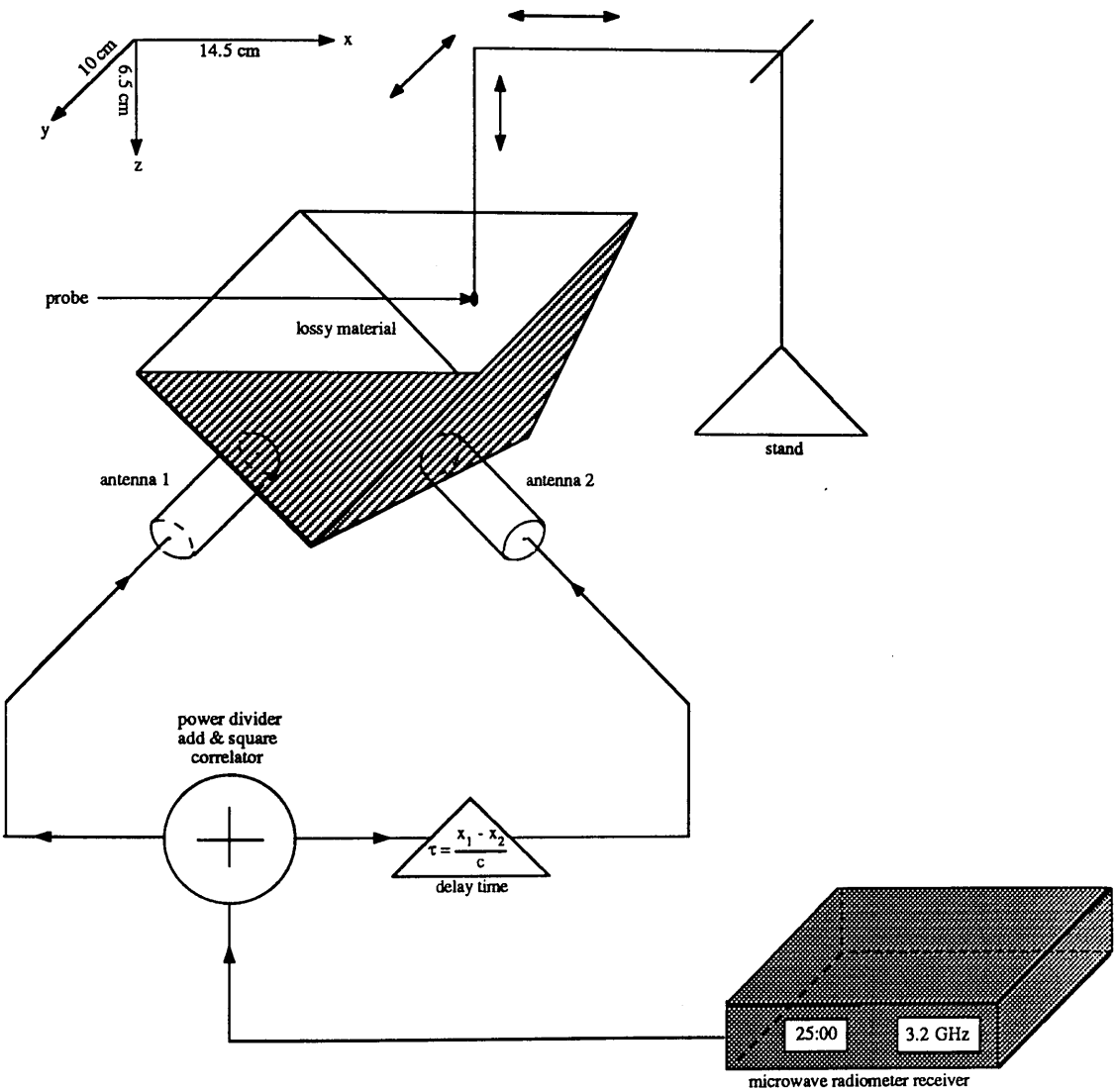

Fig. VI.1- Schematic diagram of the crossed-pair antenna

$$R_+ = \frac{1}{2}\ \overline{(E_1 + E_2)}^{\,2} = \frac{1}{2}E_1^2 + \frac{1}{2}E_2^2 + E_1 E_2 \qquad \text{(VI.1)}$$

The output from the other output port is the difference of the two input signals. Thus the sum with 180° phase shift between the signals (half the power of each) is given by:

$$R_- = \frac{1}{2}\ \overline{(E_1 - E_2)}^{\,2} = \frac{1}{2}E_1^2 + \frac{1}{2}E_2^2 - E_1 E_2 \qquad \text{(VI.2)}$$

The two outputs are alternately selected by the *SPDT* switch, at a switch frequency about 1 KHz. The switch is followed by the square law tunnel diode detector. The resulting *AF* square wave is processed as in a single channel Dicke-switched radiometer i.e. *AF* amplification, synchronous detection and low pass filtering. The output from the synchronous detector is the magnitude of the square wave which is defined by:

$$R_+ - R_- = 2\,E_1 E_2 \cos\theta \qquad \text{(VI.3)}$$

which is the required correlated signal.

VI. 2. 2- Phase switching:

The phase switching is a necessary part of the *add and square* correlator design. It separates the correlated component of the signal, $E_1 E_2$, from the total power component $(E_1^2 + E_2^2)/2$. The advantage of the *add and square* signal from the detector is that it is easier to amplify than a *d.c.* signal of the same magnitude. The position at the end of the radiometer channel for the hybrid and switch after the *IF* amplifier neglect the loss of the different components of the system noise. Since there is no front-end switch the overall system noise of a

channel is less than for a Dicke-switched radiometer. However, because phase switching is performed at the end of the receiver it will not eliminate the unwanted coherent signals. The unwanted coherent signals introduced anywhere in the microwave or *IF* stages will bi-phase modulated along with the actual signal and will contribute to the final output. The unwanted coherent signal cannot be measured.

VI. 2. 3- Practical problems:

VI. 2. 3. 1- Phase balance:

The path length difference between the channels should be adjusted in order to give the maximum signal. The path length difference in the microwave and *IF* parts must be corrected separately, because the system uses the upper and lower *IF* sidebands from the mixer and any correcting phase difference. At the microwave frequencies, the lower sideband is inverted which is not the case for the upper sideband. The sensitivity of the phase balance in the *IF* section is better than 3^{o}. The phase balance between the hybrid outputs is also good at less than 0.2^{o} difference. This phase balance has been studied by Newton, (1986).

VI. 2. 3. 2- Hybrid amplitude balance:

The signal from channel *A* into port 1 of the hybrid is divided equally between the two output ports with negligible difference in amplitude. The signal from channel *B* into port 2 is unequally divided, with a difference of 4%. Newton, (1986) found that the sensitivity for the *add and square* correlation radiometer was about 0.06 K. Recent modification to the microwave correlation radiometer has improved the performance of the radiometer channels.

VI. 3- Receive patterns:

VI. 3.1- Computer modelling:

A theoretical study using computer modelling of the crossed-pair antenna system for radiometer temperature measurement shows the variation of the field pattern relative to the distance between the antennas, and phase switching. Numerical calculations have been carried out to determine the optimum penetration depth for a variety of midline distances and phase switching of the crossed antennas.

Figures VI.2.1 and VI.2.2 show the prototype of the crossed-pair antenna considered in this work and the analytical diagram of them where the separation between antenna *1* and *2* is represented by *b* and the midpoint apertures distance is *d*.

Figures. VI. 3.1, VI. 3.2, VI. 3.3, and VI. 3.4 show the effect of spacing and phasing the crossed antennas. The midpoints of apertures are separated by different distances, *b*, and different phases to establish the maximum penetration depth that can be achieved. Figures VI. 3.1 and VI. 3.2 show the computational analyses of the above arrangement operating at a frequency of 3.2 GHz. Fig. VI. 3.1 represents the case where the two antenna paths are in phase and Fig. VI. 3.2 represents the case where the phase difference is $\frac{\pi}{6}$. The distance in both Figures between the antennas as shown in Fig. VI. 2.2 is b = 10 cm. These Figures illustrate the effect of the phase change in one antenna on the correlated signal. In Fig. VI.3.2 the received signal from the microwave correlation radiometer antennas is more widely spread in the tissue close to the antenna/tissue interface. This results in the signal received from close to the tissue surface being of little significance, with a very small penetration depth being achieved.

In Fig. VI.3.1 with the antenna paths in phase the received signal is distributed along a line between the center-point of the antenna apertures. The total power of the signal is equally spaced into regions along this axis and thus the maximum penetration depth in each region is diminished. Where the distance

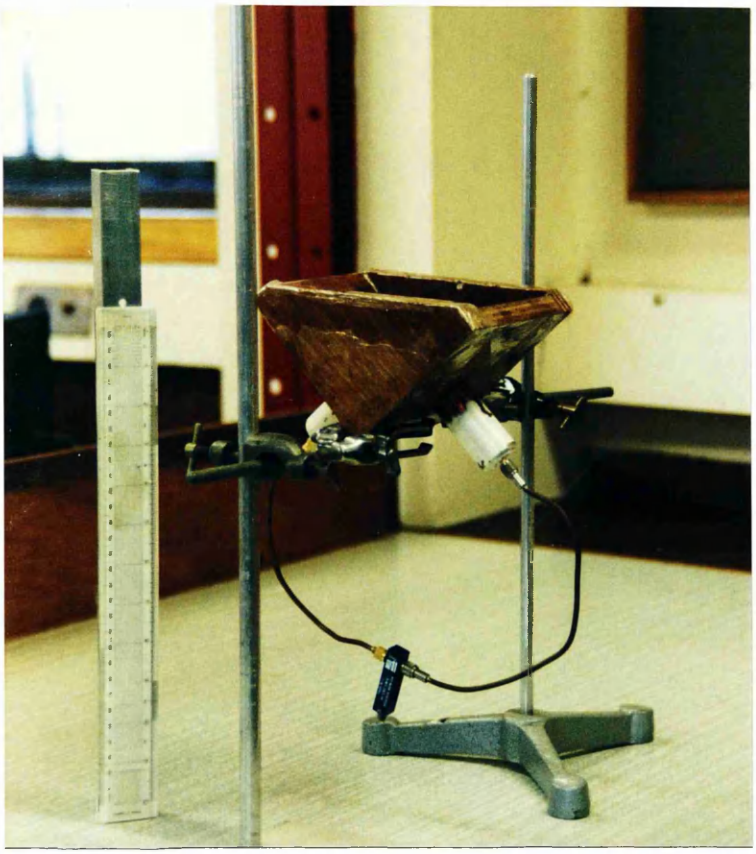

Fig. VI.2.1- Prototype of the crossed-pair antenna

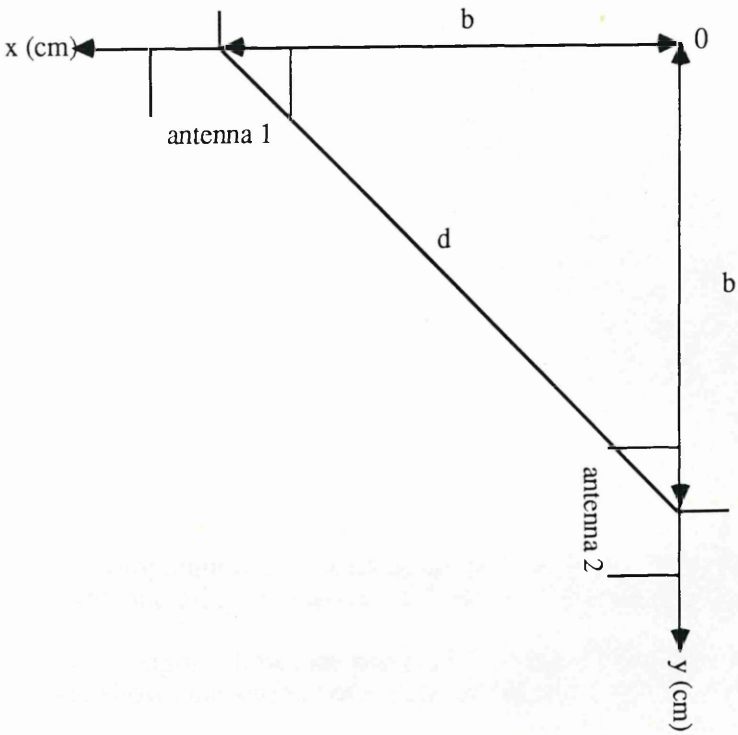

Fig. VI.2.2- The analytical diagram for the computational analyses

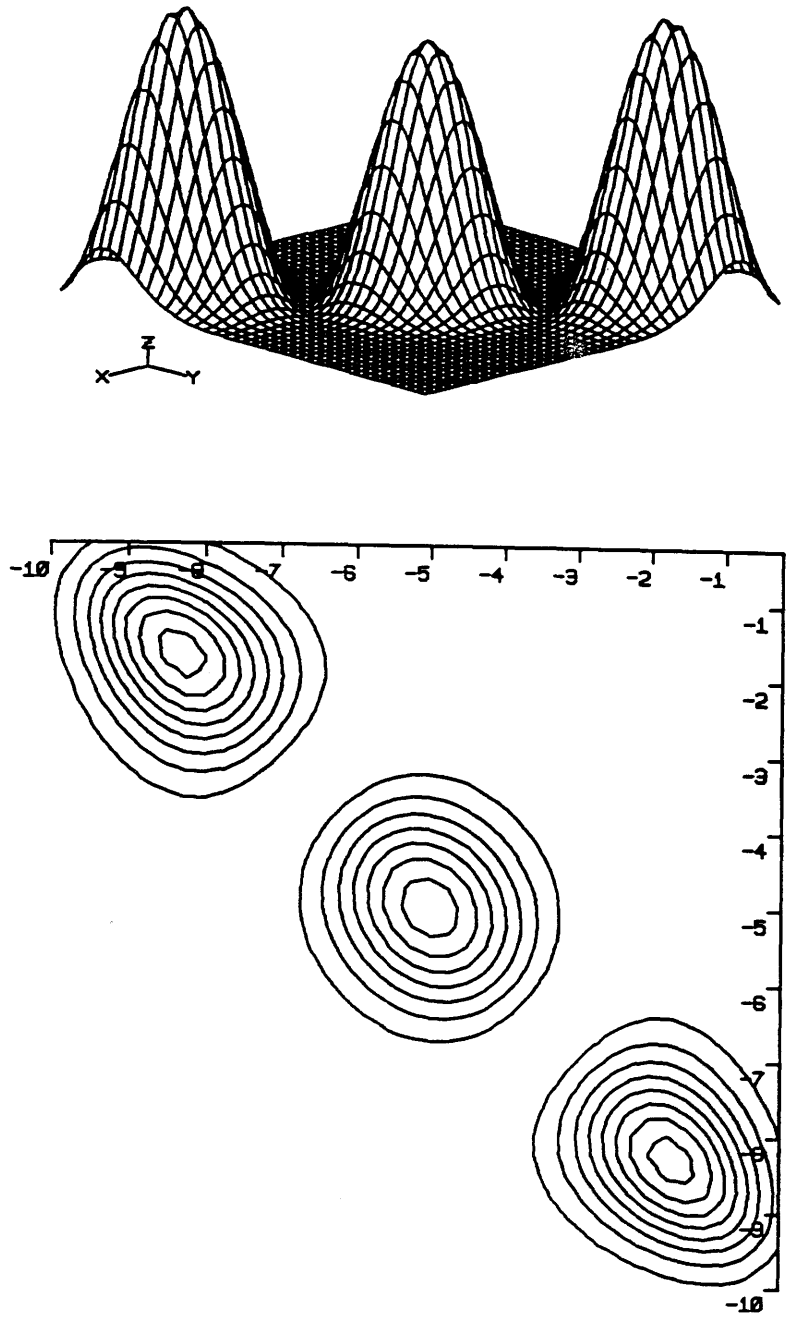

Fig. VI.3.1- The computational correlation signal of crossed-pair antenna at the operating frequency 3.2 GHz (antennas are in phase and b = 10 cm).

The top figure shows the penetration depth of the signal and lower one shows the surface of the spread signal.

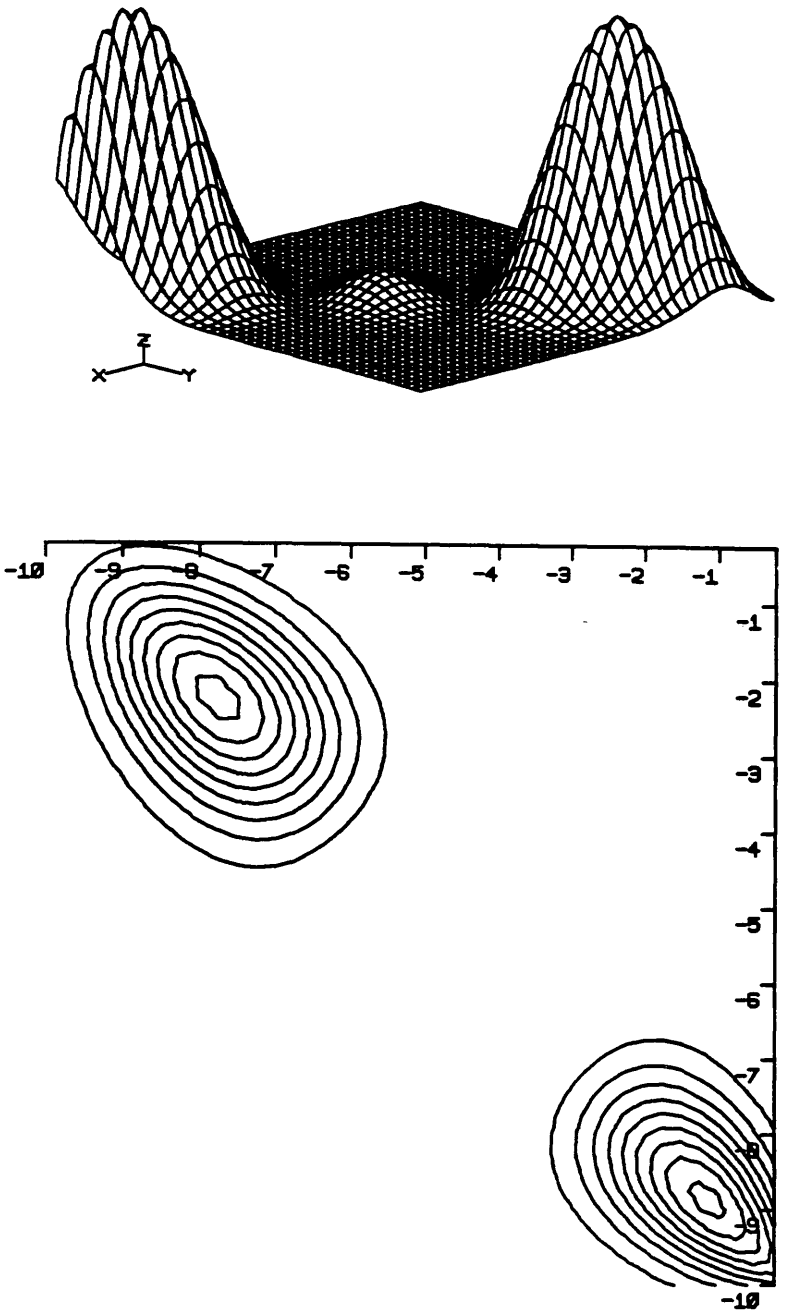

Fig. VI.3.2- The computational correlation signal of crossed-pair antenna at the operating frequency 3.2 GHz .
(antenna 2 is phased by $\frac{\pi}{6}$ and b = 10 cm).

The top figure shows the penetration depth of the signal and lower one shows the surface of the spread signal.

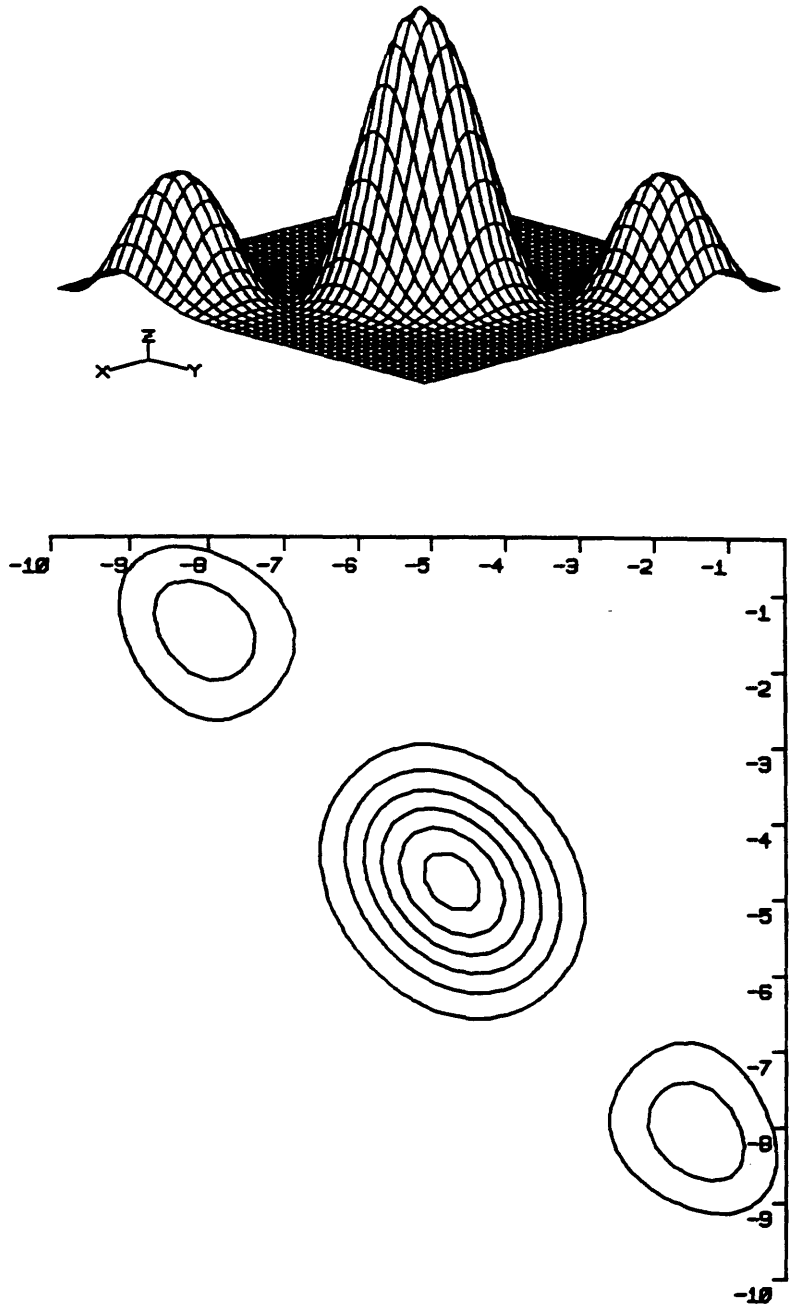

Fig. VI.3.3- The computational correlation signal of crossed-pair antenna at the operating frequency 3.2 GHz (antennas are in phase and b = 9.5 cm).

The top figure shows the penetration depth of the signal and lower one shows the surface of the spread signal.

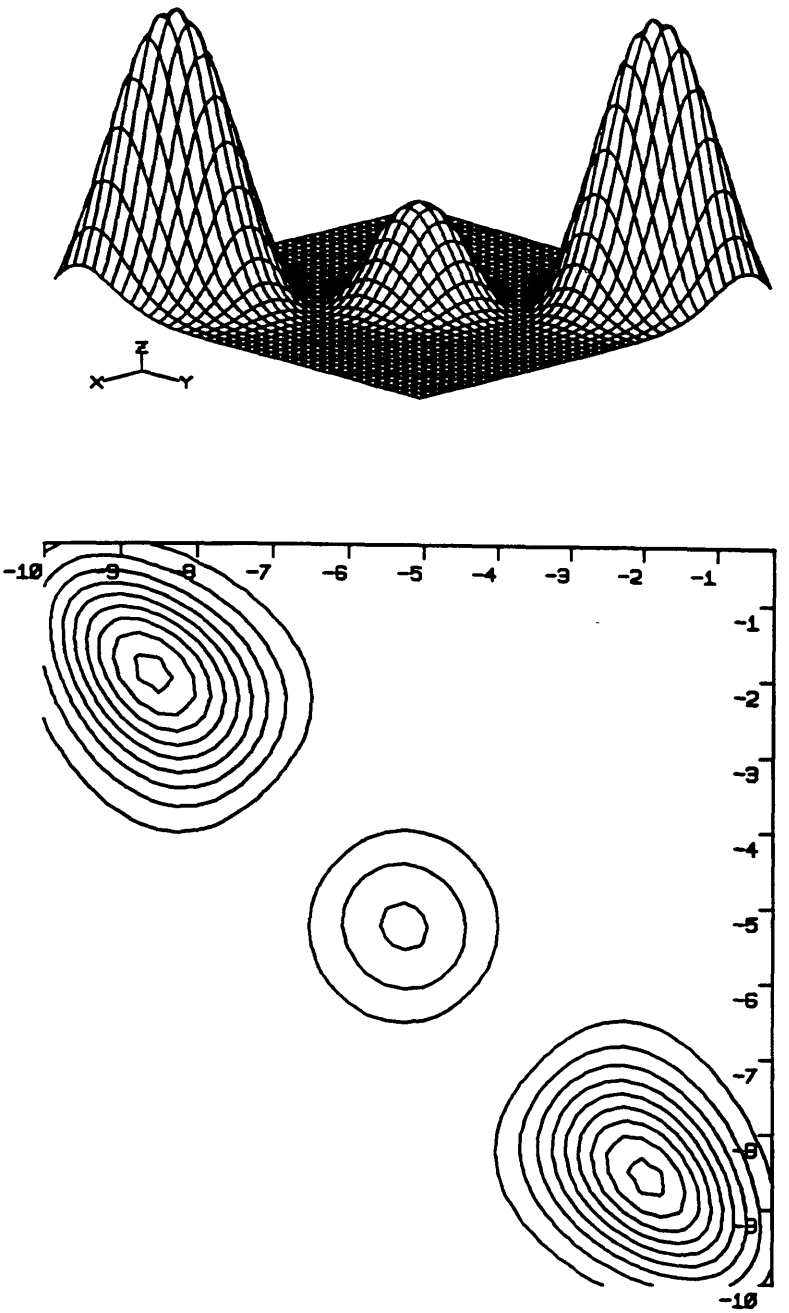

Fig. VI.3.4- The computational correlation signal of crossed-pair antenna at the operating frequency 3.2 GHz .
(antenna 2 is phased by $\frac{\pi}{6}$ and b = 9.5 cm).

The top figure shows the penetration depth of the signal and lower one shows the surface of the spread signal.

between the antennas is equal to 10 cm the strength of the received signal is very poor. Fig. VI.3.3 and VI.3.4 present the same analyses except that the distance between the antennas is b = 9.5 cm. Fig. VI.3.3 shows that the received signal is greatest in the middle of the viewed region and that the signal close to the antenna aperture is very poor. Thus, as the distance between the antennas decreases the results become more encouraging. For Fig. VI.3.4 where the antennas are $\frac{\pi}{6}$ out of phase the signal is still spread near the apertures and the signal from the centre of the viewed region is very low. Although this separation distance is also not suitable, it merits further investigation.

At various distances between 7.5 cm and 3.5 cm the total signal is centered in the middle of the viewed region for case where the antennas are in phase and close to one antenna aperture where they are $\frac{\pi}{6}$ out of phase. These results are represented by Figures VI.3.5, VI.3.6,. VI.3.7, VI.3.8, VI.3.9, VI.3.10, VI.3.11, VI.3.12,VI. 3.13 and VI.3.14.

From these Figures we conclude that the separation between the antenna apertures and the phase change give some indication of the penetration depth of the signal and the surface which can be scanned.

The numerical analysis shows that the contour patterns have a maximum at a significant depth where the antennas are in phase and the interference patterns have one central fringe in the investigated volume

The interference pattern has two central fringes. This study shows that the closer the antennas are to each other and the nearer in phase with each other the better the information at maximum depth.

The maximum number of contour patterns of the output correlated signal is found at 10 cm distance between antennas and in phase, where the radiation is more diffuse in the viewed field. If the distance between the antennas is less than 10 cm and the signals are in phase (from for example 7.5 cm), the number of contours is one and it contains the total signal. If the distance is greater than 10 cm the radiation

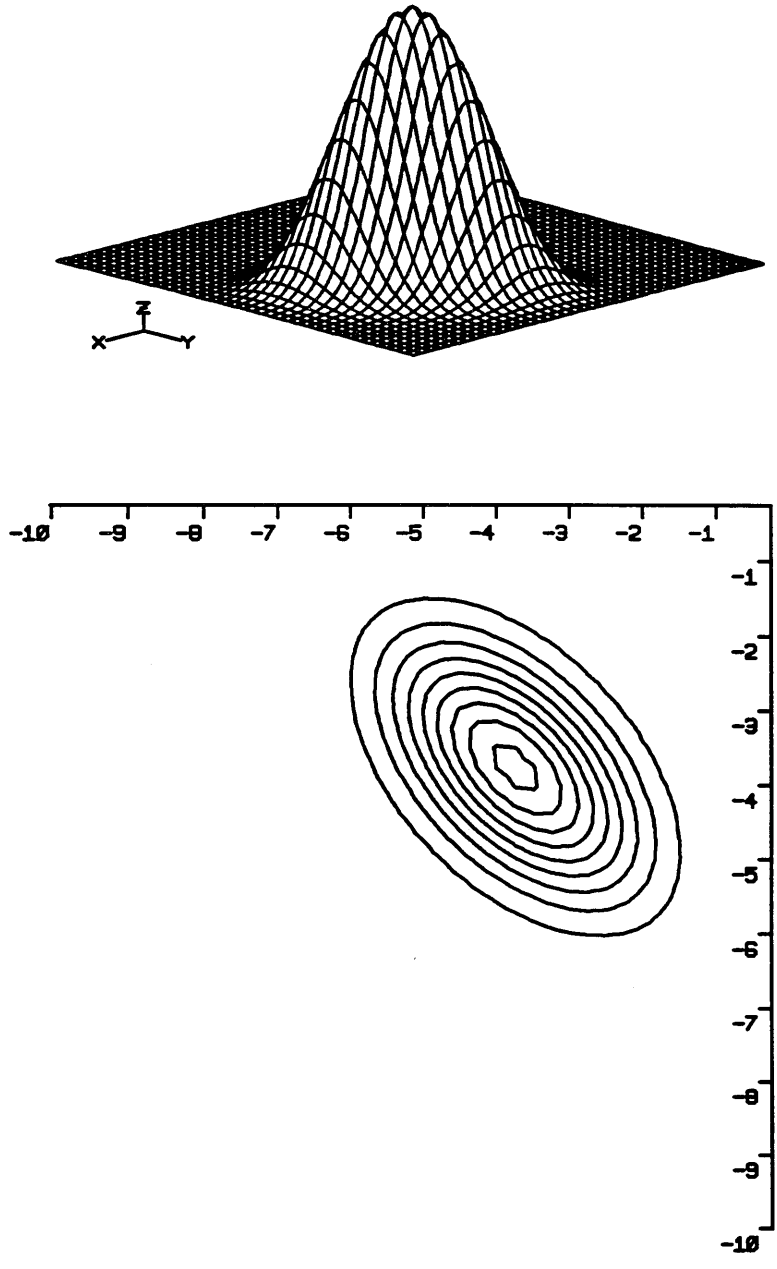

Fig. VI.3.5- The computational correlation signal of crossed-pair antenna at the operating frequency 3.2 GHz (antennas are in phase and b = 7.5 cm).

The top figure shows the penetration depth of the signal and lower one shows the surface of the spread signal.

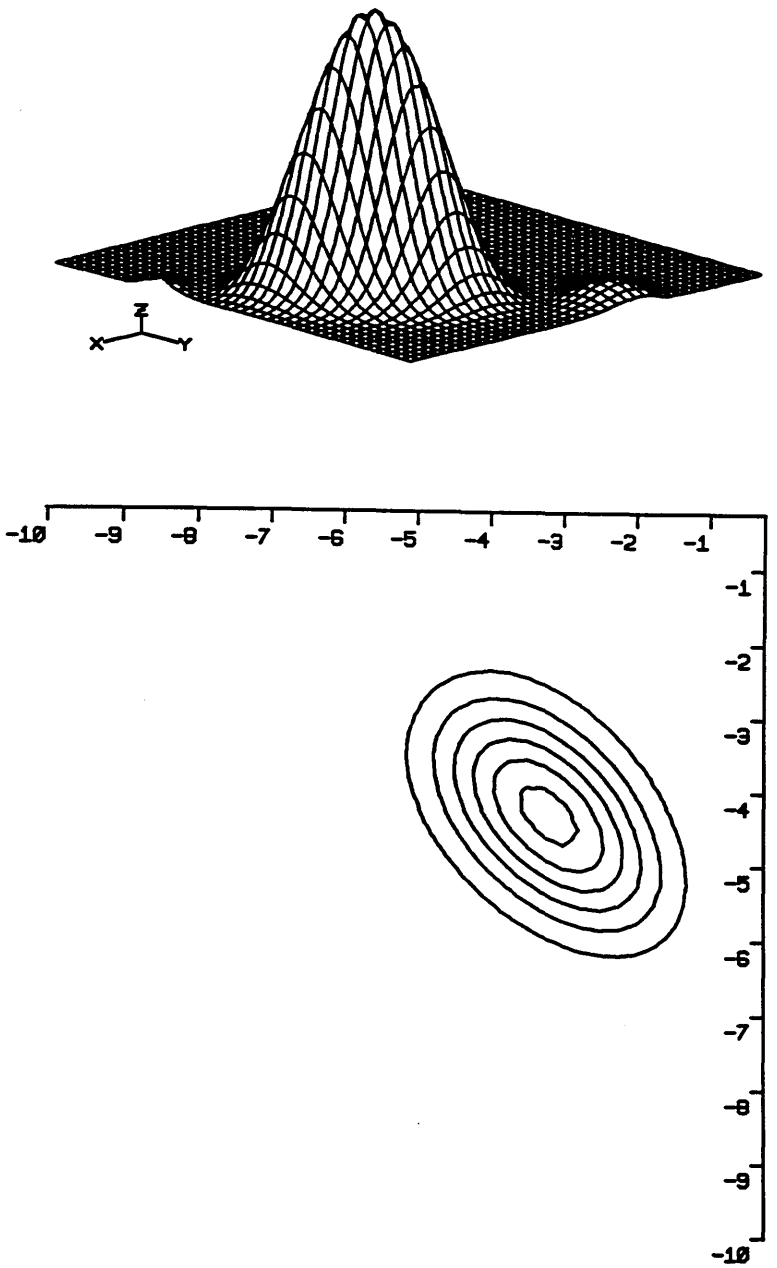

Fig. VI.3.6- The computational correlation signal of crossed-pair antenna at the operating frequency 3.2 GHz .
(antenna 2 is phased by $\frac{\pi}{6}$ and b = 7.5 cm).

The top figure shows the penetration depth of the signal and lower one shows the surface of the spread signal.

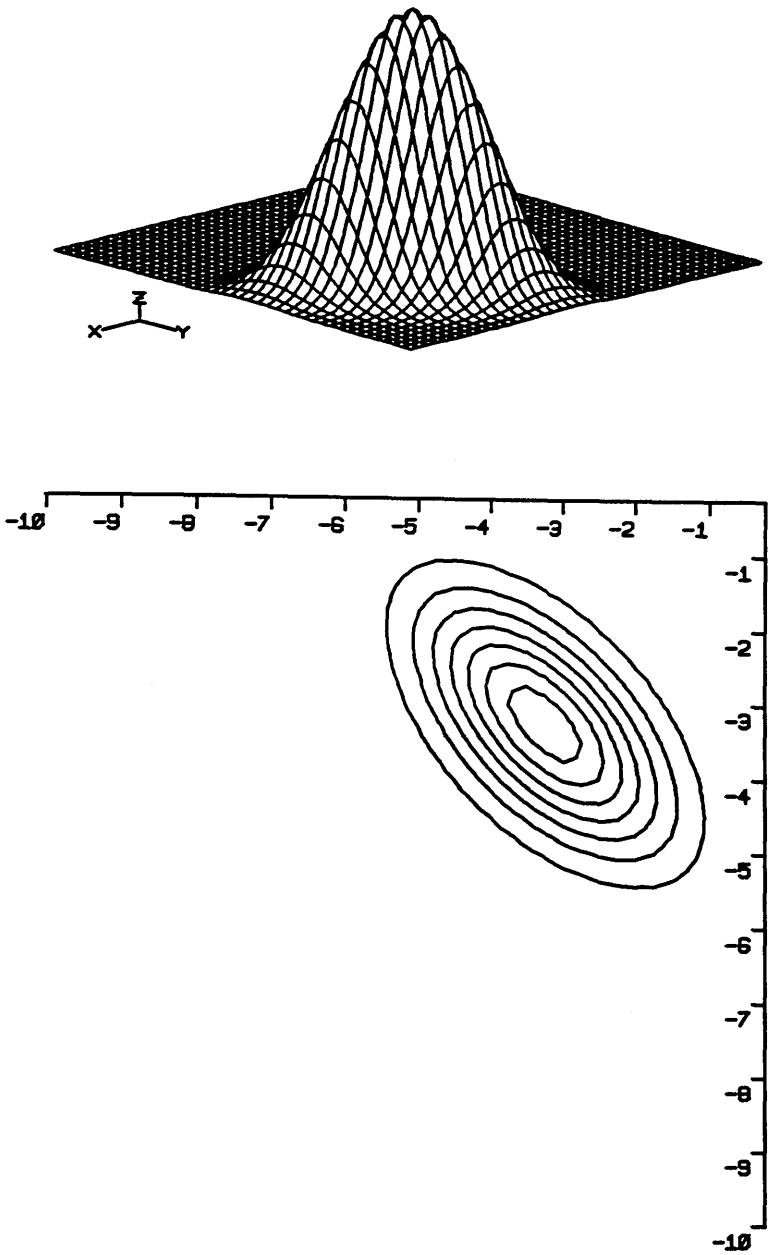

Fig. VI.3.7- The computational correlation signal of crossed-pair antenna at the operating frequency 3.2 GHz (antennas are in phase and b = 6.5 cm).

The top figure shows the penetration depth of the signal and lower one shows the surface of the spread signal.

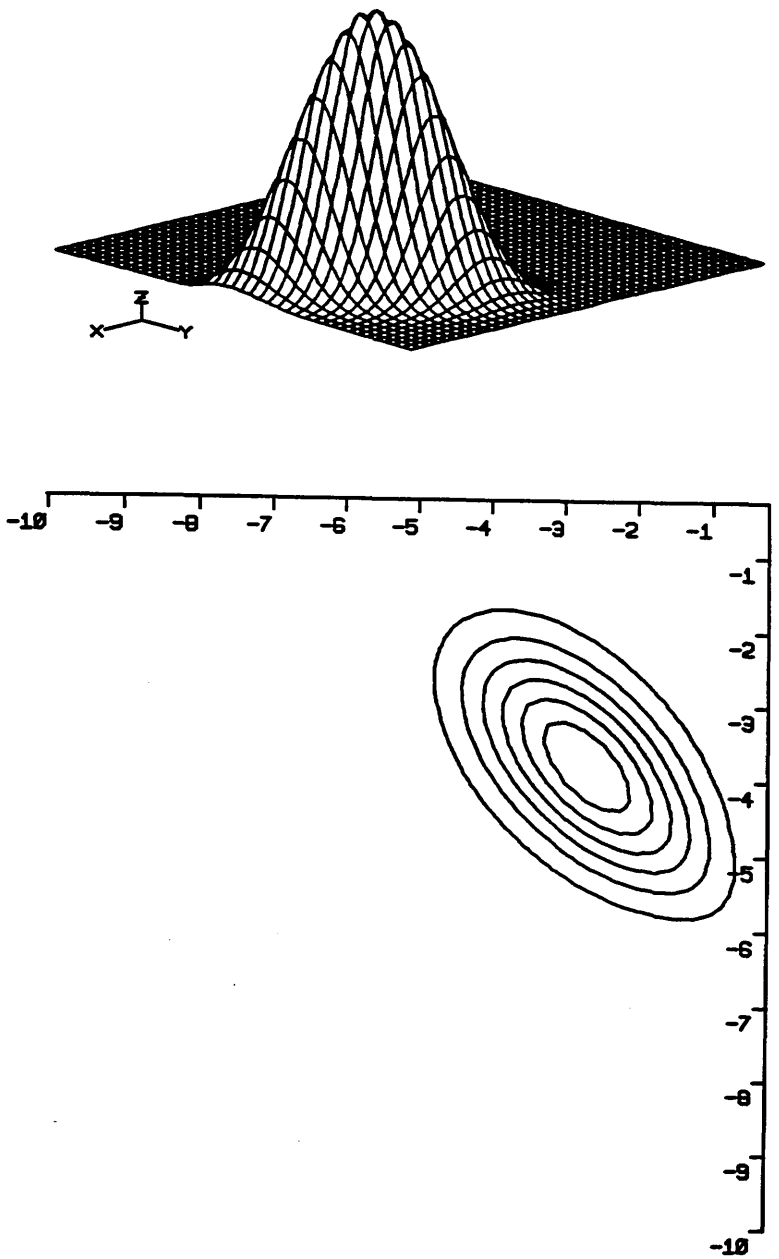

Fig. VI.3.8- The computational correlation signal of crossed-pair antenna at the operating frequency 3.2 GHz .
(antenna 2 is phased by $\frac{\pi}{6}$ and b = 6.5 cm).

The top figure shows the penetration depth of the signal and lower one shows the surface of the spread signal.

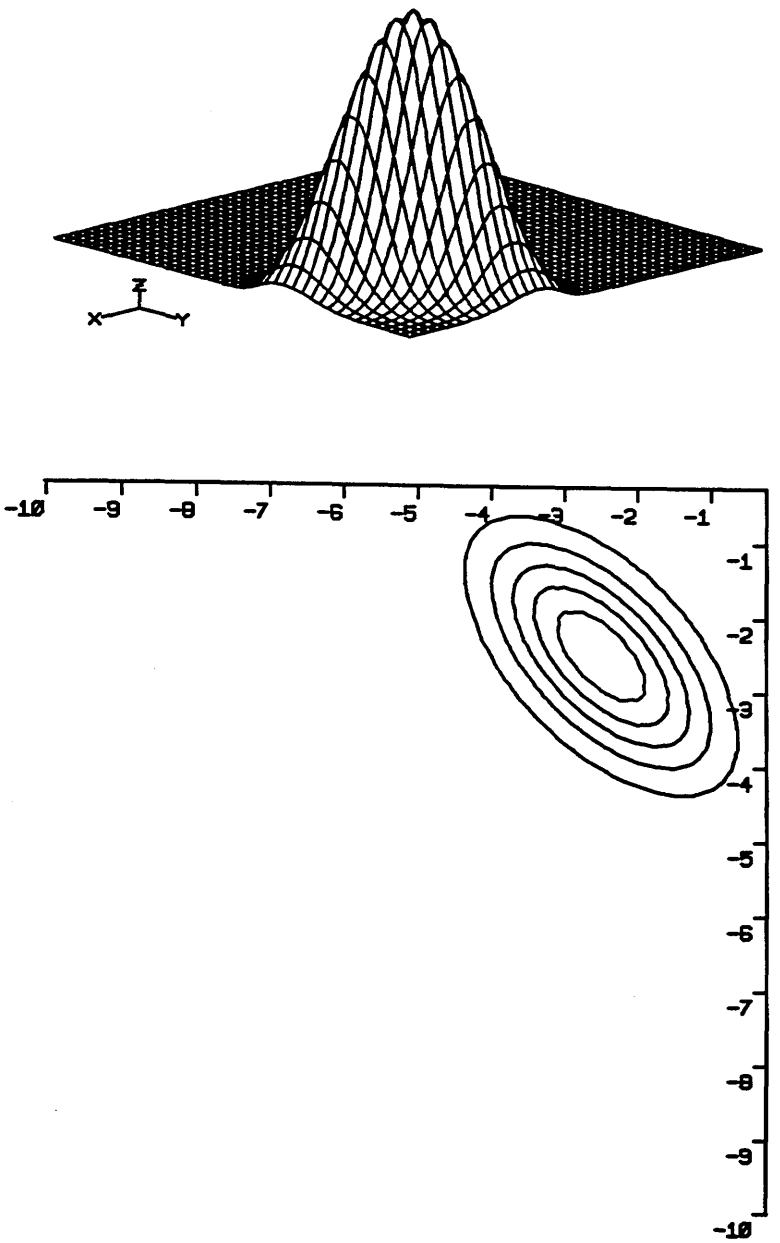

Fig. VI.3.9- The computational correlation signal of crossed-pair antenna at the operating frequency 3.2 GHz (antennas are in phase and b = 5 cm).

The top figure shows the penetration depth of the signal and lower one shows the surface of the spread signal.

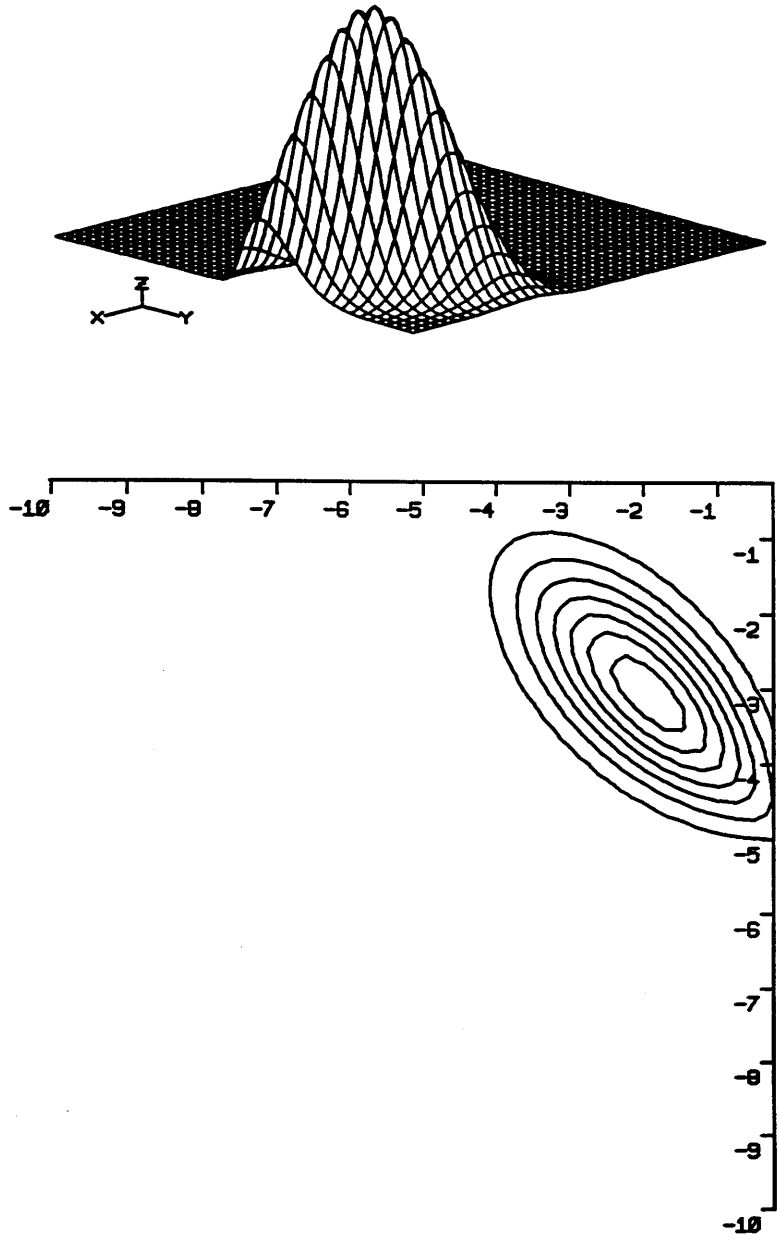

Fig. VI.3.10- The computational correlation signal of crossed-pair antenna at the operating frequency 3.2 GHz .
(antenna 2 is phased by $\frac{\pi}{6}$ and b = 5 cm).

The top figure shows the penetration depth of the signal and lower one shows the surface of the spread signal.

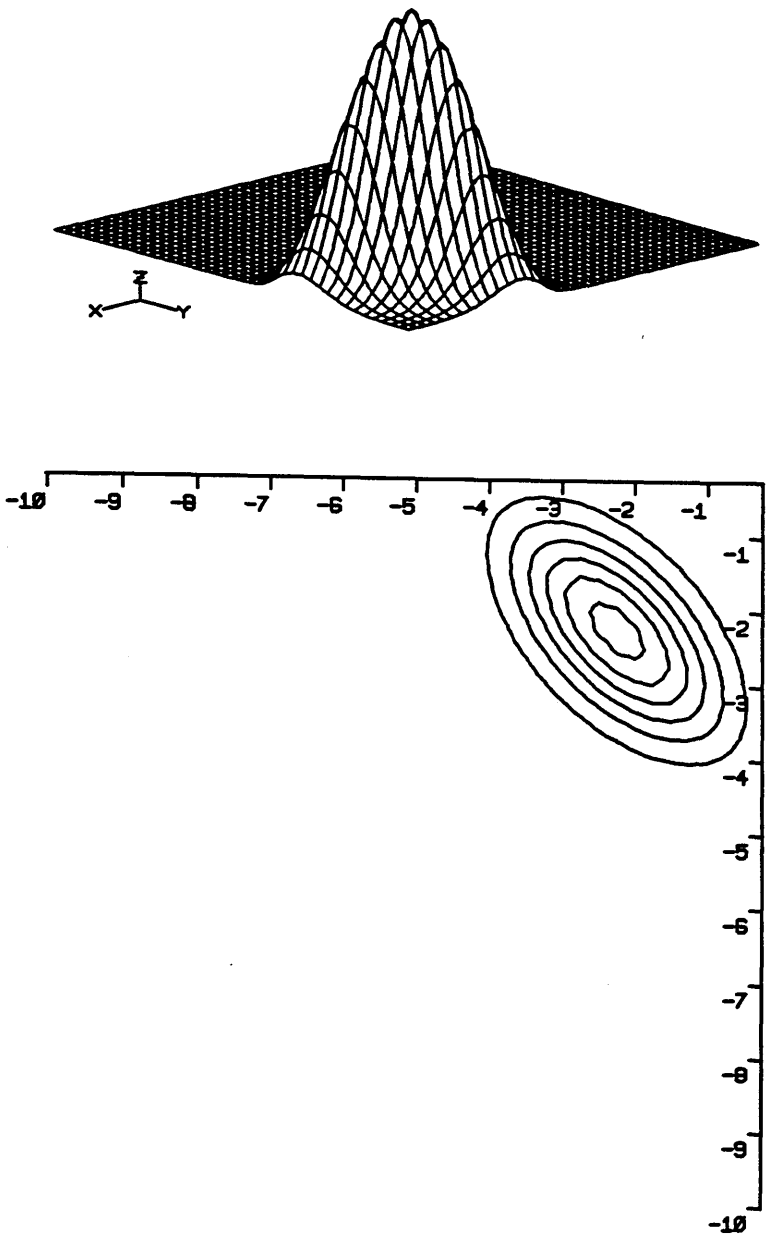

Fig. VI.3.11- The computational correlation signal of crossed-pair antenna at the operating frequency 3.2 GHz (antennas are in phase and b = 4.5 cm).

The top figure shows the penetration depth of the signal and lower one shows the surface of the spread signal.

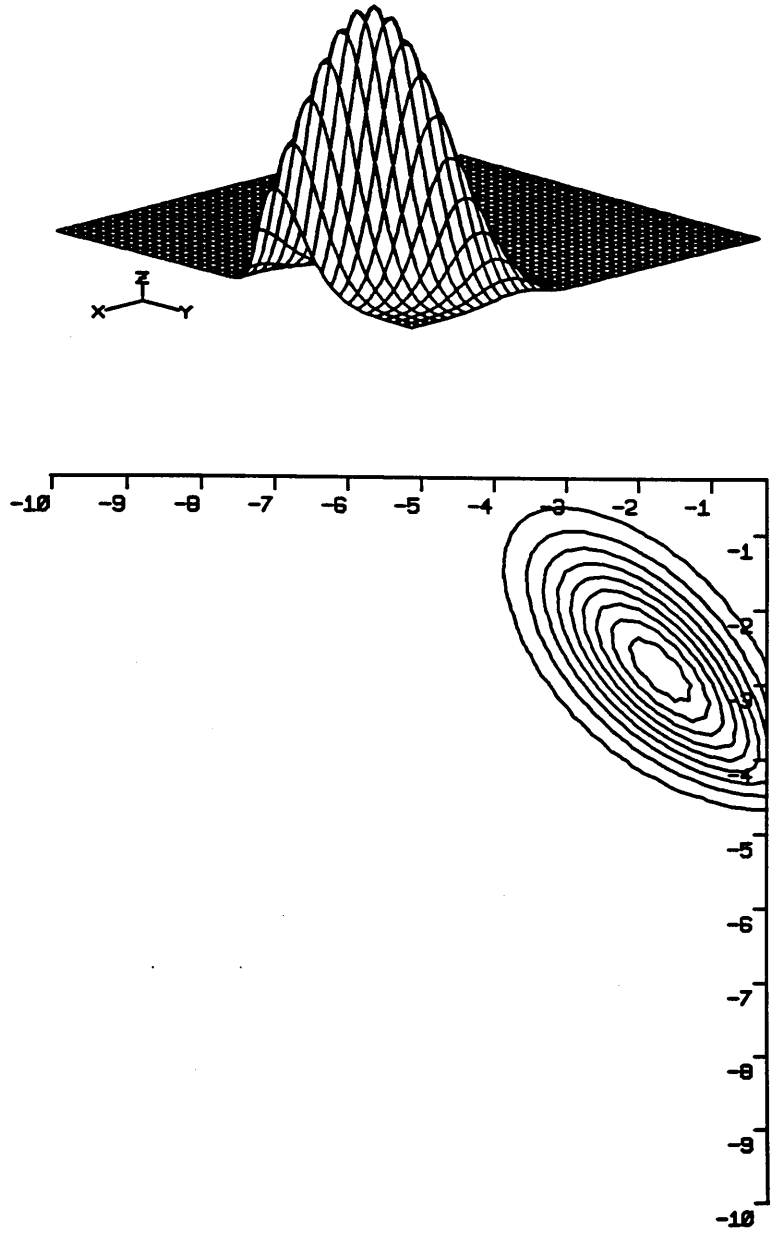

Fig. VI.3.12- The computational correlation signal of crossed-pair antenna at the operating frequency 3.2 GHz .
(antenna 2 is phased by $\frac{\pi}{6}$ and b = 4.5 cm).

The top figure shows the penetration depth of the signal and lower one shows the surface of the spread signal.

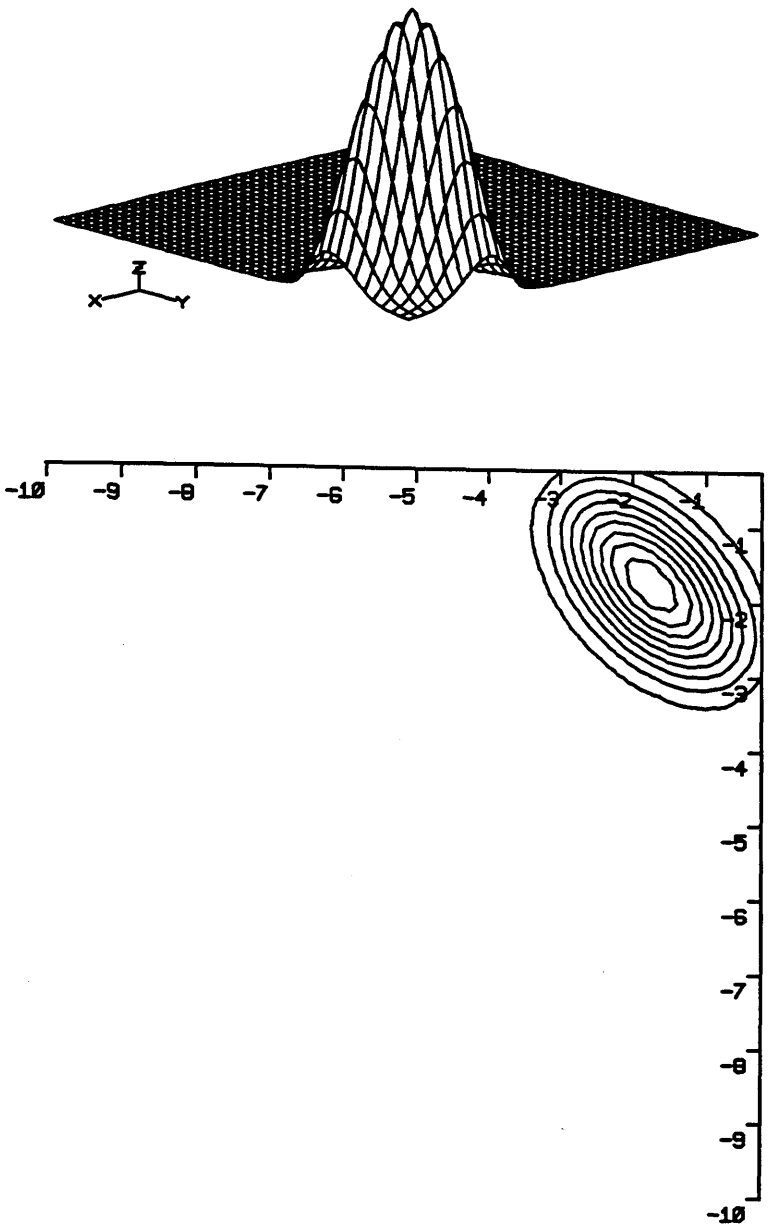

Fig. VI.3.13- The computational correlation signal of crossed-pair antenna at the operating frequency 3.2 GHz (antennas are in phase and b = 3.5 cm).

The top figure shows the penetration depth of the signal and lower one shows the surface of the spread signal.

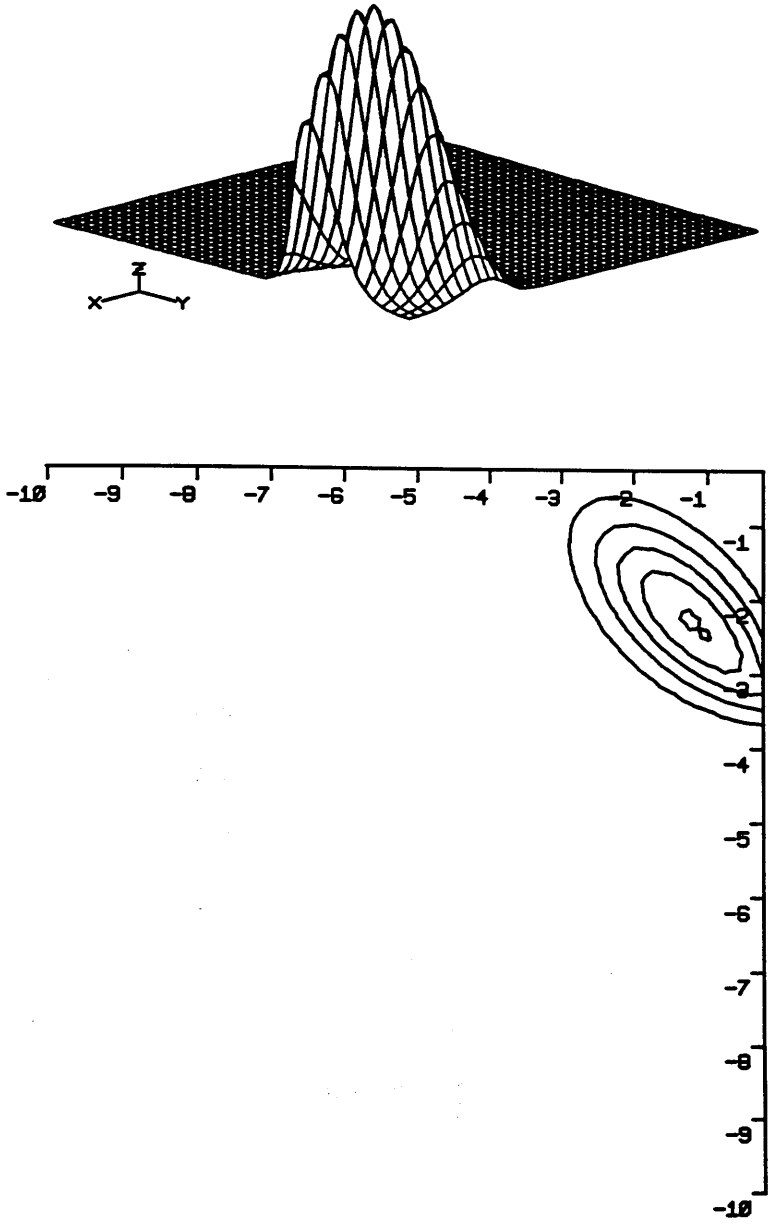

Fig. VI.3.14- The computational correlation signal of crossed-pair antenna at the operating frequency 3.2 GHz .
(antenna 2 is phased by $\frac{\pi}{6}$ and b = 3.5 cm).

The top figure shows the penetration depth of the signal and lower one shows the surface of the spread signal.

field will be very weak and the radiated region very small, so the distance should be limited. These numerical analyses show that for different positions as the spacing between the antennas increased the volume of overlap of the two antennas and the received pattern is reduced. So, the total magnitude of the signal at a given point in the field of view is also reduced. This could be become an increase in the distance between the antennas leads to a greater number of interference fringes.

Figures VI.3 give the modelling of the correlation radiometry at the operating frequency of 3.2 GHz for different distances of b between the two apertures of the antennas. The antennas are oriented so that the product of the two antenna received patterns is at a maximum depth. To achieve this the antennas are separated a certain distance and angled in towards each other in order to view a common point in the tissue. There is a limit to the distance separating between the antennas and the corresponding phase shift.

For the experimental arrangement chosen in this work, the midpoint aperture separation is 3.4 cm (2.5 cm between the antennas) and the antennas are in phase at a frequency of 3.2 GHz.

The received pattern of the correlation radiometer was measured in the muscle phantom material by the technique described in the beginning of the chapter. A small probe (constructed from semi-rigid coaxial cable) radiating wideband noise from a diode noise source is scanned across the field of view of the correlation radiometer antennas as shown in (Fig. VI. 1). The output reading of the radiometer is recorded for each position thus building up a grid of the antenna receive pattern. The antennas are orientated so that the product of the two antenna patterns is a maximum at a predetermined depth.

VI. 3.2- The experimental measurements:

from the theoretical analyses a separation of 3.4 cm was selected (2.4 cm separation between the antennas) between the apertures of the antennas with the microwave radiometer receiver operated at a frequency of 3.2 GHz to obtain

experimental measurements to compare with the numerical prediction, Figures V.3.1, VI.3.2, VI.3.3, VI.3.4, VI.3.5, VI.3.6, V.3.7, VI.3.8, VI.3.9, VI.3.10, VI.3.11, VI.3.12, VI.3.13, VI.3.14.

Fig. VI. 4 shows the experimental measurements using the microwave radiometer receiver with a noise source of the contour pattern of a phantom material which is similar to a high water content tissue ($\varepsilon_{rd}' = 75.9$, $\sigma_d = 2.6\ sm^{-1}$). These measurements have been done for the grid of 10 cm × 10 cm and 1 cm × 1 cm for the displacement of the probe. This shows the maximum received signal at the depth z = 2 cm and x = y = 4 cm of the viewed region; and the spread signal on the surface. Most of the significant signal is found between 3 and 7 cm in the y direction and between 3 and 6 cm in the x direction. These measurements give encouraging results for the crossed-pair antenna correlation radiometry for the treatment of limbs joint and breast disease because they show the expected form which is the interference pattern from the addition of the two antenna signals. These results are similar to that found by Mamouni.

Figure VI. 5 shows a series of x and y direction plots taken at different depths z and at a frequency of 3.2 GHz in de-ionised water ($\varepsilon_{rd}' = 75.9$, $\sigma_d = 2.6\ sm^{-1}$) for the same arrangement of crossed-pair antenna such as one given in Fig. VI. 1 with the antennas 180° out of phase. For z = 0 and 0.5 cm the received signal is very weak and reaches a maximum at y = 7 cm and at x = 9 cm. For z = 1 and 2 cm the maximum received signal is at y = 4 cm and at x = 5 cm and for z = 3 and 4 cm the maximum signal found is close the antenna apertures.

Figure VI.6 also shows a series of x and y direction plots in the de-ionised water, at 3.2 GHz and with the same antenna arrangement and with the crossed-pair antennas in phase. At z = 0, 0.5, 1 and 2 cm the received signal is very weak. At z = 3 cm and 4 cm the maximum received signal occurs close to the antenna on the x axis and at 5 cm on the y axis.

From these figures it was found that the maximum received signal of

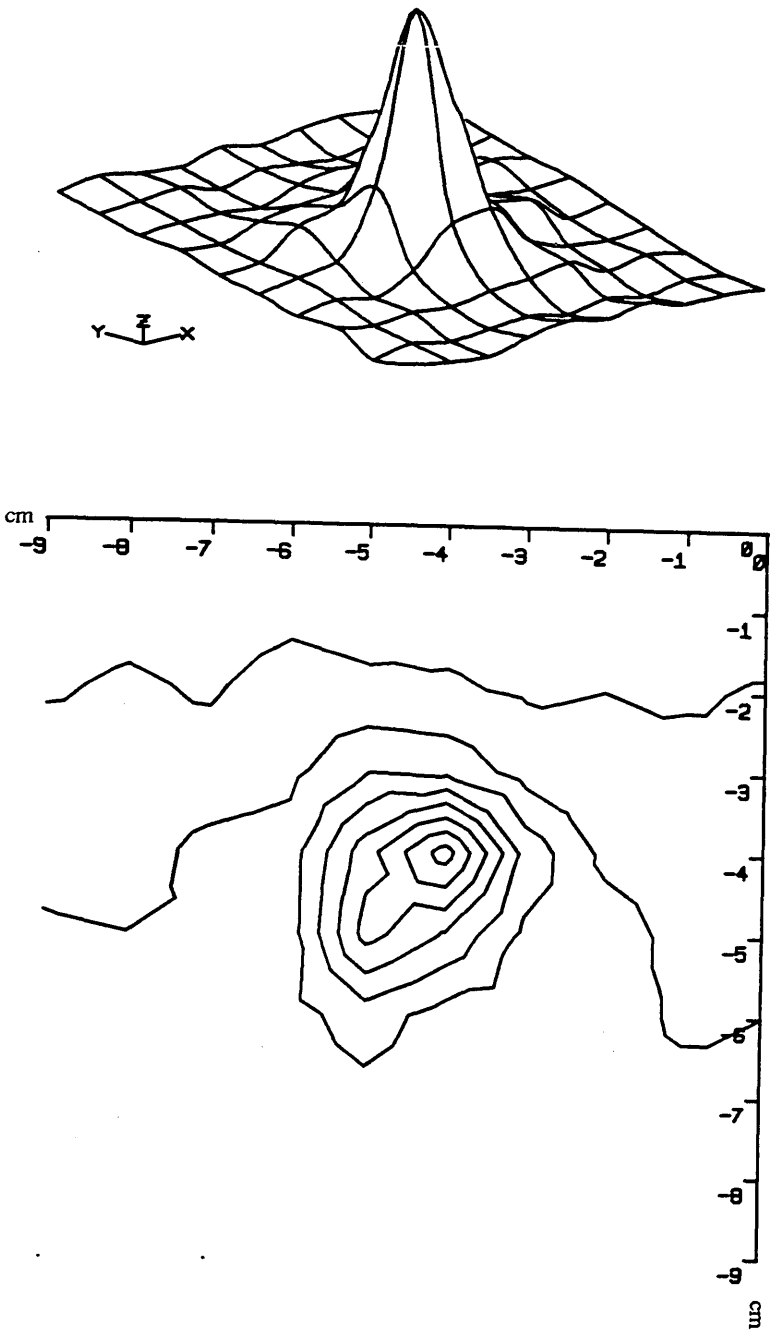

Fig. VI.4- The measured correlated signal of crossed-pair antenna at 3.2 GHz in the de-ionised water. The separation distance between the midpoint apertures is 3.4 cm.

The top figures shows the maximum received signal at the depth z = 2 cm, x = y = 4 cm and the lower one shows the spread signal in the viewed surface.

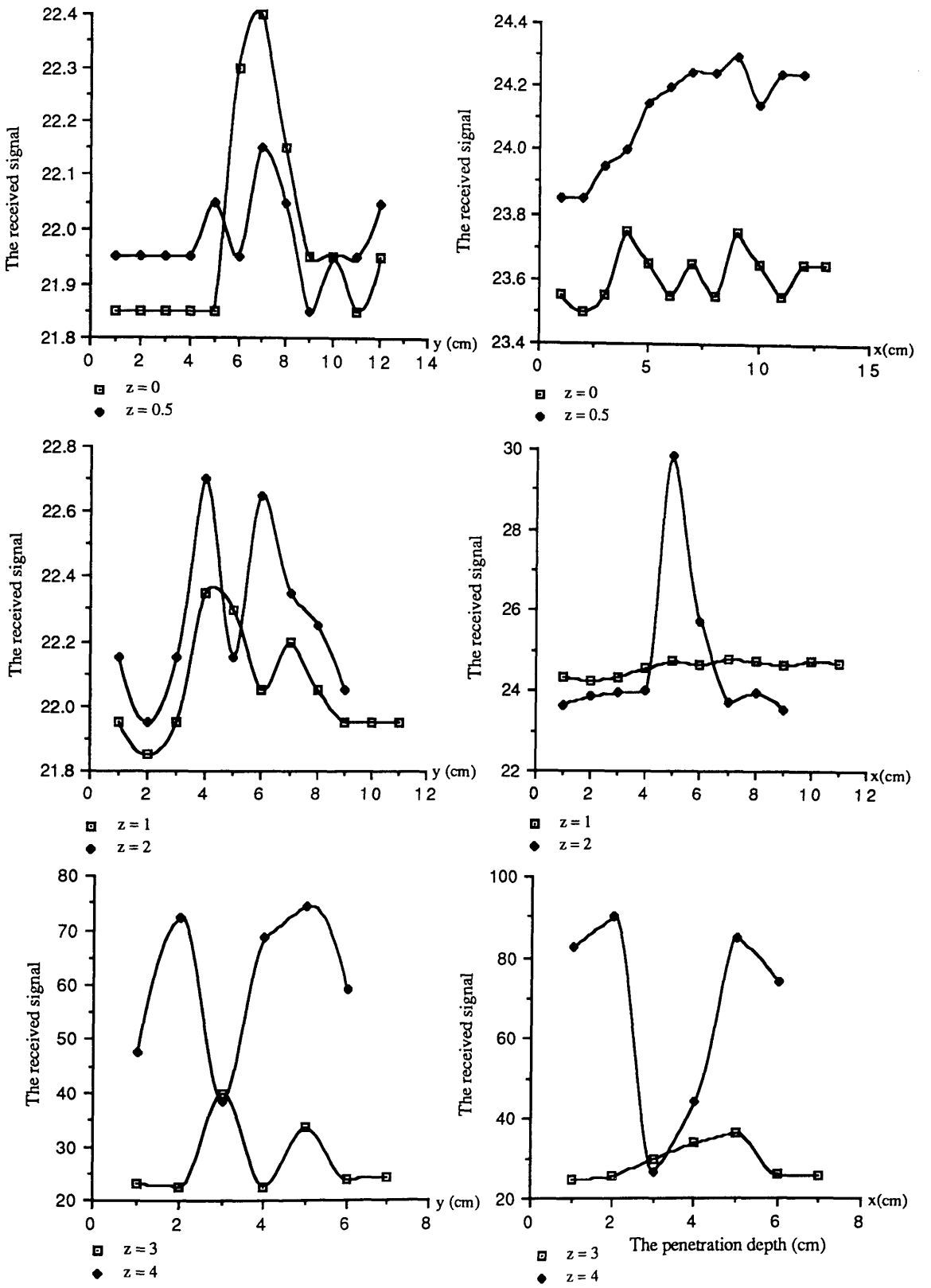

Fig. VI. 5- The received signal of crossed-pair antenna (180° phased) using the de-ionised water at 3.2 GHz of the operating microwave radiometer receiver and at different depths z.

a- along y direction
b- along x direction.

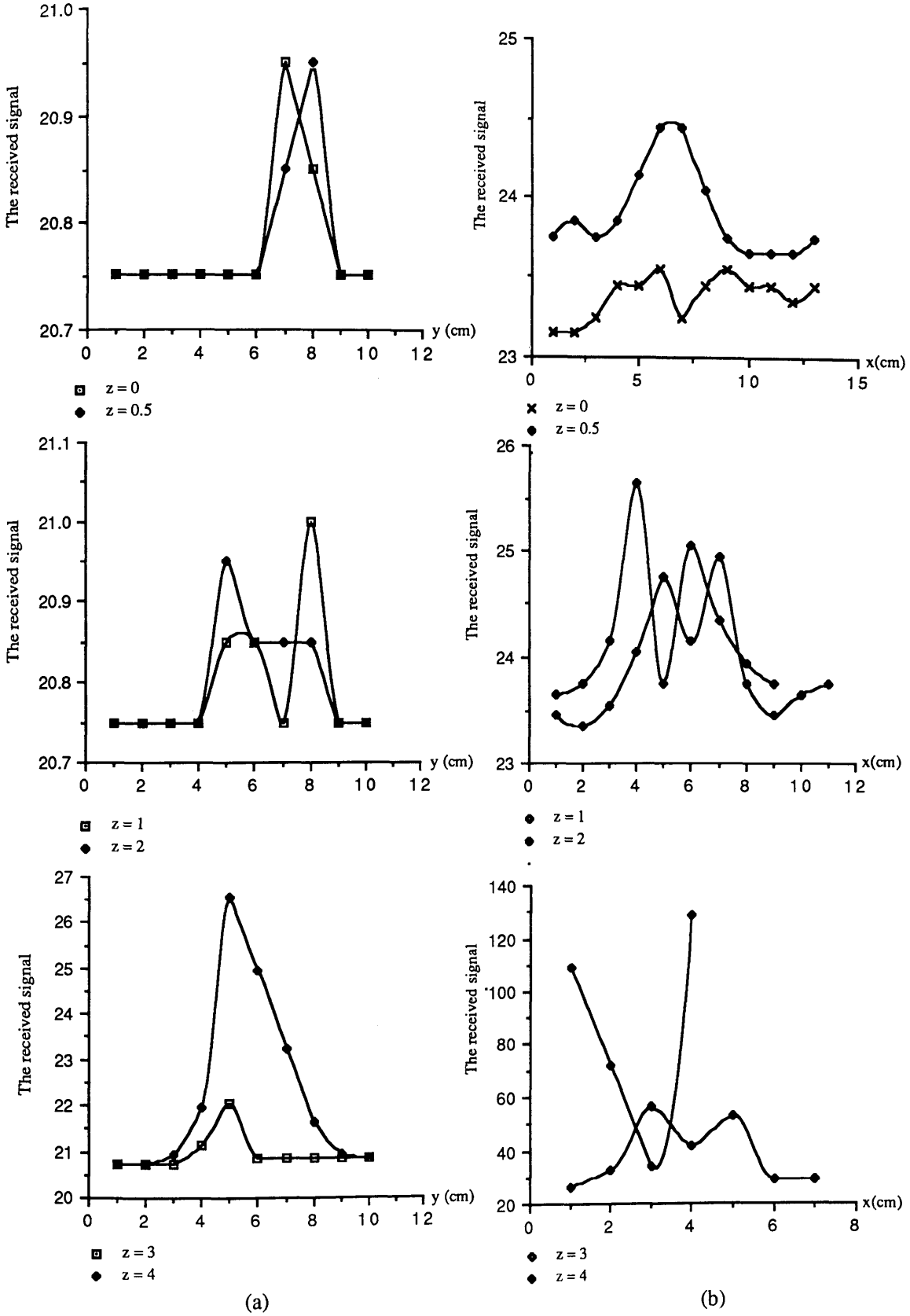

Fig. VI.6- The received signal of crossed-pair antenna in phase using the de-ionised water at 3.2 GHz of the operating microwave radiometer receiver and at different depths z.

a- along y direction
b- along x direction

crossed-pair antenna 180° out of phase is at the depth 4 cm for two positions x = 2 cm and x = 5 cm, close to the antenna apertures. However, the maximum of the received signal from the radiometer for y direction is at 4 cm depth for the positions 2 cm and 5 cm. For the second case where the antennas are in phase the maximum received signal is at the depth z = 4 cm for both directions at 2 cm and 5 cm positions. That leads to the conclusion that the maximum received signal from the microwave radiometer for both directions is similar at the depth of 4 cm. The maximum received correlated signal occurs at a depth of 4 cm on the y axis where the antennas are in phase.

Figures VI. 7 and VI.8 show series of x and y plots in muscle phantom material (sucrose solution $\varepsilon_{rd}' = 25$, $\sigma_d = 3.18\ sm^{-1}$) with the same antenna arrangement as before. The maximum received signal is at 4 cm at position 1 cm and 6 cm for x direction and at the position 5 cm in y direction for both arrangements in phase and 180° out of phase. The correlated received signal from the crossed-pair antenna has also a maximum at depth of 4 cm for these phantom materials on the y axis.

This work agrees with results using a similar pair of antennas separated by 4.4 cm from the mid-point of the apertures and angled at 48° to each other in muscle phantom materials Newton, (1986). The maximum penetration depth which can be achieved is 2.5 cm.

Figure VI. 9 shows the penetration depth in de-ionised water and in a 50% sucrose solution for the above antennas arrangement in phase and at 180° out of phase. This shows that the received signal decreasing with increasing penetration depth z, this fall-off in terms of e^{-1}. The maximum penetration depth for both phantom materials is at z = 4.5 cm depth, so at small values of the penetration depth significant information can be obtained for the microwave correlation radiometer with high-water content lossy dielectric materials.

Figure VI. 10 presents the scanning of crossed antennas with a small probe and the same arrangement with a noise source through the x axis (see Fig. VI.10) in

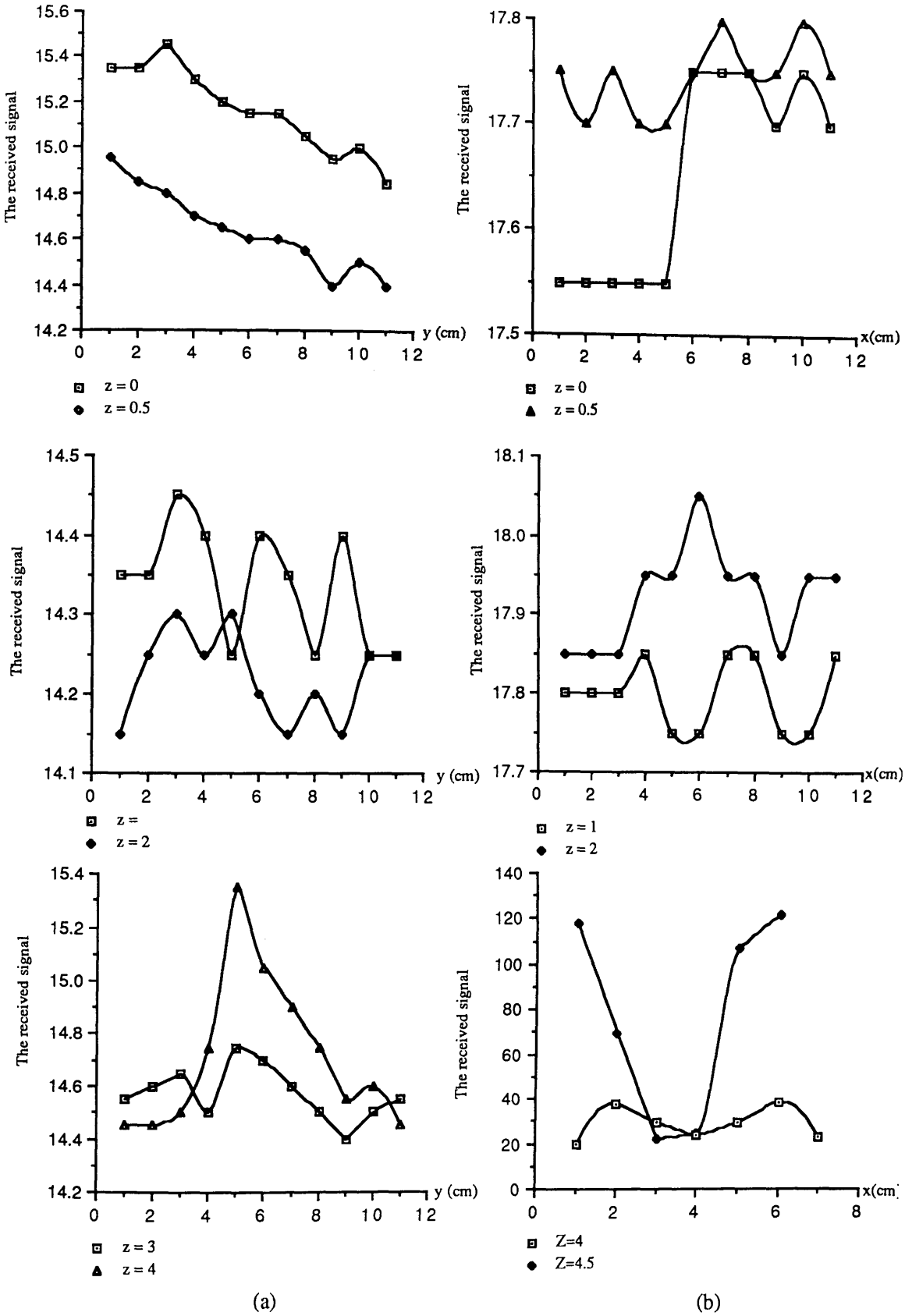

Fig. VI. 7- The received signal of crossed-pair antenna (180^{o} phased) using a 50% sucrose solution at 3.2 GHz of the operating microwave radiometer receiver and at different depths z.

a- along y direction
b- along x direction.

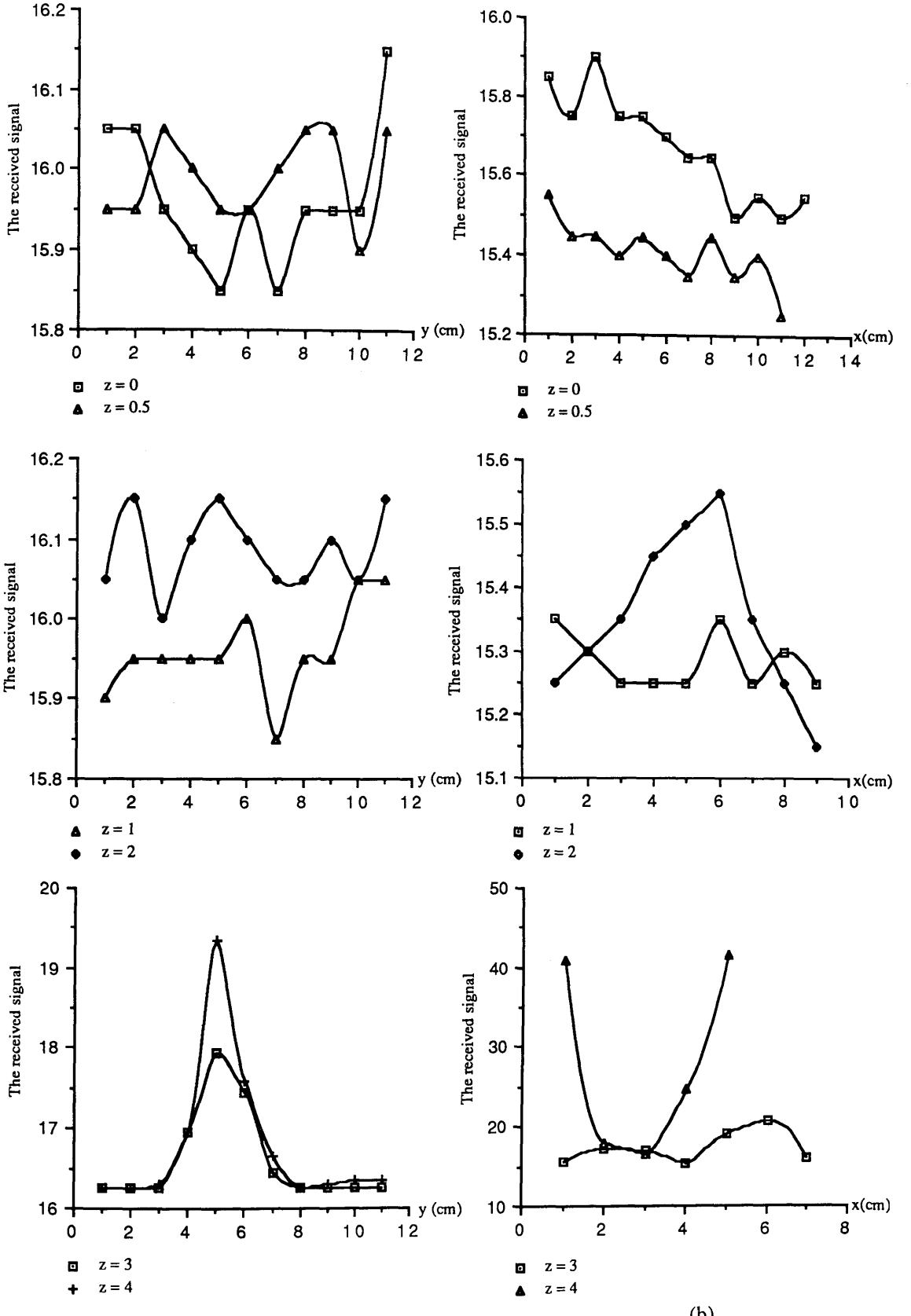

Fig. VI. 8- The received signal of crossed-pair antenna in phase using a 50% sucrose solution at 3.2 GHz of the operating microwave radiometer receiver and at different depths z.

a- along y direction
b- along x direction.

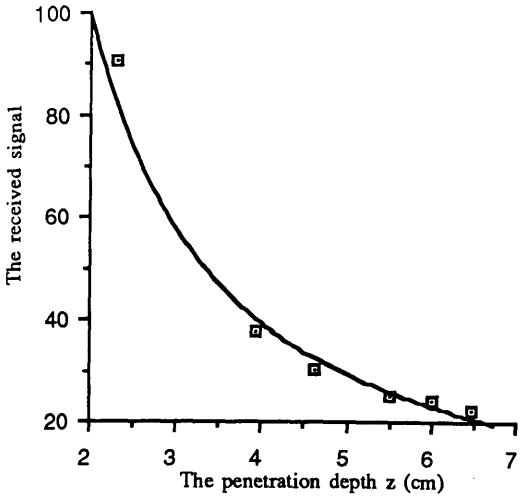

(a)

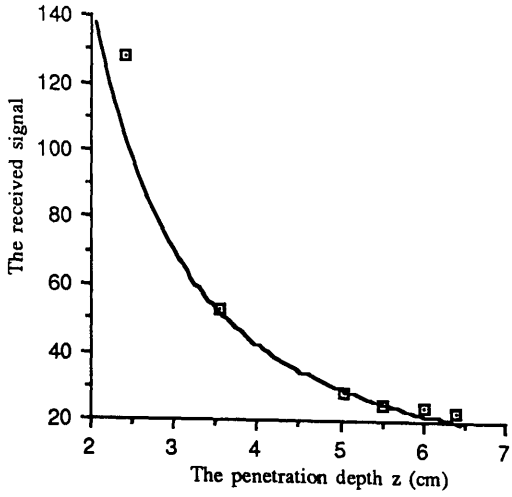

(b)

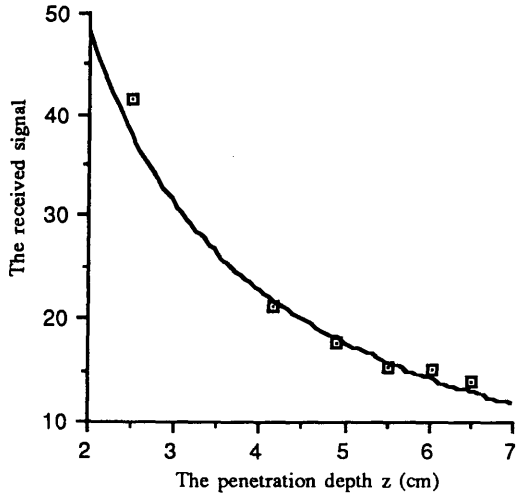

(c)

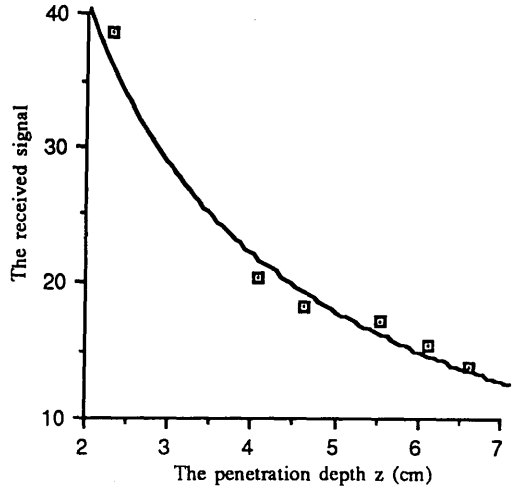

(d)

Fig. VI.9- The penetration depth for muscle phantom material at 3.2 GHz of crossed-pair antenna.

a- The de-ionised water and the antennas are 180° phased

b- The de-ionised water and the antennas are in phase

c- 50% sucrose solution and the antennas are in phase

d- 50% sucrose solution and the antennas are 180° phased

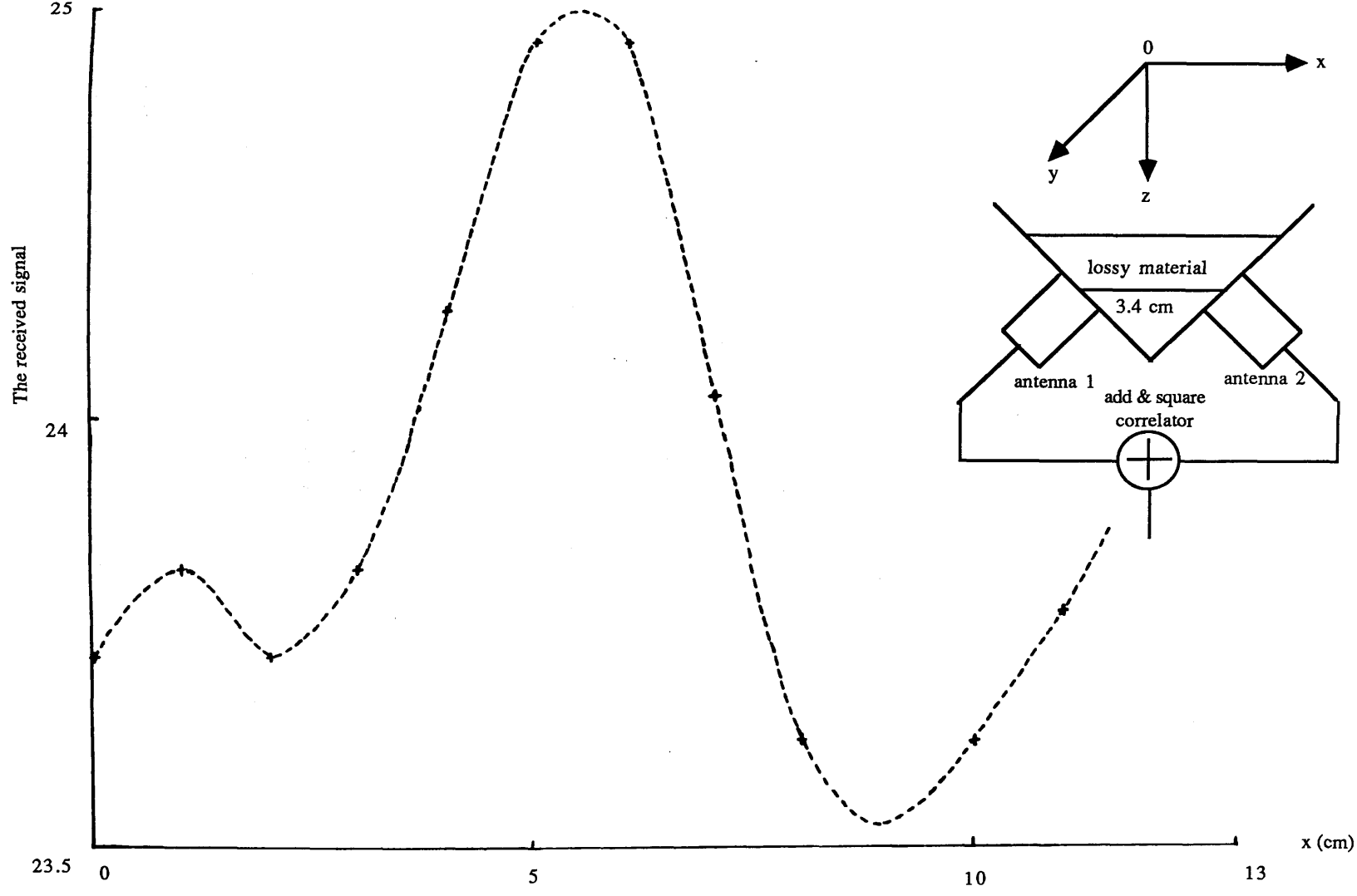

Fig. VI. 10- The variation of the correlated signal along x direction in the de-ionised water at 3.2 GHz using microwave radiometer receiver (z = 6 cm, y = 0).

de-ionised water at z = 0.5 cm depth and at a frequency of 3.2 GHz. It shows clearly the behaviour of the correlated signal for a single frequency for a perpendicular arrangement of the antennas. The numerical analysis agrees well with the experimental measurements are in good agreement.

In comparing these results with those of Newton, (1986) the present work considered several cases of correlation using cylindrical and rectangular waveguide antennas. With TE_{11}-mode cylindrical waveguide antennas, angled 48° to each other and the mid-point of the apertures separated by 4.4 cm, the maximum received signal is at a depth of 2.5 cm, When the same antennas are placed side by side in parallel, the pattern obtained is very small. With TE_{01}-mode rectangular waveguide antenna with an aperture 0.5 × 2.3 cm and length 4.5 cm (internal dimensions) the closest separation that is possible for the aperture midline is 0.72 cm. The antennas are arranged parallel to each other, the maximum received signal is at z = 1 mm and the penetration depth is about 0.5 cm. These TE_{01}-mode rectangular waveguide antennas have also been considered with the antennas separated by 1.75 cm from each other and the orientated is at 30°. The signal still does not have a maximum received signal at a significant depth and the interference pattern has six fringes. The investigated operating frequency range was 2.5 - 3.5 GHz.

Mamouni, (1988) studied two cases where the antennas were angled at 30° and placed in parallel using TE_{01} rectangular waveguide antennas, with an aperture of 2.2 × 4.4 cm and length of 10 cm (internal dimensions), using a frequency range of 2.5 - 3.5 GHz. The method is described in Chapter V.

Figure V. 11 shows the experimental analyses (data collected from Mamouni, 1988) at a frequency of 3 GHz and at depth z = 2 cm, the TE_{10} -mode rectangular waveguide antennas were angled 30° and close together and moved parallel to the surface of the material.

Fig. VI. 12 shows the same pair of the antennas placed in parallel side by side for the frequency band 2.5 - 3.5 GHz and at the depth z = 2 cm. The minimum

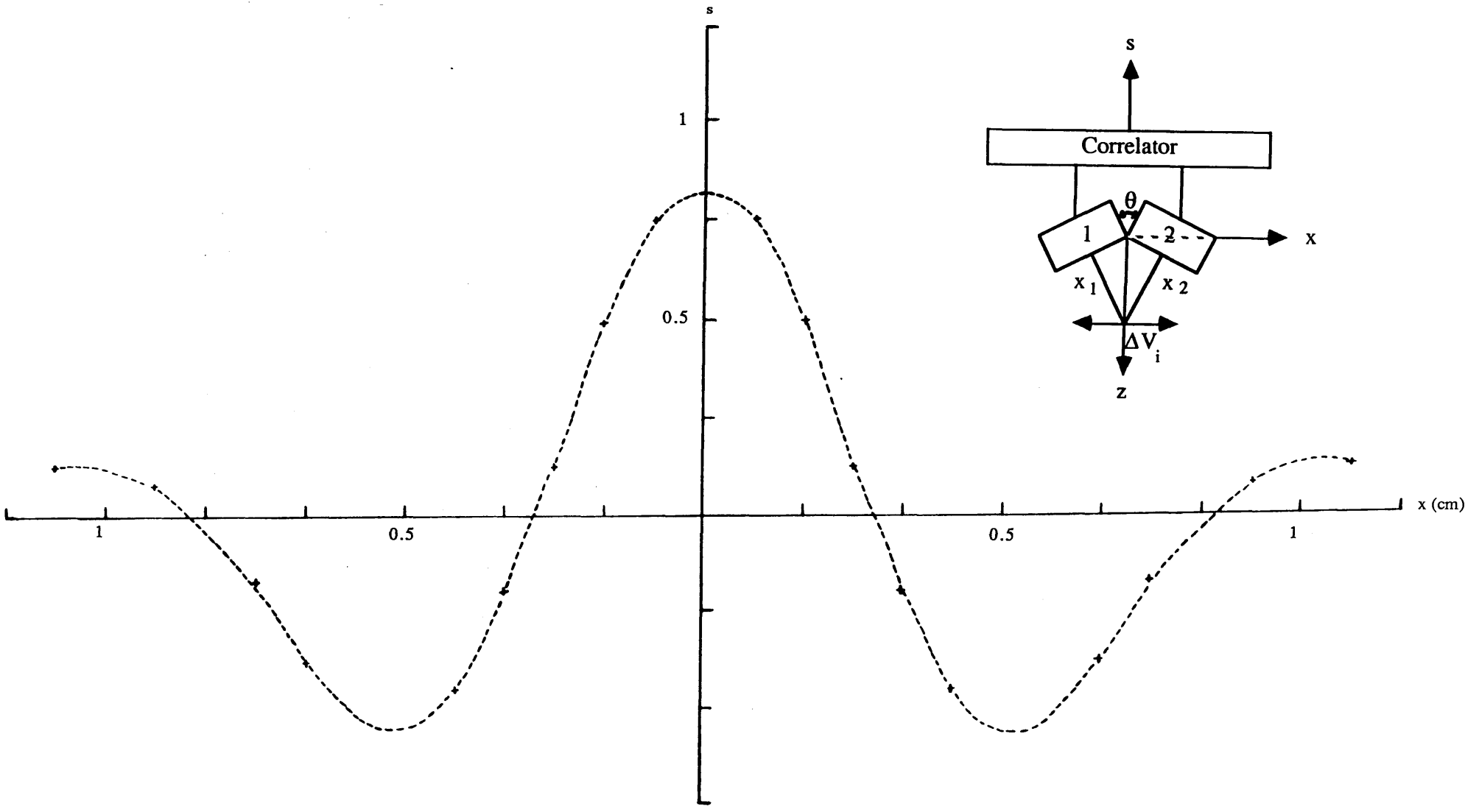

Fig. VI. 11- The correlated received signal in water at 3 GHz (y = 0, z = 2 cm and $\theta = 30^{\circ}$)
data collected from Mamouni, 1988.

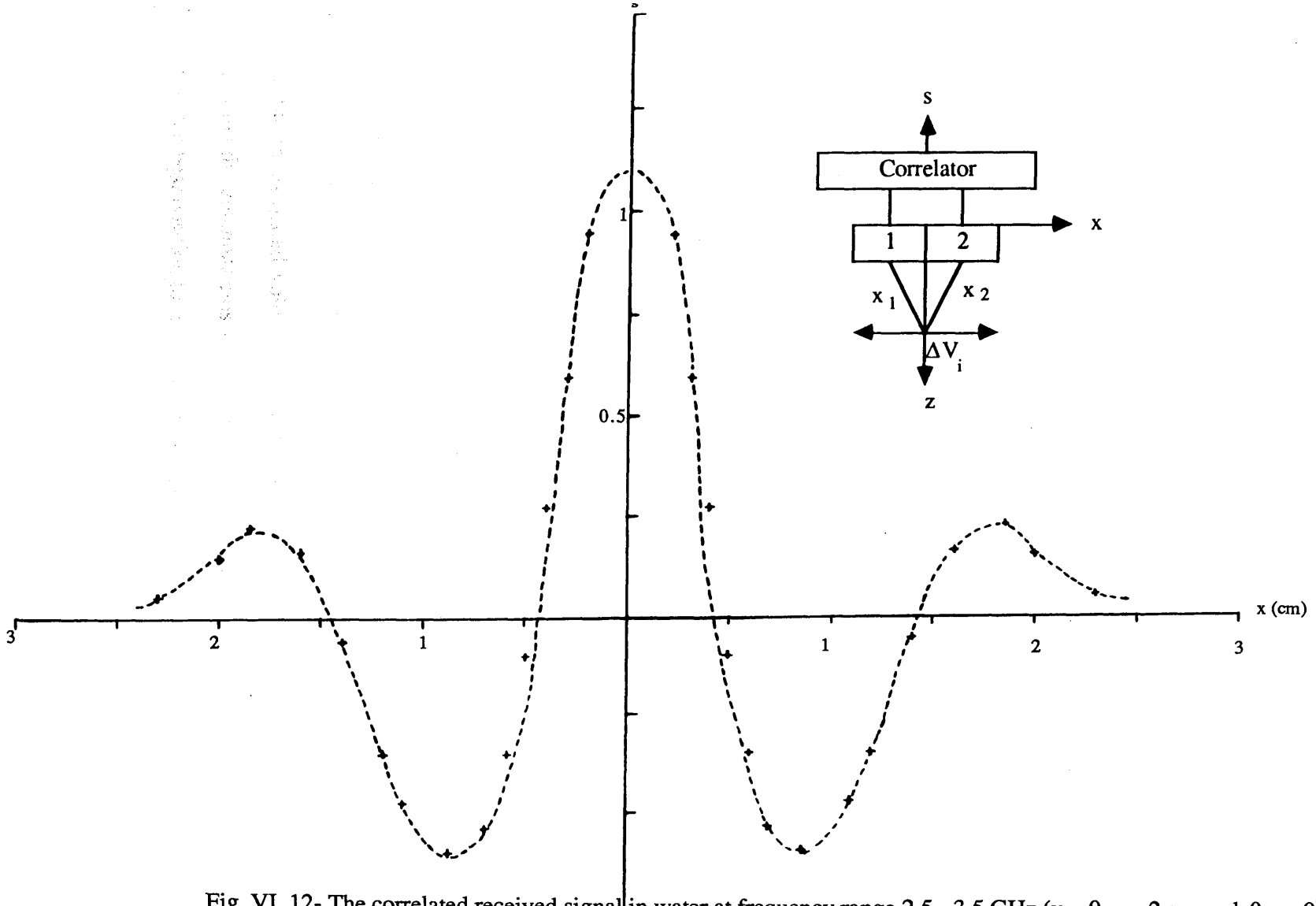

Fig. VI. 12- The correlated received signal in water at frequency range 2.5 - 3.5 GHz (y = 0, z = 2 cm and $\theta = 0^{o}$) data collected from Mamouni, 1988.

separation distance between the antennas is 0.72 cm and the maximum received signal in the lossy material which can be achieved was at a distance of 0.5 cm. It was found that the experimental and the numerical analyses were in agreement.

In conclusion, it was found that a perpendicular arrangement for these antennas, if placed close enough together and the received signals were in phase, gave a simple centered received signal. The maximum penetration depth that can be achieved was about z = 4 cm (2.5 cm from the bottom of the container as shown in Fig. VI.1) in the de-ionised water and in the 50% sucrose solution at 3.4 cm distance from the antenna apertures.

VI. 4- Conclusion:

The purpose of investigating microwave correlation radiometry was to improve the existing method for monitoring microwave hyperthermia induction and microwave temperature measurement up to several centimeters into the tissue for breast and limb joint disease treatment with negligible interaction from surface tissues.

A cross-positioned antenna arrangement was considered for this work. This system of antennas gives a pattern of investigated volume resulting from the product of the individual antenna received patterns. The received signal is modulated by a series of interference fringes with the positive and negative components cancelling out in the total output reading. The system does not respond to uniform temperature distributions and gives a signal only where there are regions in the investigated volume at different temperatures. This can be improved by placing the antennas closer together. A series of numerical analyses were made to find the best position for the antennas which can be obtained to achieve a maximum depth in the viewed region with negligible interaction from its surface tissues.

In the numerical analyses the antennas were placed at a range of distances between 10 cm and 3.5 cm from each other. These measurements were taken, as

illustrated in Figures VI.3, with the received signals at the antennas being, first, in phase with each other, and, secondly, out of phase by $\frac{\pi}{6}$. The best numerical results were achieved when the antennas were placed 3.5 cm from each other and in phase. The experimental arrangement selected correspond to 3.4 cm from the midpoints of the antenna apertures gives the expected pattern form. It was proved that at certain limits of spacing and phase of antennas a maximum depth of received signal can be obtained.

Several groups have published work on microwave correlation radiometry considering the problem of antenna spacing (as discussed in section V.1), in relation to a maximum depth, for detecting thermal gradients. These problems can be avoided by reduction in sensitivity due to the limited volume of the individual antenna received signal patterns. The arrangements as were suggested by The Microwave Thermography Group at Lille University, France, and by Newton, (1986) did not give significant results.

The technique of the present work is simple to use and to analyse. The output from the radiometer is an average over a fairly large volume of phantom dielectric material simulated biological tissue and is affected by dielectric properties and material or tissue structure as well as the actual temperature, so that it is important that the received signal pattern is as simple and predictable as possible.

In practice the crossed-pair antenna arrangements show encouraging results for biomedical application especially for the present Glasgow interest in breast and limb joint diseases.

Chapter VII

Electromagnetic field measurements and the nonresonant perturbation technique

VII.1- Introduction and literature review:

Microwave radiometry techniques have been used extensively in medical applications for monitoring tissue temperature and for electromagnetic field detection in biological tissues. Microwave receiving patterns from biological tissue have been analysed to investigate subcutaneous body temperature. Since temperature increase in the tissue resulting from deposition of microwave energy, is proportional to the square of the electric field strength in the tissue, through the antenna reciprocity law, the response to thermal radiation must have the same pattern (Slater, 1942). There are, two ways to determine the receiving pattern: a) by measuring the electric field pattern, or b) by scanning the temperature pattern using a microwave thermographic system such as a microwave radiometer. These techniques are constantly being improved given encouraging results for microwave hyperthermia induction. The Microwave Thermography Group at Glasgow University has developed and applied *nonresonant perturbation*, to assist the development of the medical application of microwave hyperthermia induction and microwave thermographic temperature measurement. Both these techniques require the electromagnetic field patterns of the spatial applicators or the antennas used to be known.

The *nonresonant perturbation* technique is a relatively simple method for accurately measuring electromagnetic field impedance in open or closed systems at high frequencies, giving amplitude, phase and spatial information about the electromagnetic fields associated with a structure (Land, 1984). It has certain

similarities to the resonant perturbation technique, but it can be applied to measurement situations where, due to radiative or dissipative power loss, a suitable resonance cannot exist, or where it is unsuitable or inconvenient to set up or measure in the standing wave pattern of the resonant perturbation method. The technique is characterized by the fact that the frequency at which measurements are made remains fixed. That is, this frequency is independent of measurement of the field perturbing object within the device.

Perturbation techniques have been used for the measurement of electromagnetic fields in microwave devices. Harries, (1937); Maier and Slater, (1952) presented a resonant perturbation method for the measurement of the direction and strength of electromagnetic fields in microwave structures. Land, (1987b) presented a new method for a resonant perturbation measurement of electromagnetic field distribution in high frequency structures and for the measurement of material properties in cavities with known fields. This technique has been restricted to low-loss systems which can support a resonance of suitable high Q-factor. Cullen and Parr, (1955) described a perturbation method using mechanical modulation of the perturber for measuring electromagnetic fields of an antenna. They found that the reflected electromagnetic wave rapidly becomes weaker as the distance from the antenna increases and its detection proved very difficult. In spite of these difficulties, a perturbation method of field measurement was more attractive than a direct method, because a smaller disturbance of the field to be measured would result. This benefit has been partly due to the fact that the perturbing element is not electrically connected to the remainder of the apparatus. Electric field measurements have been preferred in microwave devices in which resonance cannot be employed. The microwave device may prove too lossy to support resonance. This has lead to the introduction of the *nonresonant perturbation* technique to measure the electromagnetic field strength.

Nonresonant perturbation techniques have been presented and analysed for transmission coefficient measurement (Kino, 1955 and Lagerstrom, 1957), the

change in the propagation constant of the microwave device being calculated in terms of the field strength and the parameters of the perturbing object. Following this work interest developed in *nonresonant perturbation* measurements in which the input reflection coefficient of the object is measured. Mallory, (1961) considered the *nonresonant perturbation* technique to measure electric and magnetic field strengths within structures where energy is transferred to charged particles. Steele, (1966) developed a more rigorous and general justification for this measurement technique. He presented a theory for measuring the electric and magnetic fields at various points within an electromagnetic system. This theory applies the Lorentz reciprocity theorem and is similar to the theory developed by Jaynes, (1965) to calculate the change in the input impedance of a cavity when it is perturbed. Land, (1984) presented a further developed theory of the *nonresonant perturbation* technique for measuring field impedances in open or closed, low or high loss radio-frequency and microwave structures. He compared the results obtained with Steele's results for closed boundary surfaces. Comparison of these results showed that for the case considered by Steele there is agreement except for a factor of two probably due to an error in Steele's paper (Eq. 11 Steele's paper). Land confirmed his results by comparison with Cullen and Parr's analysis and measurement of perturber reflection coefficients in TE_{01}-mode rectangular waveguide. Recently Land, (1988) has carried out investigations using the *nonresonant perturbation* techniques for measuring the distribution of electromagnetic fields in high loss biological phantom materials.

VII. 2- Electromagnetic fields measurements "Literature review":

Microwave radiometry techniques have been applied to determine the electromagnetic fields patterns in low- and high-water content tissues using different types and sizes of applicators or antennas. Several workers have measured the penetration depth of the relative electric field from an applicator or an antenna

aperture comparing, it with the plane-wave penetration depth and derived the configuration of the electric field.

Electromagnetic fields at microwave frequencies have special biological significance since they can readily be transmitted through, absorbed by, and reflected by biological tissue boundaries to varying degrees (Mamouni et al., 1983), depending on body size (Guy, 1971b; Johnson and Guy, 1972), tissue properties, and frequency. The electromagnetic field configurations have been analysed in biological tissues for special simplified cases such as plane, cylindrical, or spherical layers of tissue exposed to plane wave. The human body is covered by a thin layer of skin next to a thicker layer of subcutaneous fat over muscle or other tissue of high water content. The absorption and reflective properties of tissues exposed to near-zone or radiation fields in the low frequency range of the microwave band is strongly related to the geometry and dielectric properties of the different tissue layers. Electromagnetic fields receiving patterns, using frequencies in the range of 0.3 to 3.0 GHz, offer one of the most promising and widely employed methods for hyperthermia treatment since it includes the possibility of selective controlled receiving pattern of specific tissue volumes.

Larsen et al., (1978) described a technique for electromagnetic fields analysis in the high frequency band (3 - 30 MHz). The method consists of using an electrode interface characterised by an equivalent polarisation impedance in series with the sample impedance. This method has not given encouraging results nor discomfort for the patient. Taylor, (1984) demonstrated that in the near field configuration of suitably designed applicators, the penetration depth of the electromagnetic wave can greatly exceed the usual skin depth. Numerical analyses have been carried out to improve the characteristics of the antenna or applicator used for medical purposes. An effective penetration depth has been achieved using this applicator of about 3.2 cm for muscle or organ tissues ($\varepsilon'_r = 50$, $\varepsilon''_r = 30$) and could be increased up to 7 cm for very high permittivity tissues (Franconi et al., 1986). The characteristics of the electromagnetic power absorption have been found

to vary significantly with the polarisation, frequency, size, and dielectric properties of the medium (Massoudi et al., 1977; Barber et al., 1979; and Barber, 1977).

King et al., (1983) investigated the behaviour of insulated antennas for localized heating as in the hyperthermic treatment of tumours. The antenna was constructed from flexible gold plated electrodes. Numerical predictions of the electric field were compared with the experimental measurements. They found that the electromagnetic power rapidly decreased with radial distance and in addition that the technique was very expensive.

Johnson and Guy, (1972) described electromagnetic wave effects from the lower radio-frequency up to higher microwave frequencies where the wavelength was large compared to cell size. They considered different types of tissue layers (plane, spherical and cylindrical) exposed to plane-waves where propagation characteristics in biological tissues may be examined to demonstrate how radiation has been absorbed when the size of the tissue surface was large compared to the wavelength. The near-zone fields were analysed in order to show the dependence on source size and distribution. They found that the penetration depth for tissues of low-water content was as much as 10 times greater than that for tissues of high-water content. The near-field measurements of antennas have been briefly presented by Baird et al., (1988).

Guy, (1971a) presented experimental analyses of electromagnetic fields induced for several phantom materials simulating human fat, muscle, and bone. These materials have complex dielectric properties (ε'_r = 4.6 to 6.2, ε''_r = 0.17 to 0.55 and ε'_r = 49 to 58, ε''_r = 0.33 to 1.7) which closely resemble the properties of human tissues reported by Schwan et al., (1954) and Schwan et al., (1956). The dielectric properties have been measured by a standard method described by Von Hippel where the thickness of dielectric in a coaxial transmission line to the input and termination impedance should be known. Rectangular aperture sources were used for plane layers and various sources for the other layers. Guy, (1971b) carried out the study of electromagnetic fields in biological material. Computer modelling

has been used to select an aperture size and source distribution to provide the best subcutaneous penetration depth in the tissue layers. The electromagnetic field of a rectangular aperture source in direct-contact with biological tissue has been discussed. The method used has proved that it was valid for both far- and near-zone fields and involved the use of a thermographic system for recording temperature distributions. It has been found that minimum depth receiving ratio is achieved through the use of a simple TE_{10}-mode aperture source distribution one wavelength in height and between one and two wavelength in width. The method used by Guy, (1971b) has been extensively employed to determine the temperature distribution in biological tissues. This method, when used properly, was very fast and convenient. However, it required expensive equipment (a high power source, a thermographic camera and preferably minicomputer). It may also prove unsuitable at the applicator development stage, for it does not provide any information about the direction of the electric field.

Gajda et al., (1979) presented a simple system for mapping the electric field pattern in a simulated tissue and described its performance Fig.VII.1 . It consisted of a mapping system operating at frequencies between 2 and 4 GHz, a microwave generator, a test applicator, a container with liquid phantom tissue material, an electric field probe, a detector, an amplifier (swr meter) and an x-y recorder. Muscle simulating tissue (a mixture of 30% glycerol and 70% water) has been used at a frequency of 2.45 GHz. A liquid phantom tissue material of permittivity ($\varepsilon'_r = 48$, $\varepsilon''_r = 14$) and bromopentane ($\varepsilon'_r = 5.9$, $\varepsilon''_r = 0.8$) as fat tissue simulator were considered. One of the major advantages of this technique was that only the electric properties of the simulating tissues needed to be matched to the actual tissue properties; the thermal properties were unimportant. This allowed for greater choice of simulating materials. The probe consisted of a section of a 3.5 mm semi-rigid coaxial line with an exposed section of the inner conductor. The other end of the coaxial line was connected to the square-law diode detector. The quantity measured

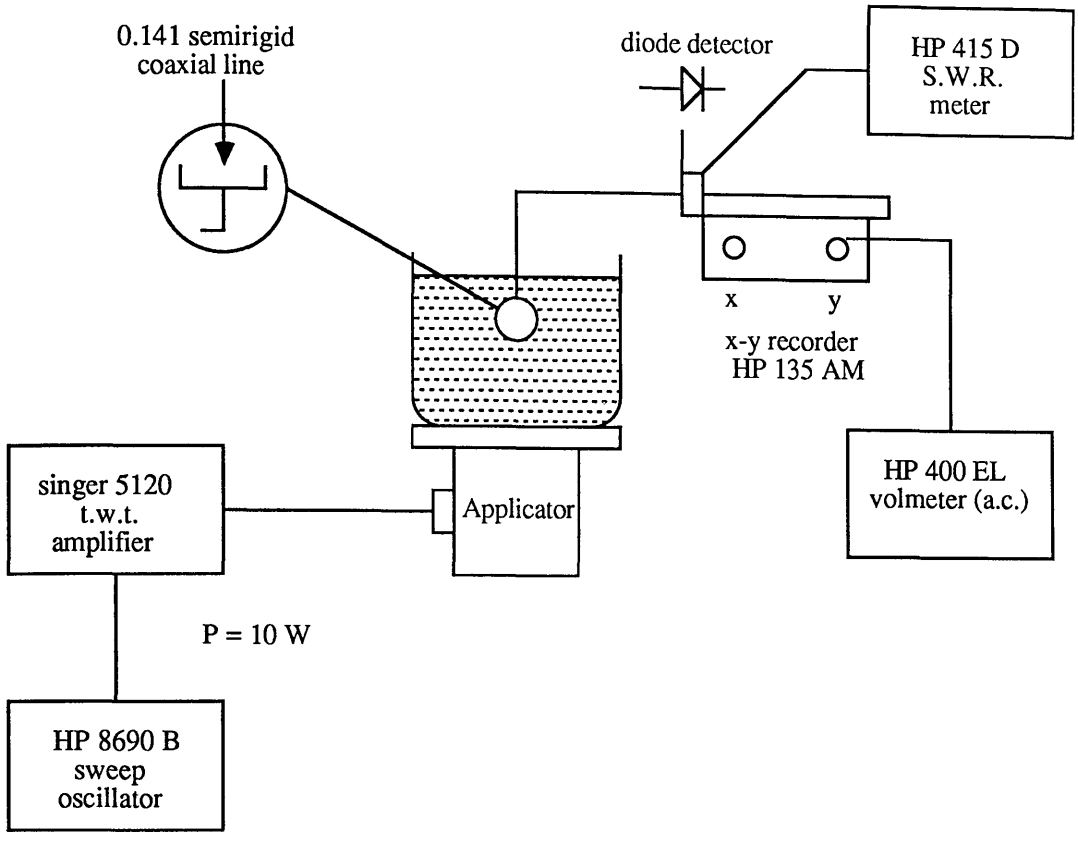

Fig. VII.1- Diagram of the electric field measurement system [from Gajda et al., 1979]

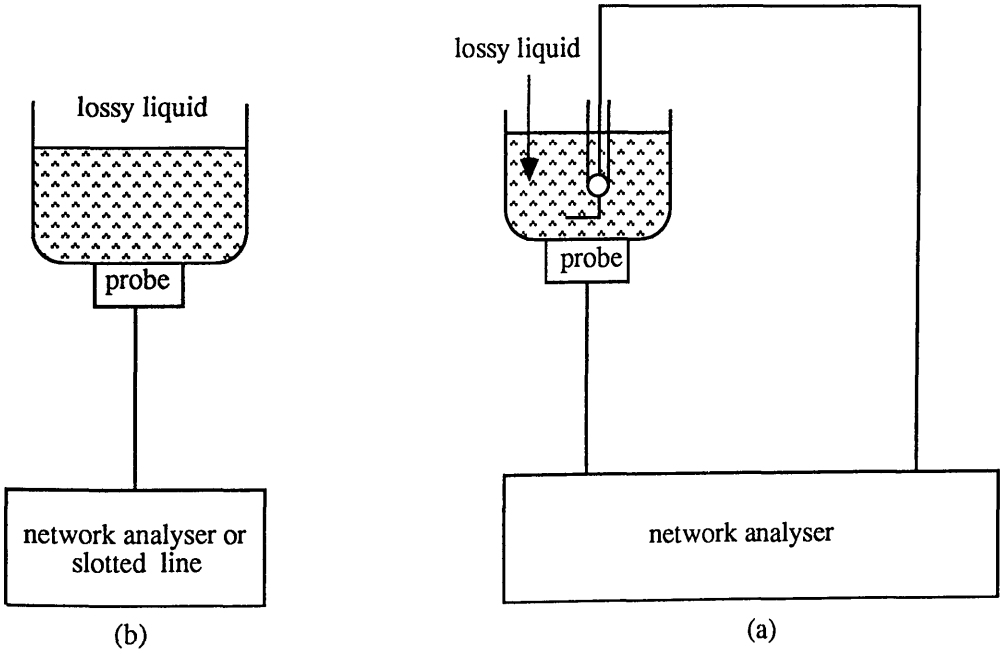

Fig. VII.2- The experimental arrangement used for measurements of
a) the reflection coefficient and
b) the propagation in lossy medium.
[Audet et al., 1980]

in this arrangement was the *rms* value of a squared electric field intensity (E^2) in a direction parallel to the probe. Gajda et al. analysed the near-field patterns in simulated muscle tissue of the squared value of the electric field strength at 2 mm from the aperture of an applicator operating at 2.45 GHz and the patterns of the electric field across the symmetry line of the applicator at different distances from the radiating aperture. The electric field can be detected up to 25 mm from the aperture of the applicator.

Cheever et al., (1987) discussed the effective penetration depth from a TE_{10}-mode rectangular waveguide antenna radiating into a lossy medium with dielectric properties resembling those of tissue. The permittivity range of the simulating muscle tissue considered were (ε'_r = 8 to 10.8, ε''_r = 8.2 to 10.5) and for fat tissue (ε'_r = 74 to 77, ε''_r = 11 to 17), the measurements have been carried out at several frequencies 3.1, 3.9 and 4.7 GHz and different aperture widths. The antenna has been mounted on a movable jig and the transmission coefficient detected by a network analyser. The effective penetration was measured and the calculated depths agreed with the plane-wave penetration depths. From these calculations it is shown that the near-field patterns of the antenna depend strongly on both the aperture width (which should be limited) and the material properties of the medium.

Theoretical and experimental analyses of the electromagnetic interactions with tissues have been presented by Cheung et al., (1981). They improved techniques for applicator design before approaching the practical aspects of the electromagnetic field configuration. Loading the empty space of the waveguide applicator with lossless dielectric material can lead to significant reductions in aperture size which are required for direct contact applicators. The electric field intensity (E^2) for four applicators of different sizes all operating at 2.45 GHz have been examined using a 3-axis implantable *E*-field probe immersed in a liquid tank filled with tissue equivalent material (80% water and 20% ethanol). Near-field as well as far-field cross-section scans have been determined. Cheung et al. found that

the smaller the applicator the larger was the on-axis attenuation into tissue (wider beam). A major problem they encountered in the electromagnetic heating was reflection at the tissue interfaces. There were two areas of concern, the first was the air-tissue interface immediately adjacent to the applicator which reflected a significant amount of energy. The second was the interface between tissues of different electrical properties such as muscle, fat and so on.

Audet et al., (1980) discussed the interaction of radiating structures with lossy materials and studied theoretically as well as experimentally measured near-field configurations. Before this, they investigated the performance of the antennas for measuring the complex permittivity of materials and studies of electromagnetic field patterns close to the antenna aperture in bi-layered biological tissues. They used two models to calculate the reflection coefficient and the effective penetration depth. The first model consisted of two rectangular waveguide antennas where one of them was oversized and the ratio between their cross-section was less than 25%. The second model consisted of a parallel plate waveguide filled with a dielectric and radiating into a medium with a different dielectric constant. Fig. VII.2 shows the practical arrangement for measuring the reflection coefficient and the propagation in the lossy medium. These measurements were carried out in the *X*-band using a standard air-filled waveguide, coaxial line transitions and dielectric loaded antennas ($\varepsilon' = 4$) in contact with a lossy dielectric material (water and chloroform). The experimental results were compared with numerical modelling. For very lossy dielectric material with a high-water content ($\varepsilon'_r = 64$, $\sigma_d = 15.25\ sm^{-1}$) differences were very small. However, for a less lossy medium, such as chloroform ($\varepsilon'_r = 4.48$, $\sigma_d = 0.45\ sm^{-1}$) differences were very significant. It was found that the penetration depth depends not only on the properties of the tissue but also on the parameters of the applicator. Figures VII.3 and VII.4 show the relative electric field dependence on the distance of the probe aperture in muscle and in fat respectively at 3 GHz (data collected from Audet et al., 1980). These show that the penetration depth decreases exponentially with the distance from the

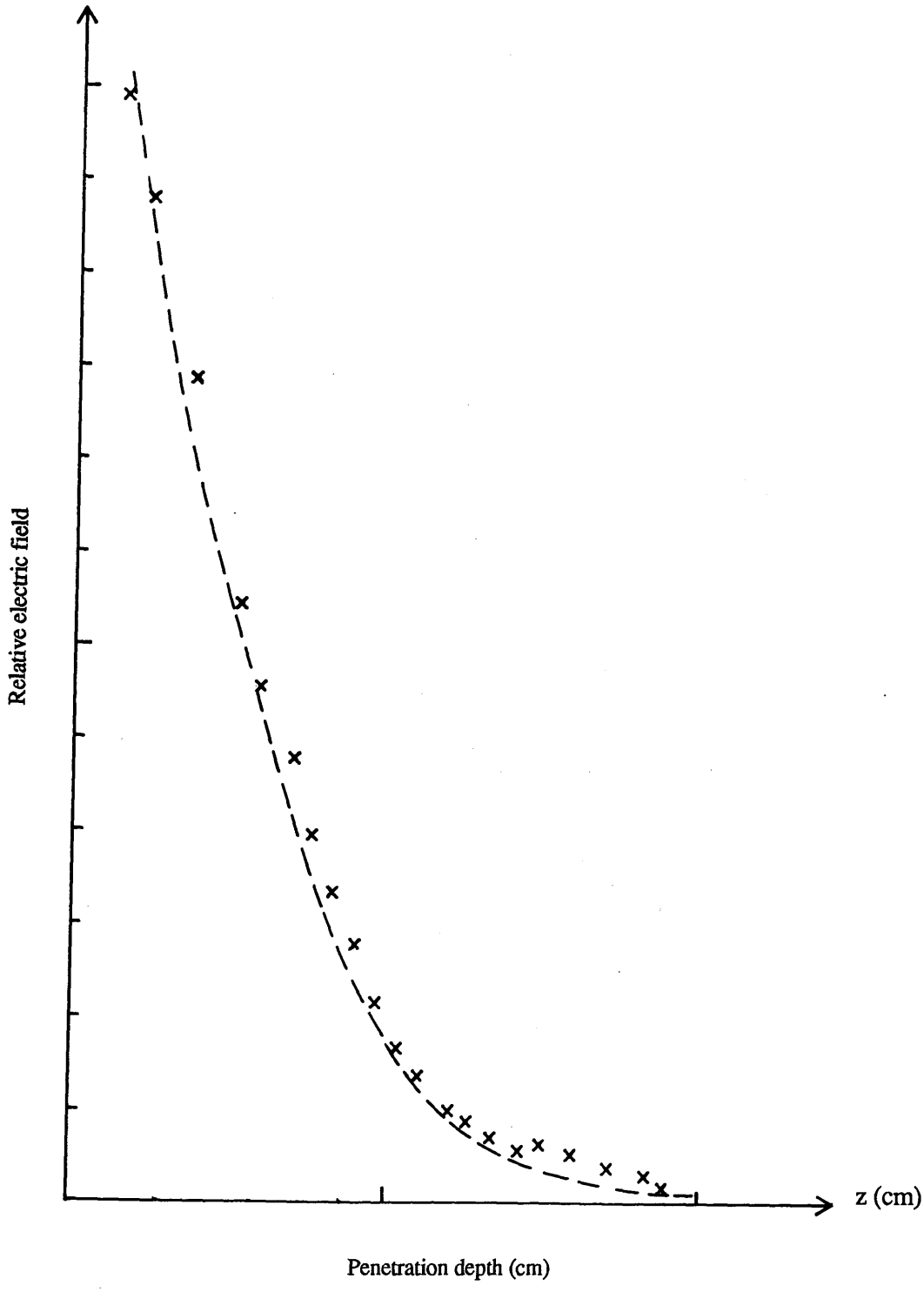

Fig. VII.3- The relative electric field in muscle ($\varepsilon_r = 46$, $\sigma = 2\ sm^{-1}$) depending on the distance from the probe at 3 GHz. (data collected from Audet et al., 1980)

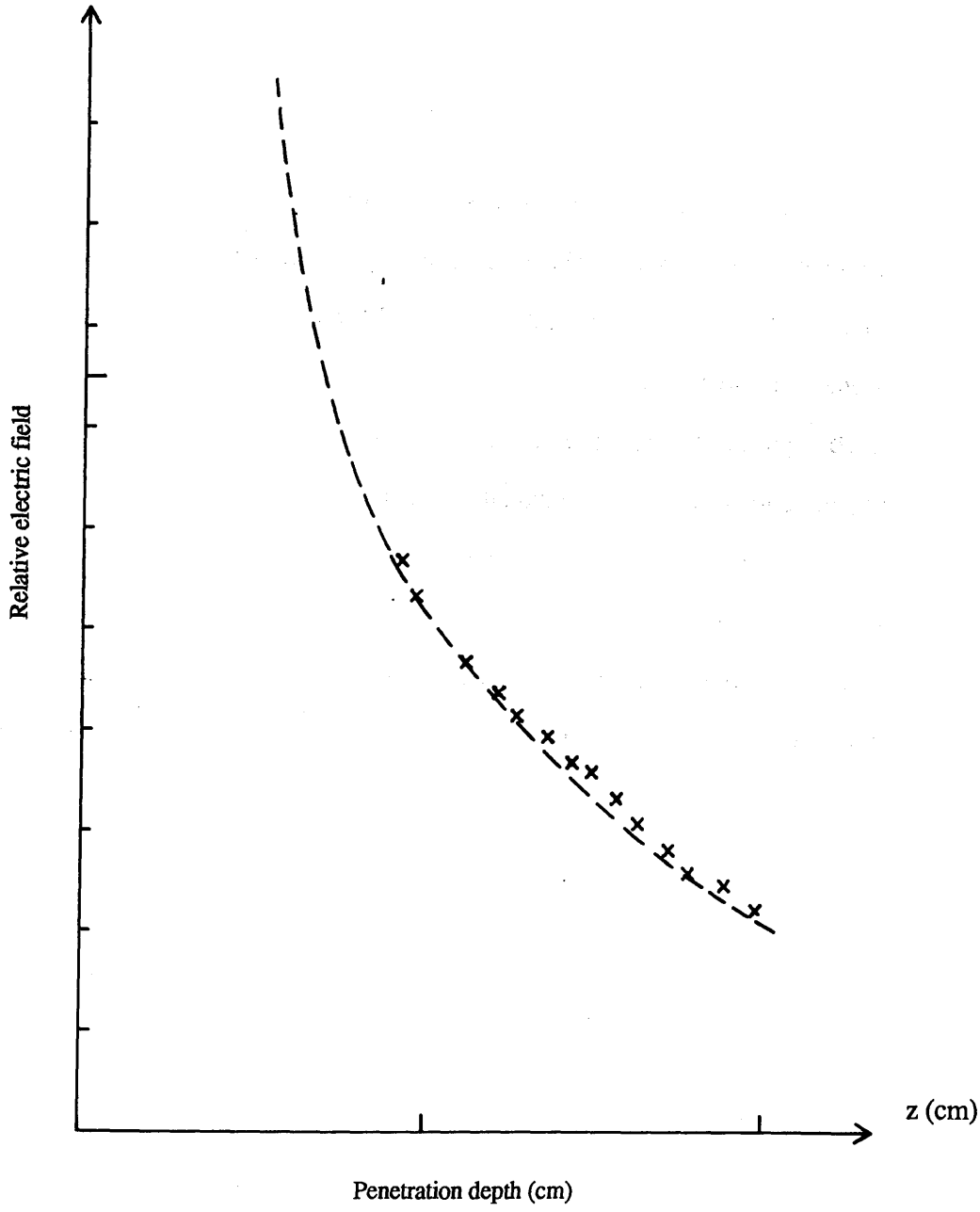

Fig. VII. 4- The relative electric field in fat ($\varepsilon_r = 5.55$, $\sigma = 0.133\ sm^{-1}$) depending on the distance from the probe at 3 GHz. (data collected from Audet et al., 1980)

aperture of the probe.They found that the method used was valid only for lossy materials such as muscle in particular conditions where the dielectric constant of the material filling the probe was low.

Robillard et al., (1980) presented experiment analyses of the electromagnetic field using a similar technique to Audet et al., (1980). This technique consisted of a TE_{01}-mode rectangular waveguide applicator (probe) in contact with a lossy material. They measured the effective penetration depth as well as the plane-wave penetration depth and the dielectric properties for different probes at frequencies 1, 3, and 9 GHz. Numerical analyses were verified by experiment and they concluded that the electromagnetic field configuration strongly depended on tissue dielectric properties and also on the characteristics of applicator (probe). Fig. VII.5 illustrates the variation of the electromagnetic field configuration with a lateral position of the probe in simulated low-water content tissue and high-water content tissue at a frequency of 3 GHz (data collected from Robillard et al., 1980). The relative electric field (E^2) in low-water content phantom such as chloroform is larger than in high-water content phantom material such as water. It can be seen that the penetration depth in low-water content tissue is greater than in those of high-water content tissue. This shows that the chloroform material is a good low-water content phantom. Robillard, (1981) carried out investigations to improve this technique, analysing the electromagnetic field configuration and the dielectric properties. More probes have been considered at the operating frequencies 1, 3, 3.2 and 9 GHz. He also considered the measurement conditions (temperature) of the water. The dielectric phantom materials used were chloroform and bromopentane as the low-water content phantom, water and acetone as the high-water content phantom, the effective penetration depth and the plane-wave penetration depth were compared.

Robillard et al., (1982) developed the computation of the thermal signals obtained by microwave radiometry from a probe or applicator in contact with tissue.

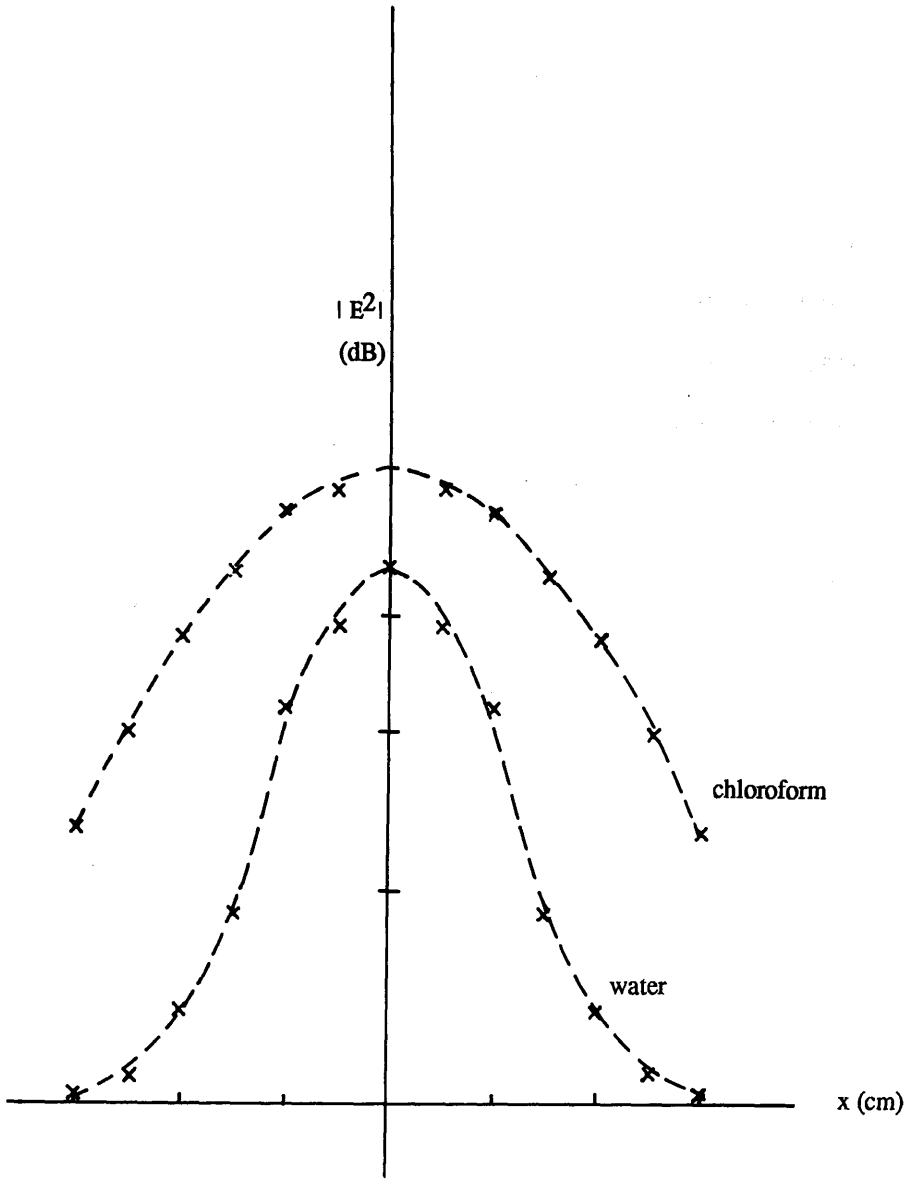

Fig. VII.5- The relative electric field configuration at a frequency of 3 GHz with a TE_{01}-mode rectangular waveguide probe (2.16 cm × 1 cm, $\varepsilon_r = 16$) data collected from Robillard et al., 1980.

This method has been already discussed by N'Guyen et al., (1980b). Robillard et al., investigated the reflection coefficient at the interface and the behaviour of the electromagnetic field on the axis of the system (penetration depth) for muscle phantom material such as water ($\varepsilon'_r = 77.85$, $\sigma_d = 2.44\ sm^{-1}$) at depth z = 5 mm and a fat phantom material such as chloroform ($\varepsilon'_r = 6.08$, $\sigma_d = 0.166\ sm^{-1}$) at the penetration depth z = 2 cm. These respectively represented the limit of the detection of the electric field at any point in the lossy material. Two different probes were used operating at a frequency of 3.2 GHz. These analyses have been verified experimentally for the same probes and frequency. Robillard et al. found that the thermal structure depended both on the characteristics of the structure and on the measurement conditions and showed how it is possible to achieve a determination of the temperature distribution in the tissue.

Mizushina et al., (1984) presented data of a three-band microwave radiometer using a single antenna in contact with a dielectric medium (water). A cylindrical container filled with water at ambient temperature in which a plastic container was inserted also filled with water at a different temperature and placed at a range of depths. They found that the measured penetration depths for tap water were 40.6 mm for the frequency band of 1 - 2 GHz, 18.6 mm for the frequency band of 2 - 3 GHz and 10.6 mm for 3 - 4 GHz. It was demonstrated that it was possible to measure surface layer temperature, subjacent layer temperature and the depth of boundaries between the layers and hence to define the electromagnetic field configurations.

Bocquet et al., (1986) first studied the geometrical characteristics (depth and size) and the temperature of a local thermal volume in a lossy material. The technique was based on the processing of radiometer data at 1.5 GHz and 3 GHz. The experimental analyses were carried out using water as phantom dielectric material. A probe was placed on the bottom of a container filled with water at ambient temperature. A cylinder of known volume, placed at a predetermined depth was filled with water at a slightly different temperature. The output signal was

expressed as a "brightness" temperature from the microwave radiometer. They measured the temperature (the output signal) in relation to the penetration depth for various diameters of the cylindrical volume. This method has widely been discussed and improved by Mamouni, (1988).

Christensen and Durney, (1981) examined the basic characteristic of electromagnetic fields at both high and low frequencies with various applicators. They investigated some of the basic aspects which govern heating patterns from various devices, such as penetration depth which depend on the characteristics of the applicator.

Swicord and Davis, (1981) described the calculation of field distributions (near-field) and energy deposition around small open-end coaxial antenna in lossy material. The operating frequency was 2.45 GHz. For a dielectric material with a permittivity of 30, a loss tangent of 0.3, it was noted that 90% of the power had been absorbed within a radius of 2 mm. It was calculated that the square of the electric field was a constant and did not depend on an antenna impedance match.

VII. 3- Theory of the *nonresonant perturbation* technique:

The Lorentz reciprocity theorem has been applied (Steele, 1966; Land, 1984) to analyse the behaviour of the electromagnetic field in a system which has just one waveguide (or transmission line) port through which electromagnetic energy is permitted to pass into its interior (Fig.VII.6). The system may be lossy (in its walls, its interior, or both) or lossless.

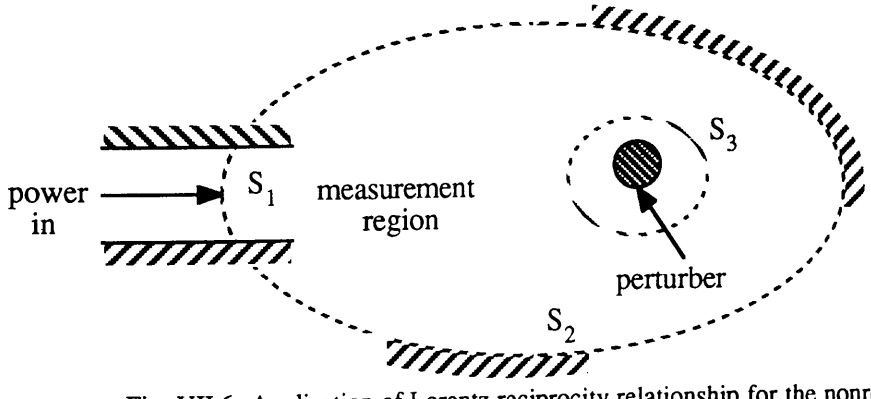

Fig. VII.6- Application of Lorentz reciprocity relationship for the nonresonant perturbation technique (Land, 1984).

The closed surface S lies entirely within the cavity walls except where it crosses the input port. In the above diagram the integration of the sum of the individual surfaces S_1, S_2 and S_3 is given by S. Surface S_1 represents the input port in a plane normal to the waveguide axis through which power is introduced into the measurement region and at which reflected power is measured. Surface S_2 is a part of the surface surrounding the measurement region other than S_1. Surface S_3 surrounds a small object introduced into the measurement region to perturb the pre-existing electromagnetic fields at the point where the fields are to be measured. Two different electromagnetic fields are considered in the measurement region. E_1, H_1 are the electric and magnetic fields in the absence of a perturbing object, and E_2, H_2 are the fields in presence of a perturbing object within the measurement region. The integral of Eq. VII.1 is evaluated for each of the three surfaces.

$$\int_S (E_1 \times H_2) \cdot ds - \int_S (E_2 \times H_1) \cdot ds = 0 \qquad \text{(VII.1)}$$

Surface S_1

Surface S_1 defines the measurement port through which high frequency power W_i at angular frequency ω is introduced into the measurement region, and at which a change in field reflection coefficient $\Delta\Gamma$ is measured on induction of the perturber. For practical measuring systems the input power W_i is constant and the integration is given by Eq. VII.4.

$$E_1 = (1 + \Gamma_1) E_{1i} \qquad H_1 = (1 - \Gamma_1) H_{1i} \qquad \text{(VII.2)}$$

$$E_2 = (1 + \Gamma_2) E_{2i} \qquad H_2 = (1 - \Gamma_2) H_{2i} \qquad \text{(VII.3)}$$

where Γ_1 and Γ_2 are the reflection coefficient in absence and in presence of the

perturber.

$$\int_{S_1} \left[(E_1 \times H_2) - (E_2 \times H_1) \right] . ds = 4 (\Gamma_2 - \Gamma_1) W_i \qquad \text{(VII.4)}$$

Surface S_2

The surface S_2 formed by conducting or power absorbing parts, the fields are rapidly attenuated with depth of penetration so that on surface S_2 the integral is then taken as zero.

Surface S_3

The surface integral is transformed to the volume integral over the volume v occupied by the perturber with surface S_3. The material in the region of this volume is taken to be a lossy dielectric material characterised by its permittivity ($\varepsilon^* = \varepsilon' - i\varepsilon''$), conductivity σ, and permeability μ_o. A dielectric perturber of the permittivity and the permeability ε_p and μ_p have been considered for the applications in the present work. Here the magnetic field does not need to be known and measurement data analysis can be considerably simplified if a dielectric rather than a conducting perturber is used. Since it does not interact with the magnetic field Maxwell's equations are applied for harmonic fields of angular frequency ω in the complex notation:

$$\text{Curl } E_1 = - i\omega\mu H_1$$

$$\text{Curl } H_1 = i\omega\varepsilon E_1$$

$$\text{Curl } E_2 = - i\omega\mu_p H_2$$

$$\text{Curl } H_2 = i\omega\varepsilon_p E_2$$

The integral Eq.VII.1 becomes:

$$\int_{S_3} (E_1 \times H_2) - (E_2 \times H_1) . ds = i\omega(\varepsilon_p - \varepsilon) \int_v (E_1 . E_2) dv$$

$$+ i\omega(\mu - \mu_p) \times \int_v (H_1 . H_2) \, dv \qquad \text{(VII.5)}$$

By the combination of these equations the surface integral from S_3 is given by:

$$\int_v \left[i\,\omega(\varepsilon' - \varepsilon_p) + (\omega\,\varepsilon'' + \sigma) \right] E_1 . E_2 \, dv \qquad \text{(VII.6)}$$

Equation VII.1 then gives:

$$\Delta\Gamma = - \int_v \left[i\,\omega(\varepsilon' - \varepsilon_p) + (\omega\,\varepsilon'' + \sigma) \right] \left(\frac{E_1 . E_2}{4\,W_i} \right) dv \qquad \text{(VII.7)}$$

where $\Delta\Gamma$ is the change in reflection coefficient caused by the introduction of the perturber into fields E_1, H_1.

VII.4- Application of *nonresonant perturbation* technique:

In biological materials electromagnetic power loss is due to dielectric losses, particularly Debye relaxation loss in water, and conduction loss due to electrolytic conduction in aqueous solutions. These losses are characterized by a dielectric loss factor ε''_d and the conductivity σ_d or by the effective loss factor ε''_e or the effective conductivity σ_e at the angular frequency ω, with the relative permittivity ε'_{rd} and the dielectric loss tangent $tan\,\delta$. In an electric field of amplitude E the power dissipation density, is $\frac{1}{2}\,\sigma_e E^2$. These factors are defined by:

$$\sigma_e = \omega \varepsilon''_d + \sigma_d \qquad \sigma_d = \omega \varepsilon_o \varepsilon''_{rd}$$

$$\varepsilon''_{rd} = \frac{\varepsilon''_d}{\varepsilon_o} \qquad \varepsilon''_e = \varepsilon''_d + \frac{\sigma_d}{\omega}$$

$$\varepsilon'_{rd} = \frac{\varepsilon'_d}{\varepsilon_o} \qquad \tan\delta = \frac{\varepsilon''_e}{\varepsilon'_d}$$

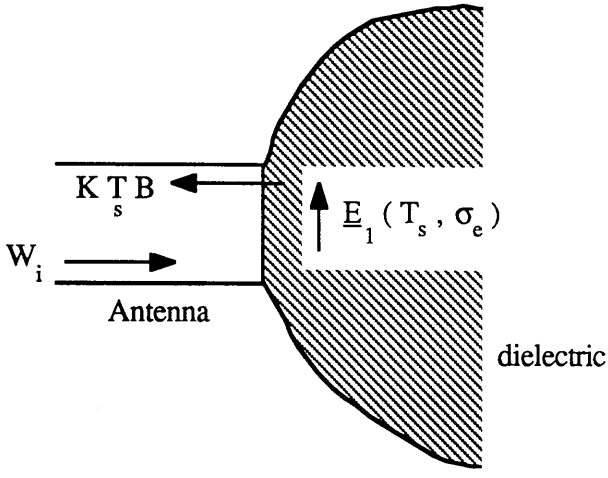

Fig. VII.7- Diagram of antenna in contact to a dielectric material shown the direction of the electric field inside the dielectric medium.

If a power W_i from an antenna is dissipated in a volume of dielectric material (Fig. VII.7) then,

$$W_i = \begin{cases} \frac{1}{2}\int_{vol} \sigma_e E_1^2 \, dv \\ \\ \frac{1}{2}\sigma_e \int_{vol} E_1^2 \, dv \end{cases} \qquad \text{for a uniform material} \qquad \text{(VII.8)}$$

If a thermal source at temperature T_s is applied, then in the Rayleigh-Jeans region, over a bandwidth B, thermal equilibrium requires that

$$K T_s B = \frac{1}{2} \sigma_e \int_{vol} E_1^2 \, dv \qquad \text{(VII.9)}$$

where K is Boltzmann's constant.

In a general case the normalized power dissipation pattern will be the pattern of,

$$\frac{\sigma_e (\underline{r}) E_1^2 (\underline{r})}{2W_i} \qquad \text{(VII.10)}$$

where $\underline{r}$ is the position vector.

The thermal signal received from a volume of material will be of the form,

$$KB T_{rec} = K B \int_{vol} c(\underline{r}) T(\underline{r}) \, dv \qquad \text{(VII.11)}$$

where c ($\underline{r}$) is the relative contribution from a volume element at $\underline{r}$.

If the source region is at a uniform temperature T_s then the thermodynamic equilibrium requires equality of power entering and leaving the antenna and both reciprocity theorem (Slater, 1942) and Principle of Detailed Balance require that the patterns of power dissipation and received signal contribution be the same at all frequencies. The received signal contribution pattern is the same as the heating pattern, and so

$$c (\underline{r}) = \frac{\sigma_e (\underline{r}) E_1^2 (\underline{r})}{2W_i} \qquad \text{(VII.12)}$$

This relationship is now applied for the measurement of radiometer antenna

response patterns.

VII.5- Microwave radiometer antenna response:

For effective practical microwave thermographic measurements the radiometer antenna must produce a large plane-wave far-field zone with a minimal near-field zone to give maximum signal contribution with depth in the viewed material. For thermal signal modelling it is then convenient to analyse the viewed region using a contribution of the plane-wave, varying as $e^{-2\alpha z}$ where α is the field attenuation constant and z is the depth within the material, and an antenna response or weighting function $W(z)$. Source temperature variations are for the present assumed to be planar, perpendicular to the z, antenna axis, and to fill completely the antenna beam, so that $T(\underline{r}) \rightarrow T(z)$ and $c(\underline{r}) \rightarrow W(z)\, e^{-2\alpha z}$.

Microwave radiometer antenna response is generated by the process shown in the diagrams below. These show the antenna/body interface. Fig. VII.8 represents the configuration of the near-field and far-field zones. The response pattern of the near-field zone is very different from the far-field zone where the field is perpendicular to the antenna axis. Fig. VII.9 shows if an element dz of the body tissue is considered the microwave signal will be generated from that element and the microwave signal in the region between dz element and the antenna is attenuated by the factor $e^{-2\alpha z}$, where α is the attenuation constant power of region z. The microwave signal received is the integral of the signal from the dz element over the z region. The antenna response pattern inside body tissue is taken to behave as presented in Fig. VII.10. The radiometer receiver gives the temperature of the viewed region weighted by the complete antenna response pattern.

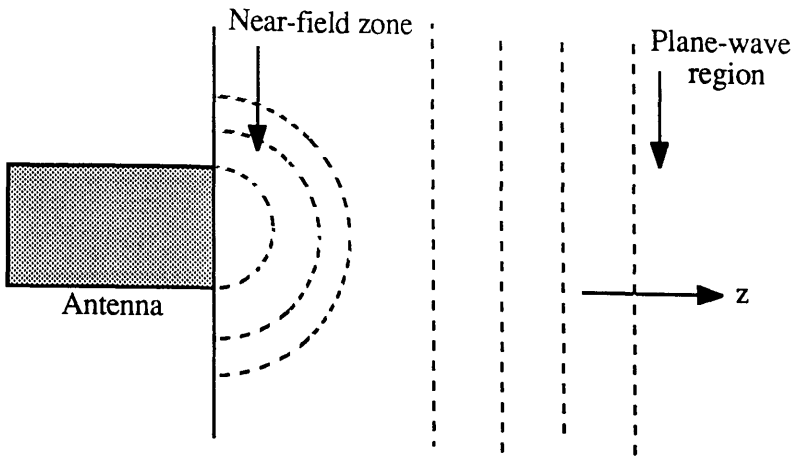

Fig.VII.8- The configuration of the near- and far-field zones.

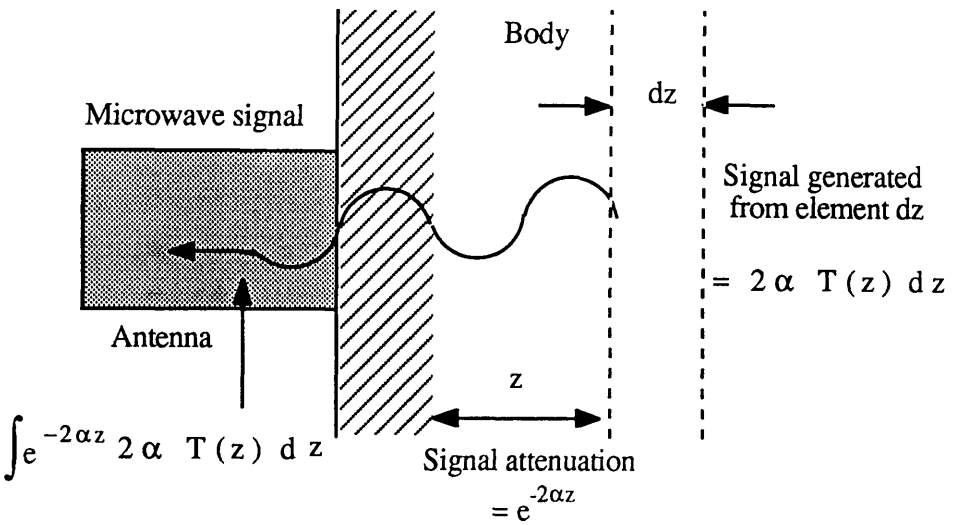

Fig.VII.9- The behaviour of the microwave signal inside body tissue.

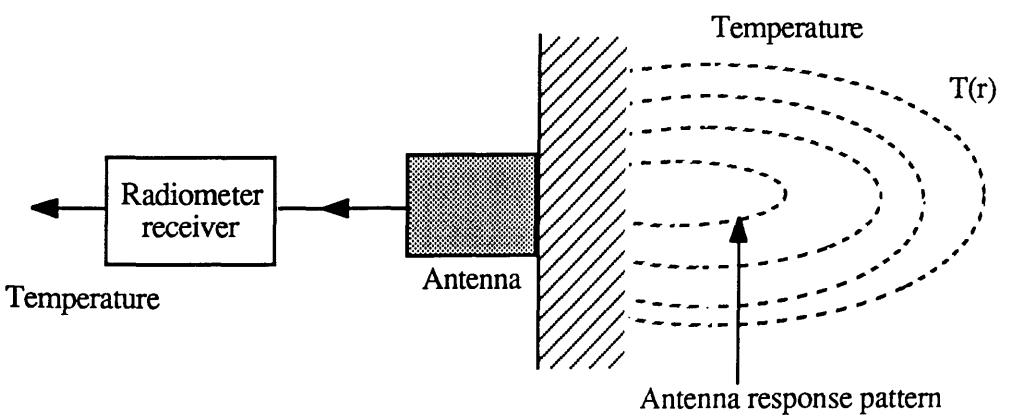

Fig. VII.10- The microwave radiometer antenna configuration into body tissue.

The total power obtained from the microwave radiometer is given by:

$$2\alpha \int_{v_p} W(r)\, e^{-2\alpha r}\; T(r)\, dr \qquad \text{(VII.13)}$$

where $W(r)\, e^{-2\alpha r}$ is the wanted function for the region r.

The factor $e^{-2\alpha z}$ is available from measurements of the viewed material dielectric properties. The dielectric lossy materials can be characterised electrically by the relative permittivity ε'_{rd} and the loss factor ε''_{rd}. Electromagnetic radiation usually propagates in tissues as plane-wave which can be fully described by reduced wavelength (λ_{eff}), the power attenuation constant 2α, and the penetration depth δ. They are related to ε'_{rd} and ε''_{rd} by:

$$\lambda_{eff} = \frac{\lambda_o}{\sqrt{\varepsilon'_{rd}}} \left[\frac{1}{2}\left(1 + \left(\frac{\varepsilon''_{rd}}{\varepsilon'_{rd}} \right)^2 \right)^{\frac{1}{2}} - \frac{1}{2} \right]^{-\frac{1}{2}} \qquad \text{(VII.14)}$$

$$2\alpha = \frac{4\pi}{\lambda_o} \sqrt{\varepsilon'_{rd}} \left[\frac{1}{2}\left(1 + \left(\frac{\varepsilon''_{rd}}{\varepsilon'_{rd}} \right)^2 \right)^{\frac{1}{2}} - \frac{1}{2} \right]^{\frac{1}{2}} \qquad \text{(VII.15)}$$

or by:

$$2\alpha = 2\omega \left[\frac{\mu_o \varepsilon'_d}{2} \left(1 + \left(\frac{\varepsilon''_e}{\varepsilon'_d} \right)^2 \right)^{\frac{1}{2}} - 1 \right]^{\frac{1}{2}} \qquad \text{(VII.16)}$$

For a reasonable approximation the attenuation power constant 2α for biological materials is given by:

$$2\,\alpha = 2\pi \frac{\sqrt{\varepsilon'_{rd}}}{\lambda_o} \tan\delta \qquad \text{(VII.17)}$$

or by:

$$2\alpha = \frac{Z_o\,\sigma_e}{\sqrt{\varepsilon_{rd}'}}, \qquad \text{with } Z_o = \sqrt{\frac{\mu_o}{\varepsilon_o}} = 377\ \Omega \qquad \text{(VII.18)}$$

$$\delta = \frac{1}{2\,\alpha} \qquad \text{(VII.19)}$$

where λ_o is the free space wavelength, λ_{eff} is always smaller than λ_o.

The variation of the dielectric electromagnetic fields in the direction of propagation is very interesting because the fields for a very lossy medium and a less lossy medium are very different. These variations show the behaviour of the plane-wave and the near-field configurations. The penetration depths are determined for those mediums, the results show that proper selection of the characteristics of the perturber is important. The *nonresonant perturbation* gives the change in the field reflection coefficient at the antenna aperture in a lossy dielectric material where the integration is over a perturbing volume V_p of loss-free dielectric material of relative permittivity ε'_{rd}.

The cross-sectional variation of the antenna beam can most conveniently be investigated with a small dielectric sphere (Fig. VII.11). The advantages of using a dielectric sphere perturber are independence from field direction and no interaction with the magnetic field.

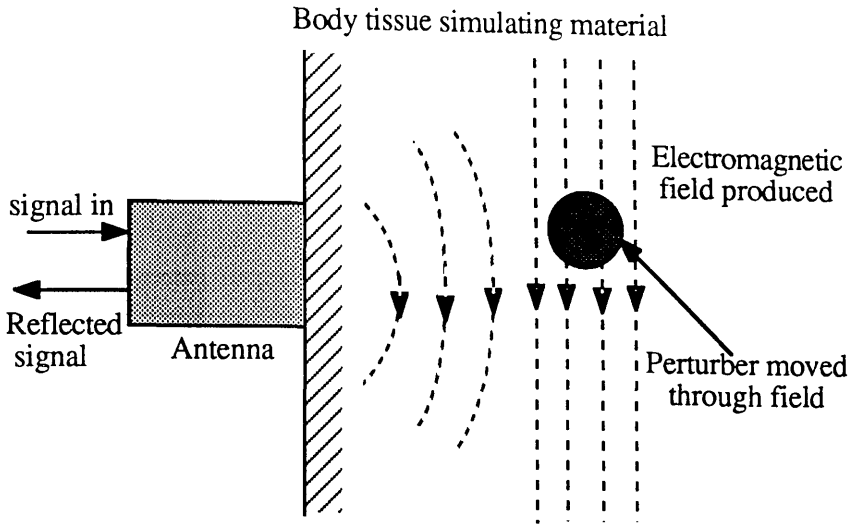

Fig. VII.11- Diagram of antenna in contact to body tissue or simulate dielectric material using a sphere perturber.

The magnitude of the reflected signal change due to the perturber thus gives a direct measurement of the square of the electric field strength at the measurement point. The reflection coefficient is given by:

$$\Delta\Gamma = \left(\frac{\pi a^3 \varepsilon'_{rd} \omega}{\varepsilon'_{rp} + 2\varepsilon'_{rd}} \right) \left[i (\varepsilon'_{rd} - \varepsilon'_{rp}) + \varepsilon''_{rd} \right] \frac{E_1^2 (r)}{W_i} \qquad \text{(VII.20)}$$

The radius of the sphere a is chosen to be always much less than the wavelength in the measurement region dielectric. This complex reflection coefficient contains both phase and amplitude information. The phase term is not normally required and the amplitude $|\Delta\Gamma|$ is measured giving directly the form of the spatial response $c(\underline{r})$.

A thin dielectric sheet perturber parallel to the electric field (Fig. VII.12) can be used to investigate the effective penetration depth from the antenna aperture of lossy dielectric phantom material. The electric field in the dielectric phantom material is the same in the absence and in the presence of the dielectric perturber, $\underline{E}_1 = \underline{E}_2$, if the sheet is thin compared to the wavelength so that the reflection coefficient becomes:

$$\Delta\Gamma = -\frac{\omega\varepsilon_o}{4W_i}\left[\, i\,(\varepsilon'_{rd} - \varepsilon'_{rp}) + \varepsilon''_{rd} \,\right] \int_{v_p} E_1^2\,(\underline{r})\, dv \qquad \text{(VII.21)}$$

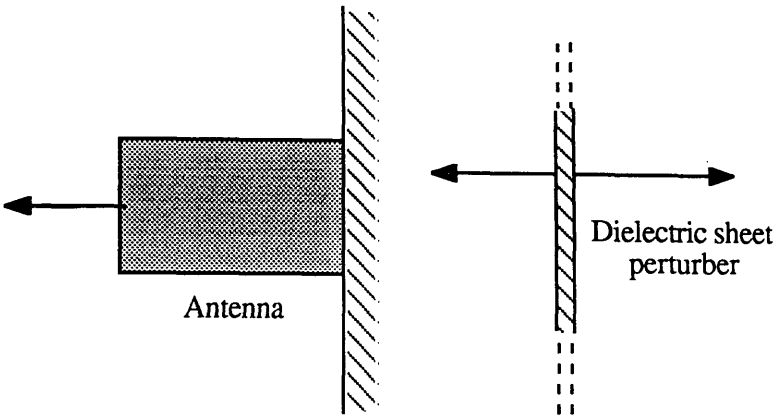

Fig. VII.12- Diagram of antenna in contact to body tissue or similar dielectric material using a sheet perturber.

$$\Delta\Gamma = \frac{-t}{2\varepsilon''_{rd}}\left(\, i\,(\varepsilon'_{rd} - \varepsilon'_{rp}) + \varepsilon''_{rd} \right)\left(\frac{\omega\varepsilon''_d}{2W_i} \int_{cs} E_1^2\,(z)\, ds \right) \qquad \text{(VII.22)}$$

where t is the thickness of the sheet dielectric perturber and expression VII.21 is integrated over the whole antenna beam cross-section.

For regions where the restriction on the field direction holds within reasonably the variation of the magnitude of $|\Delta\Gamma|$ will give the wanted axial response directly. In the near-field zone regions the field will have a component perpendicular to the sheet perturber as shown in Fig. VII.13.

Here,

$$\underline{E}_1 \cdot \underline{E}_2 = E_1\, E_2 \cos(\theta - \phi)$$

$$= E_1^2\left[\frac{\varepsilon'}{\varepsilon'_p}\cos^2\theta + \sin^2\theta \right] \qquad \text{(VII.23)}$$

the factor $\frac{\varepsilon'}{\varepsilon'_p}$ is of interest as it gives a large reflection coefficient change on perturbation and the factor cos 2θ is important since often ε' is rather greater than ε'_p.

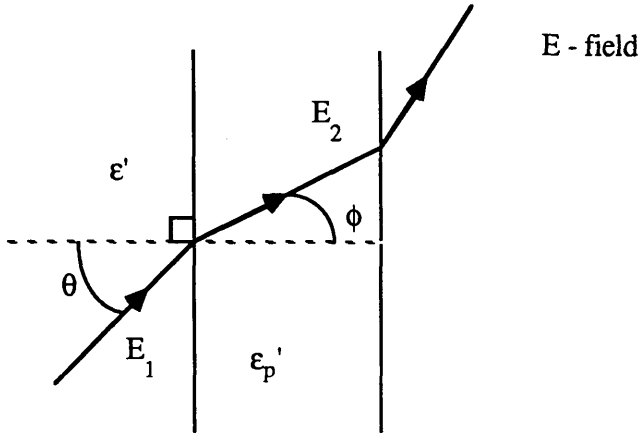

Fig. VII.13- Diagram for the electric field existing before and after the introduction of the perturber.

If the dielectric sheet perturber is moved to the face of the antenna (Fig. VII.14) the electric field E_1 can be expressed in terms of the input power W_i (Ramo, 1946)

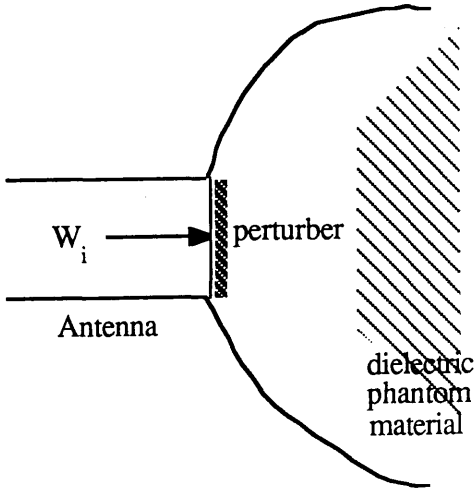

Fig. VII.14- Diagram of the antenna with the perturber the same size as the antenna aperture.

$$W_i = \frac{1}{2}\int_{cs} \mathrm{Re}\,(E_1 H_1^*)\,ds \quad \text{with} \quad \frac{E_1}{H_1} = \left[\frac{\mu_o}{\varepsilon'_d - j\varepsilon''_e}\right]^{\frac{1}{2}} \qquad \text{(VII.24)}$$

thus

$$W_i = \frac{1}{2\sqrt{\mu_o}}\int_{cs} \mathrm{Re}\left[\sqrt{\varepsilon'_d - j\,\varepsilon''_e}\,\right]^* E_1^2\,ds \qquad \text{(VII.25)}$$

$$= \frac{\sqrt{\varepsilon'_{rd}}}{2\sqrt{2}\,Z_o}\left[1 + \left[1 + \left(\frac{\varepsilon''_{rd}}{\varepsilon'_{rd}}\right)^2\right]^{\frac{1}{2}}\right]^{\frac{1}{2}}\int_{cs} E_1^2\,ds \qquad \text{(VII.26)}$$

and the magnitude of the perturber induced reflection coefficient is given by:

$$|\Delta\Gamma| = \frac{\sqrt{2}\,\pi\,t}{\lambda_o}\left[\frac{(\varepsilon'_{rd} - \varepsilon'_{rp})^2 + \varepsilon''^2_{rd}}{\varepsilon'_{rd} + \varepsilon'_{rd}\left[1 + \left(\frac{\varepsilon''_{rd}}{\varepsilon'_{rd}}\right)^2\right]^{\frac{1}{2}}}\right]^{\frac{1}{2}} \qquad \text{(VII.27)}$$

where λ_o is the free-space measurement wavelength.

Figure VII.15 shows the general behaviour of the relative electric field dependence with the penetration depth into a dielectric medium from a waveguide type antenna. The value of $Ln\,(E)^2$ falls approximately linearly with distance from the aperture along the central axis perpendicular to the plane of the aperture. The distance over which $Ln\,(E)^2$ is reduced by a factor of $e^{-2\alpha z}$ which is defined as the effective penetration depth and the antenna response function will be

$W(z)\, e^{-2\alpha z}$. The effective penetration depth is less than the plane-wave penetration depth at a given frequency. The difference between the plane-wave penetration depth and the effective penetration depth for low permittivity dielectric material is very significant (will be discussed in Chapter VIII). The antenna response (near-field zone) is always lower than the plane-wave (far-field region) as is shown below because of the relatively higher losses in the near field zone.

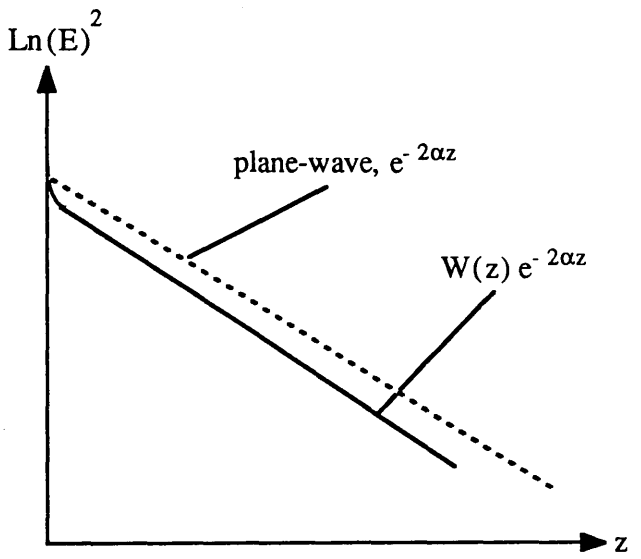

Fig.VII.15- The square of the electric field dependence of the penetration depth.

VII. 6- *Nonresonant perturbation* measurement system:

Nonresonant perturbation technique is used to investigate the improvement of electromagnetic field measurements in simulated biological tissue using the Glasgow TE_{11}-mode cylindrical waveguide antenna.

The *nonresonant perturbation* system for the square of the electric field measurements consists of two branches (Fig.VII.16) with WG10 waveguide and waveguide components for microwave section of the equipment . The first branch consists of a signal generator with a crystal synchroniser set in the frequency range of 3.2 - 3.35 GHz (f_o), connected to an isolator and a set-level 10 dB attenuator.

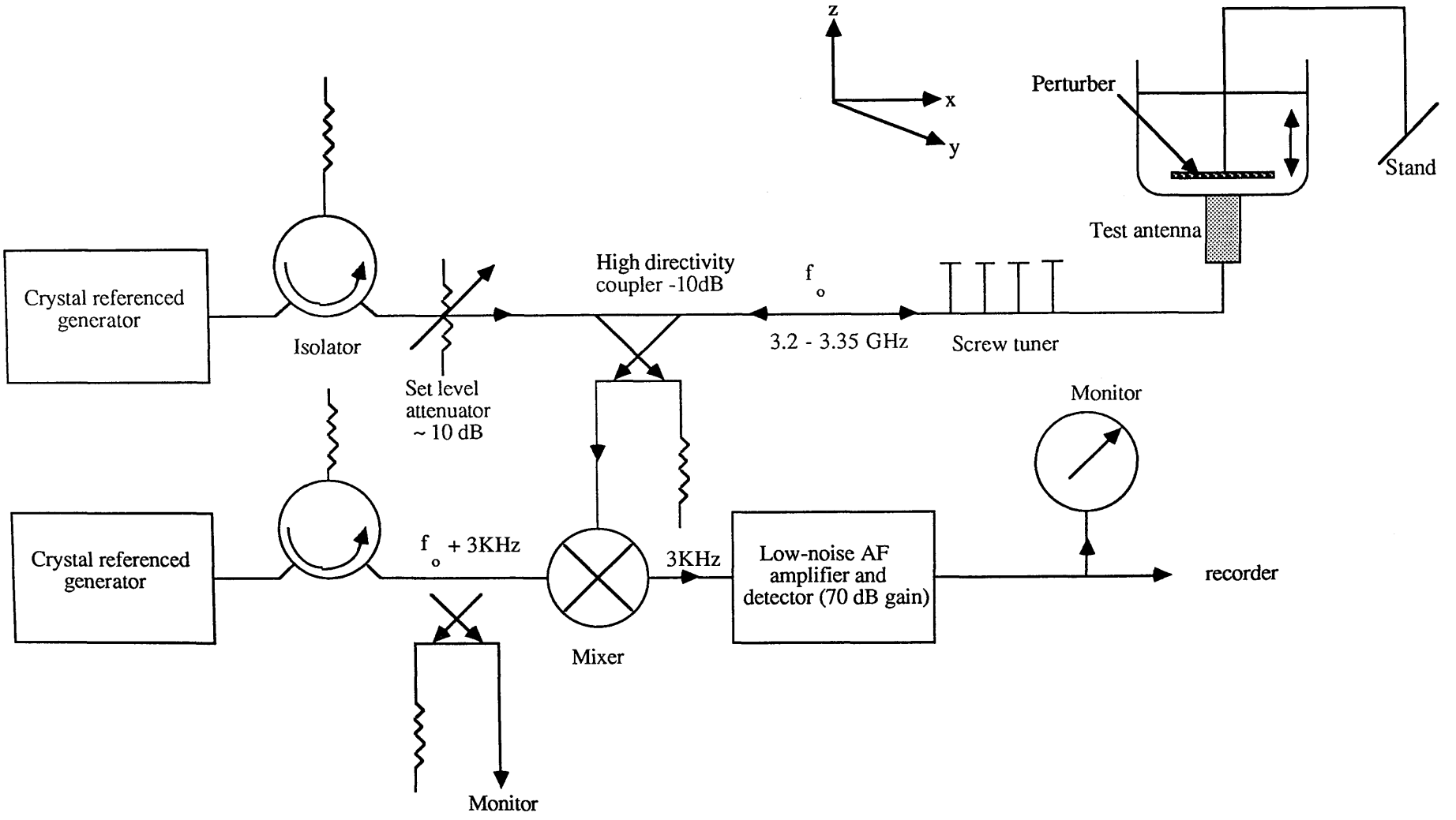

Fig. VII.16- Nonresonant perturbation system for measurement technique.

The reflected signal due to the perturber from the test antenna in contact with dielectric lossy materials is carried out by a high-directivity coupler, well matched with balanced mixer to avoid the loss of signal inherent in the use of a directional coupler of about 10 dB gain. A precision screw tuner is used to zero the signal appearing at the balanced mixer reflected-signal port in the absence of the perturber. This balanced mixer carried out the input signal from the second branch, also which consists of signal generator with a crystal synchroniser in the frequency range of 3.2 - 3.35 GHz connected to an isolator and a monitor at the frequency of $f_o + 3$ KHz. The output from the balanced mixer at the frequency of 3 KHz is amplified by a low noise AF amplifier of 70 dB gain and after that detected by a detector. The output is given by two instruments a digital meter and x-y recorder. Fig. VII.17 and VII 18 show an example of the equipment set up for the *nonresonant perturbation* technique.

Three known types of dielectric perturber were used. Two types of dielectric sheet perturbers both had similar geometry in that they consisted of a circular dielectric sheet perturber 26 mm in diameter, 1.6 mm in thickness and a larger dielectric sheet perturber is approximately 72 mm × 70 mm, 1.6 mm in thickness. The first type the dielectric sheet perturber was paxolin $\varepsilon'_r \approx 2$, in the second the dielectric sheet perturber was nylon $\varepsilon'_r \approx 3$. These perturbers were moved through the phantom dielectric material along the direction of the antenna axis (z-direction) to find the effective penetration depth which can be achieved from the antenna aperture. The third type was a spherical dielectric perturber 6.35 mm in diameter, moved in x-z plan plane from the antenna aperture to obtain detailed the electric field configuration in the lossy dielectric material.

For the TE_{11}-mode cylindrical waveguide antennas investigated and for different dielectric phantom materials and dielectric perturbers used for the *nonresonant perturbation* method, reflection coefficients from about 0.5 to 10^{-4} must be measured. A special stable, sensitive linear reflectometer system has been developed for this technique (Land, 1984), in which the measurement frequency

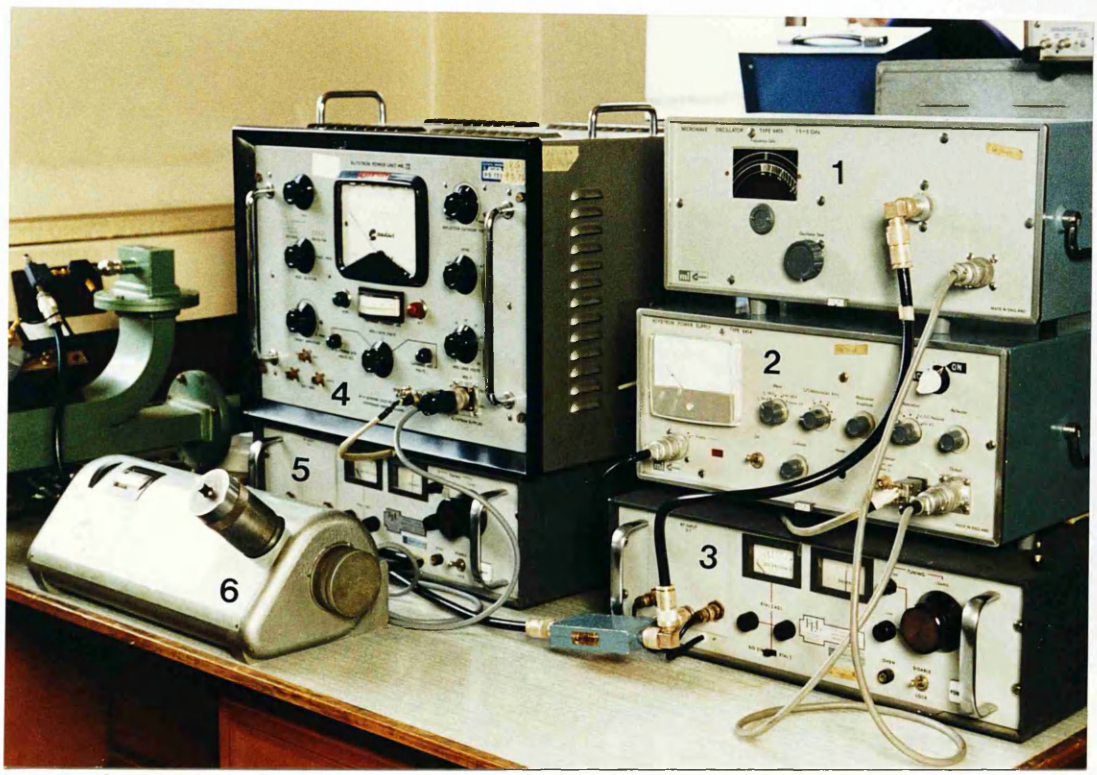

Fig. VII.17- The signal generators system used for the nonresonant perturbation technique to measure the electric field configurations.

1 - Microwave oscillator type 6455 (1.5 - 5 GHz)

2 - Klystron power suply type 6454

3 - Klystron synchroniser model 133 - AK

4 - Klystron power unit MK. IV

5 - Phase lock synchroniser model 133 - AK

6 - Sanders oscillator type CLC 2-4

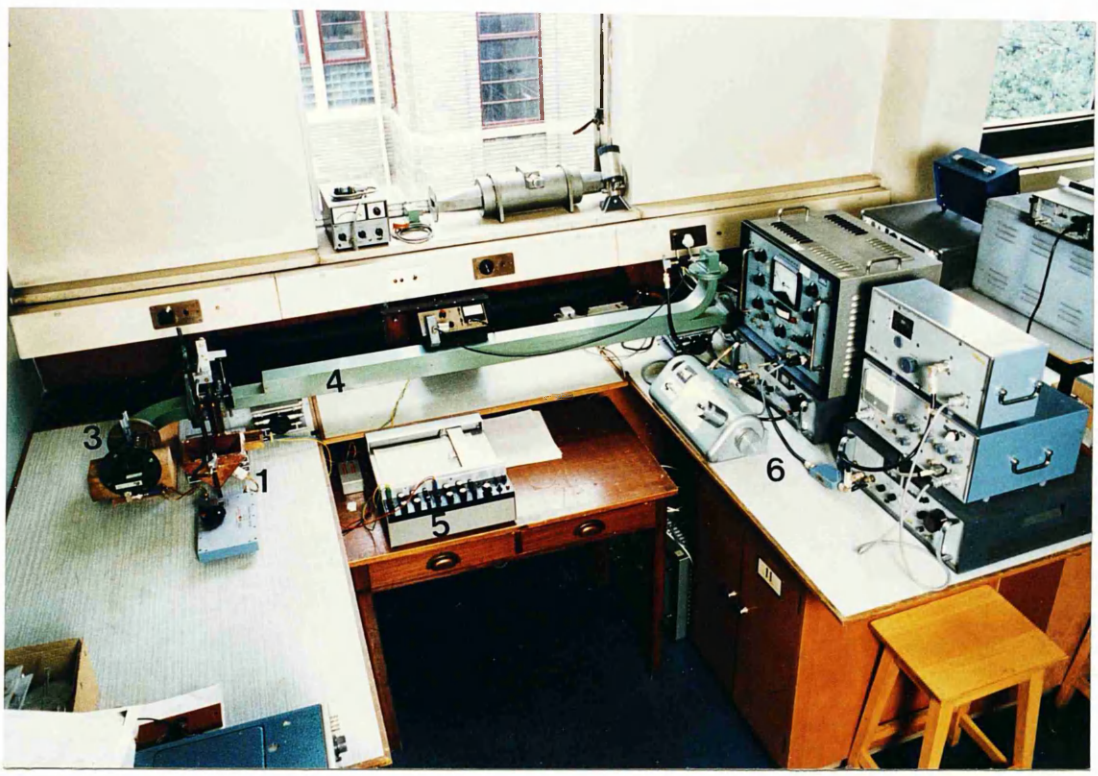

Fig. VII.18- The equipment set-up used for the nonresonant perturbation technique.

1 - Test antennas

2 - Phantom dielectric container

3 - Tuner section

4 - WG10 waveguide

5 - x-y recorder

6 - Signal generators system

signal is heterodyned with a stabilised local oscillator signal to allow the reflection coefficient signal to be measured at 3 KHz. The critical measurement parts of the reflectometer, the isolator, WG10 waveguide components for mechanical and electrical stability is required. This linear reflectometer system allows a wide measurement range of reflection coefficient from 1 for calibration to value less than 10^{-4}.

The previous measurement of reflection coefficient requires special care and is based first on moving the dielectric sheet perturber from the dielectric phantom material container to set the reflection coefficient to zero and after that to put a dielectric sheet perturber with the same size as the antenna on the top of it to measure the total reflected signal. This method is useful for checking the accuracy of the technique. This technique provides approximately 50% reflection to the main transmission line.

Chapter VIII

Nonresonant perturbation technique Practical Implementation

VIII. 1- Introduction:

In the last Chapter the concepts of the *nonresonant perturbation* technique were developed theoretically and the experimental technique was described. In this Chapter the measurements made using this technique are described and the results presented. The application of this technique to measure the electromagnetic field configuration and the effective penetration depth of a single TE_{11}-mode cylindrical waveguide antenna is considered and a crossed-pair TE_{11}-mode cylindrical waveguide antenna system has been similarly measured to investigate the microwave correlation signal. The electromagnetic fields configurations of these antennas have been investigated extensively to determine the field strength, direction and the penetration depth of the dissipated power (see section VII.5).

The medical techniques of microwave hyperthermia induction, microwave thermographic temperature measurement, and active microwave tissue imaging, all require the electromagnetic field configurations of the special applicators or antennas used to be known. These applicators or antennas often comprise of short lengths of rectangular or cylindrical waveguide (as discussed in Chapter IV) loaded with a low-loss dielectric material to achieve good coupling to body tissues. The high microwave attenuation in biological materials requires the field configurations to be measured close to the antenna aperture in the near-field zone as explained in Chapter VII. The *nonresonant perturbation* technique can be used to measure electromagnetic fields in lossy material close to the antenna aperture (Fig. VII.16). In particular this is applied in the present work to measure accurately the effective

penetration depths of waveguide type antennas in several different dielectric phantom materials with properties simulating body tissues.

VIII. 2- Method of Measurement:

The measurements were made using the system described in section VII.6 operating at the frequency of 3.35 GHz for different dielectric lossy materials. The aperture of the antenna was placed in contact with a lossy dielectric material filling a container with dielectric walls. The dimensions of the container and the level of the lossy liquid above the antenna aperture have been selected in order to avoid the boundary reflections. It is 95 mm in diameter and 105 mm in depth and the level of a lossy dielectric material was 70 mm from the antenna aperture (Fig. VIII.1). Two known types of dielectric sheet perturber were used in the present work. Both had similar geometry in that they consisted of a circular dielectric sheet perturber 26 mm in diameter, 1.6 mm in thickness and a larger dielectric sheet perturber is approximately 72 mm × 70 mm, 1.6 mm in thickness. The first type the dielectric sheet perturber was paxolin $\varepsilon'_r \cong 2$, in the second the dielectric sheet perturber was nylon $\varepsilon'_r \cong 3$. A thin dielectric sheet perturber with the same diameter as the antenna or larger has been placed in dielectric perpendicular to the antenna axis and in the centre of the antenna aperture. This perturber was moved through the phantom dielectric material along the direction of the antenna axis (z-direction) to find the effective penetration depth which can be achieved from the antenna aperture. A spherical dielectric perturber 6.35 mm in diameter and a thin sheet dielectric perturber 26 mm in diameter were also moved in x-z plan plane from the antenna aperture to obtain the detailed electric field configuration in the lossy dielectric material. The perturber was moved by steps of 0.508 mm in z-direction and 2 mm in x-direction. The reflected signal was recorded on an x-y plotter and on a digital meter. The x-y recorder (Fig. VIII.2) plotted the reflected signal, which is proportional to the magnitude of $|\Delta\Gamma|$ of Eq.VII.6.

The dielectric properties were measured by the *cavity resonant frequency*

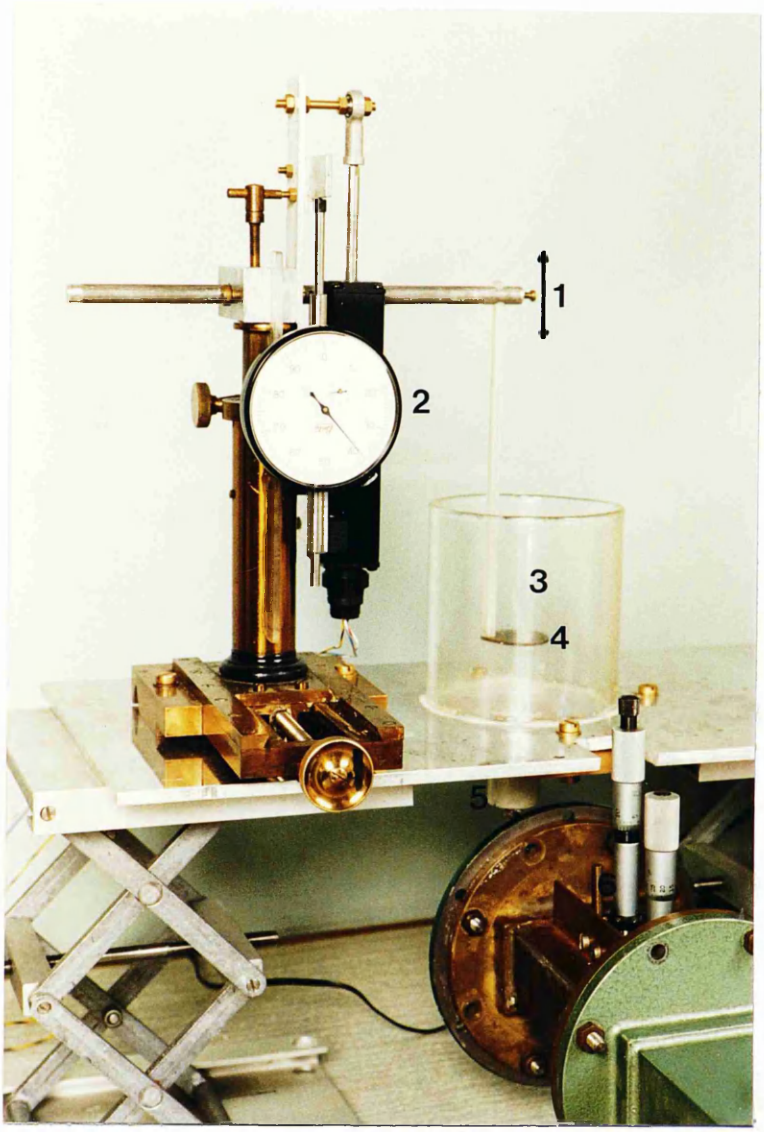

Fig. VIII.1- The experimental arrangement of the electric field measurements.

1 - Perturber movement

2 - Perturber axial position gauge

3 - Phantom dielectric liquid

4 - Sheet perturber

5 - Antenna

6 - Matching unit

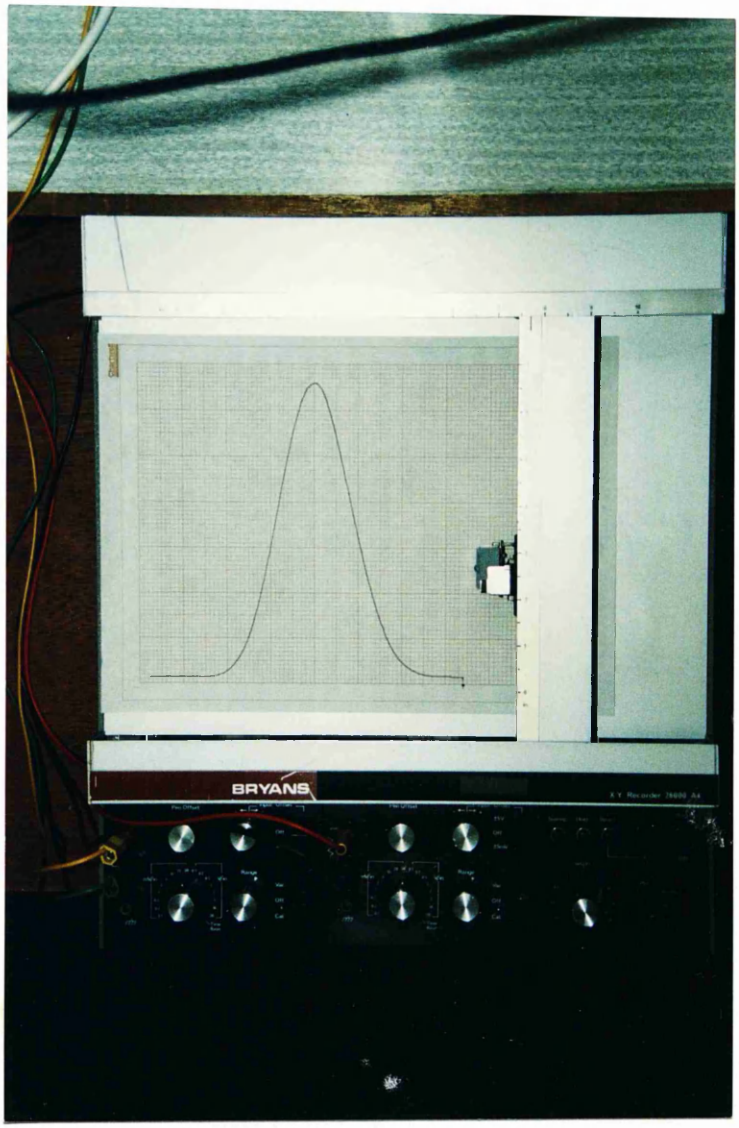

Fig. VIII.2- View of x-y recorder used for measurements showing the relative electric field configuration recorded across an antenna aperture in phantom dielectric material. Horizontal scale is 7 mm per major chart division.

perturbation technique (Land, 1987b). A resonant cavity has a thin glass tube across it in the direction of E-field. The cavity resonance mode is TM_{010}. The tube has bore of about 1 mm diameter as shown below.

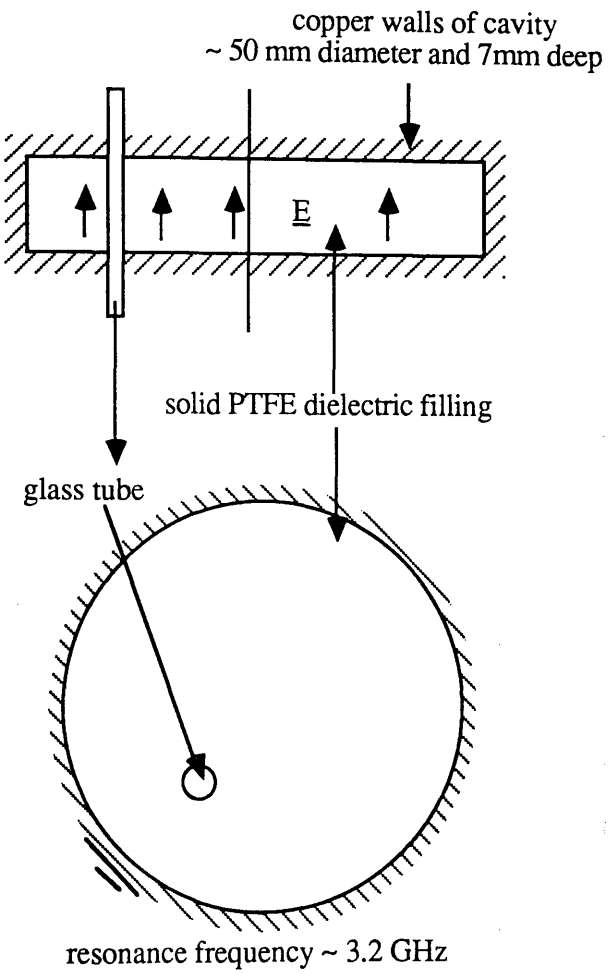

The changes in *cavity resonant frequency* and *cavity Q-factor* between the tube being empty and filled with the test dielectric are measured. For the relatively small perturbations caused these give respectively the relative permittivity ε'_r and the effective conductivity σ_e or loss factor ε''_r of the tested liquid. The cavity and sample tube are calibrated using de-ionised water as the standard. The accuracy of the measurements are about ε'_r ±2% and ε''_r ±5%.

VIII. 3- Measurement results:

The model based on the above analytical expressions measures relative values of dissipated power on the aperture and in the lossy dielectric material medium. The square of the electric field distribution is an important parameter in determining the reflection coefficient $|\Delta\Gamma|$. For high permittivity phantom materials the influence of the perturber is small and needs only be known approximately, as seen by equation VII.23. Another important parameter of the applicator or antenna radiating into a lossy medium is the penetration depth of the electromagnetic waves in that medium. The field decays largely exponentially as explained before (section VII.5 pp. 130-131), so that property can lead to defining the effective penetration depth. The exponential decay has been assumed to be close to a *TEM* wave propagating along the axis of the system. For the *TEM* wave the power penetration depth is:

$$\delta_{TEM} = \frac{1}{2\alpha_{TEM}} = \frac{c\,\varepsilon_o\sqrt{\varepsilon'_{rd}}}{\sigma_d} \qquad \text{(VIII.1)}$$

where α_{TEM} is the attenuation constant of the plane wave.

The experimental investigation of the electric field configurations was carried out at the operating frequency of 3.35 GHz for a single TE_{11}-mode cylindrical waveguide antenna loaded with low-loss dielectric material (Fig. II.4). Several different liquid dielectric phantom materials (Tab. VIII.1) have been chosen to simulate high-water content tissue such as muscle and low-water content tissue such as fat to measure the electromagnetic field configurations produced by the antenna. The values of the dielectric properties of these dielectric phantom material are similar to the dielectric properties of human tissue measured at 3 GHz and 37 °C (Tab. IV.3). From Tab. IV.3 and Tab. VIII.1 the similarity of the dielectric properties of the dielectric phantom material with the dielectric properties of human tissues and organs are very significant. The permittivities of human tissues and organs are close to dielectric phantom material used in this work, whereas the loss

factors are lower than the dielectric phantom material.

Table VIII.1- The dielectric properties at a frequency of 3.35 GHz and room temperature from high-water content tissue to low-water content tissue.

solutions	ε'_{rd}	ε''_{rd}	$\sigma_d(sm^{-1})$
75% chloroform & 25% alcohol	6.5 ± 0.02	2.58 ± 0.05	0.48 ± 0.05
50% sucrose	25 ±0.02	18 ± 0.05	3.18 ± 0.05
2/3 de-ionised water & 1/3 glycerol	40 ± 0.02	20 ± 0.05	3.5 ± 0.05
2/3 de-ionised water & 1/3 glycerol	52 ± 0.02	26 ± 0.05	4.8 ± 0.05
50% sucrose & 50% saline	56 ± 0.02	22 ± 0.05	3.9 ± 0.05
2/3 de-ionised water & 1/3 glycerol	60.3 ± 0.02	23 ± 0.05	4.2 ± 0.05
saline	74 ± 0.02	22 ± 0.05	4.0 ±0.05
de-ionised water	75.9 ± 0.02	26 ± 0.05	2.6 ± 0.05

The measurements of the relative electric field (E^2) along the antenna axis with dielectric sheet perturbers, $\varepsilon'_{rd} \cong 2$ and $\varepsilon'_{rd} \cong 3$, 2 6 mm in diameter have been considered for most of the dielectric phantom material except for the chloroform and alcohol mixture a large sheet perturber has been considered. Those sheet perturbers were moved through the dielectric phantom material to analyse the configuration of the electric field. The results of the measurements were given in the below figures covering from high- to low-water content tissues.

It is very clear from the figures that the relative electric field falls off

essentially as $e^{-2\alpha z_o}$ and that an effective attenuation constant which is the inverse of the effective penetration depth. This can be obtained from the measured data.

Fig. VIII.3 shows the effective penetration depth and the plane-wave penetration depth for a relatively lossy dielectric phantom lossy material such as de-ionised water (ε'_{rd} = 75.9, σ_d = 2.6 sm^{-1}). It shows the measured data and it illustrates that for high-water content tissue the antenna field and the plane-wave are nearly co-incidental. The ratio of the effective attenuation constant to the plane-wave attenuation constant is about 1:1. Also, in this case the reflected signal can be detected up to 25 mm from the antenna aperture. The effective penetration depth is approximately 17.9 ± 0.5 mm.

Fig. VIII.4 shows the effective penetration depth at 3.35 GHz in saline (ε'_{rd} = 74, σ_d = 4.0 sm^{-1}). The maximum depth which can be achieved is less than 20 mm from the antenna aperture. At about 15 mm the reflected signal strength starts to drop quickly and is slightly divergent from the plane-wave. This may be due to residual mismatch in the measuring equipment. The effective penetration depth is about 13 ± 0.5 mm compared with the plane-wave penetration depth which is about 13.1 ± 0.5 mm. The ratio of the effective attenuation constant to the plane-wave attenuation constant is about 1:1.

Fig. VIII.5 shows the effective penetration depth variation with respect to the reflected signal for a high-water content phantom simulating whole blood. This is a mixture of the de-ionised water and glycerol (ε'_{rd} = 60.3, σ_d = 4.2 sm^{-1}). In this case there is a larger difference between the measured and plane-wave penetration distances, 9.4 ± 0.5 mm and 11.2 ± 0.5 mm respectively. This difference may be due to the error in the measurement of the effective conductivity of the dielectric, or change in dielectric properties caused by evaporation or change in temperature.

Fig. VIII.6 presents the effective penetration depth of phantom dielectric material simulating muscle with properties as given in Tab. IV.3 (50% sucrose and

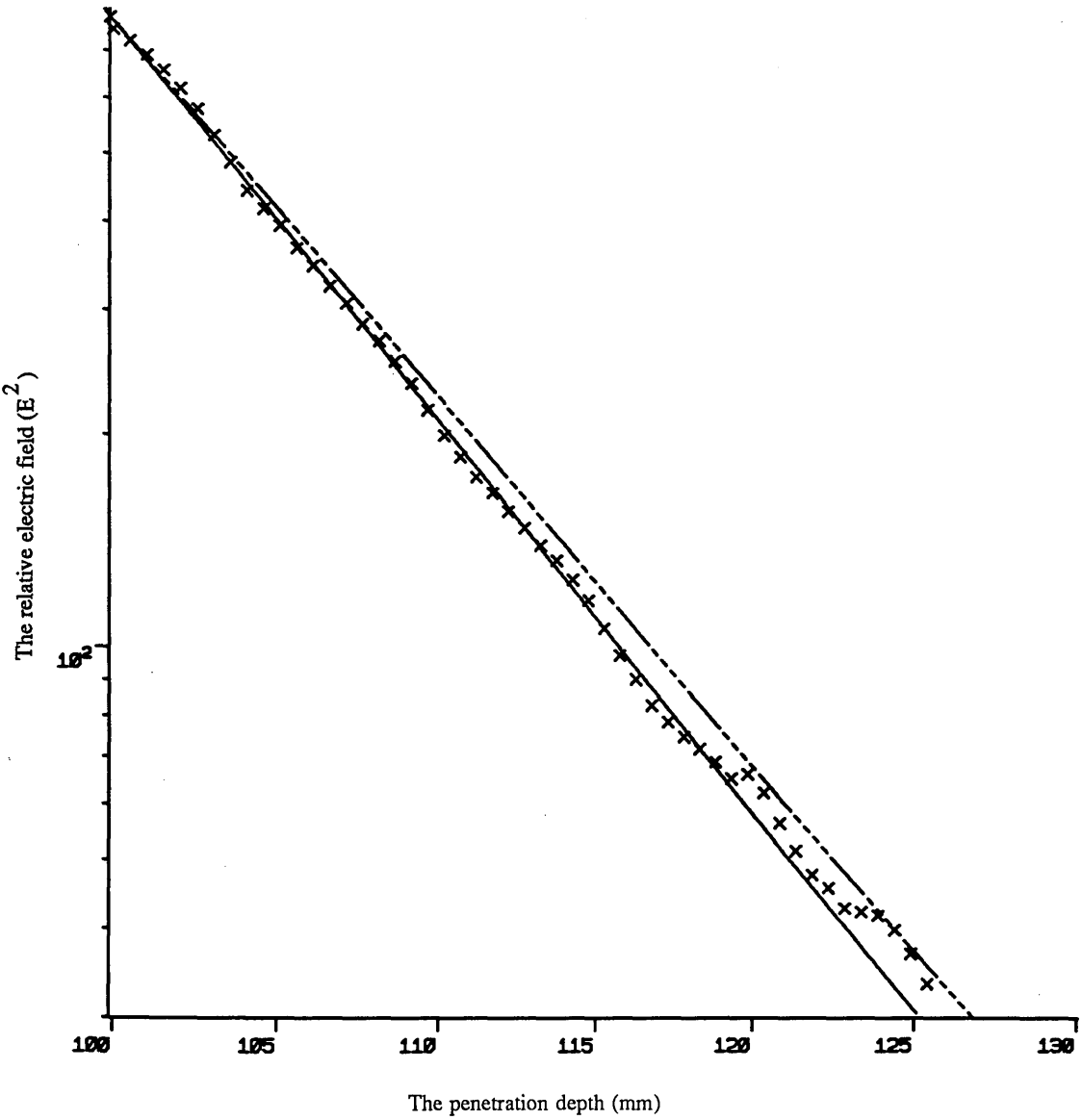

Fig. VIII.3- The relative electric field in the de-ionised water depending on the distance from the antenna aperture at 3.35 GHz for the dielectric constant ($\varepsilon'_{rd} = 75.9$, $\sigma_d = 2.6\ sm^{-1}$)

Plane-wave

Best fit curve

× measured data

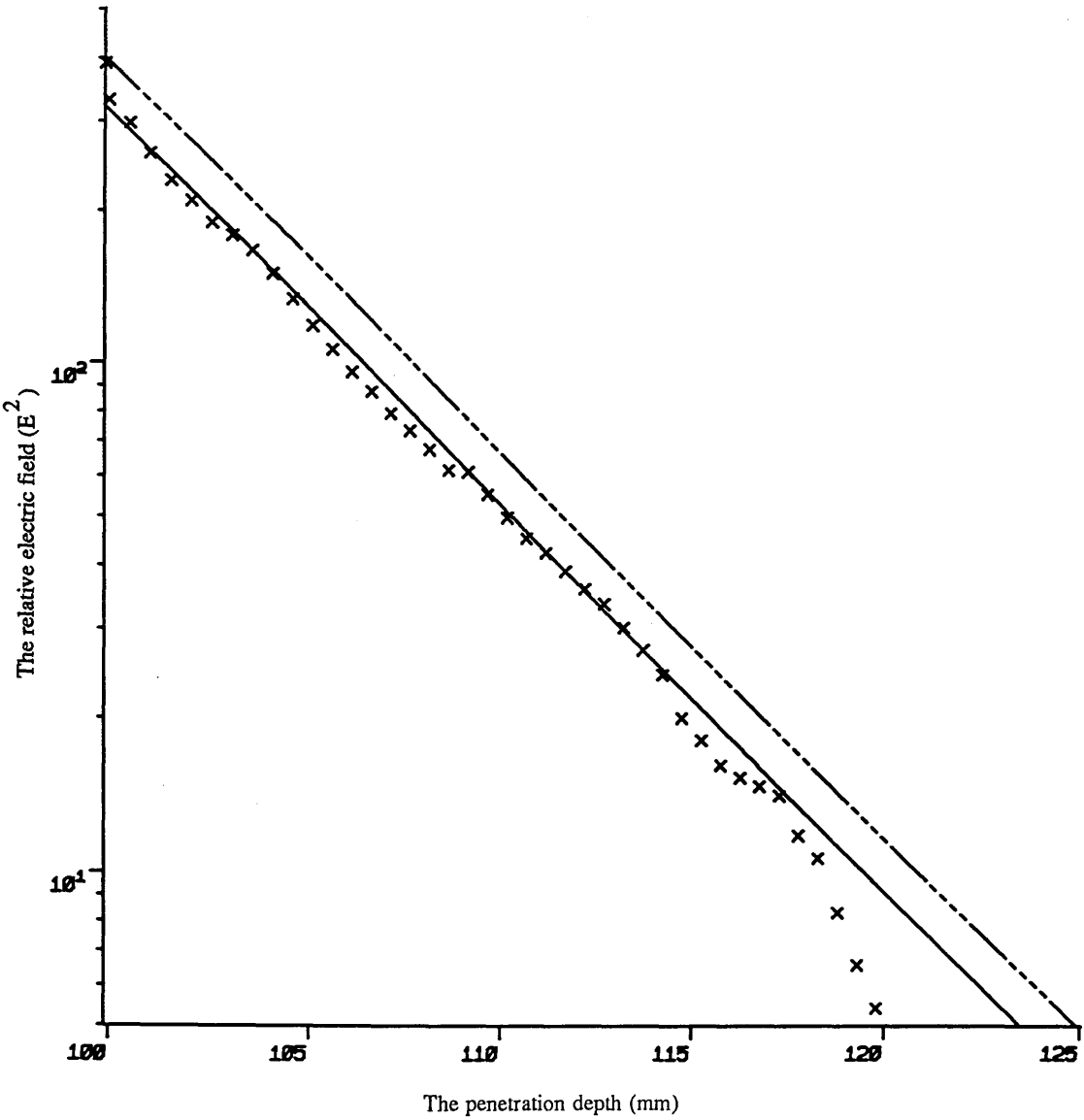

Fig. VIII.4- The relative electric field in a saline solution depending on the distance from the antenna aperture at 3.35 GHz for the dielectric constant ($\varepsilon'_{rd} = 74$, $\sigma_d = 4.0$ sm^{-1})

Plane-wave

Best fit curve

× measured data

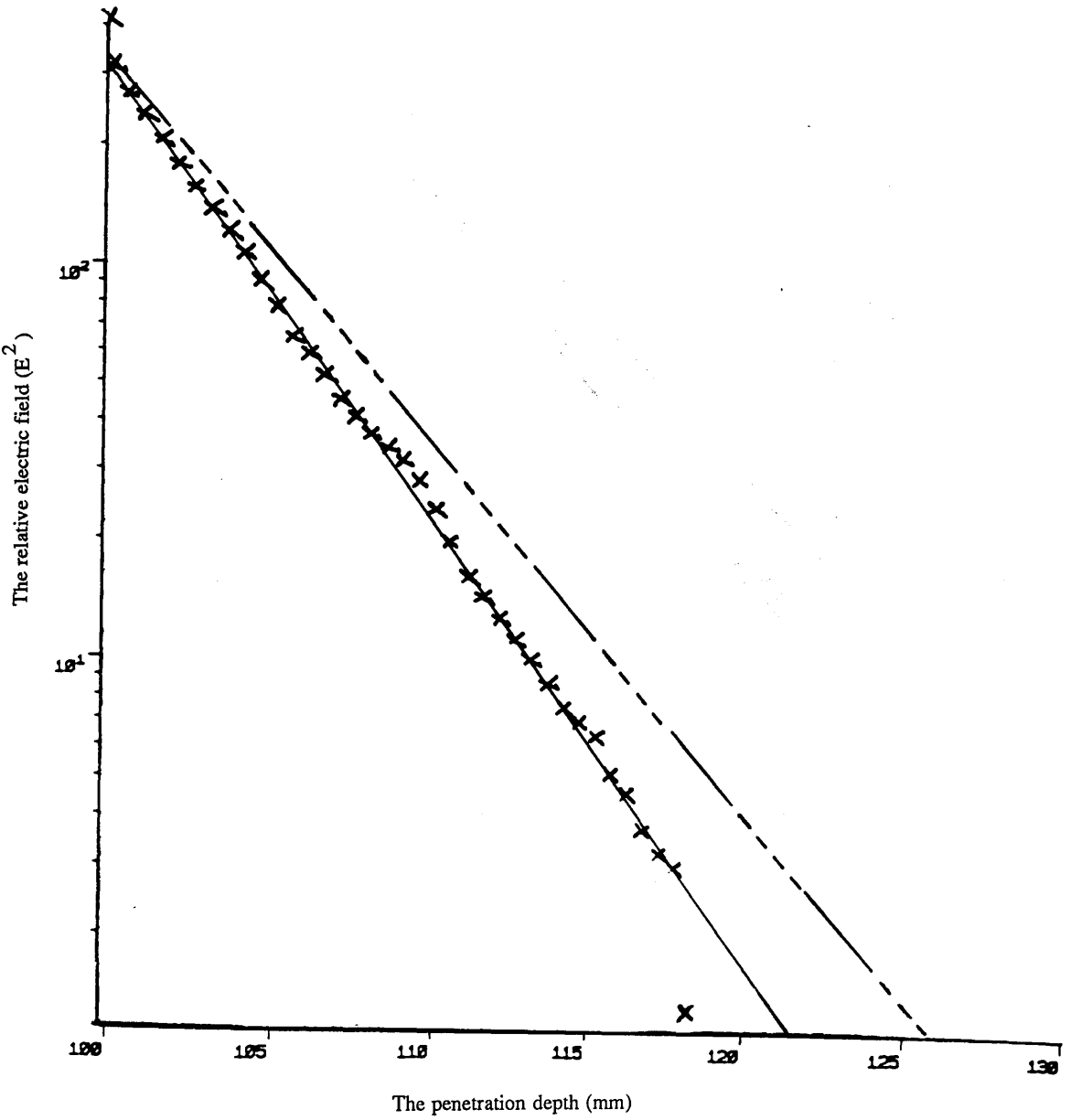

Fig. VIII.5- The relative electric field in a mixture of de-ionised water and glycerol depending on the distance from the antenna aperture at 3.35 GHz for the dielectric constant ($\varepsilon'_{rd} = 60.3$, $\sigma_d = 4.22\ sm^{-1}$)

———— - - - - ———— Plane-wave

———————— Best fit curve

× measured data

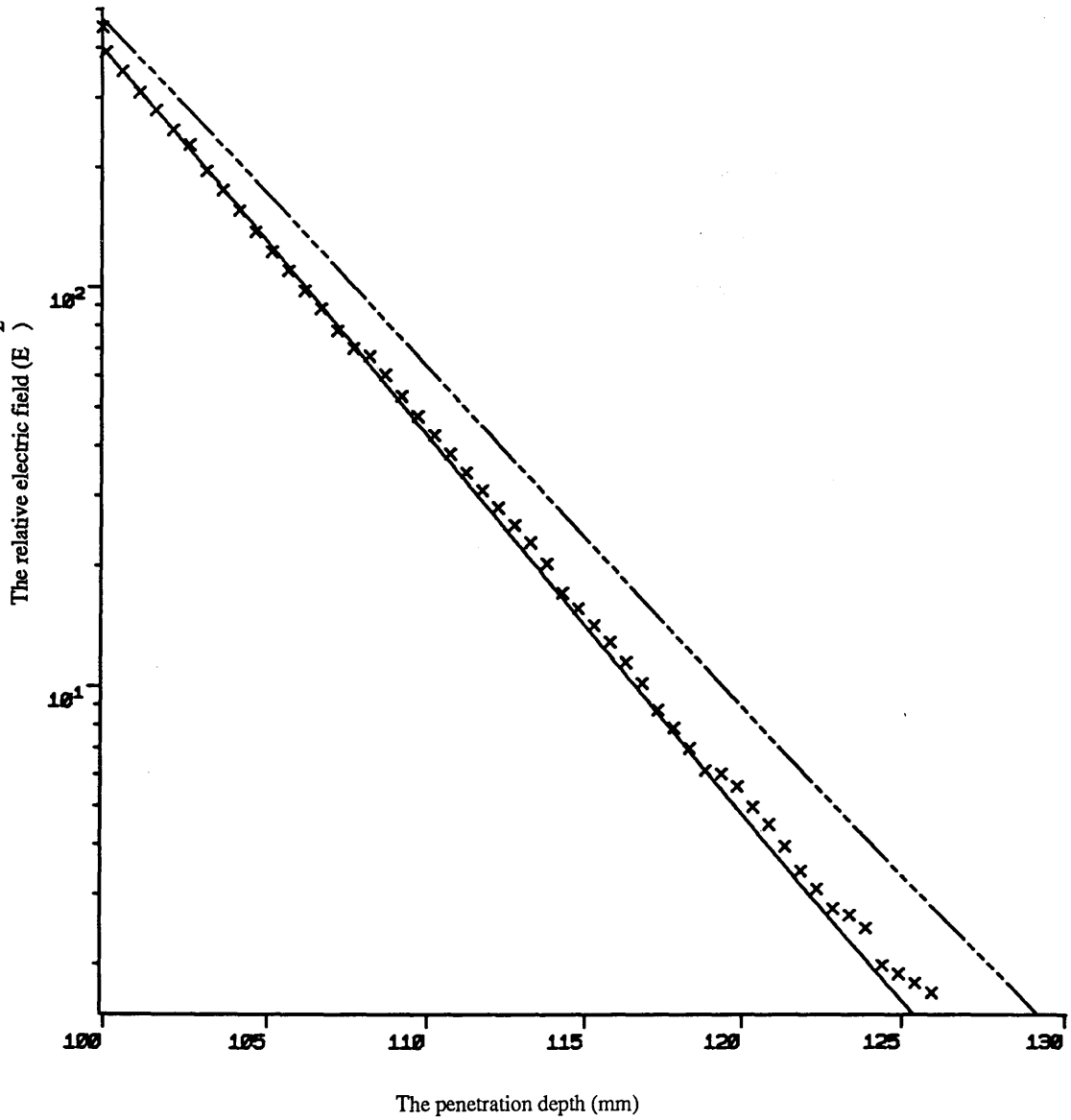

Fig. VIII.6- The relative electric field in a saline solution depending on the distance from the antenna aperture at 3.35 GHz for the dielectric constant (ε'_{rd} = 56, σ_d = 3.9 sm^{-1})

Plane-wave

Best fit curve

× measured data

50% saline solution, $\varepsilon'_{rd} = 56$, $\sigma_d = 3.9$ sm^{-1}) where the effective penetration depth, $\delta_{eff} = 10.5 \pm 0.5$ mm, is different from the plane-wave penetration depth, $\delta_{TEM} = 11.7 \pm 0.5$ mm.

Fig. VIII.7 shows the effective penetration depth variation with respect to the reflected signal for a high-water content such as muscle tissue, using de-ionised water and glycerol, ($\varepsilon'_{rd} = 52$, $\sigma_d = 4.8$ sm^{-1}). In this case the plane-wave penetration depth differs only slightly from the measured penetration depth. The effective penetration depth is 9.4 ± 0.5 mm and the plane-wave penetration depth is 9.6 ± 0.5 mm. The ratio of the effective attenuation constant to the plane-wave attenuation constant is approximately 1:1. The reflected signal can be detected up to 28 mm from the antenna aperture.

Figs. VIII.8 and VIII.9 present the effective penetration depth of a medium- and high-water content dielectric lossy material simulating muscle and breast tissues given in Tab. IV.3 (de-ionised water and glycerol, $\varepsilon'_{rd} = 40$, $\sigma_d = 3.5$ sm^{-1} and sucrose, $\varepsilon'_{rd} = 25$, $\sigma_d = 3.18$ sm^{-1}). The effective penetration depth is lower than the plane-wave penetration depth.

Fig. VIII.10 presents the effective penetration depth of a low-water content phantom such as a mixture of chloroform and alcohol ($\varepsilon'_{rd} = 6.5$, $\sigma_d = 0.48$ sm^{-1}) which is very similar to a fat tissue. The plane-wave penetration depth is significantly different to the measured data. The penetration depth in this medium can be achieved up to 22 mm, but the reflected signal decreases exponentially and after 20 mm the reflected signal is very hard to detect. The dielectric sheet perturber used in this case (approximately 72 mm × 70 mm) is larger than the diameter of the antenna in order to extend beyond the edge of the antenna field. The relative permittivity of the dielectric sheet perturber is about 2.1. The effective penetration depth is about 22.44 mm and the plane-wave penetration depth is equal approximately to 32.40 mm.

Fig. VIII.10.1 shows the antenna response in the water at 3.25 GHz using a dielectric sheet perturber. The plane-wave penetration depth compared with the

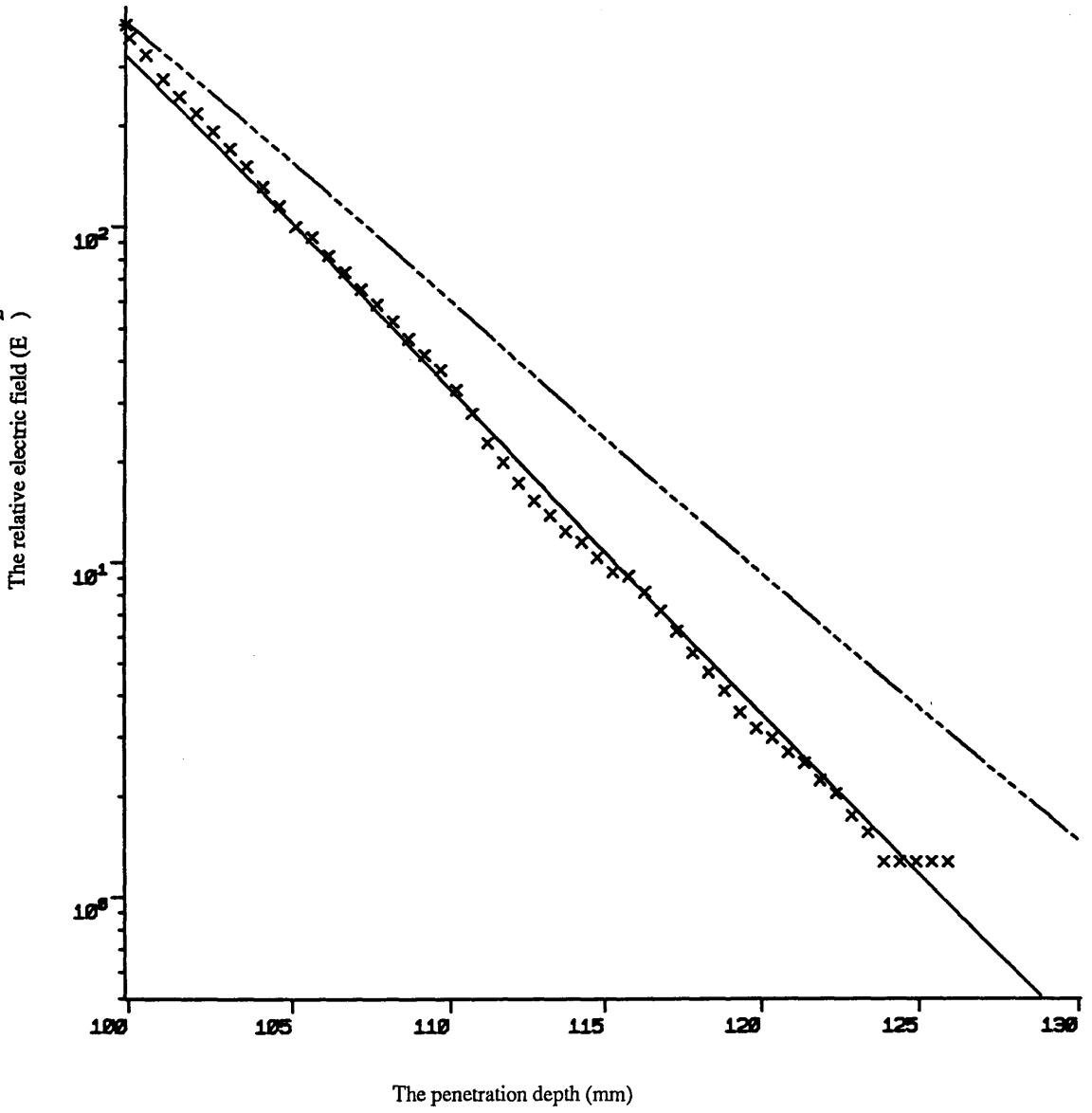

Fig. VIII. 7- The relative electric field in a mixture of de-ionised water and glycerol depending on the distance from the antenna aperture at 3.35 GHz for the dielectric constant($\varepsilon'_{rd} = 52$, $\sigma_d = 4.8\ sm^{-1}$)

——— Plane-wave

——— Best fit curve

× measured data

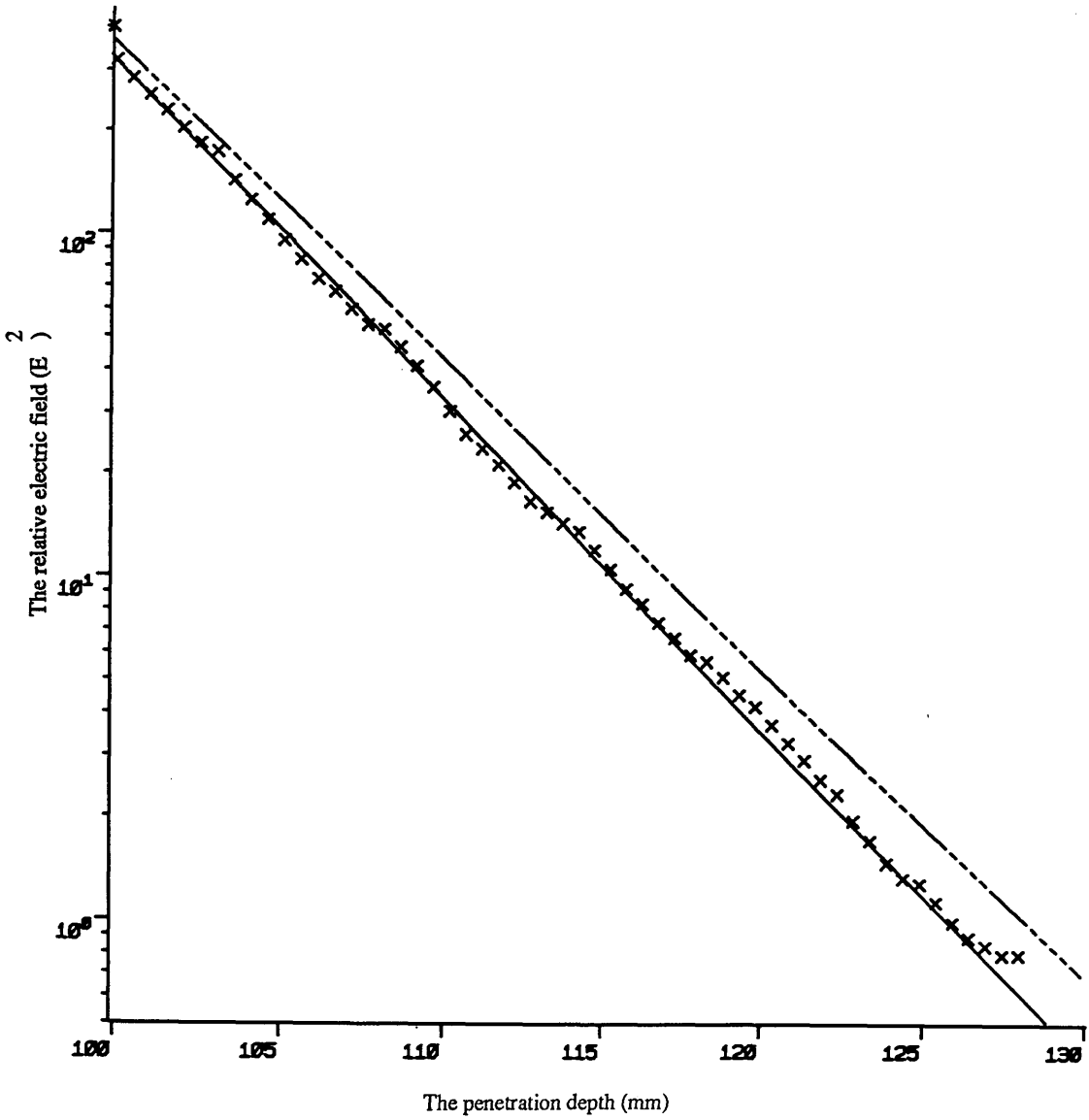

Fig. VIII. 8- The relative electric field in a mixture of de-ionised water and glycerol depending on the distance from the antenna aperture at 3.35 GHz for the dielectric constant($\varepsilon'_{rd} = 40$, $\sigma_d = 3.5\ sm^{-1}$)

———— Plane-wave

———— Best fit curve

× measured data

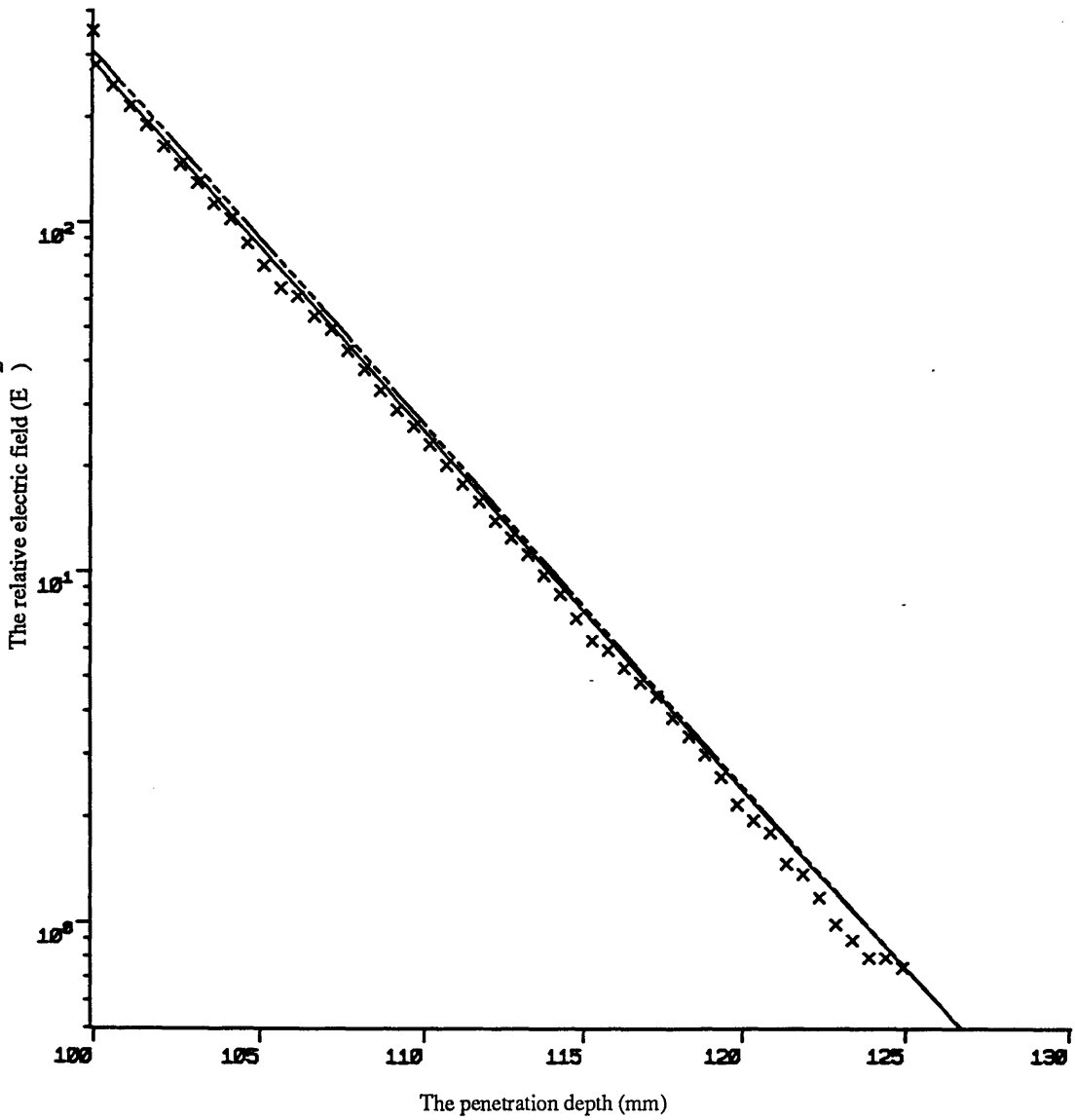

Fig. VIII.9- The relative electric field in a sucrose solution depending on the distance from the antenna aperture at 3.35 GHz for the dielectric constant ($\varepsilon'_{rd} = 25$, $\sigma_d = 3.18\ sm^{-1}$)

Plane-wave

Best fit curve

× measured data

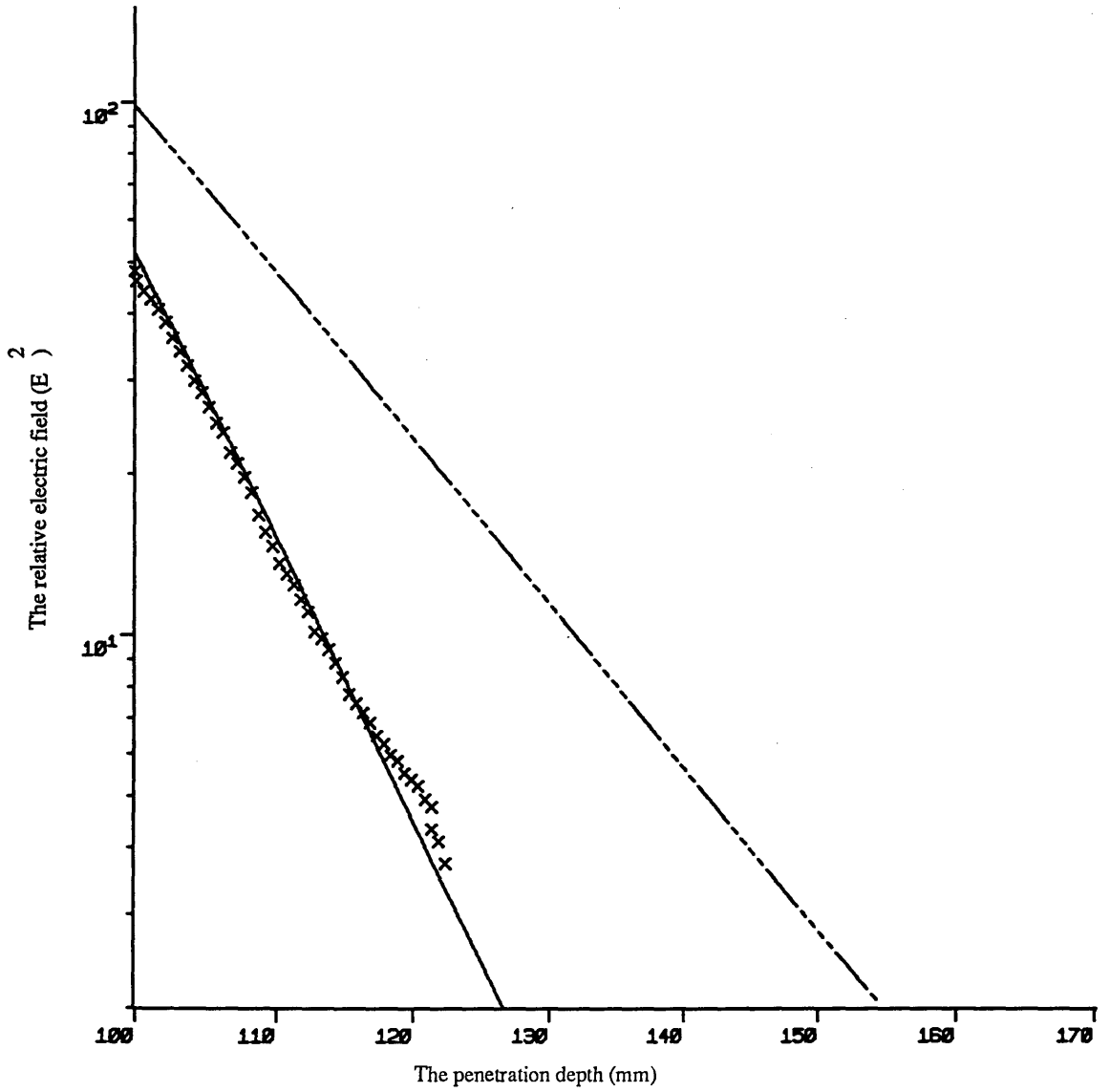

Fig. VIII. 10- The relative electric field in a simulated fat tissue (25% alcohol and 75% chloroform) depending on the distance from the antenna aperture at 3.35 GHz for the dielectric constant ($\varepsilon'_{rd}=6.5$, $\sigma_d=0.48\ sm^{-1}$)

Plane-wave

Best fit curve

× measured data

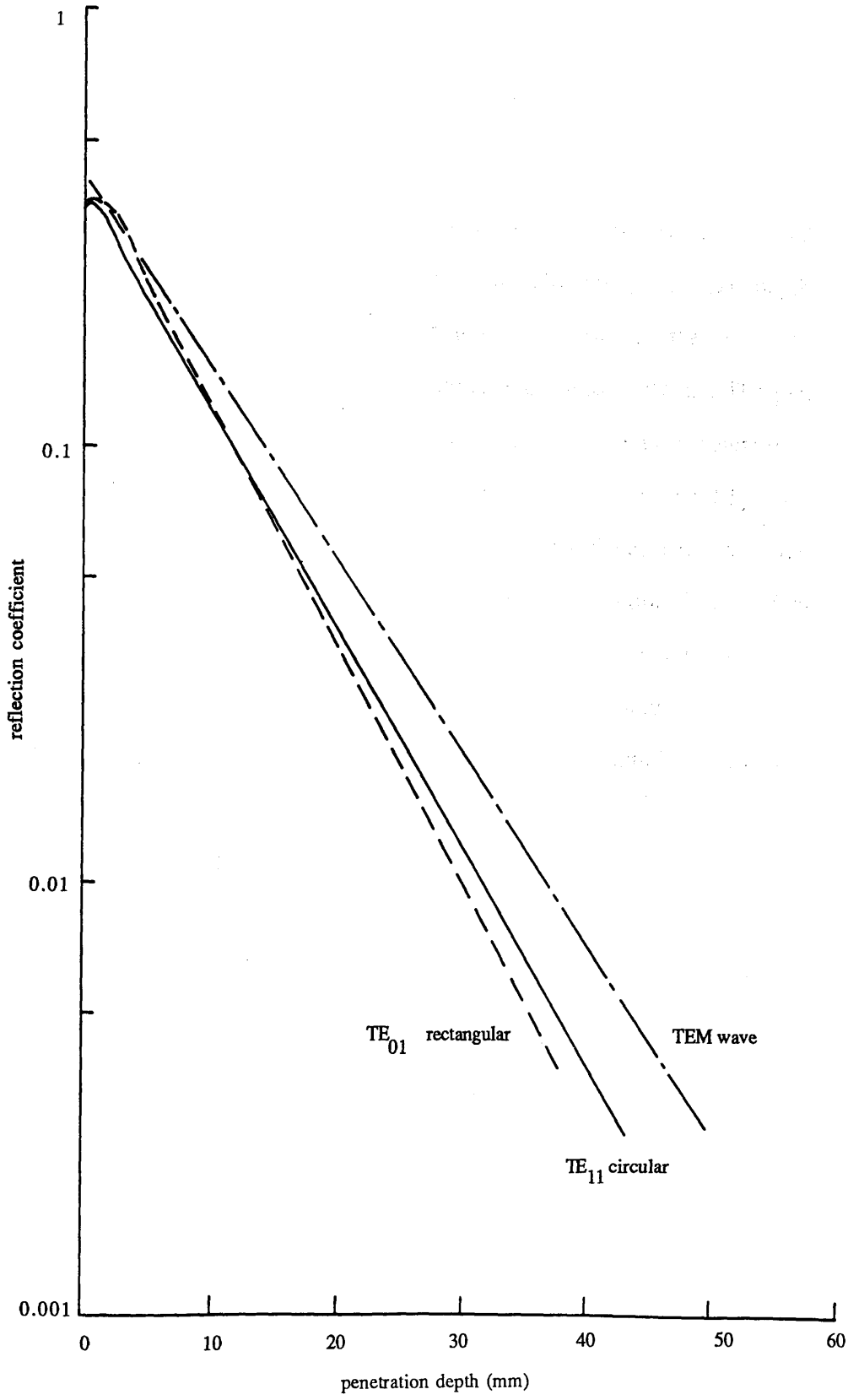

Fig. VIII.10.1- The comparison of the relative electric field of TE_{01}-rectangular waveguide antenna and TE_{11} -cylindrical waveguide antenna with TEM wave in the de-ionised water ($\varepsilon'_{rd} = 76$, $\sigma_d = 2.7\ sm^{-1}$) at a frequency of 3.2 GHz.

effective penetration depth for a TE_{11}-mode cylindrical waveguide antenna used in the present work and by the Microwave Thermography Group at Glasgow University and with a TE_{01}-mode rectangular waveguide antenna used by the Microwave Thermography Group at Lille University, France. A TE_{01}-mode rectangular waveguide antenna is loaded with a medium-loss dielectric ($\varepsilon'_r = 25$), 2.9 cm × 6 cm in dimensions. It was found that the effective penetration depth of the TE_{11}-mode cylindrical waveguide antenna is closer to the plane-wave penetration depth than a TE_{01}-mode rectangular waveguide antenna. The plane-wave penetration depth of the lossy dielectric material (de-ionised water) used is about 19.7 ± 0.5 mm and the effective penetration depth of the TE_{01}-mode rectangular waveguide antenna is about 16.7 ± 0.5 mm and the effective penetration depth of the TE_{11}-mode cylindrical waveguide antenna is about 17.8 ± 0.5 mm. The ratio of the effective penetration depth of a TE_{01}-mode rectangular waveguide antenna to the plane-wave penetration depth is about 0.85 and the ratio of the effective penetration depth of a TE_{11}-mode cylindrical waveguide antenna to the plane-wave penetration depth is about 0.9.

Table VIII.2 illustrates the dielectric properties of the dielectric phantom material at a frequency of 3.35 GHz and at room temperature. The dielectric properties of the dielectric phantom materials simulating to high-, medium- and low-water content tissues which are similar to the dielectric properties of the biological material have been taken in consideration. These dielectric materials were in contact with a TE_{11}-mode cylindrical waveguide antenna. For high- and medium-water content tissues the permittivities (ε'_{rd} = 25 to 76 approximately) are very high compared with low-water content tissue permittivity (ε'_{rd} = 6.5).

The plane-wave attenuation constants were approximately similar to the effective attenuation constants except for the low-water content tissue where the plane-wave attenuation constant was approximately half of the effective attenuation constant which was the expected value.

The effective penetration depths were always lower than the plane-wave

Table VIII.2- Dielectric properties of phantom dielectric material at a frequency of 3.35 GHz and at room temperature.

solutions	ε'_{rd}	ε''_{rd}	σ_d (sm^{-1})	$2\alpha_{TEM}$ (m^{-1})	$2\alpha_{eff}$ (m^{-1})	δ_{eff} (mm)	δ_{TEM} (mm)	$\frac{\delta_{eff}}{\delta_{TEM}}$
75% chloroform & 25% alcohol	6.5±0.02	2.58±0.05	0.48±0.05	70.98±2	102.48±5	32.4±0.2	22.4±0.5	0.69
50% sucrose	25±0.02	18±0.05	3.18±0.05	239±2	237±3	9.6±0.2	9.7±0.5	1.01
23/3 de-ionised water & glycerol*	40±0.02	20±0.05	3.5±0.05	209±2	223±5	11±0.2	10.3±0.5	0.94
2/3 de-ionised water & glycerol**	52±0.02	26±0.05	4.81±0.05	251±2	244±3	9.2±0.2	9.4±0.5	0.98
50% sucrose & 50% saline	56±0.02	22±0.05	3.9±0.05	196±2	220±3	11.7±0.2	10.5±0.5	0.90
2/3 de-ionised water & glycerol***	60.3±0.02	23±0.05	4.2±0.05	205±2	244±3	11.2±0.1	9.4±0.5	0.84
saline	74±0.02	22±0.05	4±0.05	175±2	176±3	13.1±0.2	13±0.5	0.99
de-ionised water	75.9±0.02	13.7±0.05	2.6±0.05	121±2	129±3	19±0.2	17.9±0.5	0.94

penetration depths by a low percentage except for low-water content tissue. So the ratio of the effective penetration depths with the plane-wave penetration depths must be less than 1 in the medium- and high-water content tissues and approximately half in the low-water content tissue. In the case of a medium-water content tissue the ratio was approximately 1. This may be due to an error in the measurement of the effective conductivity of the dielectric, or mismatch in the measuring equipment.

Fig. VIII.10.2 illustrates the dependence of the ratio of the effective penetration depth and the plane-wave penetration depth with the square root of the relative permittivity of the dielectric lossy materials.This approximate relationship is the measure of the relative wavelength in the dielectric which is the factor which will determine how much the beam spreads out and is given by the equation:

$$\frac{\delta_{eff}}{\delta_{TEM}} = 0.030\sqrt{\varepsilon'_{rd}} + 0.710 \qquad \text{(VIII.2)}$$

The relative wavelength in the dielectric phantom materials is given by:

$$\lambda_{rd} = \frac{\lambda_o}{\sqrt{\varepsilon'_{rd}}} \qquad \text{(VIII.3)}$$

where λ_o is the free-space measurement wavelength. The relative wavelength in the dielectric phantom materials is small compared to the free-space wavelength in the measurements. From this equation we found that the relative wavelength in high-water content tissue is smaller than that in the low-water content tissue. So, the ratio can be written as:

$$\frac{\delta_{eff}}{\delta_{TEM}} = \frac{2.7 \times 10^{-3}}{\lambda_{rd}} + 0.71 \qquad \text{(VIII.4)}$$

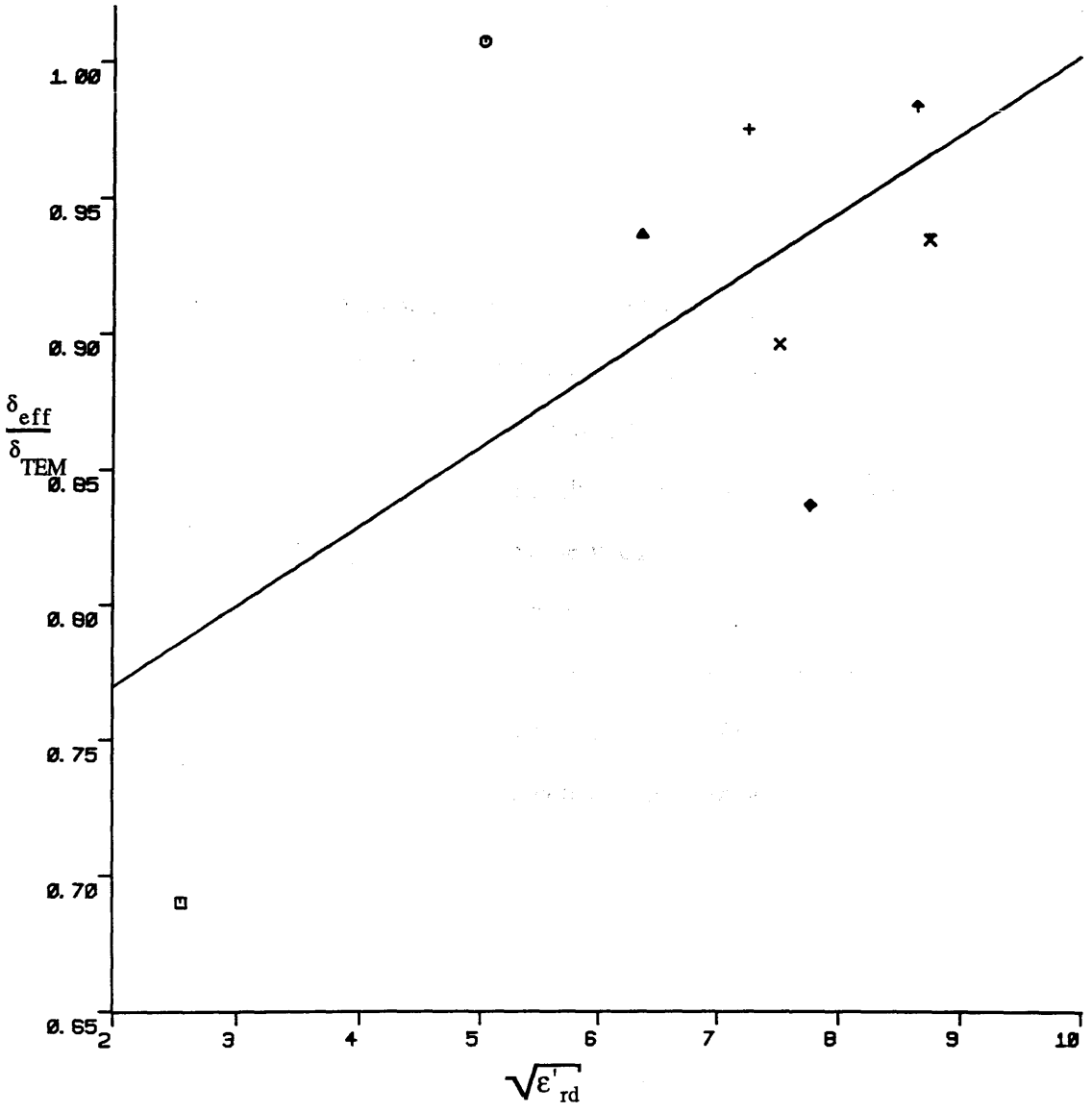

Fig. VIII.10.2- Variation of the ratio of the effective penetration depth to the plane - wave penetration depth with the square root of the relative permittivity of the dielectric lossy materials.

- chloroform (6.5,2.58)
- sucrose (25, 18)
- de-ionised water & glycerol (40, 20)
- de-ionised water & glycerol (52, 26)
- sucrose & saline (56, 22)
- de-ionised water & glycerol (60.3, 23)
- saline (74, 22)
- deionised water (75.9, 13.7)

The numbers between brackets are the relative permittivity and the loss factor.

From this equation we can see that the factor 2.7×10^{-2} is the guide wavelength λ_g of the TE_{11}-mode cylindrical waveguide antenna (m) at a frequency of 3.35 GHz. Equation VIII.4 becomes:

$$\frac{\delta_{eff}}{\delta_{TEM}} = \frac{1}{10}\left(\frac{\lambda_g}{\lambda_{rd}}\right) + 0.71 \qquad \text{(VIII.5)}$$

The ratio of the effective penetration depth to the *TEM* wave penetration distance is inversely proportional to the ratio of the relative wavelength in the dielectric material to the guide wavelength and reduced by a factor of 10.

Fig. VIII.10.3 shows the linear relationship between the plane-wave power attenuation constant, $2\alpha_{TEM}$, the former value is calculated from the dielectric properties of the phantom dielectric lossy materials using Eq. VIII.1, and the ratio of the plane-wave power attenuation constant to the effective power attenuation constant, $2\alpha_{eff}$. This relationship is necessary to account for the effects of the antenna in any tissue with a given power attenuation constant and is given by the equation:

$$\frac{2\,\alpha_{TEM}}{2\,\alpha_{eff}} = 1.8 \times 10^{-3}\, 2\alpha_{TEM} + 0.566 \qquad \text{(VIII.6)}$$

For the high-water content tissue the effective penetration depth is closer to the plane-wave penetration depth than will be expected in tissue of the same power attenuation constant. The smaller wavelength in these liquids is due to the higher dielectric constant than will be found in the tissue (Tabs. IV.3 and VIII.2), resulting in reduced diffraction effects.

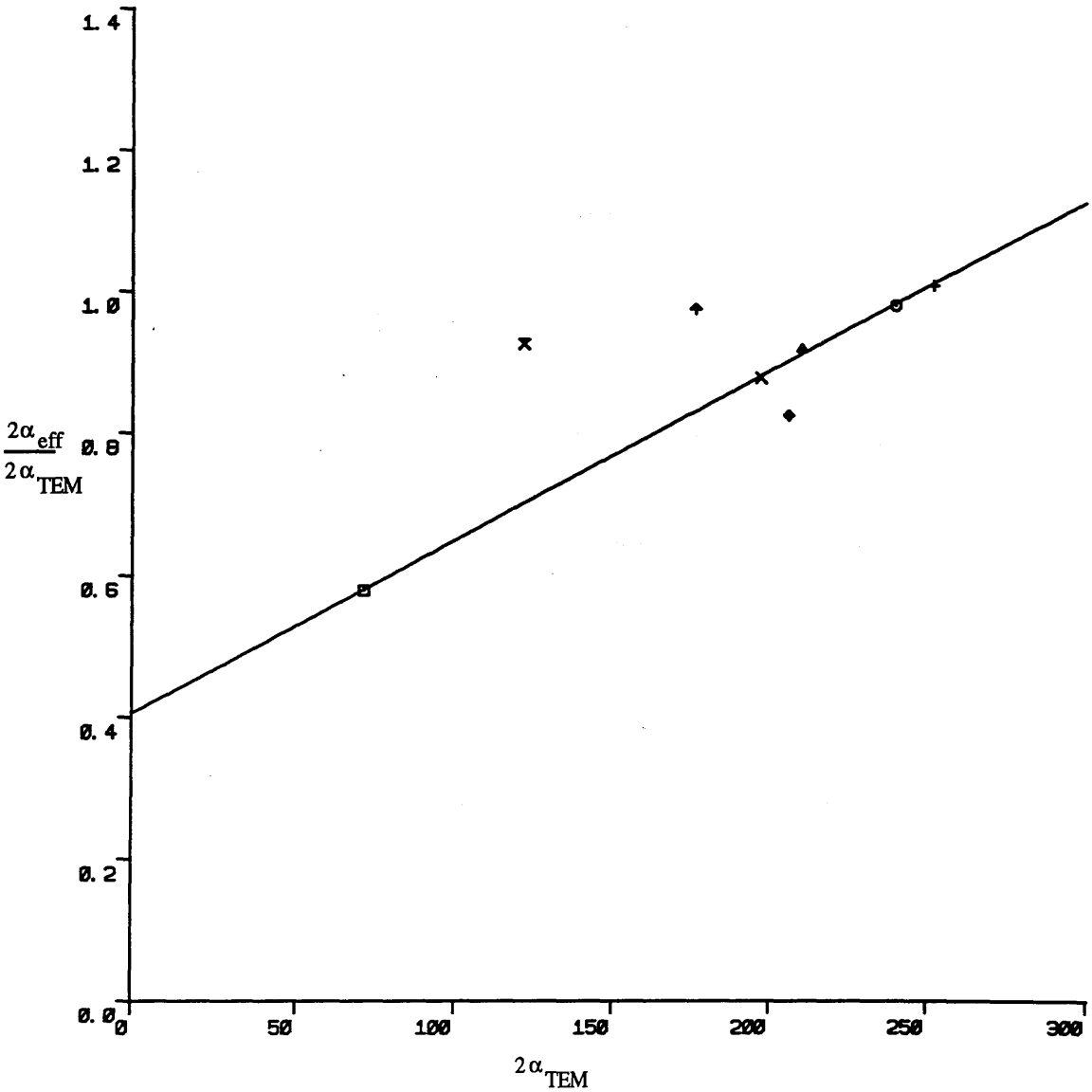

Fig. VIII.10.3- Variation of the ratio of the effective attenuation constant to the plane - wave attenuation constant with the plane-wave attenuation constant.

- chloroform (6.5,2.58)
- sucrose (25, 18)
- de-ionised water & glycerol (40, 20)
- de-ionised water & glycerol (52, 26)
- sucrose & saline (56, 22)
- de-ionised water & glycerol (60.3, 23)
- saline (74, 22)
- deionised water (75.9, 13.7)

The numbers in brackets are the relative permittivity and the loss factor.

Table VIII.3- The measured and calculated antenna face reflection coefficients of the dielectric phantom materials at a frequency of 3.35 GHz and room temperature.

solutions	ε'_{rd}	$\lvert\Delta\Gamma\rvert_{mea}$	$\lvert\Delta\Gamma\rvert_{cal}$
75% chloroform & 25% alcohol	6.5 ± 0.5	0.066 ± 0.01	0.098 ± 0.05
50% sucrose	25 ± 0.5	0.35 ± 0.01	0.30 ± 0.05
2/3 de-ionised water & 1/3 glycerol	40 ± 0.5	0.40 ± 0.01	0.36 ± 0.05
2/3 de-ionised water & 1/3 glycerol	52 ± 0.5	0.39 ± 0.01	0.42 ± 0.05
50% sucrose & 50% saline	56 ± 0.5	0.45 ± 0.01	0.42 ± 0.05
2/3 de-ionised water & 1/3 glycerol	60.3 ± 0.5	0.39 ± 0.01	0.44 ± 0.05
saline	74 ± 0.5	0.45 ± 0.01	0.49 ± 0.05
de-ionised water	75.9 ± 0.5	0.46 ± 0.01	0.48 ± 0.05

The reflection coefficient given in Tab. VIII.3 $|\Delta\Gamma|$ is approximately 50% for the high-water content dielectric lossy material, approximately 30% for medium-water content tissue and 10% for low-water content tissue. The fact that the measured reflection coefficients at the face of the antenna are generally close to those given by the approximate expression (Eq. VII.23) shows that the field is indeed mostly transmitted from the antenna outwards.

Near-field patterns in simulated muscle and fat tissues obtained from the measurements of the fields in the *E* and *H* planes of the antenna using a spherical dielectric perturber. A spherical dielectric perturber was moved in x-z plan plane from the antenna aperture in the dielectric phantom material. The corresponding results at the operating frequency of 3.35 GHz are given in Figs VIII.11 to VIII.17.

The near-field patterns of high-water content dielectric phantom materials simulating muscle and breast tissues were presented in Figs. VIII.11, VIII.12, VIII.13, VIII.14 and VIII.15 at a constant frequency and for distances ranging from 0 to 28 mm from the antenna aperture. The field patterns are larger than the antenna aperture because the electric field E is not all transverse and also the field travels "sideways" slightly. This shows the phase change and leads to the reduction in the reflection coefficient.

Figs. VIII.16 and VIII.17 present configurations of the square of the electric field for medium- and low-water content tissues such as 50% sucrose and a mixture of 75% chloroform and 25% alcohol at the operating frequency of 3.35 GHz and for distances ranging from 0 to 20 mm. For a low-water content the near-field zone is significantly different from the plane-wave region as discussed in Chapter I. The reflected signal from the antenna is very difficult to detect because the relative permittivity of the dielectric lossy material is almost the same as the relative permittivity of the dielectric perturber and also because of the reflection in the medium caused by the dielectric wall of the container. So we have minimized the reflection in the lossy liquid by covering the container with an isolating material.

Fig. VIII.18 presents the near-field configuration of a simulated muscle tissue such as a mixture of 200 grams of sucrose and 300 grams of de-ionised water at the operating frequency of 3.35 GHz for distances of 23 mm and 35 mm from the antenna aperture for two similar antennas using a sphere 6.35 mm in diameter as dielectric perturber with the relative permittivity is approximately 2. These plots have been taken with the x-y recorder. The top plot shows the power density (E^2) variation with the lateral position at a depth of 23 mm obtained by a single TE_{11}-mode cylindrical waveguide antenna. It can be seen that the antenna used for the measurement is not symmetric in both sides of the aperture. This is due to an asymmetry in the arrangement of the internal coaxial to waveguide transition of the antenna. The bottom plot shows the same measurement with similar antenna

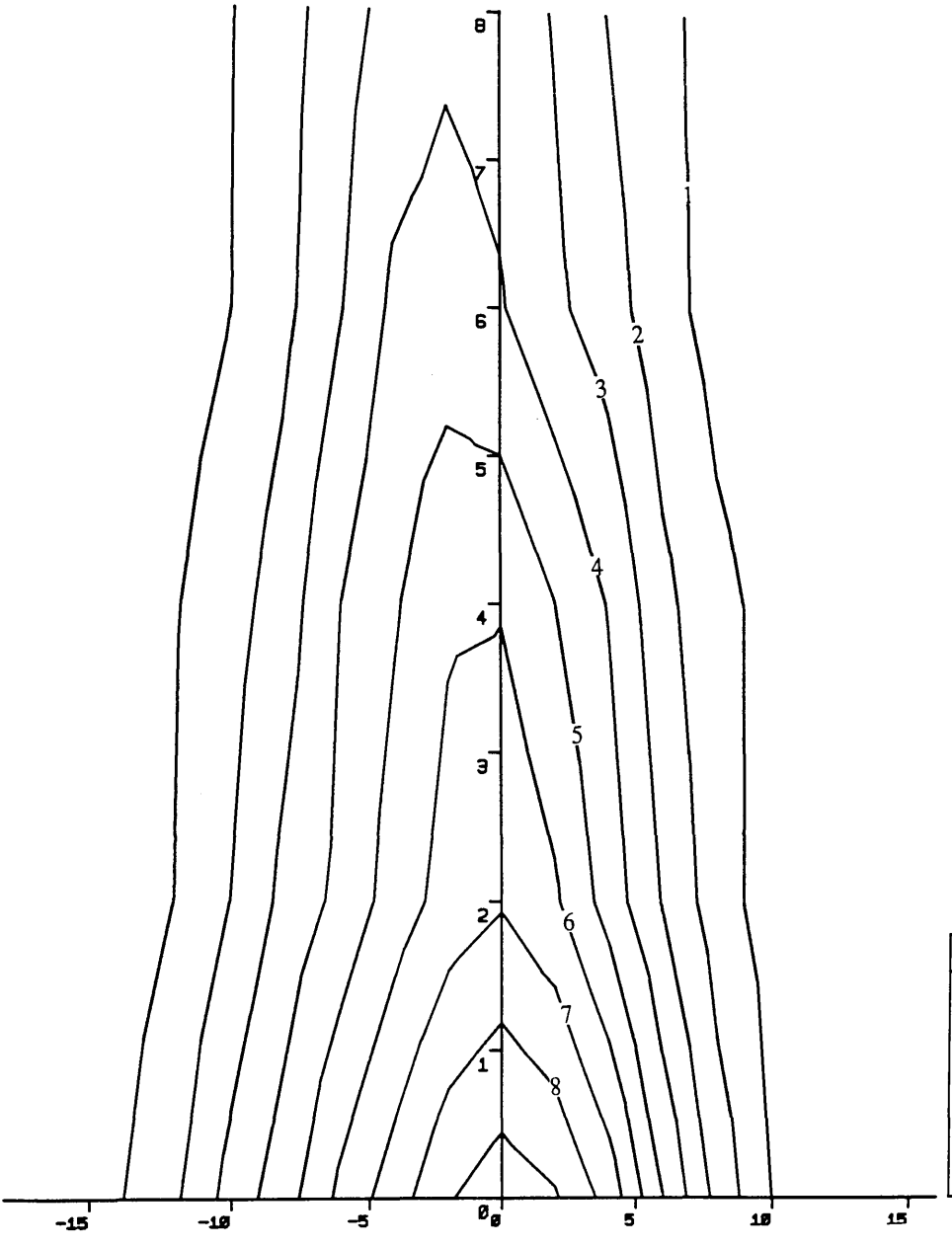

Contours	Key
1	20
2	40
3	60
4	80
5	100
6	120
7	140
8	160
9	180

Fig. VIII. 11- The relative electric field configuration in the de-ionised water at 3.35 GHz for different distances from the antenna apetrure.

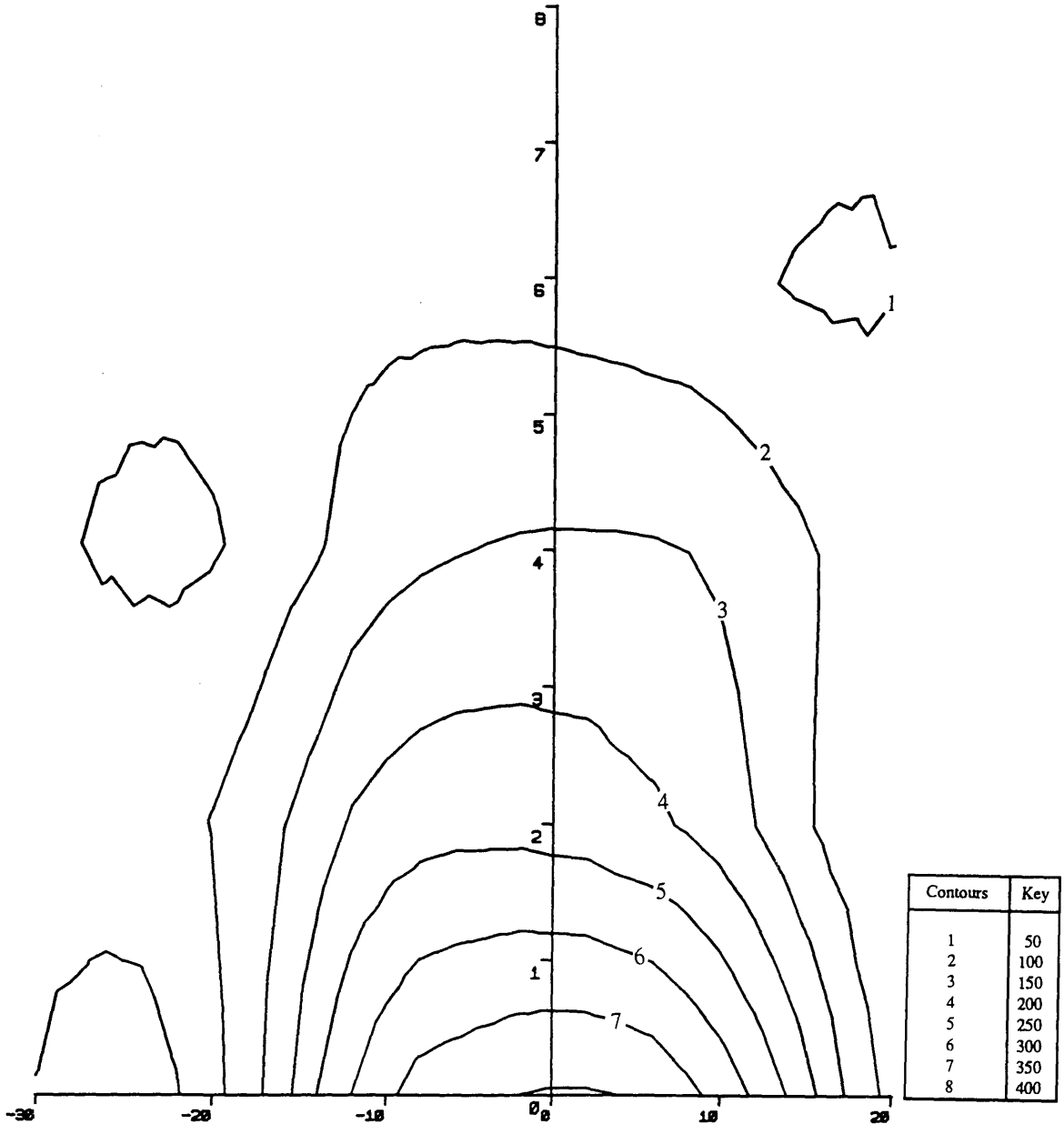

Fig. VIII.12- The relative electric field configuration in a saline solution at 3.35 GHz for different distances from the antenna aperture.

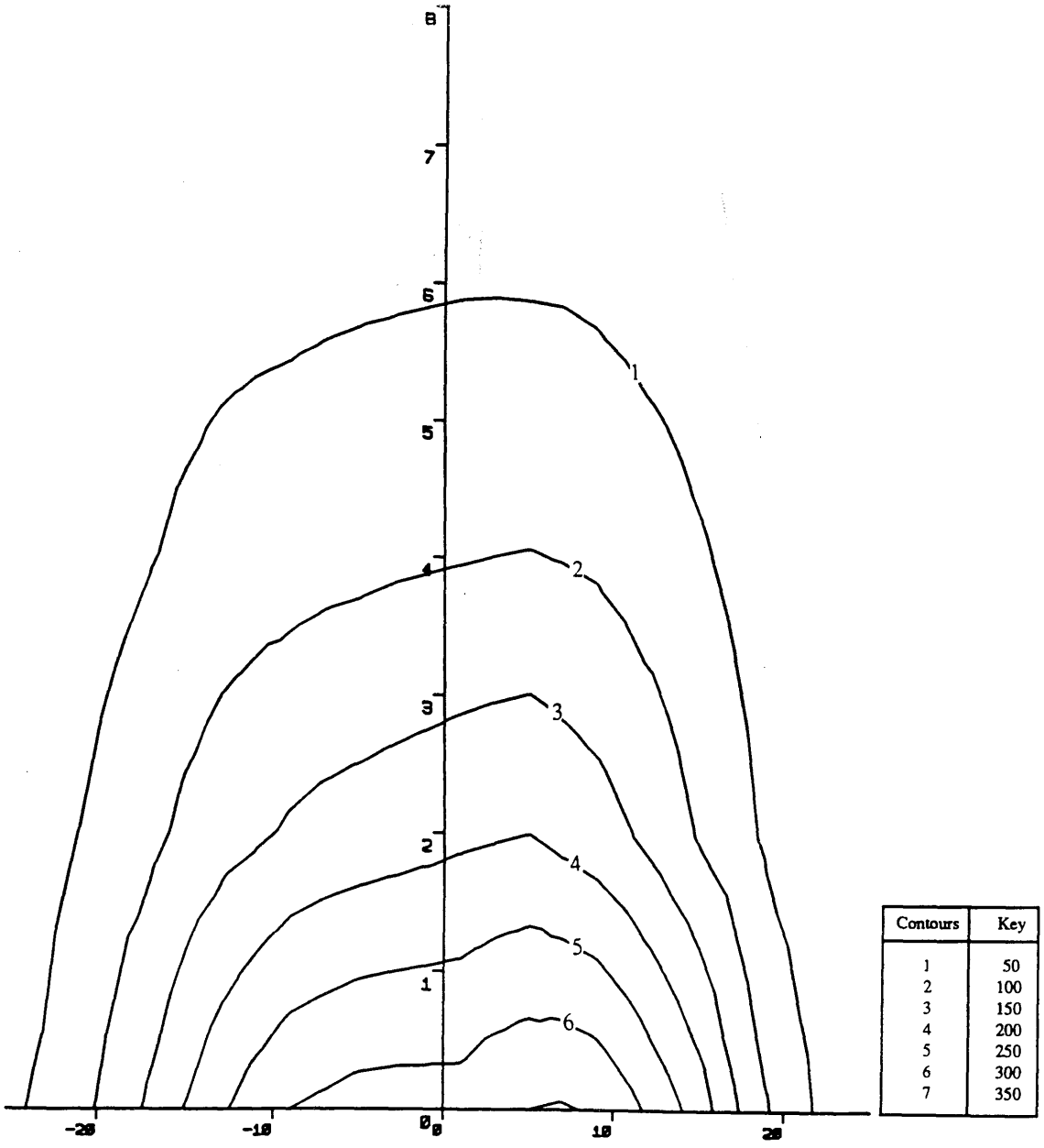

Fig. VIII.13- The relative electric field configurtation in a mixture of glycerol and de-ionised water aat 3.35 GHz for different distances from the antenna aperture.

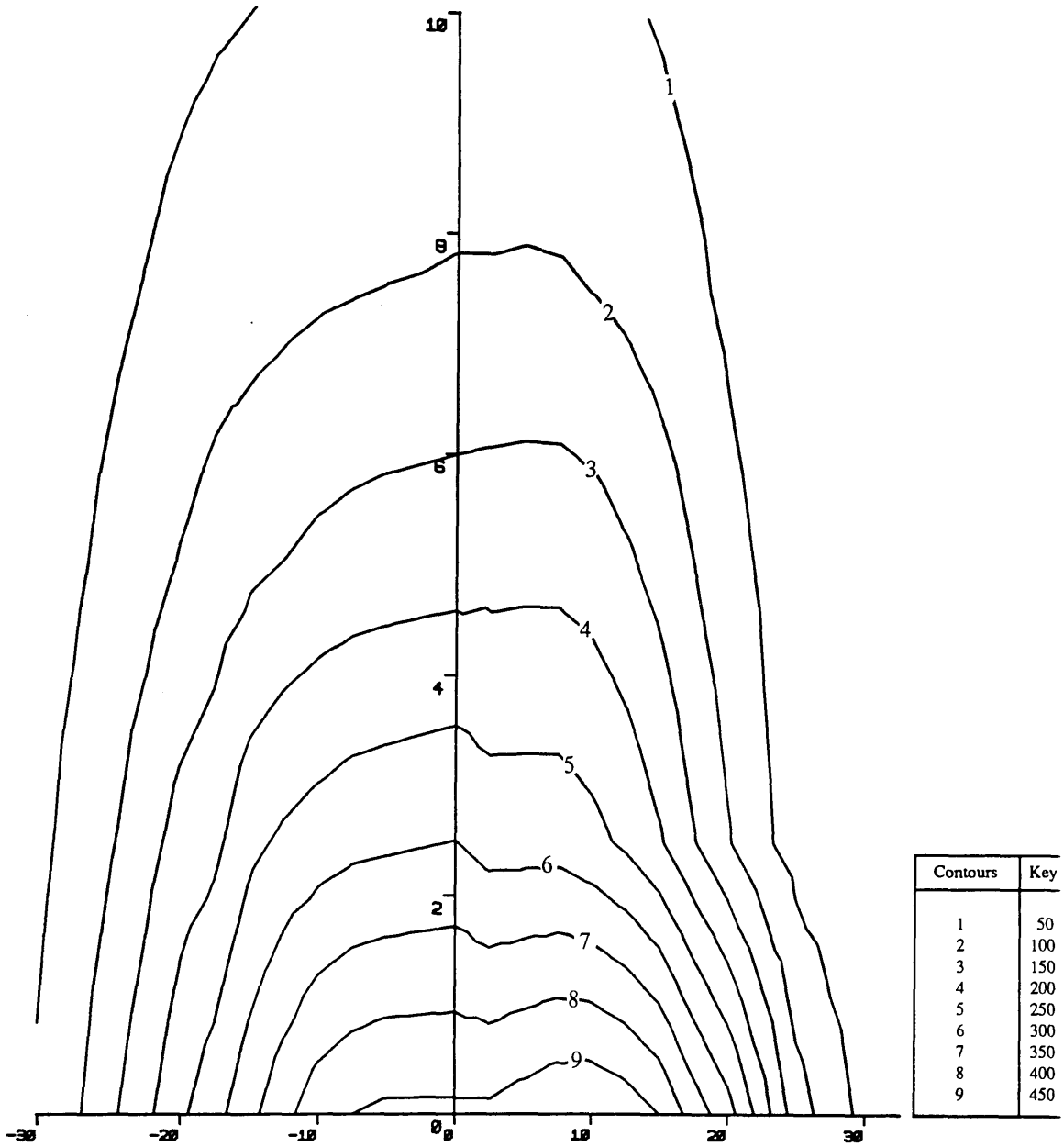

Contours	Key
1	50
2	100
3	150
4	200
5	250
6	300
7	350
8	400
9	450

Fig. VIII.14- The relative electric field configuration in a mixture of sucrose and saline at 3.35 GHz for different distances from the antenna aperture.

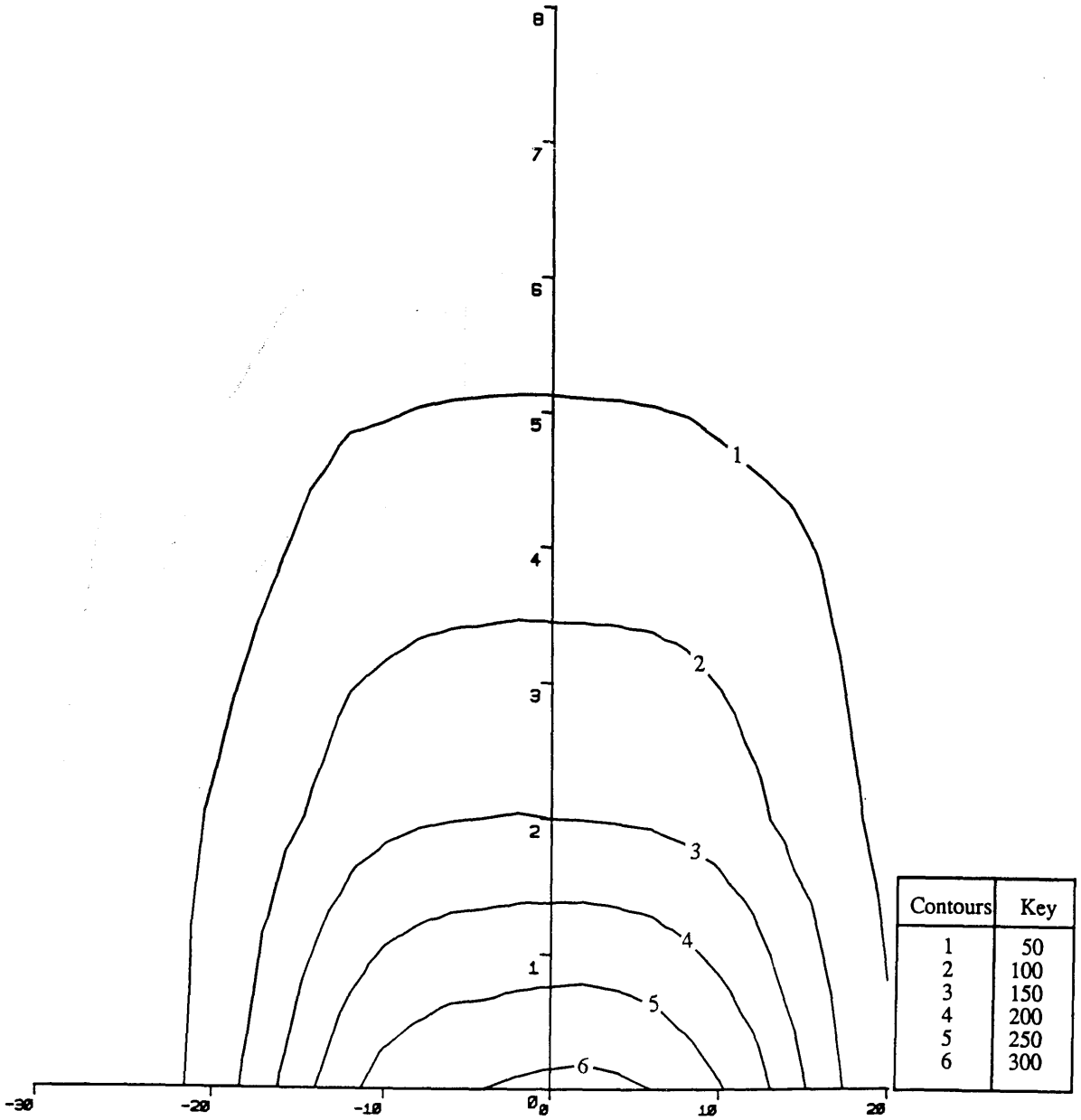

Fig. VIII.15- The relative electric field configuration in a mixture of glycerol and de-ionised water but the relative permittivity of this solution is lower than the one shown in Fig. VIII.13.
The operating frequency is 3.35 GHz for different distances from the antenna aperture.

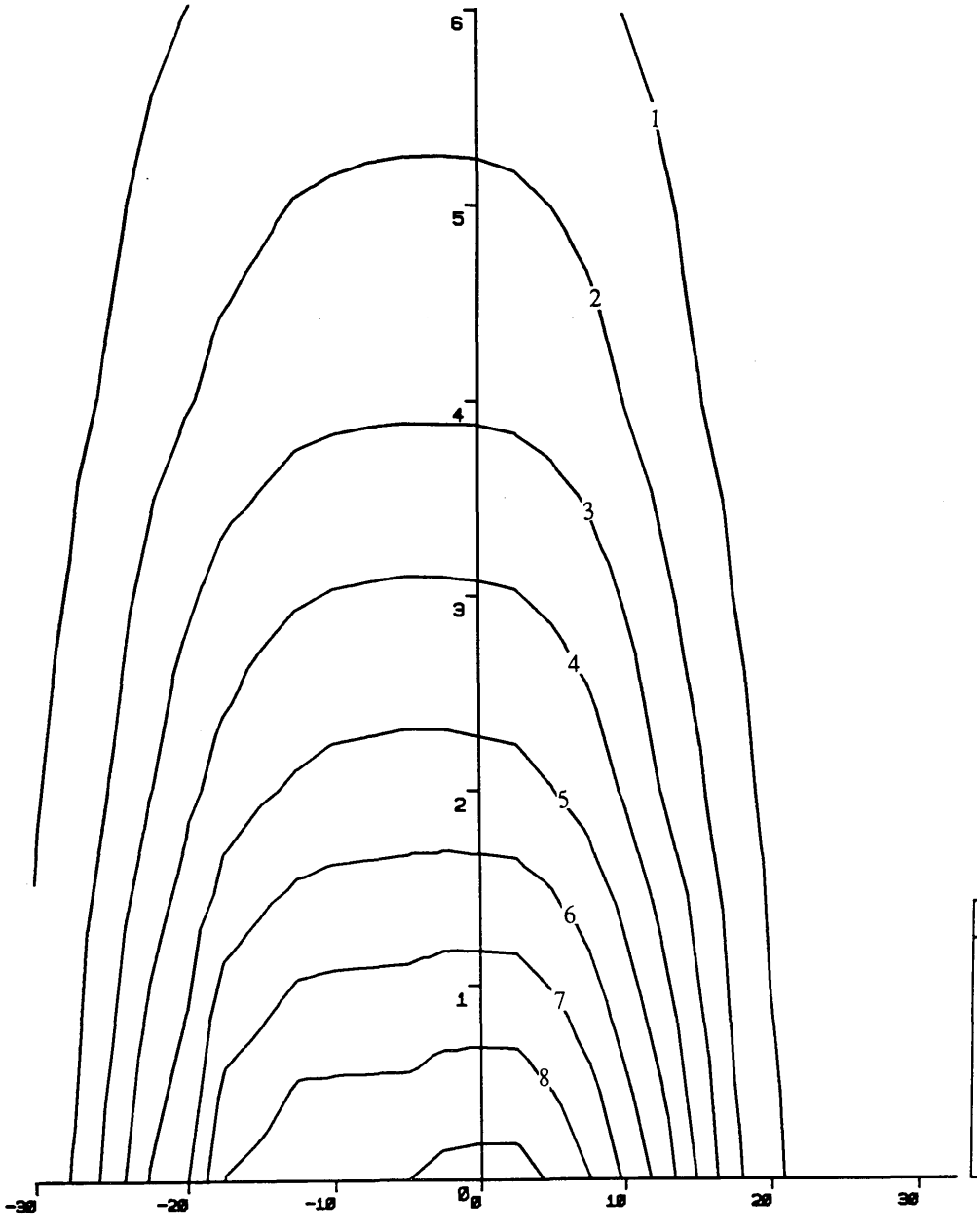

Contours	Key
1	100
2	200
3	300
4	400
5	500
6	600
7	700
8	800
9	900

Fig. VIII.16- The relative electric field configuration in a sucrose solution at 3.35 GHz for different distances from the antenna aperture.

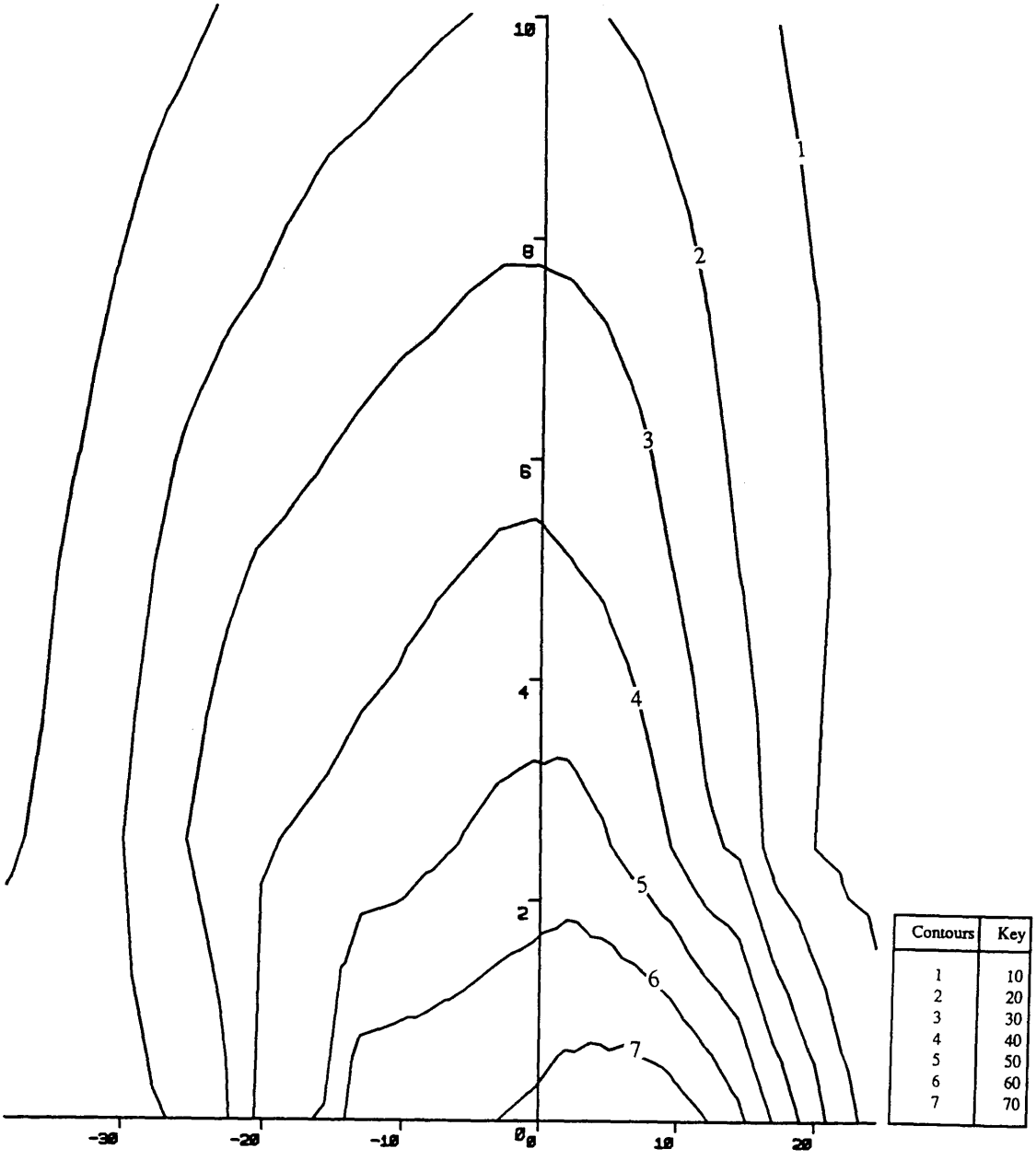

Fig. VIII.17- The relative electric field configuration in a mixture of alcohol and chloroform at 3.35 GHz for different distances from the antenna aperture.

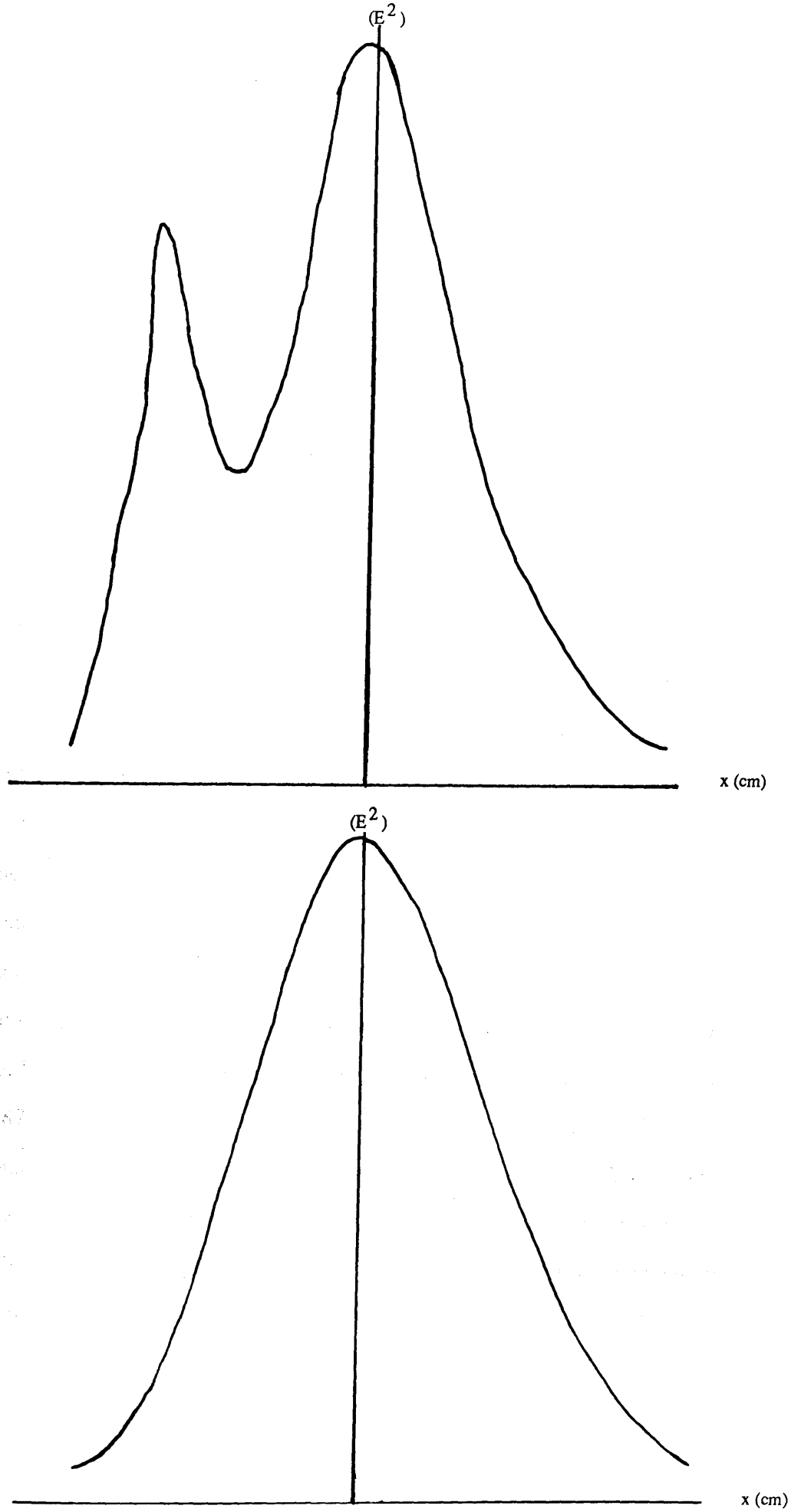

Fig. VIII.18- Comparison of the relative electric field configuration in simulating muscle tissue of two TE_{11}- cylindrical waveguide antennas.

at a depth of 35 mm from the antenna aperture. The power density (E^2) is distributed symmetrically across the aperture and shows that the antenna used is better than the first one in this respect. These measurements further illustrate the information about the antenna response pattern that can be provided by *nonresonant perturbation.*

The experimental measurements of the effective penetration depths are close to the plane-wave penetration depths for medium- and high- water content tissues and with significant difference for low-water content tissue.
The electric field in the dielectric phantom material is formed to fall-off exponentially with distance from the antenna.
. For low-water content tissue the power density decreases very slowly comparing to high- and medium-water content tissues. These results are as the expected forms.

These measurements have shown that there are three limiting cases for the penetration depth in tissue, the plane-wave penetration depth and the penetration depth determined by the waveguide antenna mode, the geometry of the waveguide antenna (Fig. VIII.10.1) and the size of the antenna aperture. For the plane-wave penetration depth, the upper limit is approached when the medium is lossy or the antenna aperture is large and the lower limit, in which the antenna aperture determines the penetration depth, is approached when the antenna aperture is electrically small. These limitations have been studied by Cheever et al., (1987). Tab. VIII.4 illustrates collected calculated and measured data from Cheever et al., (1987) of the effective penetration depths for apertures radiating into water or ethanol compared with the plane-wave penetration depth. Two different limiting cases have been considered for the effective penetration depth, in the case where $\tan \delta < 0.25$ and $\log(\omega^2 \mu_o \varepsilon_o \varepsilon' a^2) > 1$, the effective penetration depth δ is given approximately by:

$$\delta = \frac{\delta'}{a} \qquad \text{(VIII.4)}$$

where a is the aperture width and δ' is the effective penetration depth in the case

where $\tan \delta \cong 1$. This is defined by:

$$\delta' = \frac{\lambda_o}{2\pi\sqrt{2\,\varepsilon'}} \left[\left(1 + \left(\frac{\varepsilon''}{\varepsilon'} \right)^2 \right)^{\frac{1}{2}} - 1 \right]^{-\frac{1}{2}} \qquad \text{(VIII.5)}$$

where λ_o is the free-space wavelength.

Table VIII.4- The calculated and measured penetration depths for different apertures sizes compared with the plane-wave penetration depth (from Cheever et al., 1987).

Aperture Width (cm)	Frequency (GHz)	Liquid	Permittivity		Penetration depth (cm)		
			ε'_r	ε'_r	δ_{cal}	δ_{mea}	δ_{TEM}
7.3	3.1	ethanol	10.8	10.5	.56	.6	.53
7.3	3.9	"	9.1	9.3	.46	.4	.44
4.8	3.9	"	9.1	9.3	.46	.4	.44
4.8	4.7	"	8.0	8.2	.41	.4	.39
1.5	3.9	"	9.1	9.3	.20	.2	.44
1.5	4.7	"	8.0	8.2	.21	.2	.39
7.3	3.1	water	77.0	11.0	1.01	1.02	1.23
7.3	3.9	"	75.0	16.0	.67	.7	.67
4.8	3.9	"	75.0	16.0	.64	.6	.67
4.8	4.7	"	74.0	17.0	.49	.5	.52
1.5	3.9	"	75.0	16.0	.49	.5	.67
1.5	4.7	"	74.0	17.0	.47	.4	.52

The Microwave Thermography Group at Lille University, France have also studied the penetration depth and patterns of TE_{01}-mode rectangular waveguides (Mamouni, et al. 1983). The numerical calculations were carried out to determine the effective penetration depth from a variety of waveguide aperture sizes operating at frequencies of 1, 3 and 9 GHz, and filled with dielectric of relative permittivity 1 to 25. The effective penetration depth in two types of homogeneous tissues was

calculated; one representing the dielectric properties of muscle and the second the dielectric properties of fat.

VIII. 4- The *nonresonant perturbation* technique using crossed-pair antennas:

The concept of the microwave correlation radiometry has been discussed theoretically and the "*add-and-square*" technique for the correlation of thermal radiation from two antennas was used in the experiments described in Chapters V and VI. A two antenna microwave correlation radiometer integrates radiation over a distance that is of fixed time delay differential to the two antennas and also is within the volume of tissue common to both antennas. This distance is defined such that the difference in transit time of the radiation from any point P within that volume to each of the antennas is a constant τ (Fig. V. 5b), where $\tau = \frac{x_1 - x_2}{c}$.

The same arrangement investigated in Chapters V and VI which uses two identical antennas, with a fixed distance between them, and with their axes at 90 ° (Fig. V.5a) is investigated in this Chapter using the *nonresonant perturbation* technique as shown in Fig. VIII.1. The process in section VIII.2 has been applied using a sphere 6.35 mm in diameter as dielectric perturber which was moved across the phantom dielectric material parallel to the line joining the midpoints of the antenna apertures (in x-direction). Fig. VIII.19 shows an example of the *nonresonant perturbation* system coupled with a microwave crossed-pair antenna arrangement. Several phantom dielectric materials have been used to investigate the correlated power density (E^2) at a certain depth with different lateral positions and for phase differences between the antennas from 0° to 180° at a frequency of 3.35 GHz.

Fig. VIII.20 shows the relationship of the power density (E^2) at a depth of 30 mm in a position close to the plane of symmetry with lateral positions of dielectric perturber and for several phase differences between the antennas in simulated muscle tissue such as a mixture of 200 grams sucrose and 300 grams de-

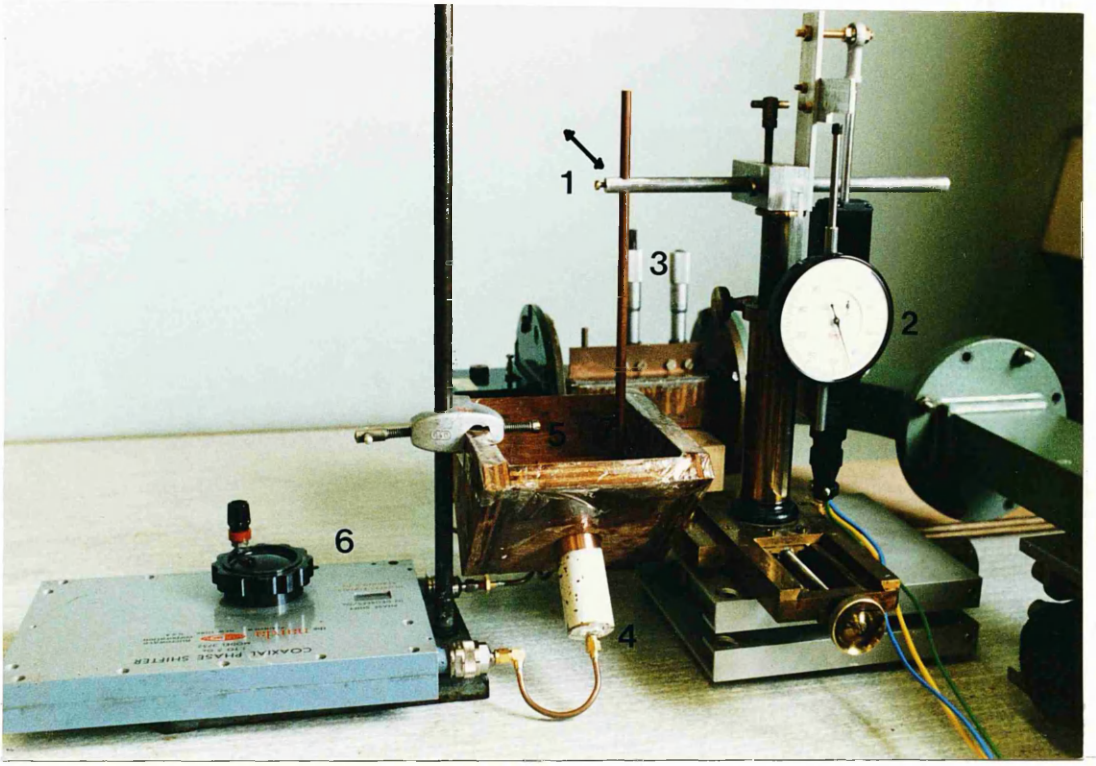

Fig. VIII.19- The experiment arrangment of a crossed-pair antenna of the electric field measurements.

1 -Perturber movement

2 -Perturber axial position gauge

3 -Matching unit

4 -Crossed-pair antenna

5 -Phantom dielectric liquid container

6 -Coaxial phase shifter

7 -Dielectric perturber

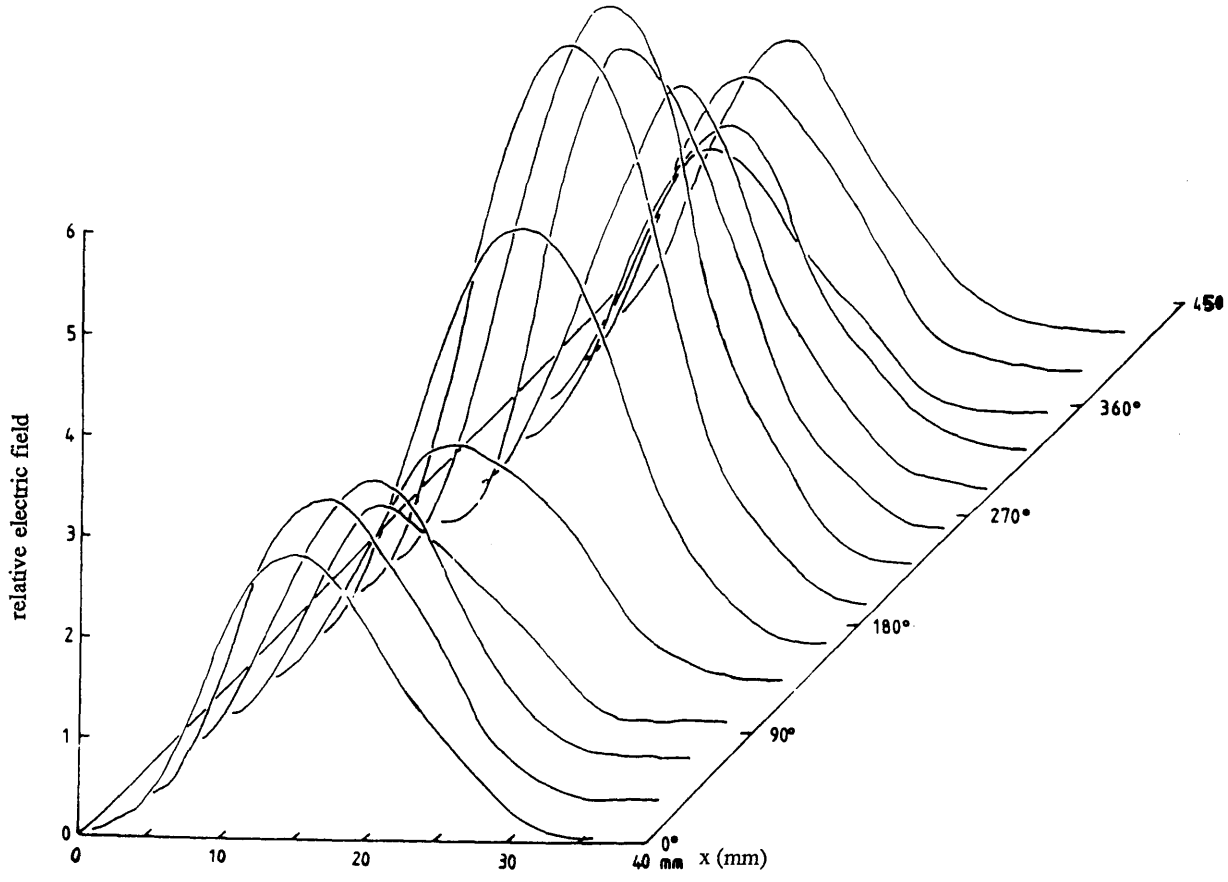

Fig. VIII.20- The variation of the power density with the lateral position and the phase at a depth of 30 mm.

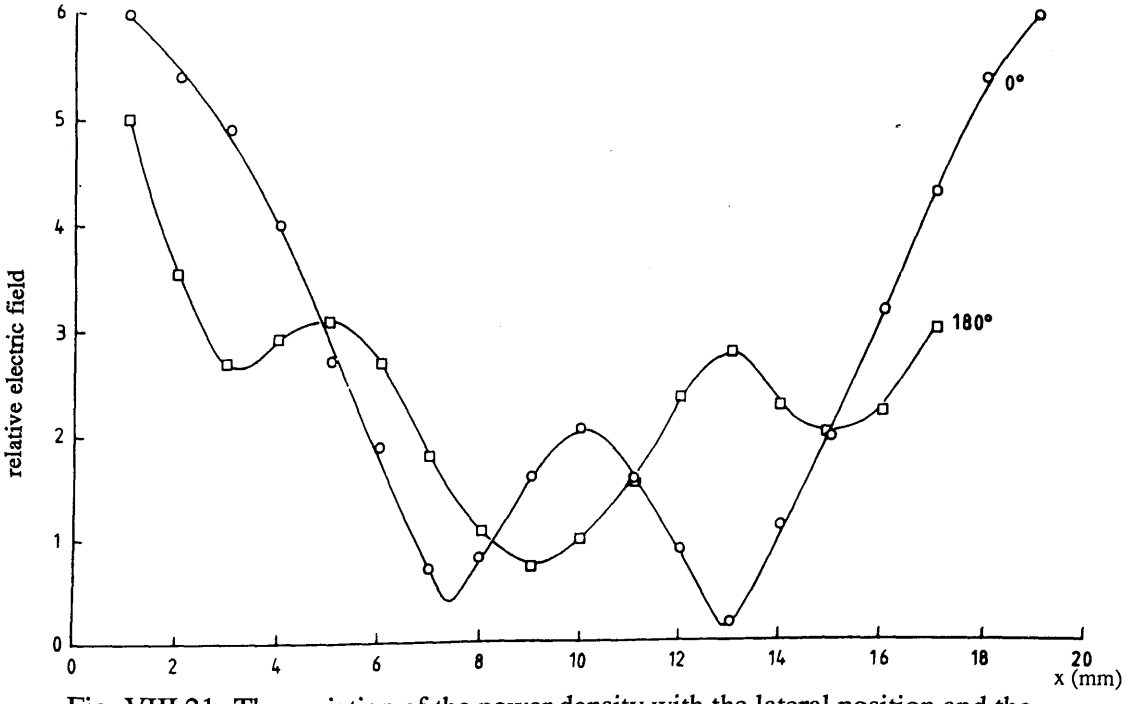

Fig. VIII.21- The variation of the power density with the lateral position and the phase at a depth of 15 mm.

ionised water ($\varepsilon'_{rd} = 47$, $\sigma_d = 34\ sm^{-1}$). The power density was measured for the phase difference range of 0° - 450° between the antennas. The maximum power density which could be achieved was located between phase differences of 180° and 270°. When the phase was lower than 180° or greater than 270° the power density was approximately the same. The power density was minimum at 0° and maximum at 180°.

Figs. VIII.21 and VIII.22 show the comparison of the power density (E^2) for depths of 15 mm and 20 mm with the lateral position. Two cases have been considered in phase and 180° out of phase between the antennas in simulated muscle tissue such as sucrose. The maximum power density for the case where the antennas were in phase was located at both sides of the antennas. At a depth of 15 mm the power density was greater than the results received at a depth of 20 mm. In the midline of the antennas the power density was very weak. For the case where the antennas were at 180° out of phase the power density was approximately half of the one obtained in phase. We concluded that the power density was maximum for the case where the antennas were in phase and at a depth of 15 mm.

Fig. VIII.23 shows the comparison of the power density (E^2) for different phases 0°, 125° and 180° at a depth of 30 mm with the lateral position. The maximum power density was located at both sides of the antennas. At the center the power density was very weak. For the cases where the antennas were 180° and 125° out of phases the power density in the midline of the antennas was approximately half of the maximum power in both sides. We concluded that the power density was maximum for the three cases close to the antenna aperture and minimum in the midline of the antennas. So, the correlated signal is weak.

The crossed antenna pair system shows the combination of the exponential fall-off of the fields expected for each antenna combined with the interference pattern from the summation of the two antenna fields. This pattern can be varied as expected by varying the relative phase of the signals of the two antennas. This has been presented in Chapters V and VI using the de-ionised water and a 50% sucrose

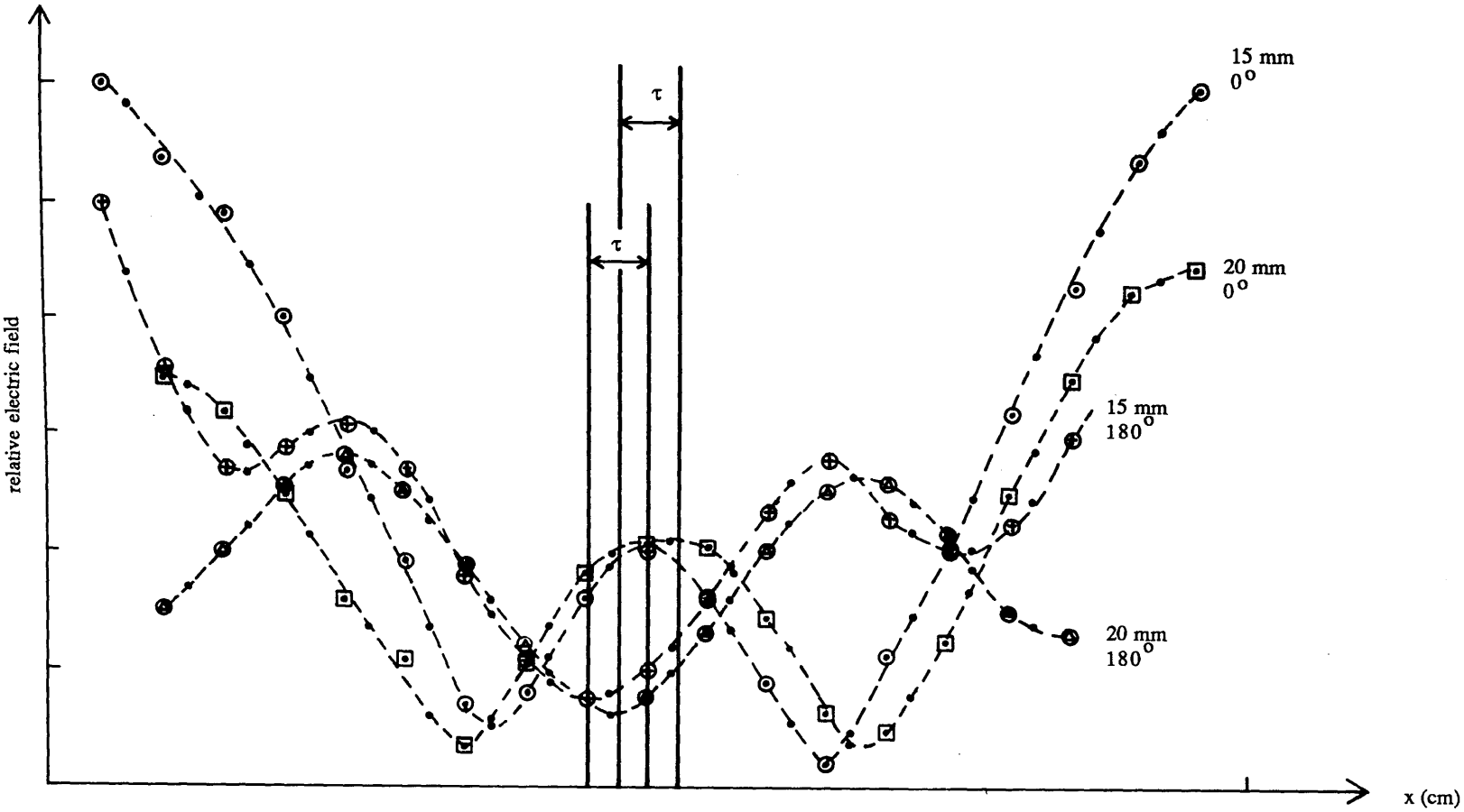

Fig. VIII.22- Comparison of the power density with the lateral position at 15 mm and 20 mm depths.

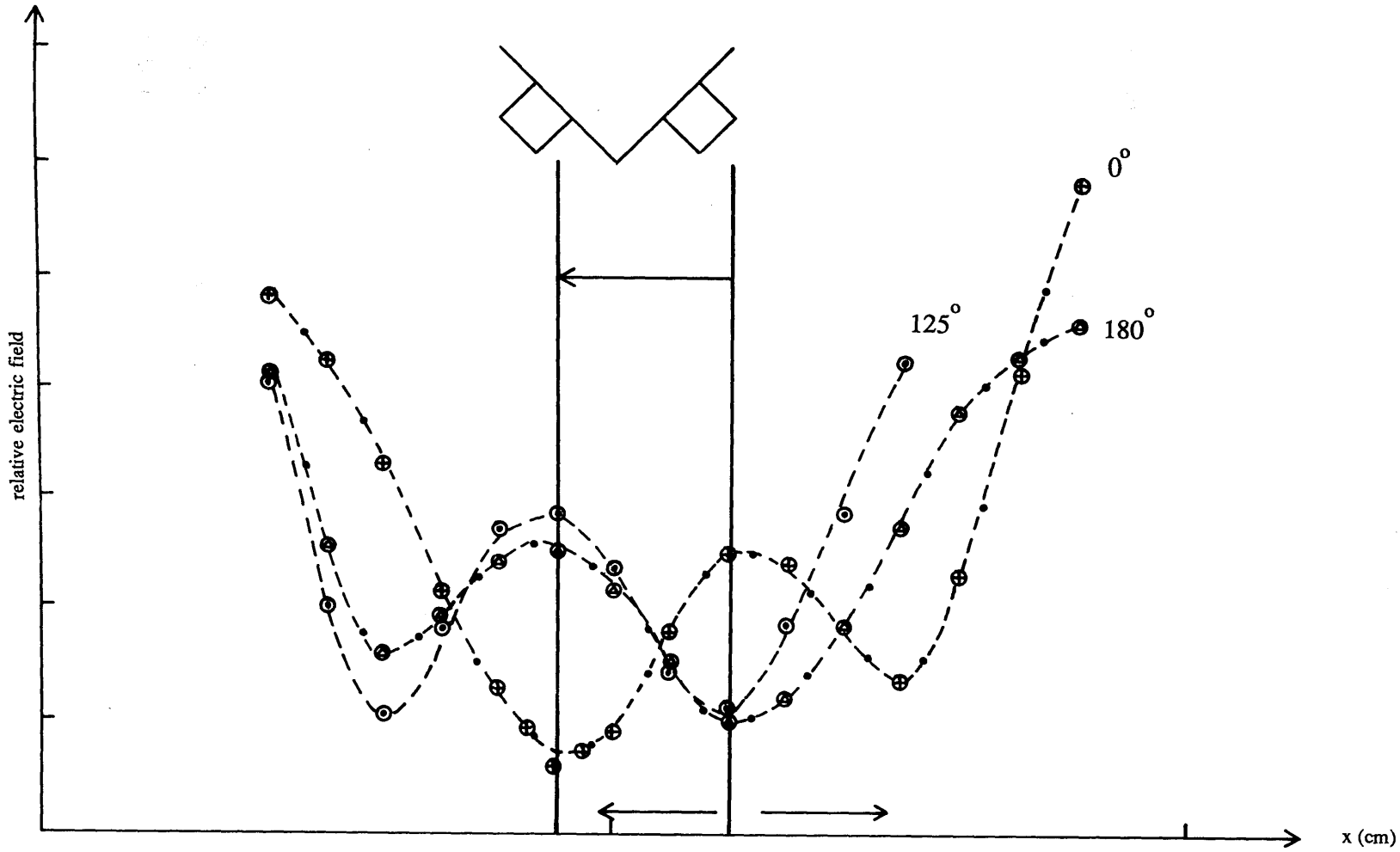

Fig. VIII.23- The variation of the power density with the lateral position for phases of 0° ,125° and 180° at depth of 30 mm.

solution as dielectric phantom materials. Two cases have been considered in phase and 180^{o} out of phase. It has seen that the interference pattern from the summation of the two signals is small comparing to the signal from each antenna and the pattern varied with the phase change.

Mamouni et al., (1983) studied the relationship between the relative electric field and the penetration depth for single microwave thermography antenna and for two microwave correlation thermography antennas. The microwave correlated signal was more visible when was located at a depth of about one or two centimeters than when was near the surface and the classical microwave signal was proportional to the penetration depth and decreased as the depth decreased. They found that the microwave correlated signal was weaker than that measured by single antenna (Fig. VIII.24).

VIII.5- Conclusion:

In the present work the *nonresonant perturbation* reflection coefficient in lossy dielectric phantom materials has been measured to find the effective penetration depth and the near-field configuration of the electromagnetic fields of a dielectric loaded TE_{11}-mode cylindrical waveguide antenna of the type used for clinical microwave thermography. It was found that the effective penetration depth depends not only on the properties of the dielectric phantom material and on the dielectric properties of the sheet perturber, but also on the parameters of the antenna and that it was usually smaller than that calculated for a plane-wave in the same dielectric material. It has been proved that a TE_{11}-mode cylindrical waveguide antenna gives more encouraging results than using a TE_{01}-mode rectangular waveguide antenna.

The *nonresonant perturbation* technique has given more encouraging results of form expected. The antenna studied produces fields in which the *TEM* wave is the most important component because the penetration distances measured

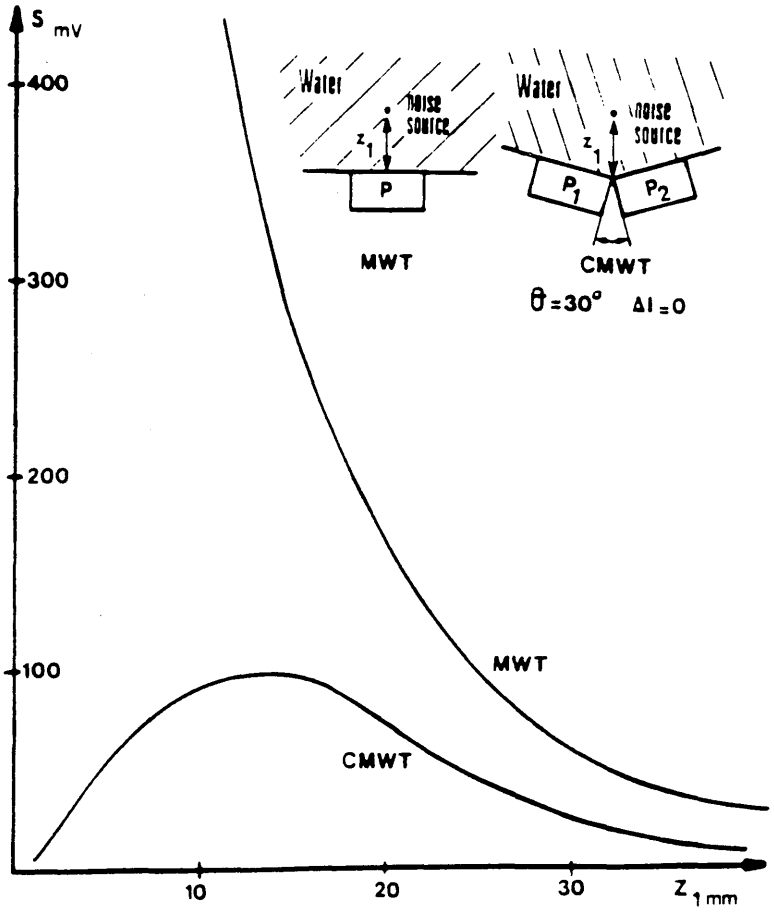

Fig. VIII.24- The Comparison of the output noise source signal S in water of the data obtained by MWT (single antenna) and CMWT (correlated antennas).

[from Mamouni et al., 1983]

and *TEM* distances are similar, as well as the antenna aperture reflection coefficient are similar. The effective penetration depths in simulated muscle tissue or in high-water content tissues are very close to the plane-wave for certain phantom materials. The plane-wave in a lossy dielectric material is usually greater than that obtained by experimental analysis. The effective penetration depth for less lossy medium such as chloroform which is approximately identical to a fat tissue is compared with the plane-wave. It shows a difference that is very significant. This technique provides a large plane-wave far-field zone with minimal near-field zone to give maximum signal contribution with depth in the investigated material.

The near-filed configuration of the electromagnetic fields of a single TE_{11}-mode cylindrical waveguide antenna in contact with a lossy dielectric material has been described. It shows that the configuration of the electric field for a high-water content tissues are, as expected, close to the microwave antenna configuration (Fig. VIII.1). The measurements can be taken up to several wavelengths from the antenna aperture.

A crossed-pair of microwave antennas (microwave antenna correlation) have been used when applying to the *nonresonant perturbation* technique to investigate the relationship of the power density (E^2) with the lateral position of a rod dielectric perturber (parallel to the midpoint antenna apertures) and the power density (E^2) with the penetration depth for different phase differences between the antennas. The results obtained show that the power density was maximum near the antenna apertures and in the midline the correlated power density was very weak and approximately one third of the maximum power. Studies are being carried out in order to improve the investigation of the relative electric field (E^2) with the penetration depth.

The *nonresonant perturbation* technique described for measuring the near-field configuration of the electromagnetic fields in simulated biological tissue provides a useful, inexpensive, simple and practical way of examining the performance of microwave thermographic antennas or applicators, particularly in

development stages and improving the investigation of the medical techniques especially for hyperthermia induction and microwave thermographic temperature measurements.

This technique gives information in order to choose the characteristics of the best suited antennas for microwave thermographic temperature measurements and microwave hyperthermia induction.

Chapter IX

Conclusions

The microwave thermography technique is a relatively simple method which can be used to obtain information about subcutaneous tissue temperature patterns by measurement of the thermal radiation emitted by the body tissues at the lower microwave frequencies. The microwave temperature measured is a weighted average over the tissue temperature of the viewed volume which is influenced by several factors which include the operating frequency, the dielectric properties and the structure of the body tissues, the characteristics of the radiometer antenna and the temperature distribution in the tissue. In clinical applications it is the tissue temperature distribution which is the quantity of interest since abnormal distribution indicates sites of disease.

Microwave radiometry sensitivity is improving but there are limitations to how the system performance can be improved. The sensitivity depends on the sum of the system and source noise temperatures. The source noise temperature is fixed so that decreasing the system noise temperature becomes progressively less beneficial. The sensitivity also depends on the square root of the pre-detection bandwidth and the system response time. An improvement in the sensitivity may be achieved by increasing the pre-detection bandwidth. This is limited in a practical sense by the frequency over which the antenna may be matched to body tissue. As sensitivity is improved gain stability may limit the actual temperature resolution of the system. A simple TE_{11}-mode cylindrical waveguide microwave thermography antenna used for medical radiometry applications is capable of detecting the existence of thermal structure of viewed volume.

Microwave correlation radiometry comprises a radiometer operating at a

frequency of 3.2 GHz and a crossed-pair of antenna arrangement to view a common region at depth. The received pattern formed by the product of the individual antenna patterns gives a maximum depth in phantom dielectric material. The depth can be adjusted by changing the spacing of the antennas and the phase in an antenna path. However, the pattern is modulated by a set of positive and negative interference fringes so that the complete receive pattern has a complicated form. On uniform temperature distributions the total reading is zero with the positive and negative contributions cancelling each other out. The fringe modulation can be removed by placing the antennas closer enough together. The pattern after this modulation is simple and gives a maximum response at a known depth. The radiometer system is sensitive to temperature gradients only. Microwave correlation radiometry is not widely used in clinical application because of the complicated form of the received pattern. Only if the temperature distribution is uniform in the tissue and is known to be very simple it will be possible to interpret the output reading. In practice the temperature distribution inside the medium or in a biological tissue is unknown and in most cases is very difficult to decipher. Another factor affects the interpretation of the output reading and makes it impossible, or at the best ambiguous. This is a wide range of dielectric properties and tissue structures in the region being investigated.

For crossed-pair radiometer antennas in phase the effective penetration depth in high- and medium-water content tissues is about 2.5 cm at a frequency of 3.2 GHz. This result is similar to Newton's work, where he considered similar TE_{11}-mode cylindrical waveguide antennas angled 48^{o} to each other and separated by 4.4 cm.

This study was undertaken to improve the use of microwave radiometry as a method of non-invasive thermometry for monitoring hyperthermia induction and microwave temperature measurement. Using a single radiometer with crossed-pair antenna arrangement proved promising to give sufficient penetration depth for detecting subcutaneous body temperature. This method is encouraging for further

investigation towards improving the detection, diagnosis and scanning of breast and limb joints disease.

The *nonresonant perturbation* measurement technique is used to obtain the effective penetration depths and the near-field configurations of the electromagnetic fields of a simple TE_{11}-mode cylindrical waveguide antenna in contact with phantom dielectric lossy materials and to investigate improvement biomedical applications. A TE_{11}-mode cylindrical waveguide antenna 2.5 cm in diameter and 5.2 cm in length loaded with low-loss dielectric $\varepsilon'_r = 12$ has been used. The guide wavelength of the antenna is 2.7 cm at a frequency of 3.35 GHz and the cut-off frequency is 2.03 GHz. It was found that the effective penetration depth depends on the parameters of the antenna and that it was always smaller than that calculated for a plane-wave in the same dielectric material. It has been shown that a TE_{11}-mode cylindrical waveguide antenna gives effective penetration depth values closer to *TEM* wave penetration distances than does a TE_{01}-mode rectangular waveguide antenna in simulated tissue dielectrics. For high-water content tissue the ratio of the effective penetration depths to the *TEM* wave penetration distances is approximately 90% and for low-water content tissue is approximately 70%. This ratio is inversely proportional to the ratio of the relative wavelength in the dielectric material to the guide wavelength. This shows that when the ratio is close to 1 the relative wavelength in the dielectric material is approximately one half of the guide wavelength which is the case of the high-water content tissue. However, for the low-water content tissue the relative wavelength in the dielectric material is approximately 1.3 times of the guide wavelength.

The configuration of the electromagnetic fields of a single TE_{11}-mode cylindrical waveguide antenna in contact with a lossy dielectric material has been measured. It shows that the configuration of the electric fields for a high and low-water content tissues is, as expected, close to the microwave field within the antenna (Fig. VII.10). For low-water content tissue the electromagnetic field configuration is usually very difficult to detect because the relative permittivity of

the dielectric lossy material is almost the relative permittivity of the dielectric perturber. Two similar TE_{11}-mode cylindrical waveguide antennas were used to compare the power density (E^2) and the behaviour of the electromagnetic field in the dielectric lossy material and also to investigate how useful the *nonresonant perturbation* technique is. It was found that one of the antennas symmetry of the signalon both sides of the antenna aperture. It can be conclude that the *nonresonant perturbation* technique is very good technique to use and it shows the significant performance of the applicators or antennas used.

The field of a crossed-pair antenna of the TE_{11}-mode cylindrical antennas, coupled as for an "*add and square*" configuration radiometer, was measured using the *nonresonant perturbation* technique. The field pattern observed was of the form expected from the measurements of the individual antenna behaviour with the appropriate interference pattern superimposed. The interference pattern showed the expected variation with the relative phase of the two antennas. The measured field showed the modest maximum between the antennas in the viewed common dielectric region which was observed in the radiometric test measurements. The measurements showed, however, that interpretation of a non-uniform temperature region would be difficult because of the interference pattern, though as suggested by Leroy it may be possible to measure a temperature gradient. Our results show similarities to Leroy's Group work, shows that the field pattern is the combination of individual field patterns and the interference pattern.

The *nonresonant perturbation* technique used for measuring the near-field configuration of the electromagnetic fields in simulated biological tissue provides a useful, inexpensive, simple and practical way of examining the performance of microwave thermographic antennas or hyperthermia applicators, particularly in the development stage and improving the investigation of the microwave thermographic temperature measurements made in medical applications. This technique gives information which can help choose the characteristics of the best suited antennas for

microwave thermographic temperature measurements and microwave hyperthermia induction.

Appendix A

Radiometer sensitivity

A .1- The total power radiometer:

The purpose of noise radiometer is to deduce changes in the system input noise temperature from changes in the system detected *dc* output. This change is limited by *ac* noise which is also in the output. The sensitivity of the radiometer has been discussed in Chapter II where the equivalent temperature of this system was given by:

$$\Delta T = \left(T_s + T_{sys} \right) \sqrt{\frac{2 B_L}{B}} \qquad (A.1)$$

The derivation of ΔT is based on the analysis of the output signal of a square law detector the input signal of which is bandwidth limited noise (Evans, 1977).

A square law detector is the special case of the multiplier or correlator.If the signal into the square law detector is $x(t)$ then the detector gives an output reading $R(t)$:

$$R(t) = x(t) \times x(t) \qquad (A.2)$$

The signal $x(t)$ is a noise waveform, it can be characterised by quantities such as mean, rms, correlation, and power spectrum. The Fourier transform of the cross correlation function is being the spectral power distribution in the signal. The cross correlation function is given by:

$$C_x(t) = \overline{x(t) \times x(t-\tau)} \qquad \text{(A.3)}$$

The cross correlation function of the output reading $C_R(t)$ from the square law detector is given by:

$$C_R(\tau) = \overline{R(t) \times R(t-\tau)} \qquad \text{(A.4)}$$

$$= \overline{\left[x(t) \times x(t)\right] \times \left[x(t-\tau) \times x(t-\tau)\right]}$$

$$= \overline{x(t)x(t-\tau)} \times \overline{x(t)x(t-\tau)} +$$

$$\overline{x(t)x(t)} \times \overline{x(t-\tau)x(t-\tau)} +$$

$$\overline{x(t)x(t-\tau)} \times \overline{x(t)x(t-\tau)}$$

In terms of correlations of the input waveforms

$$C_R(\tau) = C_x(\tau) \times C_x(\tau) + C_x(0) \times C_x(0) + C_x(\tau) \times C_x(\tau)$$

so,

$$C_R(\tau) = 2C_x^2(\tau) + C_x^2(0) \qquad \text{(A.5)}$$

This is the spectral power distribution of the output reading from the square law detector. $C^2_x(0)$ is constant and measure the *dc* power in the output simultaneously. When a time τ is considered in measuring, the cross correlation function is $C_x(\tau)$. $C_x(0) = \overline{x(t) \times x(t)}$ which equals the total power in the input signal. Therefore, the *dc* power in the output equals the square of the total power in the input signal. So, the the output signal is proportional to the total power in the input signal.

Abdul-Razzak, M.M., Hardwick, B.A., Hey-Shipton, G.L., Matthews, P.A., Monson, J.R.T., Kester, R.C., (1987), "Microwave Thermography for Medical Applications" , *IEE Proceedings*, Vol. 134, Pt.A, No. 2, February, pp. 171-174

Andersen, J.Bach, Baun, Aage, Harmark, K., Heinzl, Leif, Raskmark, Povl, Overgaard, Jens, (1984), "A Hyperthermia System Using a New Type of Inductive Applicator" , *IEEE Transactions on Biomedical Engineering*, Vol., BME-31, No. 1, January, pp. 21-27

Anderson, J.B., (1985), "Theoretical Limitations on radiation into muscle tissue" , *International Journal of hyperthermia*, Vol. 1, No. 1, pp. 45-55

Assadourian, F., Rimai, E., (1952), "Simplified Theory of Microstrip Transmission Systems" , *Proceedings of IRE*, Vol. 40, No. 12, December, pp. 1651-1657

Audet, J., Bolomey, J.C., Pichot, C., N'Guyen, D.D., Robillard, M., Chive, M., Leroy, Y., (1980), "Electrical Characteristics of Waveguide Applicators for Medical Applications" , *Journal of Microwave Power*, Vol. 15, No. 3, July, pp. 177-186

Bahl, I.J., Garg, R., (1977), "Simple and Accurate Formulas for a Microstrip with Finite Strip Thickness" , *Proceedings of IEEE*, Vol. 65, No. 11, November, pp. 1611-1612

Bahl, I.J., Stuchly, S.S., (1980a), "New Microstrip Slot Radiator for Medical Applications" , *Electronics Letters*, Vol. 16, No. 19, September, pp. 731-732

Bahl, I.J., Stuchly, S.S., Lagendijk, J.J.W., Stuchly, M.A., (1982), " Microstrip Loop Radiators for Medical Applications" , *IEEE Transactions on Microwave Theory and Techniques*, Vol. MTT-30, No. 7, July, pp.1090-1093

Bahl, I.J., Stuchly, S.S., Stuchly, M.A., (1980b), "A New Microstrip Radiator for Medical Applications" , *IEEE Transactions on Microwave Theory and Techniques*, Vol. MTT-28, No. 12, December, pp. 1464-1468

Bahl, I.J., Thansandote, A., Stuchly, S.S., (1980c), "Open-Ended Rectangular Waveguides as Antennas for Medical Diagnostics" , *Journal of Microwave Power*, Vol. 15, No. 2, pp.81-86

Barber, P.W., Gandhi, OM P., Hagmann, M.J., Chatterjee, I., (1979), "Electromagnetic Absorption in a Multilayered Model of Man" , *IEEE Transactions on Biomedical Engineering*, Vol. BME-26, No. 7, July, pp. 400-405

Barber, P.w., (1977), "Electromagnetic power Deposition in Prolate Spheroid Models of Man and Animals at Resonance" , *IEEE Transactions on Biomedical Engineering,* Vol. BME-24, No.6, November, pp. 513-521

Bardati, F., Bertero, M., Mongiardo, M., solimini, D., (1987b), "Singular System Analysis of the Inversion of Microwave Radiometric Data: Applications to Biological Temperature Retrieval" , *Inverse Problems*, Vol. 3, pp. 347-370

Bardati, F., Brown, V., Bernado, Di G., (1989), "Multi-frequency Microwave Radiometry for Retrieval of Temperature Distributions in the Human Neck" , *Advances in Medical Microwave Imaging Meeting*, Lille, France

Bardati, F., Calamai, G., Mongiardo, M., Paolone, B., (1987a), "Multispectral Microwave Radiometric System: For Biological Temperature Retrieval: Experimental Tests" , *The 17th European Microwave Conference Rome Italy,* September, pp. 386-391

Bardati, F., Mongiardo, M., Solimini, D., (1985), "Retrieval of Hyperthermia induced Temperature Distribution from Noisy Microwave Radiometry Data" , *Electronics Letters*, Vol. 21, No. 18, August, pp. 800-801

Barid, R.C., Newell, A.C., Stubenrauch, C.F., (1988), "A Brief history of Near-Field Measurements of Antennas at the National bureau of Standards" , *IEEE Transactions on Antennas and Propagation*, Vol. AP-36, No. 6, June, pp. 727-733

Barrett, A.H., Myers, P.C., Sadowsky, N.L., (1980), "Microwave Thermograhy in the Detection of Breast Cancer" , *American journal Roentology*, Vol. 134, pp. 365-368

Barrett, A.H., Myres, P.C., (1986), "Basic Principles and Applications of Microwave Thermography" , *Microwave Thermography*, pp. 41-46

Bellarbi, L., Mamouni, A., Van De Velde, J.C., Leroy, Y., (1984a), "Accurate Localization of Thermal Gradients in Lossy Matrials by Correlation Microwave Thermography" , *Electronics Letters,* Vol. 20, No. 10, May, pp. 430-431

Bellarbi, L., Mamouni, A., Van De Velde, J.C., Leroy, Y., (1984b), "On Possibilities of Thermal Pattern Recognition by Correlation Microwave Thermography" , *The 14th European Microwave Conference*, pp. 645-650

Bocquet, B., Leroy, Y., Mamouni, A., Van De Velde, J. C., Delannoy J., Delvalee D., Giaux G., (1988), "Microwave Imaging Process by Multi-probe Radiometry: Present state of Exploration of the Breast", *IEE Colloquium - Medical Applications of Microwaves* -, Digest No. 1988/60, April

Bocquet, B., Mamouni, A., Hochedez, M., Van De Velde, J. C., Leroy, Y., (1986), "Visibility of Local Thermal Structures and Temperature Retrieval by Microwave Radiometry" , *Electronics Letters*, Vol. 22, No. 3, January, pp.120-121

Bolomey, J.C., Solaiman, M., (1982), "Microwave Diffraction Tomography for Biomedical Applications" , *IEEE Transactions on Microwave Theory and Techniques*, Vol. MTT-30, No. 11, pp.1998-2000

Bolton, H. C., (1900), "Evaluation of Thermometer. 1592-1743" , *Easton, PA.: The Chemical Publishing Co.*

Brown, V.J., (1989), "Development of Computer Modelling Techniques for Microwave Thermography" , *Ph.D. thesis*, University of Glasgow

Bryant, T.G., Wiess, J.A., (1968), "Parameters of Microstrip Transmission Lines and of Coupled Pairs of Microstrip Lines" , *IEEE Transactions on Microwave Theory and Techniques*, Vol. MTT-16, No. 12, pp. 1021-1027

Cabanac, M., Cunningham, D.J., Stolwijk, J.A.J., (1971), "Thermoregulatory Set Point During Exercise: a Behvioral Approach" , *Journal of Comp. Physiol. Psychol.*, vol. 76, pp.94-102

Campbell, A., "in preparation", *Ph.D. Thesis* , University of Glasgow

Cano, G., Medina, F., Horno, M., (1988), "Characteristic Impedances of Microstrip and Fin Line with Uniaxial or Biaxial Anisotropic Substrates" , *Electronics Letters*, Vol. 24, No. 19, September, pp. 1211-1212

Carr, K.L., Bielawa, R.J., Regan, J.F., El-Mehdi, A.M., Shaeffer, J., (1983), "The Effect of Antenna Match on Microwave Radiometric Thermal Patterns" , *IEEE MTT-S DIGEST*, F-5, pp. 189-191

Carr, K.L., El-Mahdi, M., Shaeffer, J., (1981), "Dual-Mode Microwave System to Enhance Early Detection of Cancer" , *IEEE Transactions on Microwave Theory and Techniques*, Vol. MTT-29, No. 3, March, pp. 256-260

Carr, Kenneth L., El-Mahdi, M., Shaeffer, J., (1982), "Passive Microwave Thermography Coupled with Microwave Heating to Enhance Early Detection of Cancer" , *Microwave Journal,* Vol. 17, pp. 125-136

Caulton, M., Hughes, J.J., Sobol, H., (1966), "Measurements on the Properties of Microstrip Transmission Lines for Microwave Integrated Circuits" , *RCA Review*, Vol. 27, September, pp. 377-391

Cetas T.C., Lehmann F., Ed., (1982), " Thermometry in Therapeutic Heat and Cold" , 3rd Edition, *Baltimore Williams and Wilkins*, pp. 35-69

Cetas, T.C., (1985), "Temperature Measurement" , *In Heat Transfer in Medicine and Biology*, Vol. 2, Shitzer, A., Eberhart, R.C., (eds.), plenum Press, pp. 373-391

Chandrasekhar S., (1939), "An Introduction to the Study of Stellar Structure" , *Dover Publications*, Inc., pp. 198-203

Chang, K., Klein, J., (1987), "Dielectrically Shielded Microstrip (DSM) Lines" , *Electronics Letters*, Vol. 23, No.10, May, pp. 535-537

Cheever, Erik, Leonard, Jonathan B., Faster, Kenneth R., (1987), "Depth of penetration of Fields from Rectangular Apertures into Lossy Media" , *IEEE Transactions on Microwave Theory and Techniques*, Vol. MTT-35, No. 9, September, PP. 865-867

Cheung, A.Y., Golding, W.M., Samaras, G.M., (1981), "Direct Contact Applicators for Microwave Hyperthermia" , *Journal of Microwave Power*, Vol. 16, No. 2, pp. 151-159

Christensen, D.A., (1983), "Thermometry and Thermography" , Storm, F.K., (Ed.), *Hyperthermia in Cancer Therapy*, Hall, Boston, pp. 223-232

Christensen, D.A., Durney, C.H., (1981), "Hyperthermia Production for Cancer Therapy: A Review of Fundamentals and Methods", *Journal of Microwave Power*, Vol. 16, No. 2, April, pp. 89-105

Cloudsley-Thompson, J.L., (1963), "The Mechanism of Heat Death" , *New Scientist*, Vol. 338, pp. 330-332

Cook, H.F., (1951a), "Dielectric Behaviour of Human Blood at Microwave Frequencies" , *Nature,* Vol. 168, pp. 247-248

Cook, H.F., (1951b), "The Dielectric Behaviour of some Types of Human Tissues at Microwave Frequencies" , *British Journal of Applied Physics*, Vol. 2, October, pp. 295-300

Cook, H.F., (1952), "A Comparison of the Dielectric Behaviour of pure Water and Human Blood at Microwave Frequencies" , *British Journal of Applied Physics*, Vol. 3, August, pp. 249-255

Coughlin, C.T., Douple, E.B., Strohbehn, J.W., Eaton, W.L., Trembly, B.S., Wong, T.Z., (1983), "Interstitial Hyperthermia in Combination with Brachytherapy" , *Radiology,* Vol. 148, July, pp. 285-288

Croswell, W.F., Rudduck, R.C., Hatcher, D.M., (1967), "The Admittance of a Rectangular Waveguide radiating into a Dielectric Slab", *IEEE Transactions on Antennas and Propagation,* Vol. AP-15, No. 5, September, pp. 627-633

Cullen, A.L., and Parr, J.C., (1955), "A New Perturbation Method for Measuring Microwave Fields in Free Space" , *IEE Proceedings,* Vol. 102, Pt. B, paper No. 1921 R, November, pp. 836-844

De Sieyes, D.C., Douple, E.B., Strohbehn, J.W., Trembly, B.S., (1981), "Some Aspects of Optimization of an Invasive Microwave Antenna for Local Hyperthermia Treatment of Cancer" , *Medical Physics,* Vol. 8, No. 2, March - April, pp. 174-183

Dicke, R.H., (1946), "The Measurement of Thermal Radiation at Microwave Frequencies" , *The Review of Scientific Instruments,* Vol. 17, No. 7, July, pp. 268-275

Draper, J.W., Boag, J.W., (1971), "The Calculation of Skin Temperature Distributions in Thermography" , *Phys . Med. Bio.,* Vol. 16, pp. 201-211

Ebert, J., (1945), "Notes on the Accurates Measurement of Small Attenuations" , *NDRC*, PIB-43, pp.414-439

Edeiken, Stanley, (1988), "Mammography and Palpable Cancer of the Breast" , *Cancer*, Vol. 61, pp.263-265

Edrich, J., (1979), "Centimeter and Millimeter Wave Thermography: A Survey of Tumour Detection" , *Journal of Microwave power*, No. 14, pp. 95-103

Edrich, J., Hardee, P.C., (1974), "Thermography and Millimeter Wavelengths" , *Proceedings of the IEEE*, Vol. 62, No. 10, October, pp. 1391-1392

Edrich, J., Hardee, P.C., (1976), "Complex Permittivity and Penetration Depth of Muscle and Fat Tissues Between 40 and 90 GHz" , *IEEE Transactions on Microwave Theory and Techniques*, Vol. MTT-24, No. 5, May, pp. 273-275

Enander, B., Larson, G., (1974), "Microwave Radiometric Measurements of the Temperature inside Body" , *Electronics Letters*, Vol. 10, No. 15, July, p.317

Enel, L., Leroy, Y., Van De Velde, J.C., Mamouni, A., (1984), "Improved Recognition of Thermal Structures by Microwave Radiometry" , *Electronics Letters*, Vol. 20, No. 7, March, pp. 293-294

England, T.S., (1950), "Dielectric Properties of the Human body for wavelengths in the 1-10 cm range" , *Nature*, Vol. 166, p.480

Evans, G., Mcleish, C.W., (1977), "RF Radiometer Handbook" , *Artech, Electronics Engineering Division of Electrical Eng. National Research Council Ottawa Ontario Canada*

Evans, Kenneth T., Gravell, I. Huw, (1973a), "Thermography" , *Mammography, Thermography and Ultrasonography in Breast Disease*, Chap. 4, pp. 103-128

Evans, Kenneth T., Gravell, I. Huw, (1973b), "Ultrsonography" , *Mammography, Thermography and Ultrasonography in Breast Disease*, Chap. 5, pp. 129-142

Fabre, J. J., and Leroy, Y., (1981), "Thermal Noise Emission of a Lossy Material for a TEM Propagation" , *Electronics Letters*, Vol. 17, No. 11, May, May, pp. 376-377

Fallone, B.G., Moran, P.R., Podgorsak, E.B., (1982), "non-invasive Thermometry with a Clinical X-ray CT Scanner" , *Med.Phys.*, Vol. 9, pp.715-721

Faris, J.J., (1967), "Sensitivity of a correlation Radiometer" , *Journal of Research of the National Bureau of Standards - C Engineering and Instrumentation*, Vol. 71C, No. 2, April - June, pp. 153-170

Foster, K.R. , Schwan, H.P., (1986), "Dielectric properties of tissue" , *In CRC Handbook of Biological Effects in Electromagnetic Fields*, Polk, C., Postwo, E., (Eds), CRC Press, Florida

Foster, K.R., Schepps, J.L., Schwan, H.P., (1980), "Microwave dielectric relaxation in Muscle: A second Look" , *Biophysics Journal*, Vol. 29, pp. 271-282

Franconi, C., Tiberio, C.A., Raganella, L., Begnozzi, L., (1986), "Low-frequency RF Twin Dipole Applicator for Intermediate Depth Hyperthermia" , *IEEE Transactions on Microwave Theory and Techniques*, Vol. MTT-34, No.5, May, pp. 612-619

Fraser, S., Land, D.V., Sturrock, R.D., (1987), "Microwave Thermography - an index of Inflammatory Joint Disease", *British Journal of Radiology*, Vol. 26, pp. 37-39

Gabor, D., (1950), "Communication Theory and Physics" , *Philosophical Magasine*, Vol. 41, pp. 1161-1187

Gajda, G., Stuchly, M.A., Stuchly, S.S., (1979), "Mapping of the Near Field Pattern in Simulated Biological Tissues" , *Electronics Letters*, Vol. 15, No. 4, February, pp. 120-121

Garg, R., Long, S.A., (1987), "Magnetised Microstrip Antenna with Pattern Control" , *Electronics Letters*, Vol. 23, No. 21, October, pp. 1149-1151

Gautherie, M., Edrich, J., Zimmer, R., Guerguin-Kern, J. L., Robert, J., (1979), "Millimeter Wave Thermography: Application to Breast Cancer" , *Journal of Microwave Power*, Vol. 14, No. 2, pp. 123-129

Gautherie, M., Ring, E.F.J., (1980), "Thermal Imaging Methods: State of Art. Infra-red microwave and Liquid Crystalls Thermography", *Acta Thermographia*, pp. 81-85

Gerner, E.W., et al., (1975), "The potential of Locatized Heating as an Adjunct to Radiation Therapy" , *Radiology*, Vol. 116, pp. 433-439

Getsinger, W.J., (1983), "Measurement and Modeling of the Apparent Characteristic Impedance of Microstrip" , *IEEE Transactions on Microwave Theory and Techniques*, Vol. MTT-31, No. 8, pp. 624-632

Ginzton, E.L., (1957), "Microwave Measurements" , *McGraw-Hill Book Company*, INC. Chap. 5, pp.235-312

Goldman, R.F., Green, E.B., Iampietro, P.F., (1965), "Tolerance of Hot, Wet Environments by Heating Men" , *Appl. Physiol.*, Vol. 20, pp. 271-277

Goldstein, S.J., (1955), "A Comparison of Two Radiometer Circuits" , *IRE Proceedings*, Vol. 43, pp. 1663-1666

Green, H.E., (1965), "The Numerical Solution of some Important Transmission Line Problems" , *IEEE Transactions on Microwave Theory and Techniques*, Vol. MTT-13, No. 5, September, pp. 676-692

Gunston, M.A.R., Weale, J.R., (1969), "Variation of Microstrip Impedance with Strip Thickness" , *Electronics Letters*, Vol. 5, No. 26, December, pp. 697-698

Gupta, K.C., Ramesh, G., Bahl, I.J., (1979), "Microstrip Lines and Slotlines" , *Artech House*, INC.

Guy, A.W., (1971a), "Analyses of Electromagnetic Fields Induced in Biological Tissues by Thermographic Studies on Equivalent Phantom Models" , *IEEE Transactions on Microwave Theory and Techniques*, Vol. MTT-19, No. 2, February, pp. 205-214

Guy, A.W., (1971b), "Electromagnetic Fields and Relative Heating Patterns due to a Rectangular Aperture Source in Direct Contact with Bilayered Biological Tissue" , *IEEE Transactions on Microwave Theory and Techniques,* Vol. MTT-19, No. 2, February, pp. 214-223

Guy, A.W., Lehmann, J.F., (1966), "On the Determination of an Optimum Microwave Diathermy Frequency for a Direct Contact Applicator" , *IEEE Transactions on Biomedical Engineering*, Vol. BME-13, No. 2, April, pp. 76-87

Guy, A.W., Lehmann, J.F., Stonebridge, J.B., Sorensen, C.C., (1978), "Development of a 915 MHz Direct-Contact Applicator for Therapeutic Heating of Tissues" , *IEEE Transactions on Microwave Theory and Techniques,* Vol. MTT-26, No. 8, August, pp. 550-556

Haimovici, N., (1982), "Three Years Experience in Direct Intra-articular Temperature Measurement" , *In Biomedical Thermology,* Gautherie, M., Albert, E., (eds.), Alan R Liss, Inc.

Hand, J.W., (1987a), "Heat Delivery and Thermometry in Clinical Hyperthermia" , *Recent Results in Cancer Research, Hyperthermia and Therapy of Malignant Tumors,* Ed. Streffer, C., Vol. 104, pp. 1-23

Hand, J.W., (1987b), "Hyperthermia. Challenging Applications of Physics in Cancer Therapy" , *Phys. Bull.*, Vol. 38, pp.111-113

Hand, J.W., Hind, A.J., (1986a), "A Review of Microwave and RF Applicators for Localized Hyperthermia" , *in Physical Techniques in Clinical Hyperthermia*, Hand, J.W., James, J.R., Eds., New York: Wiley, pp. 98-147

Hand, J.W., Johnson, R.H., (1986b), "Field Penetration from Electromagnetic Applicators for Localized Hyperthermia" , Bruggmoser, G., Hinkelbein, W., Engelhardt, R., Wannemacher, M., (Eds), *Locoregional High-frequency Hyperthermia and Temperature Measurement*, Springer, Berlin Heidelberg New York Tokyo, pp. 7-17

Harries, J.H.O., (1937), "Cavity Resonators and Electron Beams" , *Wireless Engineer*, May, p. 135

Haslam, N.C., Gillespie, A.R., Haslam, C.G.T., (1984), "Aperture Synthesis Thermography - A New Approach to Passive microwave temperature Measurements in the Body" , *IEEE Transactions in Microwave Theory and Techniques*, Vol. MTT-32, No. 8, pp.829-835

Henderson, A., James, J.R., (1988), "Magnetised microstrip Antenna with Pattern Control" , *Electronics Letters*, Vol. 24, No. 1, January, pp. 45-47

Herrick, J.F., Jelatis, D.G., Lee, M., (1950), "Dielectric Properties of Tissues Important in Microwave Diathermy" , *Fed. Proc.*, Vol. 9, p.60

Hill, Joseph C., Goldner, Ronald B., (1984), "A Stabilized Broad-band Correlator for Medical Microwave Thermography" , *Microwave Symposium IEEE MTT-S Digest*, pp. 368-370

Hill, Joseph C., Goldner, Ronald B., (1985), "The Thermal and Spatial Resolution of a Broad-band Correlation Radiometer with Application to Microwave thermography" , *IEEE Transactions on Microwave Theory and Techniques*, Vol. MTT-33, No. 8, August, pp. 718-722

Ho, H.S., Guy, A.W., Sigelmann, R.A., Lehmann, J.F., (1971), "Microwave Heating of simulated Human Limbs by Aperture Sources" , *IEEE Transactions on Microwave Theory and Techniques,* Vol. MTT-19, 224-231

Horton, R., Easter, B., Gopinath, A., (1971), "Variation of Microstrip Losses with Thickness of Strip" , *Electronics Letters*, Vol. 7, No. 17, pp.490-491

Howe, H., (1984), "Microwave Integrated Circuits An Historical Perspective" , *IEEE Tansactions on Microwave Theory and Techniques*, Vol. MTT- 32, No. 9, Spetember, pp. 991-996

Hyltin, T.M., (1965), "Microstrip Transmission on Semi-Conductor Dielectrics" , *IEEE Transactions on Microwave Theory and Techniques*, Vol. MTT-13, No. 6, November, pp. 777-781

Iskander, M.F., Durney, C.H., (1983), "Microwave Method for Measuring Changes in Lung Water" , *Journal of Mcrowave Power*, Vol. 18, pp. 265-275

Jaynes, E.T., (1965), "Application of Reciprocity Theroem to Design of Coupling System" , *Theory of Microwave Circuits, Physics Dept. Stanford University, Calif.,* Chapter 10 , Sec. 10.3, P.10

John, S., Arlftt, P., (1974), "Simple Method for the Calculation of the Characteristic Impedance of Microstrip" , *Electronics Letters*, Vol. 10, No. 10, pp. 188-190

Johnk, C.T.A., (1975), "Engineering Electromagnetic Fields and Waves" , *Wiley*, New York, Chapter 8

Johnson, C.C., Guy, A.W., (1972), "Nonionizing Electromagnetic Wave Effects in Biological Materials and Systems", *Proceedings of IEEE*, Vol. 60, No. 6, June, pp. 692-718

Johnson, R.H., (1986), " New Type of Compact Electromagnetic Applicator for Hyperthermia in the Treatment of Cancer" , *Electronics Letters*, Vol. 22, No.11. May, pp.591-593

Johnson, R.H., James, J.R., Hand, J.W., Dickinson, R.J, (1985), "Compact 27 MHz Applicators" , *Strahlentherapie*, Vol. 161, pp. 537-538

Johnson, R.H., James, J.R., Hand, J.W., Hopewell, J.W., Dunlop, P.R.C., Dickinson, R.J, (1984), "New Low Profile Applicators for Local Heating of tissue" , *IEEE Transactions on Biomedical Engineering*, Vol. BME-31, pp. 28-37

Johnson, S.A., et al., (1977), "Non-intrusive Measurement of Microwave and Ultra-sound Induced Hyperthermia by Acoustic Temperature Tomography" , *Utrsonics Symposium Proceedings, IEEE Catalogue*, No.77 Ch. 1264- 1SU, pp.977-982

Jones, C., (1987), "Medical Thermography" , *IEE Proceedings*, Vol. 134, pp.225-236

Kantor, G., (1981), "Evaluation and Survey of Microwave and Radiofrequency Applicators" , *Journal of Microwave Power,* Vol. 16, No. 2, pp. 135-150

Kantor, G., Witters, D.M., (1983), "The Performance of a New 915 MHz Direct Contact Applicator with Reduced Leakage" , *Journal of Microwave Power*, Vol. 18, pp. 133-142

Kaupp, H.R., (1967), "Characteristics of Microstrip Transmission Lines" , *IEEE Transactions on Electronic Computer*, Vol. EC-16, No.2, April, pp. 185-193

Kelly, E.J., Lyons, D.H., Root, W.L., (1958), "The Theory of the Radiometer" , *MIT Lincoln Lab. Group 312* Group Report 47.16

King, R.W.P., Trembly, B.S., Strohbehn, J.W., (1983), "The Electromagnetic Field of an Insulated Antenna in a Conducting or Dielectric Medium" , *IEEE Transactions on Microwave Theory and Techniques,* Vol. MTT-31, No. 7, July, pp. 574-583

Kino, G., (1955), "Normal Mode Theory in Perturbed Transmission Systems" , *Electronics Research Lab.*, Stanford University, Stanford, California, Rept. 84

Knight, J., (1962), "A General Expression for the output of a Dicke-type Radiometer " , *IRE Proceedings*, Vol. 50, No. 2, December, pp. 2497-2498

Ko, H.C., (1967), "Coherence Theory of Radio-Astronomical Measurements" , *IEEE Transactions on Antennas and Propagation*, Vol. AP-15, No. 1, January, pp. 10-20

Kraus, J.D., (1966), "Radio Astronomy" , *McGraw-Hill book Company*, New York

Kraus, J.D., (1984), "Electromagnetics" , 3rd Edition, *McGraw-Hill Int. Book Company*, Chap. 10, pp.395-402

Krowne, C.M., (1988), "Microstrip Conductor Losses Calculated by Full Wave and perturbational Approaches" , *Electronics Letters*, Vol. 24, No. 9, April, pp. 552-553

Kumar, A., Kumar, D., Gupta, H.C., Tripath, K.N., Mathur, P.C., (1976), "A Method for the Calculation of the Characteristic Impedance of Microstrip" , *Electronics*, Vol. 40, No. 1, pp.45-47

Lagerstrom, R.P., (1957), "Interaction Impedance measurements by Perturbation of Traveling Waves" , *Electronics Research Lab.*, Stanford University, Stanford, California, Rept. 7

Land, D.V., (1983a), "Radiometer Input Circuit Requirements for Microwave Thermography" , *Electronics Letters*, Vol. 19, No. 24, November, pp. 1040-1042

Land, D.V., (1983b), "Radiometer Receivers for Microwave Thermography " , *Microwave Journal*, Vol. 26, No. 5, May, pp. 196-201

Land, D.V., (1984), "Measurement of Radio-Frequency and Microwave Fields by Non-resonant Perturbation" ,*IEE Proceedings*, Vol. 131, Pt. H, No. 1, Februry, pp. 1-8

Land, D.V., (1987a), "A Clinical Microwave Thermography System" , *IEE Proceedings*, Vol. 134A, pp. 193-200

Land, D.V., (1987b), "Improved Method for Resonant Frequency Perturbation Measurements" , *Electronics Letters,* Vol. 23, No. 21, October, pp. 1166-1167

Land, D.V., (1988), "Application of the Nonresonant Perturbation Technique to the Measurement of High-Frequency Fields in Biological Phantom Materials" , *Electronics Letters*, Vol. 24, No.1, January, pp. 70-71

Land, D.V., Fraser, S., Shaw, R., (1986), "A Review of the Clinical Experience of Microwave Thermography" , *Journal of Medical Engineering and Techniques*, (Supp: Recent Developments in Medical and Physiological Imaging), pp. 109-113

Larsen, L.E., Jacobi, J.H., Krey, A.K., (1978), "Preliminary Observations with an Electromagnetic Method for the Noninvasive Analysis of Cell Suspension Physiology and Induced Pathophysiology" , *IEEE Transactions on Microwave Theory and Techniques*, Vol. MTT-26, No. 8, pp. 581-595

Lauer, P., Leroy, Y., Van De Velde, J.C., Mamouni, A., (1987), "Thermometry of Impedances by Correlation Radiometry" , *Electronics Letters*, Vol. 23, No. 25, December, PP. 1348-1350.

Lawson, R., (1956), "Implications of SurfaceTemperasture Measurements in the Diagnosis of Breast Cancer" , Canad.Med.Association Journal, Vol. 75, pp.309-310

Lehmann, J.F., Guy, A.W., Stonebridge, J.B., De Lateur, B.J., (1978), "Evaluation of a Therapeutic Direct Contact 915 MHz Microwave Application for Effective Deep Tissue Heating in Human" , *IEEE Transactions on Microwave Theory and Techniques*, Vol. MTT-26, No. 8, pp. 556-563

Leroy, Y., (1982), "Microwave Radiometry and Thermography: Present and Prospective" , *Biomedical Thermology*, pp. 485-499

Leung, T., Balanis, C.A., (1988), "Attenuation Distortion of Transient Signals in microstrip" , *IEEE Transactions on Microwave Theory and Techniques*, Vol. MTT-28, No. 4, pp.765-769

Lin, J.C., Kantor, G., Ghods, A., (1982), "A Class of New Microwave Therapeutic Applicators" , *Radio Science*, Vol.17s, pp. 119-123

Lindholm, C.E., Kjellén, E., Landberg, T., Nilsson, P., Hertzman, S., Persson, B., (1984), "Microwave Induced Hyperthermia and Radiotherapy. Clinical Results", *Overgaard Journal (ed) Hyperthermia Oncology*, Vol. 1, Ed. Taylor and Francis, London, pp. 341-344

Lipkin, M., Hardy, J.D., (1954), "Measurement of Some Thermal Properties of Human Tissues" , *Journal of App. Physiol.*, pp. 212-217

Lloyd Williams, K., Lloyd Williams, F.J., Handley, R.S., (1961), "Infra-red Thermometry in the Diagnosis of Breast Disease" , *The Lancet*, 2, pp. 1378-1381

Lorrain P., Corson D., (1970), "Electromagnetic Fields and Waves" , *W.H. Freeman & Co.*, San Francisco, pp. 471-472

Lüdeke, K.M., Köhler, J., (1983), "Microwave Radiometric System for Biomedical 'True Temperature' and Emissivity Measurements" , *Journal of Microwave Power* , Vol. 18, No. 6, march, pp. 276-283

Lüdeke, K.M., Köhler, J., Kanzenbach, J., (1979), "A New Radiation Balance Microwave Thermograph for Simultaneous and Independent Temperature and Emissivity Measurements" , *Journal of Microwave Power* , Vol. 14, No. 2, pp. 117-121

Lüdeke, K.M., Schiek, B., Köhler, J., (1978), "Radiation Balance Microwave Thermography for Industrial and Medical applications" , *Electronics Letters*, Vol. 14, No. 6, march, pp. 194-196

Lyons, B.E., Britt, R.H., Strohbehn, J.W., (1984), "Localized Hyperthermia in the Treatment of Malignant Brain Tumors Using an Interstitial Microwave Antenna Array" , *IEEE Transactions on Biomedical Engineering*, Vol. BME-31, No. 1, January, pp. 53-62

Maier, L.C., Slater, J.C., (1952), "Field Strength Measurements in Resonant Cavities" , *Journal of Applied Physics*, Vol. 23, p.68

Mallory, A., (1961), "A Perturbation Technique for Impedance Measurements" , *Microwave Measurement Technique Conference*, London, England

Mamouni, A., (1988), "Radiometrie microonde en champ proche: Applications médicales (Thermographie Microonde)" , *Thése pour le titre de Docteur es-sciences physiques*. L'université des Sciences et Techniques de Lille Flandres Artois, France

Mamouni, A., Bliot, F., Leroy, Y., Moschetto, Y., (1977), "A Modified Radiometer for Temperature and Microwave Properties Measurements of Biological Substances" , *The 7th European Microwave Conference, Copenhagne*, September, pp. 703-707

Mamouni, A., Dehour, P., Bocquet, J.C., Van De Velde, J.C., Leroy, Y., (1989), "Computational of Three Dimentional radiometric Signals Detected in microwave Imaging" , *Advances in Medical Microwave Imaging, Lille, France*

Mamouni, A., Leroy, Y., Houdas, Y., Moschetto, Y., (1978), "Passive Subcutaneous Temperature Measurement for Investigation of Thermoregulation" , *The 8th European Microwave Conference, Paris France*, September, pp. 543-547

Mamouni, A., Leroy, Y., Van De Velde, J.C., and Bellarbi, L., (1983), "Introduction to Correlation Microwave Thermography" , *Journal of Microwave Power*, Vol. 18, No. 3, April, pp. 285-293

Mamouni, A., Van De Velde, J.C., Leroy, Y., (1981), "New Correlation Radiometer for Microwave Thermography" , *Electronics Letters*, Vol. 17, No. 16, August, pp. 554-555

Massoudi, H., Durney, C.H., Johnson, C.C., (1977), "Long- Wavelength Electromagnetic Power Absorption in Ellipsoidal Models of Man and Animals" , *IEEE Transactions on Microwave Theory and Techniques*, Vol. MTT-25, No.1, January, pp. 47-52

McClintock, W.J., (1981), "Microwave Antenna Measurements Using Noise Correlation Techniques and Radio Stars" , The Marconi Review, Fourth quarter, pp. 244-269

Mendecki, J., Friedenthal, E., Botstein, C., Sterzer, F., Paglione, R., (1979), "Therapeutic Potential of Conformal Applicators for Induction Hyperthermia" , *Journal of Microwave Power*, Vol. 14, pp. 139-144

Meredith, R., Warner, F.L., (1963), "Superheterodyne Radiometers for Use at 70 GHz and 140 GHz" , *IEEE Transactions on Microwave Theory and Techniques*, Vol. MTT-11, No. 5, pp. 397-411

Meredith, R., Warner, F.L., Davis, Q.V., Clarke, J.L., (1964), "Superheterodyne Radiometers for Short-millimetre Wavelengths" , *IEE Proceedings*, Vol. 111, No.2, February, pp.241-256

Merie, Hylton B., (1979), "Demonstration of Focal Liver Disease by Ultrasound and Computed Tomogrphy" , *Diagnostic Ultrasound in Gastrointestinal Disease* , Ed. Kenneth, J.W. Taylor, Churchill Livingstone, pp. 35-58

Miller, C.K.S., Daywitt, W.C., Arthur, M.G., (1967), "Noise standards Measurements and Receiver Noise Definitions" , *Proceedings of IEEE*, Vol. 55, No. 6, pp. 865-877

Mirshekar-Syahkal, D., (1983), "An Accurate Determination of Dielectric Loss Effect in Monolithic Microwave Integrated Circuits Including Microstrip and Coupled Microstrip Lines" , *IEEE Transactions on Microwave Theory and Techniques*, Vol. MTT-31, No. 11, November, pp. 948-954

Mitchell, D., Wyndham, C.H., Hodgson, T., Nabaro, F.R.N., (1967), "Measurement of the Total Emissivity of Skin without the Need for Measuring Skin Temperature" , *Phys.Med.Biol.*, Vol. 12, pp.359-366

Miyakawa, M., (1981), "Study of Microwave Thermography Application to the Estimation of Subcutaneous Temperature Profiles" , *Transactions on IECE*, Japan, Vol. E-64, pp. 786-792

Mizushina, Shizuo, Oh-Ishi, Hiroyuki, Hamamura, Yoshinori, (1984), "A Three-Band Microwave Radiometer for Noninvasive Temperature Measurement" , *Microwave Symposium IEEE MTT-S Digest*, San Fransisco, May-June, pp.145-147

Myers, P.C., Barrett, A.H., (1977), Microwave Thermography: Physical Principles and Diagnostic Applications" , *Presented at the Workshop on the Physical Basis of Electromagnetic Interactions with Biological Systems, University of Maryland*, June, pp. 2-23

Myers, P.C., Barrett, A.H., (1980), "Microwave Thermography of Normal and Cancerous Breast Tissue" , *Annals of the New York Academy of Sciences*, Vol. 335, March, pp. 443-455

Myers, P.C., Sadowsky, N.L., Barrett, A.H., (1979), "Microwave Thermography: Principles, Methods and Clinical Applications" , *Journal of Microwave Power*, Vol. 14, No. 2, pp. 105-115

N'Guyen, D.D., Chive, M., Leroy, Y., Constant, E., (1980a), "Combination of Local Heating and Radiometry by Microwaves" , *IEEE Transactions on Instrumentation and Measurement*, Vol. IM-29, No. 2, June, pp.143-144

N'Guyen, D.D., Mamouni, A., Leroy, Y., Constant, E., (1979), "Simultaneous Microwave Local Heating and Microwave Thermography. Possible Clinical Applications" , *Journal of Microwave Power*, Vol. 14, No. 2, pp. 135-137

N'Guyen, D.D., Robillard, M., Chivé, M., Leroy, Y., audet, J., Pichot, Ch., Bolomey, J.Ch., (1980b), "Microwave Thermography -The Modeling of Probes- An Approach Toward Thermal Pattern Recognition" , *Conference Proceedings- The 10th European Microwave Conference*, September, Warszawa, Poland

Nasoni, R.L., Bowen, T., Dewhirst, M.W., Roth, H., (1982), "In Vivo Temperature Dependence of the Speed of Sound in Mammalian Tissue and its Possible Use in Hyperthermia" , *Nat. Cancer Inst. Monog.*, Vol. 61, pp.501-504

Neelakantaswamy, P.S., Rajaratnam, A., (1982), "Open-ended Circular Waveguide with a Curved Corrugated Disk at its Aperture as a Diathermy Applicator" , *IEEE Transactions on Microwave Theory and Techniques*, Vol. MTT-30, pp. 2005-2008

Newton, R.H., (1982), "Studies of the Feasibility of Non-invasive Thermometry by Microwave Radiometry" , *Ms.C. Thesis,* University of Aberdeen

Newton, R.H., (1986), "Non-invasive Thermography by Coorelation and Multi-Frequency Microwave Radiometry" , *Ph. D. Thesis*, University of Aberdeen

Nilsson, P., (1984), "physics and Techniques of Microwave Induced Hyperthermia in the Treatment of Malignant Tumours" , *Ph.D. Thesis*, University of Lund

North, D.O., (1942), "The Absolute Sensitivity of Radio Receivers" , RCA Review, Vol. 6, pp. 332-344

Page, R.M., Brodzinsky, A., Zirm, R.R., (1953), "A Microwave Correlator" , *IRE Proceedings*, Vol. 41, January, pp. 128-131

Paglione, R., Sterzer, F., (1981), " 27 Mhz Ridged Waveguide Applicators for Localized Hyperthermia Treatment of Deep-Seated Malignant Tumors" , *Microwave Journal*, Vol. 24, No. 2, February, pp. 71-80

Parker, D.L., (1984), "Applications of NMR Imaging in Hyperthermia: An Evaluation of the Potential for Localized Tissue Heating and Non-invasive Temperature Monitoring" , *IEEE Transactions on Biomedical Engineering*, Vol. BME-34, No. 1, January, pp. 161-167

Peronnet, G., Pichot, Ch., Bolomey, J.Ch., Jofre, L., Izadnegahdar, A., Szelles, C., Michel, Y., Guerquin-Kern, J.L., Gautherie, M., (1983), "A Microwave Diffraction Tomography System for Biomedical Applications" , *The 13th European Microwave ConferenceE, Nurnberg*, September, pp. 529-533

Plancot, M., (1983), "Contribution à L'étude Theorique, Experimentale et Clinique de L'hyperthermie Microonde Controlée par Radiometrie Microonde" , *Thesis Université des Sciences et Technique de Lille*, Chap. 3

Plancot, M., Prevost, B., Chive, M., Fabre, J.J., Ledee, R., Giaux, G., (1987), "A New Method for Thermal Dosimetry in Microwave Hyperthermia using Microwave Radiometry for Temperature Control" , *International Journal of Hyperthermia,* Vol. 3, No. 1, pp. 9-19

Pucel, R.A., Massé, D.J., Hartwig, C.P., (1968), "Losses in Microstrip" , *IEEE Transactions on Microwave Theory and Techniques*, Vol. MTT-16, No. 6, pp. 342-350

Rainwater, J. Hank, (1978), "Radiometers: Electronic Eyes That See Noise" , *Microwave Journal,* pp. 58-68

Ramo, S., Whinnery, J.R., (1946), "Fields and Waves in Modern Radio" , *Wiley and sons, INC.*, New York

Ramo, S., Whinnery, J.R., Van Duzer, T., (1965), "Fields and Waves in Communication Electronics" , *Wiley and sons, INC.*, New York, pp. 429-437

Rao, B.R., (1974), "Effect of Loss and Frequency Dispersion on the Performance of Microstrip Directional Couplers and Coupled Line Filters" , *IEEE Transactions on Microwave Theory and Techniques*, Vol. MTT-22, No. 7, pp. 747-750

Ring, E.F.J., (1986), "Skin Temperature Measurement" , *Bioengineering and Skin,* Vol. 2, pp. 15-30

Robert, J., Marchal, C., Drocourt, M., Escayne, J.M., Thouvenot, P., Gaulard, M.L., Tosser, A., (1982), "Ultrasound Velocimetry for Hyperthermia Control" , Gautherie, M., Albert, E., (Eds.), *Biomedical Thermology*, Liss, New York, pp. 555-560

Roberts, J.E., Cook, H.F., (1952), "Microwave in Medical and Biological Research" , *British Journal of Applied Physics*, Vol. 3, February, pp. 33-40

Robillard, M., (1981), "Contribution à l'Etude des Sondes et à la Reconnaicance d'Objet Thermique par Thermographie Micro-onde" , *Docteur de troisième cycle thèse,* Université des Sciences et Tecniques de Lille, France, pp. 27-34

Robillard, M., Chive, M., Leroy, Y., Audet, J., Pichot, Ch., Bolomey, J.Ch., (1982), "Microwave Thermography - Characteristics of Waveguide Applicators and Signatures of Thermal Structures" , *Journal of Microwave Power,* Vol. 17, No. 2, pp. 97-105

Robillard, M., N'Guyen, D.D., Chive, M., Leroy, Y., Audet, J., (1980), "Profondeur de pénétration et resolution spatiale de sondes atraumatique utilisées en miro-ondes" , *Symposium URSI - International Ondes Eletromagnétiques et Biologie*, Jouy en Josas, pp. 213-217.

Samaras, G.M., (1984), "Intracranial Microwave Hyperthermia: Heat Induction and Temperature Control" , *IEEE Transactions on Biomedical Engineering*,Vol. BME-31, No. 1, January, pp. 63-69

Sample, W.F., Sarti, D.A., (1979), "Diagnosis of Pancreatic Disease by Ultrasound and Computed Tomography" , *Diagnostic Ultrasound in Gastrointestinal Disease*, Ed. Kenneth, J.W. Taylor, Churchill Livingstone, pp. 85-101

Sandhu, T.S., Kolozvary, A.J., (1983),"Effect of Bolus Material and Tissue Inhomogeneities on the resonance frequency of MW microstrip applicators" , *Radiation Research*, Vol. 94, p. 594

Sandhu, T.S., Kolozvary, A.J., (1984),"Conformal Hyperthermia Applicators" , *Overgaard Journal (ed) Hyperthermia Oncology*, Vol. 1, Ed. Taylor and Francis, London, pp. 675-678

Sandhu, T.S., Kowal, H.S., Johnson, R.J.R., (1977), "Microwave Hyperthermia Applicators: Design and Dosimetry" , *Proceedings of the 2nd International Symposium on Cancer Therapy by Hyperthermia and Radiation*, Essen, June, pp. 118-121

Schaller, G., (1984a), "Inversion of Radiometric Data from Biological Tissue by an Optimisation Method" , *Electronics Letters*, Vol. 20, No. 9, April, pp. 380-382

Schaller, G., (1984b), "Microwave and Infra-red Thermograms of Hot Spots in Tissue" , *IEEE MTT-S Digest*, pp.148-149

Schneider, M.V., (1969a), "Microstrip lines for Microwave Integrated Circuits" , *The Bell System Technical Journal*, pp. 1421-1443

Schneider, M.V., (1969b), "Dielectric Loss in Integrated Microwave Circuits" , *The Bell System Technical Journal*, pp. 2325-2332

Schwan, H.P., Cartenson, E., Li, K., (1956), "The Biophysical Basis of Physical Medicine" , *Journal of American Medicine Association*, Vol. 160, No. 3, January, pp. 191-197

Schwan, H.P., Foster, K.R., (1977), "Microwave Dielectric Properties of tissue - Some Comments on the Rotational Mobility of Tissue Water" , *Biophysical Journal,* Vol. 17, pp. 193-197

Schwan, H.P., Foster, K.R., (1980), "RF-field Interactions with Biological Systems: Electrical Properties and Biophysics Mechanisms" , *Proceedings of the IEEE*, Vol. 68, No. 1, January, pp. 104-113

Schwan, H.P., Piersol, G.M., (1954), "The Absorption of Electromagnetic Energy in Body Tissue. Part 1 biophysical Aspects" , *American Journal of Physcis ans Medicine*, Vol. 33, December, pp. 370-404

Schwarzamann, A., (1967), "Microstrip plus Equations adds up to Fast Designs" , *Electronics*, Vol. 40, No. 20, October, pp. 109-112

Selawry, O.S., Carlson, J.C., Moore, G.E., (1958), "Tumor Response to ionizing Rays at Elevated Temperatures" , *Am. J. Roentgenol*, Vol. 80, pp. 833-839

Selove, W., (1954), "A DC Comparison Radiometer" , *The Review of Scientific Instruments*, Vol. 25, No. 2, February, pp. 120-122

Semet, C., Mamouni, A., Van De Velde, J.C., Robillard, M., Leroy, Y., (1984), "Système de Thermogrphie Microonde Multisonde à Balayage Electronique" , *Innov. Technol. Biol.*, Vol. 5, pp. 200-209

Shaeffer, J., El- Mahdi, M., Carr, K.L., (1981), "Microwave Radiometry Thermal Properties of Breast and Drainage Lymph node Areas" , *IEEE Frontiers of Engineering in Health Care*, pp. 102-104

Silvester, P., (1968), "TEM Wave Properties of Microstrip Transmission Lines" , *Proceedings of IEE*, Vol. 115, No. 1, January, pp. 43-48

Simpson, T.L., Tseng, B., (1976), "Dielectric Loss in Microstrip Lines" , *IEEE Transactions on Microwave Theory and Techniques*, Vol. MTT-24, pp. 106-108

Slater J.C., (1942), "Microwave Transmission" , *McGraw-Hill Book Company*, Inc., pp. 245-256

Smith, C.E., Chang, R.S., (1980), "Microstrip Transmission Line with Finite width dielectric" , *IEEE Transactions on Microwave Theory and Techniques*, Vol. MTT-36, No. 2, pp.90-94

Smith, C.E., Chang, Ray-Sun, (1985), "Microstrip Transmission Line with Finite Width Dielectric and Ground Plane" , *IEEE Transactions on Microwave Theory and Techniques*, Vol. MTT-33, No. 9, September, pp. 835-839

Sobol, H., (1971), "Applications of Integrated Circuits Technology to Microwave Frequencies" , *Proceedings of IEEE*, Vol. 59, No. 8, August, pp.1200-1211

Sorrows, H.E., Ryan, W.E., Ellenwood, R.C., (1951), "Evaluation of Coaxial Slotted Line Impedance Measurements", *Proceedings of IRE*, Vol. 39, No. 2, February, pp. 162-168

Standley, R.D., Cheung, N.K., (1988), "Performance Studies of some Microstrip Structures Using Superconducting Materials" , *Electronics Letters*, Vol. 24, No. 6, March, pp. 349-350

Steele C.W., (1966), " A Non-resonant Perturbation Theory " , *IEEE Transactions on Microwave Theory and Techniques*, Vol. MTT-14, No. 2, Febraury, pp. 70-74

Stinehelfer, H.E., (1968), "An Accurate Calculation of Uniform Microstrip Transmission Lines" , *IEEE Transactions on Microwave Theory and Techniques*, Vol. MTT-16, No. 7, pp. 439-444

Stogryn, A., (1971), "Equations for Calculating the Dielectric Constant of Saline Water" , *IEEE Transactions on Microwave Theory and Techniques*, Vol. MTT-19, No. 8, pp. 733-736

Strohbehn, J.W., Trembly, B.S., Douple, E.B., (1982), " Blood Flow Effects on the Temperature Distributions from an Invasive Microwave Antenna Array Used in Cancer Therapy" , *IEEE Transactions on Biomedical Engineering*, Vol. BME-29, No. 9, September, pp. 649-661

Strom, Leland D., (1957), " The Theoretical Sensitivity of the Dicke Radiometer " , *IRE Proceedings*, Vol. 45, No. 2, pp. 1291-1292

Strum, Peter D., (1958), " Considerations in High-Sensitivity Microwave Radiometry " , *IRE Proceedings*, Vol. 46, November, pp. 43-53

Stuchly, M.A., Stuchly, S.S., (1980), "Dielectric Properties of Biological Substances - Tabulated" , *Journal of Microwave Power*, Vol. 15, pp. 19-26

Stuchly, M.A., Stuchly, S.S., (1984), "Permittivity of Mammalian Tissues in Vivo and in Vitro Advances in Experimental Techniques and Recent results" , *International Journal of Electronics,* Vol. 56, No. 4, pp. 443-456

Stuckly, S.S., Stuckly, M.A., (1978), "Multimode Square Waveguide Applicators for Medical Applications of Microwave Power" , *Proceedings of the 8th European Microwave Conference: Microwave Exhibitions Publishers*, Sevenoaks, Kent, pp.553-557

Sutton, C.H., (1971), "Tumor Hyperthermia in the Treatment of Malignant Gliomas of the Brain" , *Trans. Am. Neurology Association*, Vol. 6, pp.195-199

Swenson, G.W., and Mathur, N.C., (1968), " The Interferometer in Radio-Astronomy " , *IEEE Proceedings*, Vol. 56, No. 12, December, pp. 2114-2130

Swicord, M.L., Davis, C.C., (1981), " Energy Absorption from Small Radiating Coaxial Probes in Lossy Media" , *IEEE Transactions on Microwave Theory and Techniques,* Vol. MTT-29, No. 11, November, pp. 1202-1208

Tanabe, E., McEwen, A., Norris, C.S., Fessenden, P., Samulski, T.U., (1983), "A Multi-element Microstrip Antenna for Local Hyperthermia" , *IEEE MTT-S International Microwave Symposium Digest*, New York, pp.183-185

Taylor, L.S., (1980), " Implantable Radiators for Cancer Therapy by Microwave Hyperthermia" , *Proceedings of the IEEE,* Vol. 68, No. 1, January, pp. 142-149

Taylor, L.S., (1984), "Penetrating Electromagnetic Wave Applicators" , *IEEE Transactions on Antennas and Propagation*, Vol. AP-32, No. 10, October, pp. 1138-1141

Tiuti, M.E., (1964), "Radio Astronomy Receivers" , *IEEE Transactions on Military Electronics*, July-October, pp. 264-272

Turner, P.F., Kumar, L., (1982), "Computer Solutrion for Applicator Heating Patterns" , *National Cancer Instutit Monogr*, Vol. 61, pp. 521-532

Uzunoglu, Nikolaos K., Nikita, Konstantina S., (1988), " Estimation of Temperature Distribution Inside Tissues Heated by Interstitial RF Electrode Hyperthermia Systems " , *IEEE Transactions on Biomedical Engineering*, Vol. BME-35, No. 4, April, pp.250-256

Vaguine, V.A., Christensen, D.A., Lindley, J.H., Walston, T.E., (1984), " Muliple Sensor Optical Thermometry System for Application in Clinical Hyperthermia" , *IEEE Transactions on Biomedical Engineering,* Vol. BME-31, No. 1, January, pp. 168-172

Vaguine, V.A., Tenable, E., Giebeler, R.H., McEwen, A.H., Halin, G.M., (1982), "Microwave Direct-Contant Applicator System for Hyperthermia Therapy Research" , *National Cancer Instrusment Monoger*, Vol. 61,pp. 461-464

Wait, David F., (1967), "The Sensitivity of the Dicke Radiometer" , *Journal of Research of the National Bureau of Standards -C Engineering and Instrumentation*, Vol. 17C, No. 2, April-June, pp. 127-152

Weber, E., (1947), "The Measurement of Attenuation" , *In Technique of Microwave Measurements*, Ed. Carol G. Monotgomery, Vol.11, Chapter 13, pp.804-853

Welch, J.D., Pratt, H.J., (1966), "Losses in Microstrip Transmission Systems for Integrated Microwave Circuits" , *NEREM Record*, pp. 100-101

Wheeler, H.A., (1964), "Transmission Line Properties of Parallel Strips by a Conformal Mapping Approximation" , *IEEE Transactions on Microwave Theory and Techniques*, Vol. MTT-12, No. 5, May, pp. 280-289

Wheeler, H.A., (1965), "Transmission Line Properties of Parallel Strips Separated by a Dielectric Sheet" , *IEEE Transactions on Microwave Theory and Techniques*, Vol. MTT-13, No.3, March, pp. 172-185

Wheeler, H.A., (1977), "Transmission Line Properties of a Strip on a Dielectric Sheet on a Plane" , *IEEE Transactions on Microwave Theory and Techniques,* Vol. MTT- 25, No. 8, August, pp. 631-647

Wickerseim, K.A., Sun, M.H., Heinemann, S.O., (1985), "16-Channel Fiberoptic Thermometry System with Multisensor Arrays for Thermal Mopping" , *33rd Annual Meeting Radiation Research Society*, los Angeles, May, p.62

Williams, D.F., Schwarz, S.E., (1983), "Design and Performance of Coplanar Waveguide Bandpass Filters" , *IEEE Transactions on Microwave Theory and Techniques*, Vol. MTT-31, No. 7, pp. 558-566

Yamashita, E., Mittra, R., (1968), "Variational Method for the Analysis of Microstrip Lines" , *IEEE Transactions on Microwave Theory and Techniques*, Vol. MTT-16, No. 4, pp. 251-256